THE ROLE OF TUMOR MICROENVIRONMENT IN PRIMARY LIVER CANCER THERAPEUTIC RESISTANCE

EDITED BY: Jiang Chen, Jian Chen, Zhigang Ren, Xiaochen Wang and Qiuran Xu
PUBLISHED IN: Frontiers in Cell and Developmental Biology and Frontiers in Oncology

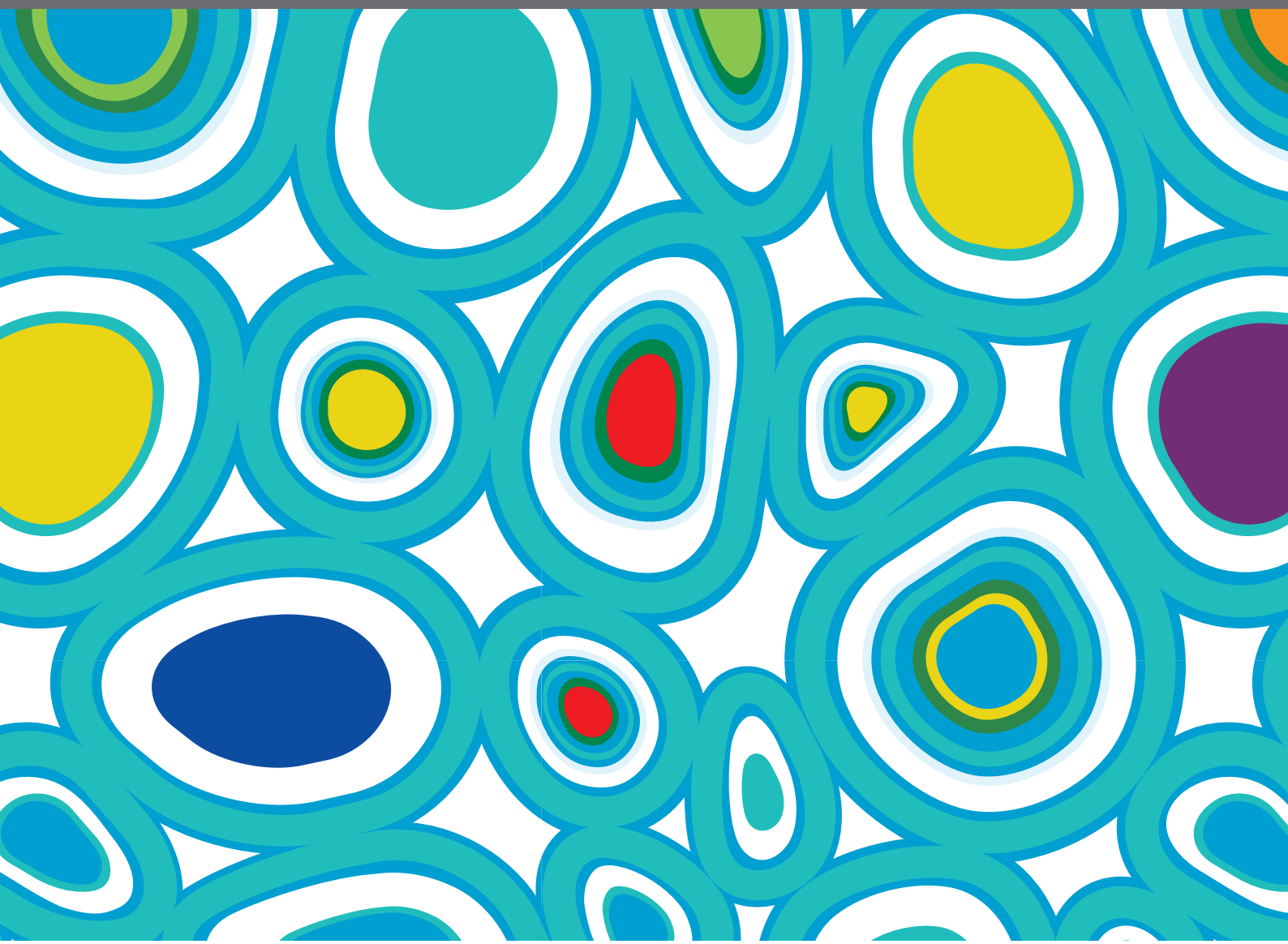

frontiers Research Topics

frontiers

ISSN 1664-8714
ISBN 978-2-88976-882-0
DOI 10.3389/978-2-88976-882-0

About Frontiers

Frontiers is more than just an open-access publisher of scholarly articles: it is a pioneering approach to the world of academia, radically improving the way scholarly research is managed. The grand vision of Frontiers is a world where all people have an equal opportunity to seek, share and generate knowledge. Frontiers provides immediate and permanent online open access to all its publications, but this alone is not enough to realize our grand goals.

Frontiers Journal Series

The Frontiers Journal Series is a multi-tier and interdisciplinary set of open-access, online journals, promising a paradigm shift from the current review, selection and dissemination processes in academic publishing. All Frontiers journals are driven by researchers for researchers; therefore, they constitute a service to the scholarly community. At the same time, the Frontiers Journal Series operates on a revolutionary invention, the tiered publishing system, initially addressing specific communities of scholars, and gradually climbing up to broader public understanding, thus serving the interests of the lay society, too.

Dedication to Quality

Each Frontiers article is a landmark of the highest quality, thanks to genuinely collaborative interactions between authors and review editors, who include some of the world's best academicians. Research must be certified by peers before entering a stream of knowledge that may eventually reach the public - and shape society; therefore, Frontiers only applies the most rigorous and unbiased reviews.
Frontiers revolutionizes research publishing by freely delivering the most outstanding research, evaluated with no bias from both the academic and social point of view. By applying the most advanced information technologies, Frontiers is catapulting scholarly publishing into a new generation.

What are Frontiers Research Topics?

Frontiers Research Topics are very popular trademarks of the Frontiers Journals Series: they are collections of at least ten articles, all centered on a particular subject. With their unique mix of varied contributions from Original Research to Review Articles, Frontiers Research Topics unify the most influential researchers, the latest key findings and historical advances in a hot research area! Find out more on how to host your own Frontiers Research Topic or contribute to one as an author by contacting the Frontiers Editorial Office: frontiersin.org/about/contact

THE ROLE OF TUMOR MICROENVIRONMENT IN PRIMARY LIVER CANCER THERAPEUTIC RESISTANCE

Topic Editors:
Jiang Chen, Zhejiang University, China
Jian Chen, BioAtla, Inc., United States
Zhigang Ren, First Affiliated Hospital of Zhengzhou University, China
Xiaochen Wang, University of Texas Southwestern Medical Center, United States
Qiuran Xu, Zhejiang Provincial People's Hospital, China

Citation: Chen, J., Chen, J., Ren, Z., Wang, X., Xu, Q., eds. (2022). The Role of Tumor Microenvironment in Primary Liver Cancer Therapeutic Resistance. Lausanne: Frontiers Media SA. doi: 10.3389/978-2-88976-882-0

Table of Contents

frontiers | Frontiers in Oncology

TYPE Editorial
PUBLISHED 27 July 2022
DOI 10.3389/fonc.2022.938557

OPEN ACCESS

EDITED AND REVIEWED BY
Luisa Lanfrancone,
European Institute of Oncology (IEO), Italy

*CORRESPONDENCE
Jiang Chen
chenjiang520@zju.edu.cn

SPECIALTY SECTION
This article was submitted to Molecular and Cellular Oncology, a section of the journal Frontiers in Oncology

RECEIVED 07 May 2022
ACCEPTED 04 July 2022
PUBLISHED 27 July 2022

CITATION
Pu Z, Ren Z, Xu Q, Wang X, Chen J and Chen J (2022) Editorial: The role of tumor microenvironment in primary liver cancer therapeutic resistance. *Front. Oncol.* 12:938557. doi: 10.3389/fonc.2022.938557

Editorial: The role of tumor microenvironment in primary liver cancer therapeutic resistance

Zhangya Pu[1], Zhigang Ren[2], Qiuran Xu[3], Xiaochen Wang[4], Jian Chen[5] and Jiang Chen[6]*

[1]Department of Infectious Disease, The First Affiliated Hospital, School of Medicine, Zhejiang University, Hangzhou, China, [2]Department of Infectious Diseases, The First Affiliated Hospital of Zhengzhou University, Zhengzhou, China, [3]Laboratory of Molecular Diagnosis, Zhejiang Provincial People's Hospital and Affiliated People's Hospital, Hangzhou Medical College, Hangzhou, China, [4]Department of Immunology, University of Texas Southwestern Medical Center, Dallas, TX, United States, [5]Department of Research and Development, BioAtla, Inc., San Diego, CA, United States, [6]Department of General Surgery, Sir Run Run Shaw Hospital, Zhejiang University, Hangzhou, China

KEYWORDS

hepatocellular carcinoma, tumor microenvironment, immune infiltration, biomarkers, prognostic model

Editorial on the Research Topic:
The role of tumor microenvironment in primary liver cancer therapeutic resistance

Hepatocellular carcinoma (HCC) is the most prevalent histological type of primary liver cancer, ranking as the sixth most common malignancy and the third leading cause of cancer-related death worldwide (1). Currently, despite the tremendous advancement in the diagnosis and treatment of HCC, especially the increasing attention paid to immunotherapies targeting the tumor microenvironment (TME), only a small population of patients benefit from it owing to the therapeutic resistance and the 5-year of overall survival remains largely unsatisfactory, with the efficacy of<18% (2–4). Hence, further integrative analyses of the diversity of TME and identification of novel diagnostic and prognostic biomarkers can not only improve immunotherapeutic responsiveness but also decode the possible new molecular mechanisms of HCC initiation and progression.

This Research Topic aims to highlight the latest valuable biomarkers, gene signature sets, and prognostic-related molecular models assisting in the diagnosis, prediction of prognosis, and evaluation of immunotherapy efficacy in HCC patients. Research articles contributing to the topic are performed by multiple bioinformatic analyses underlying publicly available online databases including TCGA (http://cancergenome.nih.gov/), ICGC (https://dcc.icgc.org/), and GEO (https://www.ncbi.nlm.nih.gov/geo/), combined with *in vivo* animal models, including tumor xenograft implantation and lung metastasis assay, and *in vitro* experimental methods, such as western blot, qRT-PCR,

immunochemistry, immunoprecipitation, dual-luciferase reporter gene assay, immunofluorescence, wound healing, transwell system, as well as tissue microarray (TMA).

Zheng et al. explored the biological function of decorin (DCN) secreted by cancer-related fibroblast in the progression of HCC. Mechanistically, they found that DCN inhibited the vascular invasion and metastasis of HCC by downregulating integrin β1protein expression. Rao et al. identified four hub genes of RPL19, RPL35A, RPL27A, and RPS12 by weighted gene co-expression network analysis (WGCNA) and further demonstrated that RPL19 was upregulated in HCC tissues than the adjacent liver tissues using TMA and public databases, and was intimately correlated to poor prognosis and suppressive immune response. Additionally, He et al. utilized the gene set variation analysis (GSVA) to construct the LIHC-unfavorable gene set (LUGs) and LIHC-favorable gene set (LFGs) associated with survival possibility after completely analyzing the differentially expressed genes (DEGs) in HCC datasets from TCGA, ICGC, and GEO databases. Next, they demonstrated that the patients in the high-LFG score group exerted immune activation, while the patients in the high-LUG score group were characterized by an immunosuppressive microenvironment. What is more, four genes of ESR1, EHHADH, CYB3A4, and ACADL were considered the crucial LIHC-progression characteristic genes (LCGs) and closely related to superior prognosis.

Recently, increasing evidence indicated the vital role of long non-coding RNAs (lncRNAs) in the carcinogenesis and progression of HCC (5, 6). Cao et al. analyzed the differentially expressed lncRNAs in the HCC cohort from TCGA database. They revealed that TMEM220-AS1 was low-expressed in HCC samples and TMEM220-AS1 curbs the proliferation and metastasis of HCC *via* regulating the miR484/MAGI1 axis.

Hitherto, limited knowledge is explicit concerning the prognostic value of skeletal muscle and adipose tissue mass and density in BCLC state B HCC patients with transarterial chemoembolization (TACE) treatment (7, 8). Li et al. evaluated the predictive function of skeletal muscle area (SM) and visceral adipose tissue (VAT) in this population of HCC patients and indicated that patients with VAT < 89.1 Hounsfield units (HU) experienced a prolonged survival possibility, showing the potential role of VAT in stratifying the intermediate stage HCC patients.

To elucidate the regulatory function of RNA post-transcriptional modification patterns in the malignant progression, prognosis, and TME of HCC. Li et al. constructed N6-methyladenosine (m6A) modification clusters of m6Acluster 1, m6Acluster 2, and m6Acluster 3, highly consistent with immune-inflamed, immune-desert, and immune-excluded, respectively. Moreover, they calculated the m6A scores for individual patients according to the differential m6A modification-related genes with prognostic values. The high m6A scores were involved with tumor progression, shorter survival possibility, and immunotherapy non-response. Additionally, the specific m6A regulator of YTHDF1 was overexpressed in HCC tissues and associated with low infiltration of $CD3^+$ and $CD8^+$ T cell types in HCC TME. Gu et al. used the HCC cohort from TCGA database to develop three 5-methylcytosine (m5C) modification subtypes and further assessed its correlation to TME, showing that Cluster-2 had a distinct survival advantage over the others. Moreover, the m5C regulator of DNMT1 was significantly upregulated in HCC samples than that in the normal tissues and was related to a poor prognosis in HCC patients. Simultaneously, upregulated expression of DNMT1 was positively correlated to several subtypes of immune cell infiltration. Xing et al. developed a prognostic model of WM-score according to the multi-layer RNA modification phenotype-related genes after integrating bioinformatic analyses of the HCC cohort in TCGA database. Later, they indicated the credible performance of WM-score value in predicting anti-tumor drug resistance and immunotherapeutic response for HCC patients.

Previous studies reported that lactate produced by aerobic glycolysis could serve as a vital signaling marker to influence the intercellular interactions, resulting in regulating the composition and function of TME. However, the specific regulatory processes are still limited (9–11). Li et al. established a lactate metabolism-related gene signature (LMRGS) using the TCGA-HCC dataset as the training cohort and the ICGC-LIRI-JP dataset was regarded as an externally validated cohort. Furthermore, they carefully evaluated the correlation of LMRGS with clinical outcomes and the TME traits of HCC patients. The results displayed that the patients within the high-LMRGS group were prone to have a shorter survival possibility and higher tumor mutation burden (TMB). Meanwhile, this population experienced a suppressed TME, with infiltrating inhibitory immune cells of follicular helper T cells and regulatory T cells and expressing repressive immune checkpoints.

This Research Topic presented the current status of updated knowledge correlated to HCC according to the comprehensive bioinformatic analyses of publicly online cancer-related databases, combined with experimental models, providing us with a variety of prognostic biomarkers or specific gene sets, as well as their predictive value of TME characteristics in HCC. We hope that this Research Topic contributes to the advancement of the diagnosis and outcome of HCC patients, especially in response to immunotherapeutic strategies.

Author contributions

ZP specialized in the Research Topic and wrote the paper text. ZR, QX, XW, JianC, and JiangC are editors of the Research Topic. All authors contributed to the article and approved the submitted version.

Acknowledgments

We put much gratitude to all authors of the manuscripts published on the specific Research Topic for their great endeavor and the reviewers for their stringent and exquisite review process. We still extend our gratitude to the editorial board of the Frontiers in Oncology for their great support.

Conflict of interest

Author JianC was employed by BioAtla, Inc.

The remaining authors declare that the research was conducted in the absence of any commercial or financial relationships that could be construed as a potential conflict of interest.

Publisher's note

References

1. Sung H, Ferlay J, Siegel RL, Laversanne M, Soerjomataram I, Jemal A, et al. Global cancer statistics 2020: GLOBOCAN estimates of incidence and mortality worldwide for 36 cancers in 185 countries. *CA Cancer J Clin* (2021) 71:209–49. doi: 10.3322/caac.21660

2. Fu Y, Liu S, Zeng S and Shen H. From bench to bed: the tumor immune microenvironment and current immunotherapeutic strategies for hepatocellular carcinoma. *J Exp Clin Cancer Res* (2019) 38:396. doi: 10.1186/s13046-019-1396-4

3. Ruf B, Heinrich B and Greten TF. Immunobiology and immunotherapy of HCC: spotlight on innate and innate-like immune cells. *Cell Mol Immunol* (2021) 18:112–27. doi: 10.1038/s41423-020-00572-w

4. Villanueva A. Hepatocellular carcinoma. *N Engl J Med* (2019) 380:1450–62. doi: 10.1056/NEJMra1713263

5. Zhou Y, Huang Y, Hu K, Zhang Z, Yang J and Wang Z. HIF1A activates the transcription of lncRNA RAET1K to modulate hypoxia-induced glycolysis in hepatocellular carcinoma cells *via* miR-100-5p. *Cell Death Dis* (2020) 11:176. doi: 10.1038/s41419-020-2366-7

6. Hu M, Fu Q, Jing C, Zhang X, Qin T and Pan Y. LncRNA HOTAIR knockdown inhibits glycolysis by regulating miR-130a-3p/HIF1A in hepatocellular ncarcinoma under hypoxia. *BioMed Pharmacother* (2020) 125:109703. doi: 10.1016/j.biopha.2019.109703

7. Marasco G, Serenari M, Renzulli M, Alemanni LV, Rossini B, Pettinari I, et al. Clinical impact of sarcopenia assessment in patients with hepatocellular carcinoma undergoing treatments. *J Gastroenterol* (2020) 55:927–43. doi: 10.1007/s00535-020-01711-w

8. Imai K, Takai K, Miwa T, Maeda T, Hanai T, Shiraki M, et al. Increased visceral adipose tissue and hyperinsulinemia raise the risk for recurrence of non-b non-c hepatocellular carcinoma after curative treatment. *Cancers (Basel)* (2021) 13:1542. doi: 10.3390/cancers13071542

9. Dong Q, Zhou C, Ren H, Zhang Z, Cheng F, Xiong Z, et al. Lactate-induced MRP1 expression contributes to metabolism-based etoposide resistance in non-small cell lung cancer cells. *Cell Commun Signal* (2020) 18:167. doi: 10.1186/s12964-020-00653-3

10. Liao ZX, Kempson IM, Hsieh CC, Tseng SJ and Yang PC. Potential therapeutics using tumor-secreted lactate in nonsmall cell lung cancer. *Drug Discovery Today* (2021) 26:2508–14. doi: 10.1016/j.drudis.2021.07.014

11. Zhang A, Xu Y, Xu H, Ren J, Meng T, Ni Y, et al. Lactate-induced M2 polarization of tumor-associated macrophages promotes the invasion of pituitary adenoma by secreting CCL17. *Theranostics* (2021) 11:3839–52. doi: 10.7150/thno.53749

frontiers in Cell and Developmental Biology

ORIGINAL RESEARCH
published: 02 July 2021
doi: 10.3389/fcell.2021.687756

m6A Regulator-Associated Modification Patterns and Immune Infiltration of the Tumor Microenvironment in Hepatocarcinoma

Jianhao Li[1,2†], Weiwei Wang[3†], Yubing Zhou[2,4†], Liwen Liu[1,2], Guizhen Zhang[1,2], Kelei Guan[4], Xichun Cui[2], Xin Liu[1,2], Maoxin Huang[5], Guangying Cui[1,2] and Ranran Sun[1,2*]*

[1] Precision Medicine Center, The First Affiliated Hospital of Zhengzhou University, Zhengzhou, China, [2] Key Laboratory of Clinical Medicine, The First Affiliated Hospital of Zhengzhou University, Zhengzhou, China, [3] Department of Pathology, The First Affiliated Hospital of Zhengzhou University, Zhengzhou, China, [4] Department of Pharmacy, The First Affiliated Hospital of Zhengzhou University, Zhengzhou, China, [5] Department of Dermatology, The First Affiliated Hospital of Zhengzhou University, Zhengzhou, China

OPEN ACCESS

Edited by:
Jiang Chen,
Zhejiang University, China

Reviewed by:
Jinyang Li,
The Rockefeller University, United States
Ke-Da Yu,
Fudan University, China
Geoffrey Joseph Markowitz,
Cornell University, United States
Zhi Li,
The First Affiliated Hospital of China Medical University, China

***Correspondence:**
Ranran Sun
fccsunrr@zzu.edu.com
Guangying Cui
cuiguangying1986@163.com

[†] These authors have contributed equally to this work

Specialty section:
This article was submitted to Molecular and Cellular Oncology, a section of the journal Frontiers in Cell and Developmental Biology

Received: 30 March 2021
Accepted: 03 June 2021
Published: 02 July 2021

Citation:
Li J, Wang W, Zhou Y, Liu L, Zhang G, Guan K, Cui X, Liu X, Huang M, Cui G and Sun R (2021) m6A Regulator-Associated Modification Patterns and Immune Infiltration of the Tumor Microenvironment in Hepatocarcinoma. Front. Cell Dev. Biol. 9:687756. doi: 10.3389/fcell.2021.687756

Background: Immunotherapy elicits durable responses in many tumors. Nevertheless, the positive response to immunotherapy always depends on the dynamic interactions between the tumor cells and infiltrating lymphocytes in the tumor microenvironment (TME). Currently, the application of immunotherapy in hepatocellular carcinoma (HCC) has achieved limited success. The ectopic modification of N6-methyladenosine (m6A) is a common feature in multiple tumors. However, the relationship between m6A modification with HCC clinical features, prognosis, immune cell infiltration, and immunotherapy efficacy remains unclear.

Materials and Methods: Here, we comprehensively evaluated m6A modification clusters based on 22 m6A regulators and systematically explored the relationship between m6A modification with tumor progression, prognosis, and immune cell infiltration characteristics. The m6Ascore was calculated by principal component analysis to quantify the m6A modifications of individual patients. Key regulators involved in immunoregulation in HCC were identified using immunohistochemistry and immunofluorescence.

Results: Three distinct m6A modification clusters were identified. The m6A clusters were significantly associated with clinical features, prognosis, and immune cell infiltration. The three clusters were highly consistent with the three tumor immune phenotypes, i.e., immune-excluded, immune-inflamed, and immune-desert. Comprehensive bioinformatics analysis revealed that high m6Ascore was closely associated with tumor progression, poor prognosis, and immunotherapy non-response. m6A regulators were dysregulated in HCC tissues. Hence, they play a role as predictors

of poor prognosis. Tissue microarray demonstrated that overexpressed YTHDF1 was associated with low $CD3^+$ and $CD8^+$ T cell infiltration in HCC.

Conclusion: Our findings demonstrate that m6A modification patterns play a crucial role in the tumor immune microenvironment and the prognosis of HCC. High YTHDF1 expression is closely associated with low $CD3^+$ and $CD8^+$ T cell infiltration in HCC.

Keywords: N6-methyladenosine, hepatocellular carcinoma, tumor microenvironment, prognosis, immune infiltration

INTRODUCTION

Hepatocellular carcinoma (HCC) is one of the major causes of cancer-related mortality worldwide and accounts for 80% of primary liver cancer (Lin et al., 2013; Siegel et al., 2018). Currently, surgical resection and percutaneous ethanol injection are the main treatment modalities for HCC (Dutta and Mahato, 2017). However, even though significant efforts have been made in HCC treatment and management, the 5-year overall survival (OS) remains poor, and has been attributed to late diagnosis, tumor recurrence, and unsatisfactory treatment (Forner et al., 2018; Yang and Heimbach, 2020). Therefore, it is imperative to develop powerful diagnostic and novel therapeutic strategies to improve the outcome of HCC.

N6-methyladenosine (m6A) is an RNA post-transcriptional modification that is most abundant in mammalian mRNA (Zaccara et al., 2019). m6A methylation is mediated by several proteins, which are categorized into three types: writers are methyltransferases, including WTAP, KIAA1429, RBM15, RBM15B, and METTL3/14/16; erasers such as FTO and ALKBH5, which are the only two identified m6A demethylases; and final function executions (readers) that include HNRNPs, YTHDF1/2/3, YTHDC1/2, IGF2BP1/2/3, and EIF3A (Chen et al., 2019; Zhen et al., 2020). Increasing evidence has identified the important roles m6A modifications play in various cellular processes and in cancer progression through regulating RNA stability, mRNA splicing and translation, and microRNA processing (Gilbert et al., 2016; Zhao et al., 2017). Meanwhile, m6A modification dysregulation has been correlated with tumor malignant progression and immunomodulatory abnormality (Shulman and Stern-Ginossar, 2020). Wang et al. (2019) revealed that upregulated METTL3 promoted dendritic cell (DC) activation and maturation, and that METTL3 downregulation inhibited T cell activation and aggregation. Han et al. (2019) demonstrated that inhibiting YTHDF1 enhanced $CD8^+$ T cell tumor infiltration and immunotherapy efficacy in a murine tumor model. However, the specific mechanism of m6A involvement in the malignant progression and immune response of HCC remains unclear.

In the present study, we integrated the information on mRNA and protein levels of m6A regulators to comprehensively evaluate the effect of m6A modification variation on HCC malignant progression, prognosis, and immune response. **Supplementary Figure 1** shows the overall study design. First, the mRNA and protein expression levels of m6A regulators in HCC were systematically explored via The Cancer Genome Atlas (TCGA) database, Gene Expression Omnibus (GEO) and a tissue microarray analysis (TMA) cohort. Then, we identified three distinct m6A modification patterns of HCC and evaluated the clinical features, prognosis value, potential mechanism, and immune infiltration of the resultant m6A clusters. Further, we explored the correlation among the YTHDF1 level, activated tumor-infiltrating lymphocytes, and related biological processes in HCC using immunohistochemistry (IHC), immunofluorescence, and comprehensive bioinformatics analysis. We reveal that m6A modification patterns play a critical role in the malignant progression and efficacy of immunotherapy in HCC.

MATERIALS AND METHODS

Data Source

The RNA-seq transcriptome data and corresponding clinicopathological information of 370 HCC and 50 normal tissues were obtained from TCGA liver hepatocellular carcinoma cohort (TCGA-LIHC)[1], 203 HCC and 175 normal tissue samples from the International Cancer Genome Consortium Liver Cancer-RIKEN-JP cohort (ICGC-LIRI-JP)[2] were downloaded. GSE36376 (non-tumor = 193, tumor = 240) and GSE76297 (non-tumor = 52, tumor = 153) were gathered through the GEO database[3], GEO) (Chaisaingmongkol et al., 2017; Cho et al., 2020).

Unsupervised Clustering for Twenty-Two m6A Regulators

A total of 22 m6A regulator genes were curated and analyzed to identify different m6A modification patterns based on previous literature. The 22 m6A regulators genes included seven writers (WTAP, KIAA1429, RBM15, RBM15B, and METTL3/14/16), 12 readers (HNRNPs, YTHDF1/2/3, YTHDC1/2, IGF2BP1/2/3, and EIF3A), and two erasers (ALKBH5 and FTO). To ensure clustering reproducibility of our approach, we selected TCGA-LIHC (training set) and ICGC-LIRI-JP (validation set) with high heterogeneity for further analysis. The HCC Patients without follow-up information were deleted. Eventually, 367 patients from TCGA-LIHC dataset and 203 patients from ICGC-LIRI-JP database were enrolled for subsequent

[1]https://tcga-data.nci.nih.gov/tcga/

[2]https://icgc.org/

[3]http://www.ncbi.nlm.nih.gov/geo/

analysis. **Supplementary Table 1** presents the detailed clinical-pathological information of TCGA and ICGC cases selected for testing database and validation set. Then, we performed unsupervised clustering to identify distinct m6A modification patterns based on the expression of 22 m6A regulators. The R package "ConsensusClusterPlus" were used to conduct the above steps and 1000 times repetitions for guaranteeing the stability of clustering. The optimal number of clusters was determined according to the consensus clustering algorithm.

Tissue Samples

A microarray of 100 HCC tumors and adjacent normal tissue samples was constructed using a core diameter of 1.5 mm. All experiments received approvals from the Ethics Committee of the First Affiliated Hospital of Zhengzhou University.

Immunohistochemistry and Immunofluorescent

Immunohistochemistry and immunofluorescent were performed as previously reported. Briefly (Li et al., 2019, 2020b), 5 μm thick TMA sections were deparaffinized and treated with hydrogen peroxide to quench endogenous peroxidase activity. Subsequently, the sections were incubated with related proteins antibodies at 4°C overnight. The immunoreactive cells were detected by Signal Stain® DAB (CST, United States) and counterstained with Hematoxylin QS (Vector Laboratories). Two experienced pathologists who were blinded to evaluate the clinicopathological data the immunostaining samples separately and they scored the samples according to the proportion of positive cells as follows: no staining, 1+; weak staining, 2+; moderate staining, 3+; strong staining, 4+; and intense staining, 5+; The score of 1+ and 2+ was defined as low expression while the other scores were defined as high expression for statistical analysis. The $CD3^+$ and $CD8^+$ T cells count were performed using ImageScope (Aperio Technologies). $CD3^+$ and $CD8^+$ T cell density were counted as cells/mm^2 and categorized into high and low groups. For Immunofluorescence, slides were incubated with HRP labeled second antibody. The slides were visualized with scanning laser confocal microscope and evaluated by Image-Pro Plus software. Detailed information of antibodies used in this study was showed in **Supplementary Table 2**.

Single-Sample Gene Set Enrichment Analysis (ssGSEA)

Single-sample gene set enrichment analysis (ssGSEA) in R package GSVA was used to quantify the infiltration levels of the immune cell types in tumor microenvironment (TME). ssGSEA applies gene signatures expressed by immune cell populations to individual cancer samples. **Supplementary Table 3** shows the detailed information of gene signatures used in this study. The deconvolution approach was used to evaluate total 24 immune cells involved in innate immunity [natural killer (NK) cells, CD56dim NK cells, CD56bright NK cells, plasmacytoid DCs, immature DCs, activated DCs, DC, neutrophils, mast cells, eosinophils, and macrophages] and adaptive immunity including B cells, $CD8^+$ T cells, Cytotoxic cells, T cells, T helper cells, Tcm (central memory T cell), Tem (effector memory T cell), TFH (Follicular helper T cell), Tgd, Th1 cells, Th17 cells, Th2 cells, and Treg (Regulatory T cell).

Gene Set Variation Analysis (GSVA) and Other Biological Pathways Analysis

The gene set variation analysis (GSVA) package was used to export the Kyoto Encyclopedia of Genes and Genomes (KEGG) pathways described in the molecular signature database and used to perform the pathway analyses of the potential mechanism of m6A clusters. Mariathasan et al. (2018) constructed a set of gene sets that stored genes associated with some biological processes, including Antigen processing and presentation (APAP), CD8 T-effector signature, Epithelial–mesenchymal transition 1 (EMT1), EMT2, EMT3, Angiogenesis, TGF-β pathway, Wnt pathway, DNA damage repair (DDR), Nucleotide excision repair (NER), DNA replication and Cell cycle (Rosenberg et al., 2016; Şenbabaoğlu et al., 2016; Mariathasan et al., 2018). The correlation between m6A modification and other biological pathways were further explored. **Supplementary Table 4** presents the detailed information of biological pathways used in this study.

Construction of m6Ascores

To quantitatively evaluate of m6A modification patterns for individual HCC patients, we established a set of scoring system. The establishment procedures of m6A scoring system were as follows: Differential analysis and Venn diagram showed that there are 236 common differential genes among three m6A clusters. Then, we conducted the univariate Cox regression analysis for each gene. These genes with the significant prognosis were extracted for next analysis. We then performed principal component analysis (PCA) to calculate m6A score using the formula:

$$\text{m6A score} = \sum \left(PC1_i + PC2_i\right)$$

where i is the expression value of each selected genes. This formula was used to calculate the m6A score for HCC patients in both the training (TCGA) and validation (ICGC) datasets.

Statistical Analysis

All statistical analyses were conducted in R (3.5.3) statistical package unless otherwise stated. Student's *t*-test (unpaired, two-tailed) was used to evaluate the differences between the two independent groups. One-way ANOVA and Kruskal–Wallis tests were used to determine difference comparisons of three or more groups. The *post hoc* comparisons of ANOVAs, Kruskal–Wallis and log rank test were performed. These results presented in **Supplementary Table 10**. Chi-square test was used to examine the correlation between m6A modification patterns and clinical features. For each significantly ectopically expressed genes the Kaplan-Meier analysis was performed using the log-rank test. Cox regression analysis of univariate and multivariate variables was used to study the relationship between the prognosis value and different variables. The P values were corrected for multiple comparisons via the Benjamini and Hochberg (BH). Unsupervised subclass mapping method (SubMap) was used to

clarify the corresponding relationship of m6A clusters between TCGA-LIHC and ICGC-LIRI cohorts[4] (Hoshida et al., 2007; Chaisaingmongkol et al., 2017). $P < 0.05$ was considered to have Significant similarity between clusters found by the SubMap method, and this P values were corrected by the Bonferroni method. The Tumor Immune Dysfunction and Exclusion (TIDE) were used to calculate TIDE scores and predict the clinical response to immune checkpoint blockade (Şenbabaoğlu et al., 2016). In all cases, $P < 0.05$ was considered statistically significant.

RESULTS

The Landscape of Genetic Variation of m6A Regulators in HCC

To explore the significant biological function of m6A regulators in hepatocarcinogenesis and tumor progression, we summarized the mRNA and protein expression levels of 22 m6A regulators in HCC and non-tumor tissues based on TCGA, ICGC, GEO, and ZZU TMA cohorts. Both the mRNA and protein expression levels of WTAP, KIAA1429, RBM15, RBM15B, METTL3, HNRNPs, YTHDF1, YTHDF2, YTHDF3, IGF2BPs, and FTO were markedly higher in HCC tissues (**Figure 1A**). Additionally, to gain insight into the cause of m6A regulator dysregulation, we explored the somatic mutations and copy number variation (CNV) alteration frequency of m6A regulators. Among 364 samples, 35 (9.62%) had m6A regulator mutations, indicating that m6A regulator somatic mutations are infrequent in HCC (**Supplementary Figure 2A**). The CNV alteration frequency study indicated that CNV alteration was prevalent in m6A regulators. Meanwhile, m6A regulators with amplified CNV (e.g., KIAA1429 and YTHDF1) were markedly upregulated in the HCC tissues (**Supplementary Figure 2B**). Univariate Cox regression analysis showed that most of the upregulated m6A regulators are potential prognostic risk factors for patients with HCC (**Figures 1B,C**). Multivariate Cox regression analysis indicated that YTHDF2 was an independent risk factor for OS and progression-free survival (PFS) (**Supplementary Figures 2C,D**). Correlation analysis indicated that there were higher correlations among m6A regulators (**Supplementary Figure 2E** and **Supplementary Table 5**). Overall, the results present large genomic and expression variations of m6A regulators between normal and HCC tissue. Concurrently, the expression of the 22 m6A regulators was closely related, playing a significant role in HCC prognosis.

Correlation of m6A Clusters With Clinical Features and Prognosis in TCGA Dataset

To explore the biological function of different m6A methylation modification patterns in HCC, we performed unsupervised clustering based on the expression of 22 m6A regulators in TCGA-LIHC dataset, and identified three distinct modification clusters. Further analysis of the m6A transcriptional profiles revealed that a significant distinction in three different m6A modification patterns. m6Acluster 1 presented moderate expression in most m6A regulators except for the IGFBPs. m6Acluster 2 was characterized by the increased expression of all m6A regulators. m6Acluster 3 exhibited significant low expression in most m6A regulators except for IGFBP1 and IGFBP2 (**Figure 2A**). We found that there were significant correlations between clinicopathological features and the m6A clusters. Lack of vascular invasion, low serum alpha-fetoprotein (AFP) level, histologic grade G1/G2, and tumor-node-metastasis (TNM) stage I/II were associated with the C1 or C3 clusters; presence of vascular invasion, advanced TNM stage (III/IV), histologic grade (G3/G4), and high serum AFP level were associated with the C2 cluster (**Supplementary Table 6**). Prognostic analysis showed the particularly prominent survival advantage in m6Acluster 1, followed by that in m6Acluster 3. m6Acluster 2 had the worst outcome (**Figures 2B,C**). And the survival advantage of m6Acluster 1 was confirmed in patients with different ages (age $\leq$ 55 or age $>$ 55) (**Supplementary Figure 3**). Further, PCA dimension reduction analysis showed that the m6A clusters were segregated into three discrete clusters (**Figure 2D**). The results suggest that different m6A modifications have significant correlation with HCC clinical characteristics and prognosis.

Correlation of the m6A Clusters With Tumor Microenvironment (TME) Immune Cell Infiltration Characteristics

Considering that the classification was based on m6A regulators, we explored whether distinct m6A clusters had different biological behaviors. First, we conducted GSVA analysis. **Figures 2E,F** and **Supplementary Table 7** show that m6Acluster 1 was markedly enriched in cytokine–cytokine receptor interaction, T and B cell receptor signaling pathways, NER, and apoptosis pathways. m6Acluster 2 presented enrichment pathways related to WNT, MAPK, and the cell cycle pathways. m6Acluster 3 was prominently associated with the TGF-β and MAPK signaling pathways. Further immune infiltration and mechanism studies demonstrated that compared with m6Acluster 2, m6Acluster 1 and 3 showed high infiltration of most immune cells, but m6Acluster 3 did not show higher $CD8^+$ positive T cell infiltration and significant survival advantage, which may be related to the immunosuppression caused by TGF-β pathway significant enrichment (**Figures 3A,B**). A surprising finding was that the m6A modification patterns had significantly distinct immune subtypes. m6Acluster 1 was classified as the immune-inflamed phenotype, characterized by adaptive immune cell infiltration. m6Acluster 2 was classified as the immune-desert phenotype, characterized by the inhibition of immunity and WNT pathway significant enrichment. m6Acluster 3 was classified as the immune-excluded phenotype, characterized by innate immune cell infiltration and TGF-β significant enrichment. To investigate the m6A-related immune phenotypes, we extracted pathway- and immune-associated key gene signatures from the published literature. We found that the mRNAs relevant to immune checkpoints and the

[4]http://genepattern.broadinstitute.org/

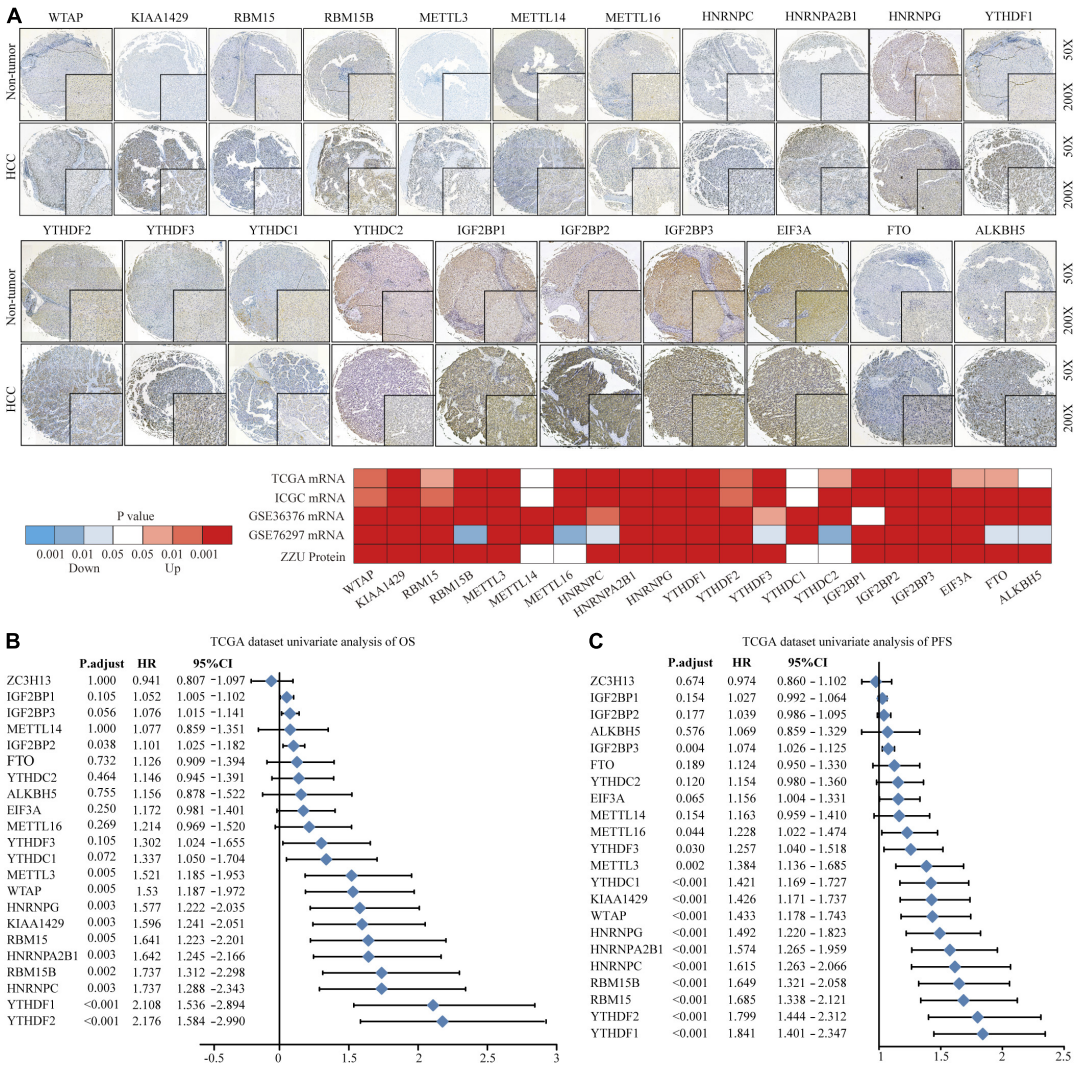

FIGURE 1 | Landscape of genetic variation of m6A regulators in HCC. **(A)** The mRNA and protein expression pattern of m6A regulators in HCC. **(B)** Univariate Cox regression analysis of OS in HCC patients. **(C)** Univariate Cox regression analysis of PFS in HCC patients.

WNT pathway were significantly upregulated in m6Acluster 2 (**Figures 3C,D**). The immune activation genes CD8A, CXCL9, and CXCL10 had significant high expression in m6Acluster 1 (**Figure 3E**), while the TGF-β pathway-related genes exhibited high expression in m6Acluster 3 (**Figure 3F**). These results demonstrate that there is a close relationship between m6A clusters and TME immune status.

Correlation of the m6A Clusters With Clinical and TME Cell Infiltration Characteristics in the ICGC Dataset

To validate the correlation of the m6A clusters with the clinical and TME cell infiltration characteristics, we focused on the ICGC cohort for external validation. Similar to TCGA dataset clustering, three fully distinct m6A modification patterns were identified. m6Acluster 1 was characterized by the decreased expression of most of the m6A regulators. m6Acluster 2 showed high expression of YTHDC1, METTL3/16, HNRNPs, RBM15, YTHDF1/2, WTAP, ALKBH5, RBM15B, and IGF2BPs; m6Acluster 3 exhibited significant upregulation of ZC3H13, YTHDC2, YTHDF3, FTO, METTL14, and EIF3A (**Figure 4A**). Clinical characteristics analysis showed that m6Acluster 2 patients had high serum AFP levels, TNM stage, and were hepatitis B virus (HBV)-positive (**Figure 4A** and **Supplementary Table 8**). Prognostic analysis also revealed that m6Acluster 2 was significantly related with poor survival (**Figure 4B**). PCA dimension reduction analysis visualization of the transcriptomic data of the three m6A clusters showed that they were segregated into three discrete clusters (**Figure 4C**). To further examine consistency in cluster formation, we used an SubMap method. The SubMap method conducted a pairwise comparison of the molecular features between each of the predetermined m6A clusters of TCGA-LIHC and ICGC-LIRI cohorts. The

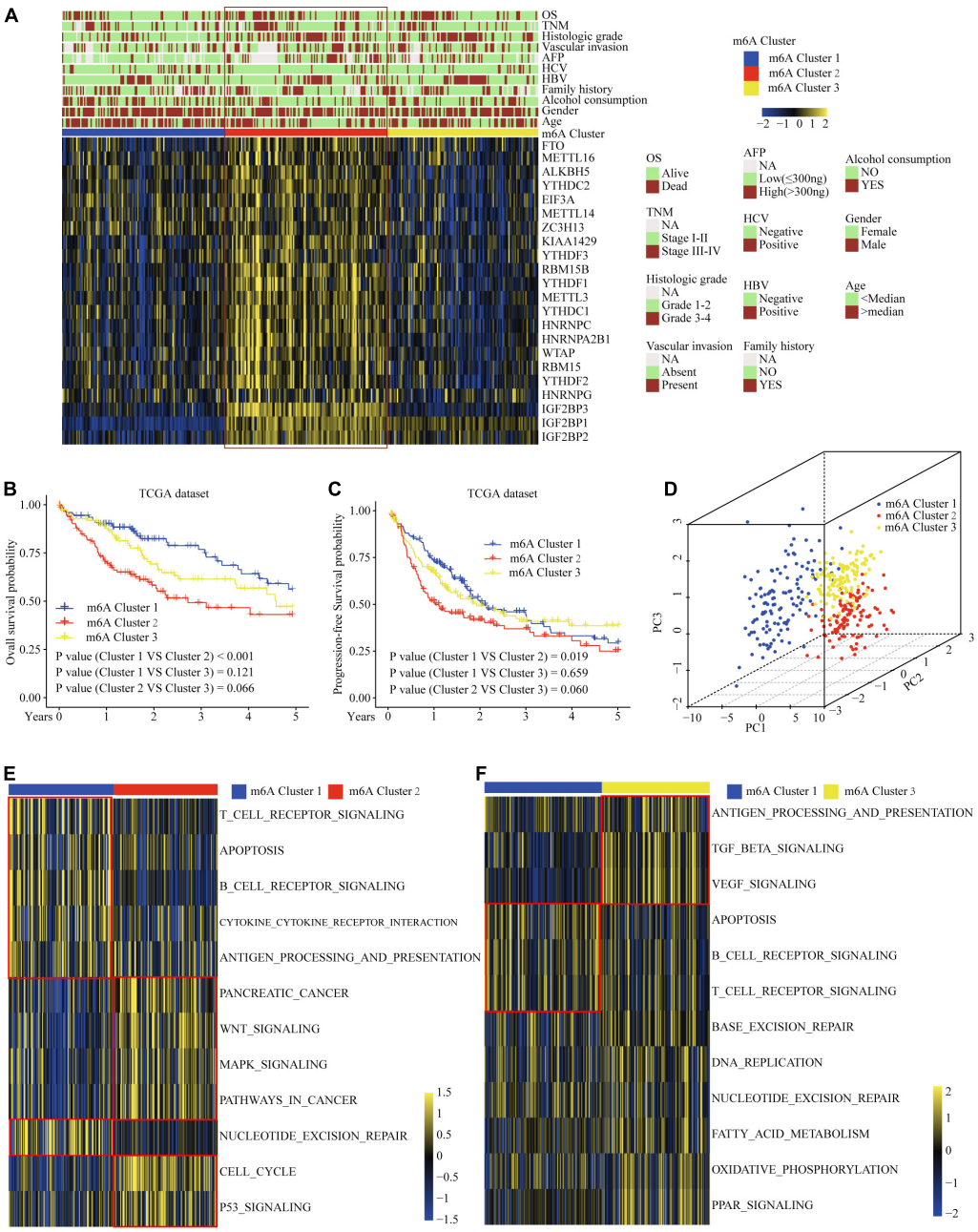

FIGURE 2 | Correlation of the m6A clusters with clinical features, prognosis and biological characteristics in TCGA dataset. **(A)** The relationship between the m6A regulators expression profiles of these three clusters and clinical features of HCC. **(B)** Overall survival analysis for the HCC patients of three clusters in the TCGA dataset. **(C)** Progression-free survival analysis for the HCC patients of three clusters in the TCGA dataset. **(D)** PCA plots of TCGA-LIHC RNA-sequence profiles for three m6A clusters. **(E,F)** GSVA enrichment score showing the activation states of biological pathways in three m6A clusters. Red box indicates the genes expression and clinical features of clusters.

result showed that the molecular features of m6A clusters between TCGA-LIHC and ICGC-LIRI cohorts are significantly similar (**Figure 4D**). Further immune infiltration and pathway score analysis indicated that m6Acluster 1 and 3 showed high immune cell infiltration, but that the TGF-β pathway was significantly enriched in m6Acluster 3. m6Acluster 2 presented the lowest level of immune cell infiltration and WNT pathway significant enrichment (**Figures 4E,F**). The results again confirm the ability of m6A regulators to distinguish different subtypes of HCC.

Upregulated YTHDF1 Reduced CD3$^+$ and CD8$^+$ T Cell Infiltration in HCC

The earlier results reveal that different m6A clusters have different immune subtypes. To explore the effect of the expression

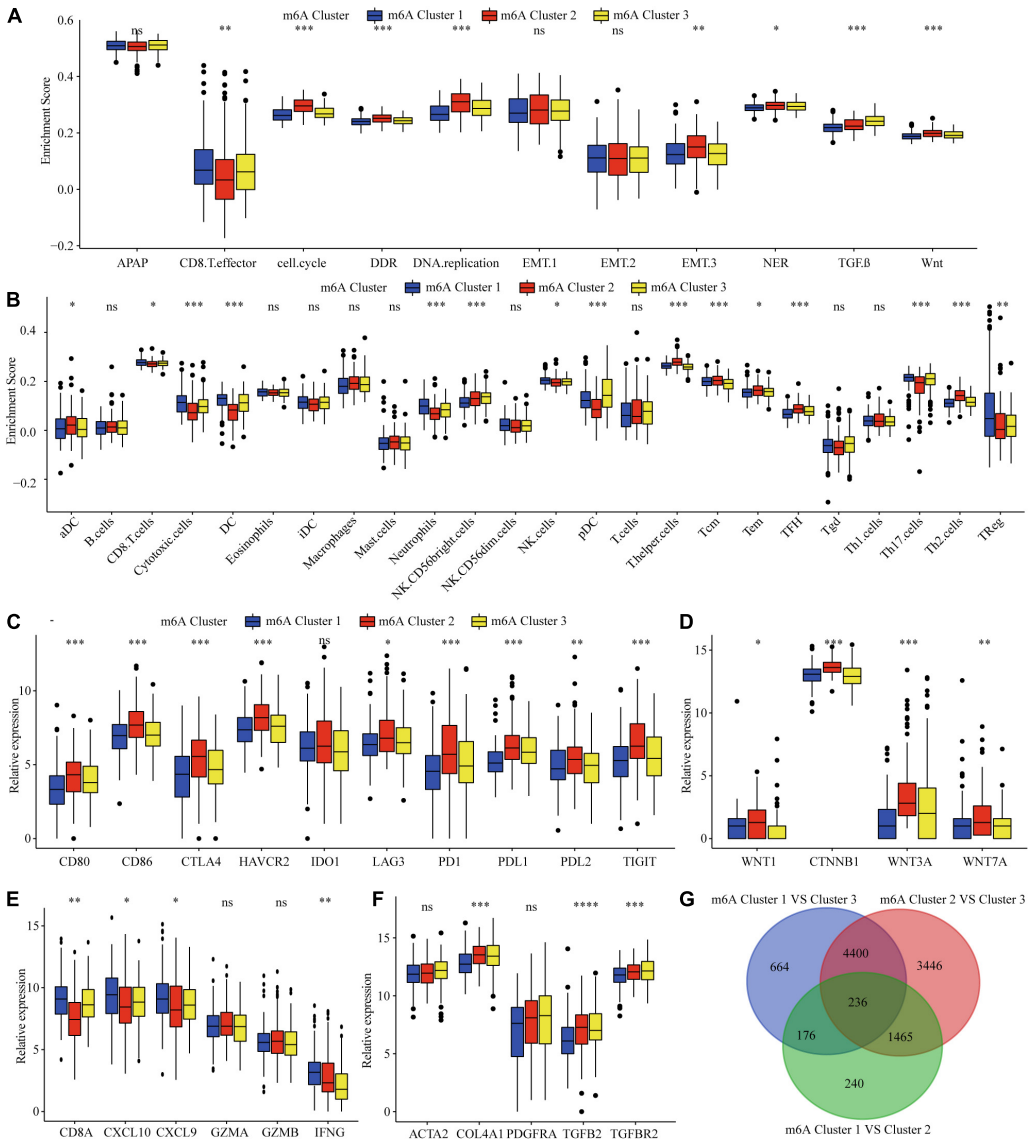

FIGURE 3 | TME immune cells infiltration, biological functions and transcriptome traits in three m6A clusters. **(A)** Difference in biological functions among three m6A clusters in TCGA dataset. **(B)** Difference in the abundance of immune infiltrating cells among three m6A clusters. **(C)** Difference in the immune-checkpoint related genes expression among three m6A clusters. **(D)** Difference in the Wnt pathway related genes expression among three m6A clusters. **(E)** Difference in the immune-activation related genes expression among three m6A clusters. **(F)** Difference in the TGF-β pathway related genes expression among three m6A clusters. **(G)** 236 m6A clusters related genes shown in Venn diagram. $^{*}P \leq 0.05$; $^{**}P \leq 0.01$; $^{***}P \leq 0.001$; $^{****}P \leq 0.0001$.

of the 22 m6A regulators on immune cell infiltration, we first examined the specific correlation between each TME-infiltrating cell type and the 22 regulators using Pearson analyses. We found significantly negative correlations between the level of immune cell infiltration, such as that by B cells, T cells, and CD cells, with the expression of most of the m6A regulators (**Supplementary Figure 4A**). Subsequently, we found that high YTHDF1 expression was closely related with poor prognosis and infiltration by numerous immune cells (**Supplementary Figures 4B–D**). Additionally, we explored the effect of YTHDF1 protein level on T cell infiltration. IHC analysis indicated that $CD3^{+}$ and $CD8^{+}$ T cell numbers were significantly decreased in the samples with upregulated YTHDF1 (**Figure 5A**). To study the essential relationship between TME immune status and YTHDF1 level in patients with HCC, we quantitatively analyzed the $CD3^{+}$ and $CD8^{+}$ T cell counts with immunofluorescence assay. The results demonstrated that YTHDF1 overexpression significantly decreased $CD3^{+}$ and $CD8^{+}$ T cell infiltration (**Figure 5B**). Based on these findings, it is evident that upregulated YTHDF1 is closely associated with poor prognosis and immune suppression in HCC. Subsequently, pathway enrichment analyses indicated that tumors with low YTHDF1 expression exhibited obvious enhancement in $CD8^{+}$ T effector cells and had inhibited cell

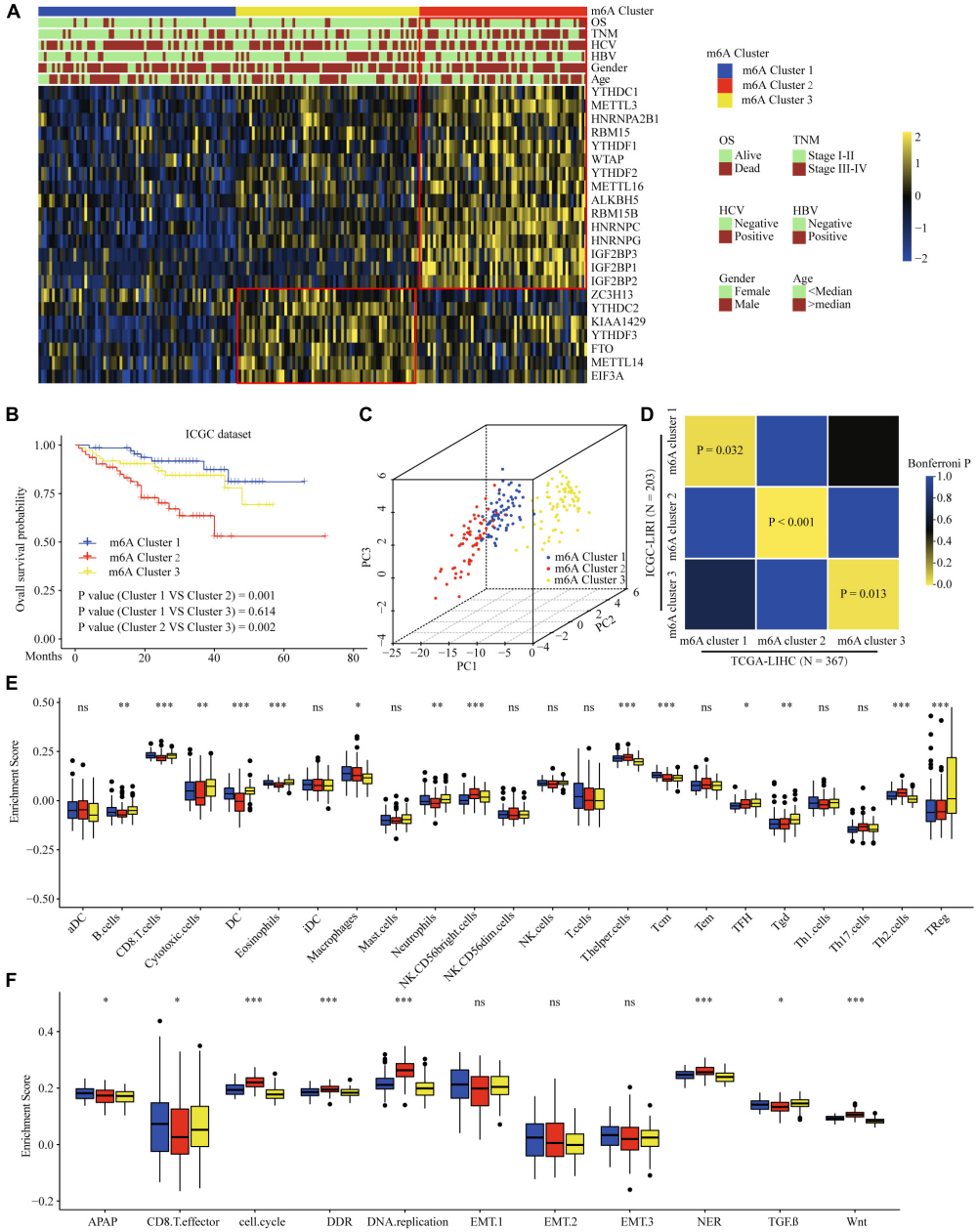

FIGURE 4 | Correlation of the m6A clusters with clinical features, prognosis and biological characteristics in ICGC dataset. **(A)** The relationship between the m6A regulators expression profiles of these three clusters and clinical features of HCC in ICGC dataset. **(B)** Survival analysis for the HCC patients of three clusters in the ICGC dataset. **(C)** PCA plots of ICGC-LIRI-JP RNA-sequence profiles for three m6A clusters. **(D)** Subclass Mapping of TCGA-LIHC and ICGC-LIRI m6A clusters. $P < 0.05$ was considered to have Significant similarity between clusters. **(E)** Difference in the abundance of immune infiltrating cells among three m6A clusters in ICGC dataset. **(F)** Difference in biological functions among three m6A clusters in ICGC dataset. Red box indicates the genes expression and clinical features of clusters. $^{*}P \leq 0.05$; $^{**}P \leq 0.01$; $^{***}P \leq 0.001$.

cycle, DDR, DNA replication, TGF-β, and WNT pathways (**Supplementary Figure 4E**).

m6A Gene Signature Subtypes and m6Ascore Performance Validation

Considering the variation and biological function of m6A modification in HCC, we explored the potential biological function of each m6A modification pattern. Differential analysis and a Venn diagram showed that there were 236 common differential genes among the three m6A clusters (**Figure 3G**). Unsupervised clustering analyses based on the 236 genes confirmed that there were three distinct m6A modification genomic phenotypes; we termed these three clusters m6A gene cluster A–C (**Figure 6A**). Clinical features analysis indicated that m6A gene cluster B exhibited more vascular invasion, AFP

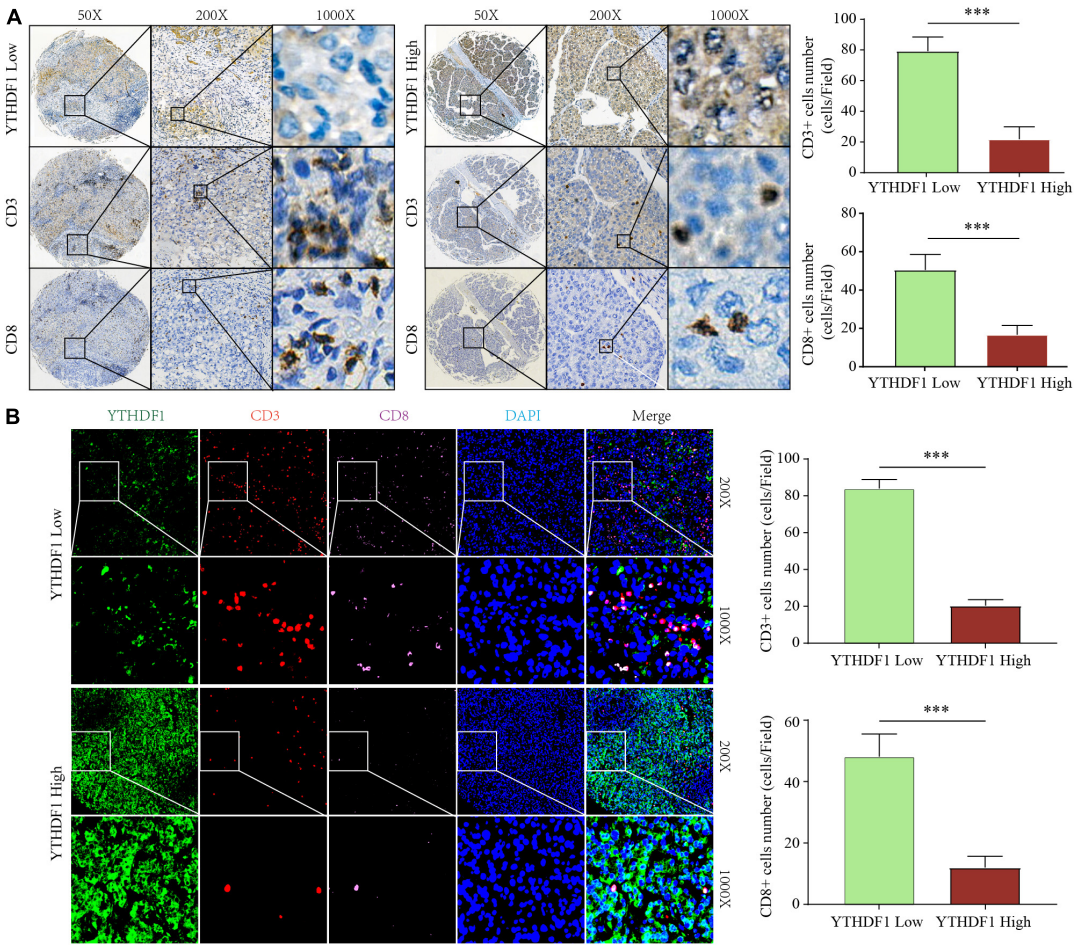

FIGURE 5 | YTHDF1 expression level closely associated with CD3 and CD8 positive T cells infiltration in HCC. **(A)** Immunohistochemistry assays showed that CD3+ and CD8 + T cell density in HCC tissues with high or low YTHDF1 expression. **(B)** immunofluorescent IHC staining of YTHDF1, CD3, and CD8 were performed on TMA-cohort. ***$P \leq 0.001$.

elevation, high histologic grade, and TNM stage (**Supplementary Table 9**). Prognostic analysis demonstrated a particularly prominent survival advantage in the m6A gene cluster A modification pattern, followed by that of m6A gene cluster C. m6A gene cluster B had the worst outcome (**Figures 6B,C**). The results again show that m6A methylation patterns are tightly associated with HCC development and progression.

To accurately evaluate the m6A methylation modification of individual patients with HCC, we selected 182 differential genes with prognostic utility to construct the patients' individual m6Ascores (**Supplementary Table 11**). To obtain the clinical and prognostic value for the patients with HCC, the best cut-off value was calculated with the survminer package, and the patients were divided into low or high m6Ascore groups. A high m6Ascore indicated worse prognosis (**Figures 7A,B**). Meanwhile, validation in an external ICGC database confirmed the prognostic value of the m6Ascore (**Figure 7C**). Thereafter, we quantitatively analyzed the m6Ascore in HCC to investigate the association between the m6Ascore and each clinicopathological characteristic. **Figures 7D–G** shows that the m6Ascores were significantly different in these groups, with TCGA dataset compartmentalized by histologic grade, vascular invasion, TNM stage, and AFP level. Univariate and multivariate Cox regression analyses were performed with TCGA and ICGC datasets. The m6Ascore was an independent prognostic factor for HCC outcome (**Figures 7H–K**).

To explore the potential biological mechanism of the m6Ascore, we tested the correlation between it and the known pathway signatures. The results indicated that a low m6Ascore could be significantly associated with $CD8^+$ T cell effector, whereas a high m6Ascore could be linked to significant enrichment of the immunosuppression and malignant progression pathways (**Figure 8A**). Furthermore, we explored the relationship among m6A modification, m6Ascore, and HCC immunotherapy. Differential analysis found that m6Acluster 1 and m6A gene cluster B had the highest m6Ascores, while m6Acluster 1 and m6A gene cluster B had the lowest m6Ascores (**Figures 8B–D**). Then, we used the TIDE algorithm to predict the likelihood of response to immunotherapy based on TCGA and ICGC datasets. A previous study had demonstrated that a

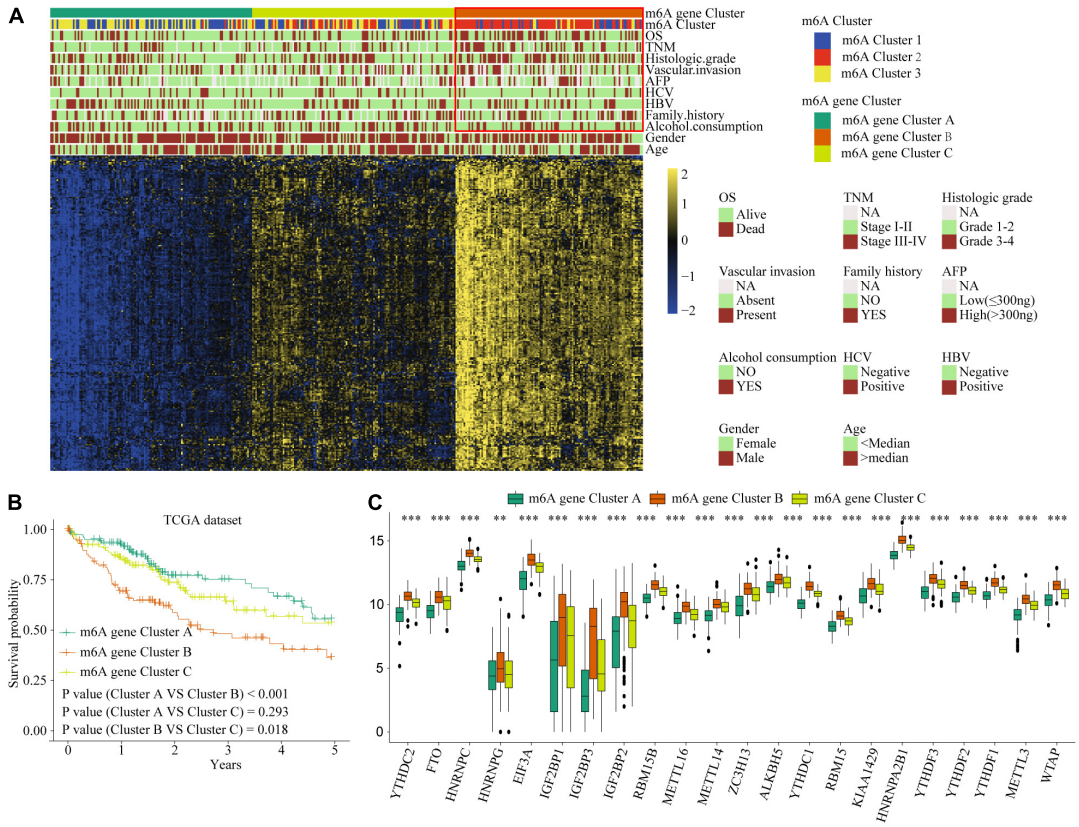

FIGURE 6 | The interrelation of the m6A scores with clinicopathological characteristics and prognostic. **(A)** Unsupervised clustering of 236 m6A related genes in TCGA cohort to classify patients into three m6A gene clusters. **(B)** Survival analysis for the HCC patients of three m6A gene clusters in the TCGA dataset. **(C)** The expression of 22 m6A regulators in three m6A gene clusters. Red box indicates the genes expression and clinical features of clusters. $^{**}P \leq 0.01$; $^{***}P \leq 0.001$.

higher TIDE score indicated worse immunotherapy response. Correlation analysis showed a significantly positive correlation between the m6Ascore and the TIDE score (**Figures 8E,G**). Meanwhile, we were very delighted to see that patients with low m6Ascores had more promising to response to immunotherapy (**Figures 8F,H**). Overall, our study indicates that the m6Ascore might be a potential biomarker for evaluating the immunotherapy effect and prognosis in HCC.

DISCUSSION

Hepatocellular carcinoma is one of the most frequently diagnosed malignancies worldwide, with poor prognosis (Dominissini et al., 2012; Meyer et al., 2012). Hence, there is an urgent need to identify powerful diagnostic and novel therapeutic strategies to improve HCC diagnosis and treatment. Numerous studies have demonstrated that harnessing the immune system against cancer has become an effective therapy option (Makarova-Rusher et al., 2015; Topalian et al., 2020). Recent clinical studies have verified that the PD-1 inhibitor nivolumab has raised hope for the successful treatment of advanced HCC (Yau et al., 2020; Kim et al., 2021). However, a small proportion of patients with HCC can benefit from immune checkpoint inhibitor therapy. Therefore, identifying novel biomarkers would allow better patient selection for individual immune and targeted therapy.

Previously studies have demonstrated that m6A modification plays a critical role in HCC progression and the shaping of TME, e.g., YTHDF1 promotes tumor progression and was closely associated with poor prognosis (Wang T. et al., 2020). Meanwhile, the study of Han et al. (2019) revealed that inhibition of YTHDF1 strengthened the ability of tumor APAP in DCs, which in turn enhanced tumor infiltrating CD8 + T cell antitumor response. YTHDF2 regulates mRNA degradation by recognizing mRNA m6A sites, and facilitates the proliferation of HCC cells (Yang et al., 2017; Zhang C. et al., 2020). In parallel, it was found that YTHDF2 suppress inflammation and angiogenesis in the tumor cell hypoxia environment (Hou et al., 2019). METTL3 enhances HCC cell growth ability (Liu et al., 2020; Yang et al., 2021). METTL14 suppresses the metastatic potential of HCC by modulating m6A-dependent tumor-suppressor primary miRNA processing (Ma et al., 2017; Shi et al., 2020). Wang et al. (2019) reported that upregulated METTL3 promoted DC activation and maturation. METTL3 downregulation inhibited T cell activation and aggregation though downregulation of co-stimulatory molecules CD80 and CD40 (Liu Y. et al., 2019). However, the specific depletion of METTL3 or METTL14 improved the therapeutic efficacy of

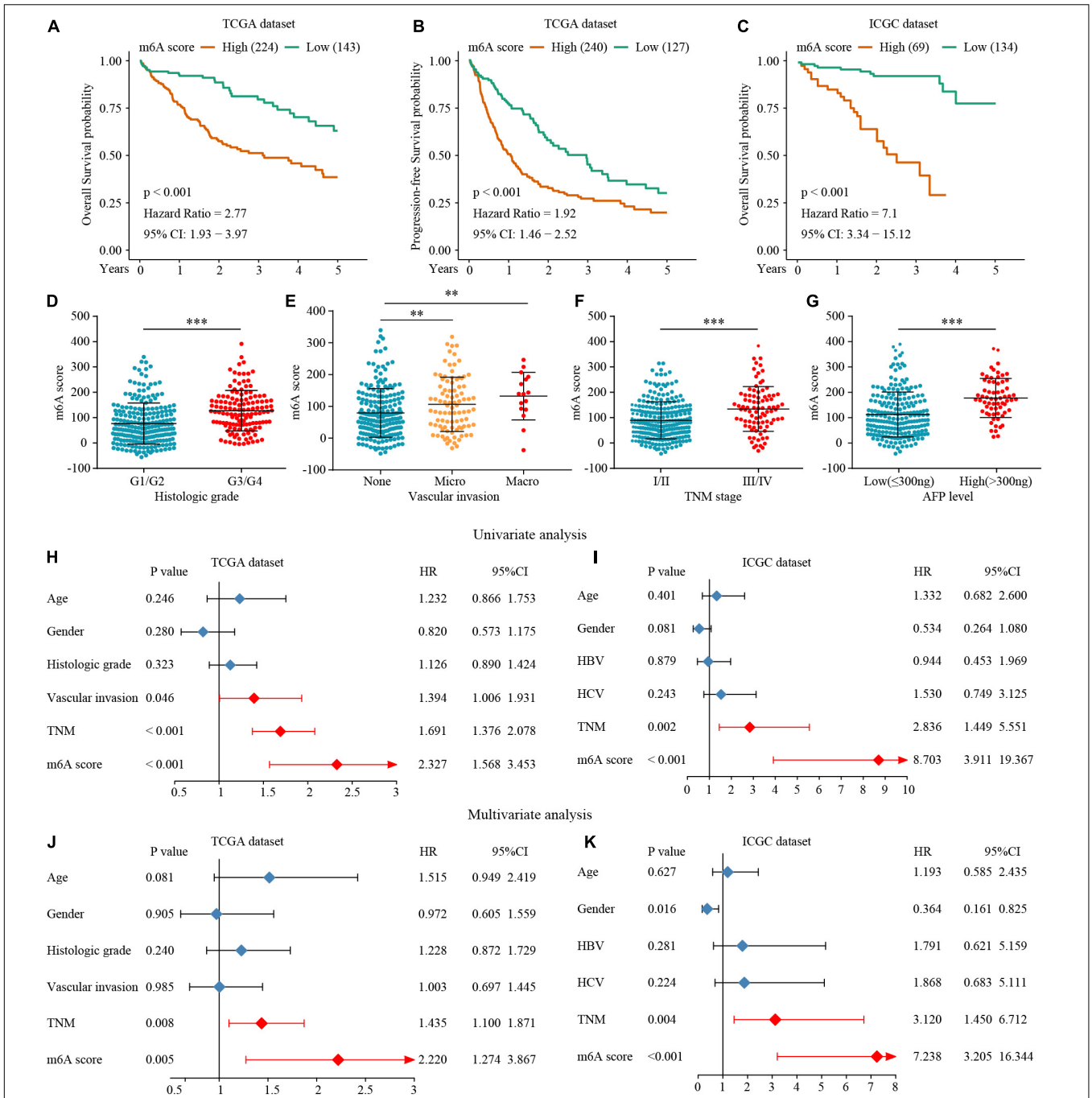

FIGURE 7 | The interrelation of the m6A scores with clinicopathological characteristics and prognosis. **(A–C)** Survival analysis for the HCC patients of m6A scores in the TCGA and ICGC dataset. **(D–G)** The relationship between the m6A scores and clinical characters. **(H–K)** The Univariate and multivariate Cox regression analyses of m6A scores in TCGA and ICGC datasets. $^{**}P \leq 0.01$; $^{***}P \leq 0.001$.

anti-PDL1 blockade (Wang L. et al., 2020). As most studies focused on single m6A regulators or analyzed public datasets only, a comprehensive and systematic study of the biological function of m6A regulator-associated modification patterns in HCC is necessary.

In the present study, we explored the m6A regulators of mRNA and protein levels based on TCGA and TMA cohorts. The survival analysis clarified the m6A-related regulator effects on the prognoses of the patients with HCC. Furthermore, three distinct m6A clusters were identified based on 22 m6A regulators. The three clusters had significantly distinct prognosis value, clinical features, immune cell infiltration, and pathway signatures. m6Acluster 1 was characterized by the significant enrichment of adaptive immunity pathways,

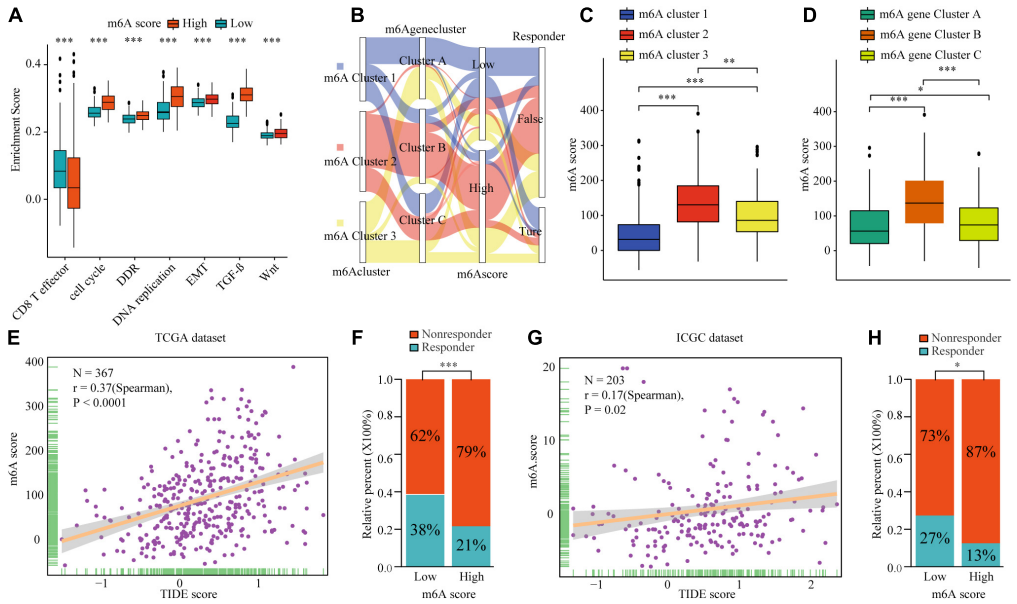

FIGURE 8 | The biological mechanism and immunotherapy value of m6Ascore. **(A)** Difference of biological functions between m6A score high and low. **(B)** Alluvial diagram showing the changes of m6A clusters, m6A gene clusters, m6A scores, and respond to immunotherapy. **(C)** Differences in m6Ascore among three m6A clusters in TCGA cohort. **(D)** Differences in m6Ascore among three m6A gene clusters in TCGA cohort. **(E–H)** Correlation analysis of m6A scores and TIDE scores and the proportion of patients with response to immunotherapy in low or high m6Ascore groups in TCGA dataset **(E,F)** and ICGC dataset **(G,H)**. $^{*}P \leq 0.05$; $^{**}P \leq 0.01$; $^{***}P \leq 0.001$.

corresponding to the immune-inflamed phenotype, m6Acluster 2 was characterized by the suppression of immunity and WNT pathway activation, corresponding to the immune-desert phenotype, and m6Acluster 3 was classified as the immune-excluded phenotype, characterized by innate immune cell infiltration and TGF-β significant enrichment. The immune-excluded and immune-desert phenotypes could be considered cold tumors. It has been indicated that the activation of WNT–β-catenin signaling mediates T cell exclusion in HCC. Further, the TGF-β pathway suppresses the effect of $CD8^+$ T cells by regulating regulatory T cells (Tregs). Mechanistically, previous study showed that m6A modification directly or indirectly involved in the regulation of cancer-related pathways such as proliferation, apoptosis, invasion and metastasis, and metabolic reprogramming (Li et al., 2021). Some investigators have found that YTHDF1 regulated the translation of FZD7 which is a key Wnt receptor by an m6A-dependent manner (Pi et al., 2021). The m6A modification of CTNNB1 promotes the expression of β-catenin and activates the Wnt pathway (Liu L. et al., 2019). Additionally, the upregulated of TCF1 regulated by IGF2BP2-mediated m6A modification activates the Wnt pathway and the expression of the downstream effector molecules (Wang K. et al., 2020). The m6A modification of the 5′-UTR and coding sequence (CDS) regions of TGF-β promotes the degradation of mRNA encoding TGF-β and thereby inhibits the TGF-β signaling pathway (Li et al., 2020a). METTL3 contributes to TGF-β induced epithelial-mesenchymal transition through the regulation of JUNB in lung cancer (Wanna-Udom et al., 2020). The immune-inflamed phenotype, known as hot tumor, demonstrates a large amount of immune cell infiltration in the TME. Consistent results were confirmed in both TCGA and ICGC datasets. The consistency of immune cell infiltration characteristics and pathway signatures confirmed the reliability of our immunophenotype classification for the different m6A clusters.

Next, we identified 236 differential genes in three distinct m6A clusters. These differential genes were considered m6A cluster-related genes. Similar to the m6A clusters, three m6A modification genomic phenotypes were identified based on the m6A cluster-related genes. Clinical features and prognosis analyses indicated that the m6A methylation pattern is tightly associated with HCC development and progression. Considering the high degree of m6A modification heterogeneity, 182 differential genes with prognostic utility were selected to construct the m6Ascores of individual patients. Patients with high m6Ascores demonstrated worse prognosis and clinical features. Meanwhile, high m6Ascores indicated significant enrichment of the cell proliferation, WNT, and TGF-β pathways, and the inhibition of $CD8^+$ T effector cells. The m6A subtype characterized by the immune-excluded phenotype exhibited a higher m6Ascore, while the pattern characterized by the immune-inflamed phenotype showed a lower m6Ascore. Additionally, TIDE analysis showed that the m6Ascore had a predictive advantage in immunotherapy for HCC. Generally, the m6A scores were closely associated with immune cell infiltration and could be used as prognostic markers for HCC. To date, there are some studies have analyzed the relationship among m6A modification patterns, m6A scores, tumor progression, and immune cell infiltration in many solid

malignancies. Consistently, Zhang B. et al. (2020) and Chong et al. (2021) identified three different m6A subtypes according to the expression of m6A regulators in colon and gastric cancer. After comprehensively evaluated the association among immune cell infiltration, prognosis, and pathway scores, three m6A patterns to different immune phenotypes (immune-inflamed, immune-excluded, and immune-desert) were constructed. Then m6A score calculated based on the m6A modification, were closely associated with tumor progression, prognosis, immune infiltration subtypes and immunotherapy response in colon cancer and gastric cancer.

Our data also reveal that YTHDF1 plays an important role in the development and immune response of HCC. We found significantly negative correlations between the level of immune cell infiltration such as that by B cells, T cells, and CD cells with the expression of most of the m6A regulators. Subsequently, we focused on YTHDF1. Han et al. (2019) demonstrated that *Ythdf1*-deficient mice exhibit an elevated antigen-specific $CD8^+$ T cell anti-tumor response because suppressing YTHDF1 in the DCs enhanced the cross-presentation of tumor antigen and the cross-priming of $CD8^+$ T cells *in vivo*. However, the immunomodulatory function of YTHDF1 dysregulation in HCC cells is unclear. In the present study, IHC and immunofluorescence demonstrated that YTHDF1 overexpression significantly decreased $CD3^+$ and $CD8^+$ T cell infiltration in HCC. Meanwhile, patients with high YTHDF1 expression exhibited obvious TGF-β and WNT pathway enhancement. These results indicate that YTHDF1 might induce immunosuppression by activating the TGF-β and WNT pathways. Our findings provide novel ideas for promoting personalized cancer immunotherapy and potential therapeutic targets for HCC.

CONCLUSION

We show that m6A modification patterns play a crucial role in the tumor immune microenvironment and prognosis of HCC. Upregulated YTHDF1 mediates m6A modification, playing a critical role in suppressing anti-tumor immune responses.

DATA AVAILABILITY STATEMENT

The datasets presented in this study can be found in online repositories. The names of the repository/repositories and accession number(s) can be found in the article/**Supplementary Material**.

ETHICS STATEMENT

This study was approved by the Institutional Review Board of the First Affiliated Hospital of Zhengzhou University. Written informed consent for participation was not required for this study in accordance with the national legislation and the institutional requirements.

AUTHOR CONTRIBUTIONS

JL, YZ, and WW performed all the experimental work. LL, XL, MH, and GZ completed the data collection. GC, KG, and XC participated in data analysis. RS and LL conceived and participated in the design of the study. JL and RS wrote the manuscript. All authors read and approved the final manuscript.

ACKNOWLEDGMENTS

We thank the many clinical doctors from the Pathology Department and Precision Medicine Center, First Affiliated Hospital of Zhengzhou University, who were involved in this study.

SUPPLEMENTARY MATERIAL

The Supplementary Material for this article can be found online at: https://www.frontiersin.org/articles/10.3389/fcell.2021.687756/full#supplementary-material

REFERENCES

Chaisaingmongkol, J., Budhu, A., Dang, H., Rabibhadana, S., Pupacdi, B., Kwon, S. M., et al. (2017). Common molecular subtypes among Asian Hepatocellular carcinoma and Cholangiocarcinoma. *Cancer Cell* 32, 57–70.e53. doi: 10.1016/j.ccell.2017.05.009

Chen, X. Y., Zhang, J., and Zhu, J. S. (2019). The role of m(6)A RNA methylation in human cancer. *Mol. Cancer* 18:103. doi: 10.1186/s12943-019-1033-z

Cho, Y. A., Choi, S., Park, S., Park, C. K., and Ha, S. Y. (2020). Expression of pregnancy up-regulated non-ubiquitous Calmodulin Kinase (PNCK) in Hepatocellular Carcinoma. *Cancer Genom. Proteom.* 17, 747–755. doi: 10.21873/cgp.20229

Chong, W., Shang, L., Liu, J., Fang, Z., Du, F., Wu, H., et al. (2021). m(6)A regulator-based methylation modification patterns characterized by distinct tumor microenvironment immune profiles in colon cancer. *Theranostics* 11, 2201–2217. doi: 10.7150/thno.52717

Dominissini, D., Moshitch-Moshkovitz, S., Schwartz, S., Salmon-Divon, M., Ungar, L., Osenberg, S., et al. (2012). Topology of the human and mouse m6A RNA methylomes revealed by m6A-seq. *Nature* 485, 201–206. doi: 10.1038/nature11112

Dutta, R., and Mahato, R. I. (2017). Recent advances in hepatocellular carcinoma therapy. *Pharmacol. Ther.* 173, 106–117. doi: 10.1016/j.pharmthera.2017.02.010

Forner, A., Reig, M., and Bruix, J. (2018). Hepatocellular carcinoma. *Lancet* 391, 1301–1314. doi: 10.1016/s0140-6736(18)30010-2

Gilbert, W. V., Bell, T. A., and Schaening, C. (2016). Messenger RNA modifications: form, distribution, and function. *Science* 352, 1408–1412. doi: 10.1126/science.aad8711

Han, D., Liu, J., Chen, C., Dong, L., Liu, Y., Chang, R., et al. (2019). Anti-tumour immunity controlled through mRNA m(6)A methylation and YTHDF1 in dendritic cells. *Nature* 566, 270–274. doi: 10.1038/s41586-019-0916-x

Hoshida, Y., Brunet, J. P., Tamayo, P., Golub, T. R., and Mesirov, J. P. (2007). Subclass mapping: identifying common subtypes in independent disease data sets. *PLoS One* 2:e1195. doi: 10.1371/journal.pone.0001195

Hou, J., Zhang, H., Liu, J., Zhao, Z., Wang, J., Lu, Z., et al. (2019). YTHDF2 reduction fuels inflammation and vascular abnormalization in

hepatocellular carcinoma. *Mol. Cancer* 18:163. doi: 10.1186/s12943-019-1082-3

Kim, C. G., Kim, C., Yoon, S. E., Kim, K. H., Choi, S. J., Kang, B., et al. (2021). Hyperprogressive disease during PD-1 blockade in patients with advanced hepatocellular carcinoma. *J. Hepatol.* 74, 350–359. doi: 10.1016/j.jhep.2020.08.010

Li, J., Chen, F., Peng, Y., Lv, Z., Lin, X., Chen, Z., et al. (2020a). N6-Methyladenosine regulates the expression and secretion of TGFβ1 to affect the epithelial-Mesenchymal transition of cancer cells. *Cells* 9:296. doi: 10.3390/cells9020296

Li, J., Rao, B., Yang, J., Liu, L., Huang, M., Liu, X., et al. (2020b). Dysregulated m6A-related regulators are associated with tumor metastasis and poor prognosis in Osteosarcoma. *Front. Oncol.* 10:769. doi: 10.3389/fonc.2020.00769

Li, J., Liu, L., Liu, X., Xu, P., Hu, Q., and Yu, Y. (2019). The role of upregulated DDX11 as a potential prognostic and diagnostic biomarker in Lung Adenocarcinoma. *J. Cancer* 10, 4208–4216. doi: 10.7150/jca.33457

Li, M., Zha, X., and Wang, S. (2021). The role of N6-methyladenosine mRNA in the tumor microenvironment. *Biochim. Biophys. Acta Rev. Cancer* 1875:188522. doi: 10.1016/j.bbcan.2021.188522

Lin, Y., Totsuka, Y., He, Y., Kikuchi, S., Qiao, Y., Ueda, J., et al. (2013). Epidemiology of esophageal cancer in Japan and China. *J. Epidemiol.* 23, 233–242. doi: 10.2188/jea.je20120162

Liu, L., Wang, J., Sun, G., Wu, Q., Ma, J., Zhang, X., et al. (2019). m(6)A mRNA methylation regulates CTNNB1 to promote the proliferation of Hepatoblastoma. *Mol. Cancer* 18:188. doi: 10.1186/s12943-019-1119-7

Liu, Y., Liu, Z., Tang, H., Shen, Y., Gong, Z., Xie, N., et al. (2019). The N(6)-methyladenosine (m(6)A)-forming enzyme METTL3 facilitates M1 macrophage polarization through the methylation of STAT1 mRNA. *Am. J. Physiol. Cell Physiol.* 317, C762–C775. doi: 10.1152/ajpcell.00212.2019

Liu, X., Qin, J., Gao, T., Li, C., Chen, X., Zeng, K., et al. (2020). Analysis of METTL3 and METTL14 in hepatocellular carcinoma. *Aging* 12, 21638–21659. doi: 10.18632/aging.103959

Ma, J. Z., Yang, F., Zhou, C. C., Liu, F., Yuan, J. H., Wang, F., et al. (2017). METTL14 suppresses the metastatic potential of hepatocellular carcinoma by modulating N(6) -methyladenosine-dependent primary MicroRNA processing. *Hepatology* 65, 529–543. doi: 10.1002/hep.28885

Makarova-Rusher, O. V., Medina-Echeverz, J., Duffy, A. G., and Greten, T. F. (2015). The yin and yang of evasion and immune activation in HCC. *J. Hepatol.* 62, 1420–1429. doi: 10.1016/j.jhep.2015.02.038

Mariathasan, S., Turley, S. J., Nickles, D., Castiglioni, A., Yuen, K., Wang, Y., et al. (2018). TGFβ attenuates tumour response to PD-L1 blockade by contributing to exclusion of T cells. *Nature* 554, 544–548. doi: 10.1038/nature25501

Meyer, K. D., Saletore, Y., Zumbo, P., Elemento, O., Mason, C. E., and Jaffrey, S. R. (2012). Comprehensive analysis of mRNA methylation reveals enrichment in 3′ UTRs and near stop codons. *Cell* 149, 1635–1646. doi: 10.1016/j.cell.2012.05.003

Pi, J., Wang, W., Ji, M., Wang, X., Wei, X., Jin, J., et al. (2021). YTHDF1 promotes gastric carcinogenesis by controlling translation of FZD7. *Cancer Res.* 81, 2651–2665. doi: 10.1158/0008-5472.can-20-0066

Rosenberg, J. E., Hoffman-Censits, J., Powles, T., van der Heijden, M. S., Balar, A. V., Necchi, A., et al. (2016). Atezolizumab in patients with locally advanced and metastatic urothelial carcinoma who have progressed following treatment with platinum-based chemotherapy: a single-arm, multicentre, phase 2 trial. *Lancet* 387, 1909–1920. doi: 10.1016/s0140-6736(16)00561-4

Şenbabaoğlu, Y., Gejman, R. S., Winer, A. G., Liu, M., Van Allen, E. M., de Velasco, G., et al. (2016). Tumor immune microenvironment characterization in clear cell renal cell carcinoma identifies prognostic and immunotherapeutically relevant messenger RNA signatures. *Genome Biol.* 17:231. doi: 10.1186/s13059-016-1092-z

Shi, Y., Zhuang, Y., Zhang, J., Chen, M., and Wu, S. (2020). METTL14 inhibits Hepatocellular carcinoma metastasis through regulating EGFR/PI3K/AKT signaling Pathway in an m6A-dependent manner. *Cancer Manag. Res.* 12, 13173–13184. doi: 10.2147/cmar.s286275

Shulman, Z., and Stern-Ginossar, N. (2020). The RNA modification N(6)-methyladenosine as a novel regulator of the immune system. *Nat. Immunol.* 21, 501–512. doi: 10.1038/s41590-020-0650-4

Siegel, R. L., Miller, K. D., and Jemal, A. (2018). Cancer statistics, 2018. *CA Cancer J. Clin.* 68, 7–30. doi: 10.3322/caac.21442

Topalian, S. L., Taube, J. M., and Pardoll, D. M. (2020). Neoadjuvant checkpoint blockade for cancer immunotherapy. *Science* 367:eaax0182. doi: 10.1126/science.aax0182

Wang, H., Hu, X., and Huang, M. (2019). Mettl3-mediated mRNA m(6)A methylation promotes dendritic cell activation. *Nat. Commun.* 10:1898. doi: 10.1038/s41467-019-09903-6

Wang, K., Jiang, L., Zhang, Y., and Chen, C. (2020). Progression of thyroid carcinoma is promoted by the m6A Methyltransferase METTL3 through regulating m(6)A Methylation on TCF1. *Oncol. Targets Ther.* 13, 1605–1612. doi: 10.2147/ott.s234751

Wang, L., Hui, H., Agrawal, K., Kang, Y., Li, N., and Tang, R. (2020). m(6) A RNA methyltransferases METTL3/14 regulate immune responses to anti-PD-1 therapy. *EMBO J.* 39:e104514. doi: 10.15252/embj.2020104514

Wang, T., Kong, S., Tao, M., and Ju, S. (2020). The potential role of RNA N6-methyladenosine in Cancer progression. *Mol. Cancer* 19:88. doi: 10.1186/s12943-020-01204-7

Wanna-Udom, S., Terashima, M., Lyu, H., Ishimura, A., Takino, T., Sakari, M., et al. (2020). The m6A methyltransferase METTL3 contributes to transforming growth factor-beta-induced epithelial-mesenchymal transition of lung cancer cells through the regulation of JUNB. *Biochem. Biophys. Res. Commun.* 524, 150–155. doi: 10.1016/j.bbrc.2020.01.042

Yang, J. D., and Heimbach, J. K. (2020). New advances in the diagnosis and management of hepatocellular carcinoma. *BMJ* 371:m3544. doi: 10.1136/bmj.m3544

Yang, N., Wang, T., Li, Q., Han, F., Wang, Z., Zhu, R., et al. (2021). HBXIP drives metabolic reprogramming in Hepatocellular carcinoma cells via METTL3-mediated m6A modification of HIF-1α. *J. Cell. Physiol.* 236, 3863–3880. doi: 10.1002/jcp.30128

Yang, Z., Li, J., Feng, G., Gao, S., Wang, Y., Zhang, S., et al. (2017). MicroRNA-145 modulates N(6)-Methyladenosine levels by targeting the 3′-Untranslated mRNA Region of the N(6)-Methyladenosine Binding YTH domain family 2 protein. *J. Biol. Chem.* 292, 3614–3623. doi: 10.1074/jbc.M116.749689

Yau, T., Kang, Y. K., Kim, T. Y., El-Khoueiry, A. B., Santoro, A., Sangro, B., et al. (2020). Efficacy and Safety of nivolumab plus ipilimumab in patients with advanced Hepatocellular carcinoma previously treated with sorafenib: the CheckMate 040 randomized clinical trial. *JAMA Oncol.* 6:e204564. doi: 10.1001/jamaoncol.2020.4564

Zaccara, S., Ries, R. J., and Jaffrey, S. R. (2019). Reading, writing and erasing mRNA methylation. *Nat. Rev. Mol. Cell Biol.* 20, 608–624. doi: 10.1038/s41580-019-0168-5

Zhang, B., Wu, Q., Li, B., Wang, D., Wang, L., and Zhou, Y. L. (2020). m(6)A regulator-mediated methylation modification patterns and tumor microenvironment infiltration characterization in gastric cancer. *Mol. Cancer* 19:53. doi: 10.1186/s12943-020-01170-0

Zhang, C., Huang, S., Zhuang, H., Ruan, S., Zhou, Z., Huang, K., et al. (2020). YTHDF2 promotes the liver cancer stem cell phenotype and cancer metastasis by regulating OCT4 expression via m6A RNA methylation. *Oncogene* 39, 4507–4518. doi: 10.1038/s41388-020-1303-7

Zhao, B. S., Roundtree, I. A., and He, C. (2017). Post-transcriptional gene regulation by mRNA modifications. *Nat. Rev. Mol. Cell Biol.* 18, 31–42. doi: 10.1038/nrm.2016.132

Zhen, D., Wu, Y., Zhang, Y., Chen, K., Song, B., Xu, H., et al. (2020). m(6)A reader: epitranscriptome target prediction and functional characterization of N (6)-Methyladenosine (m(6)A) readers. *Front. Cell Dev. Biol.* 8:741. doi: 10.3389/fcell.2020.00741

Conflict of Interest: The authors declare that the research was conducted in the absence of any commercial or financial relationships that could be construed as a potential conflict of interest.

frontiers in Cell and Developmental Biology

ORIGINAL RESEARCH
published: 19 July 2021
doi: 10.3389/fcell.2021.686547

RPL19 Is a Prognostic Biomarker and Promotes Tumor Progression in Hepatocellular Carcinoma

Benchen Rao[1,2†], Jianhao Li[1,2†], Tong Ren[3†], Jing Yang[4], Guizhen Zhang[1,2], Liwen Liu[1,2], Haiyu Wang[1,2], Maoxin Huang[5], Zhigang Ren[1,2] and Zujiang Yu[1,2*]*

[1] Department of Infectious Diseases, The First Affiliated Hospital of Zhengzhou University, Zhengzhou, China, [2] Precision Medicine Center, Gene Hospital of Henan Province, The First Affiliated Hospital of Zhengzhou University, Zhengzhou, China, [3] Department of Breast Surgery, The Affiliated Cancer Hospital of Zhengzhou University, Zhengzhou, China, [4] Department of Pharmacy, The First Affiliated Hospital of Zhengzhou University, Zhengzhou, China, [5] Department of Dermatology, The First Affiliated Hospital of Zhengzhou University, Zhengzhou, China

OPEN ACCESS

Edited by:
Giampaolo Morciano,
University of Ferrara, Italy

Reviewed by:
Danillo G. Augusto,
University of California,
San Francisco, United States
Manikandan Mayakannan,
Case Western Reserve University,
United States

***Correspondence:**
Zhigang Ren
fccrenzg@zzu.edu.cn
Zujiang Yu
johnyuem@zzu.edu.cn

[†] These authors have contributed equally to this work

Specialty section:
This article was submitted to Molecular and Cellular Oncology, a section of the journal Frontiers in Cell and Developmental Biology

Received: 27 March 2021
Accepted: 30 June 2021
Published: 19 July 2021

Citation:
Rao B, Li J, Ren T, Yang J, Zhang G, Liu L, Wang H, Huang M, Ren Z and Yu Z (2021) RPL19 Is a Prognostic Biomarker and Promotes Tumor Progression in Hepatocellular Carcinoma. Front. Cell Dev. Biol. 9:686547. doi: 10.3389/fcell.2021.686547

Background: Hepatocellular carcinoma (HCC) is one of the most common malignancies, and the therapeutic outcome remains undesirable due to its recurrence and metastasis. Gene dysregulation plays a pivotal role in the occurrence and progression of cancer, and the molecular mechanisms are largely unknown.

Methods: The differentially expressed genes of HCC screened from the GSE39791 dataset were used to conduct weighted gene co-expression network analysis. The selected hub genes were validated in The Cancer Genome Atlas (TCGA) database and 11 HCC datasets from the Gene Expression Omnibus (GEO) database. Then, a tissue microarray comprising 90 HCC specimens and 90 adjacent normal specimens was used to validate the hub genes. Moreover, the Hallmark, Gene Ontology (GO) and Kyoto Encyclopedia of Genes and Genomes (KEGG) databases were used to identify enriched pathways. Then, we conducted the immune infiltration analysis.

Results: A total of 17 co-expression modules were obtained by weighted gene co-expression network analysis. The green, blue, and purple modules were the most relevant to HCC samples. Four hub genes, RPL19, RPL35A, RPL27A, and RPS12, were identified. Interestingly, we found that all four genes were highly expressed in HCC and that their high expression was related to a poor prognosis by analyzing the TCGA and GEO databases. Furthermore, we investigated RPL19 in HCC tissue microarrays and demonstrated that RPL19 was overexpressed in tumor tissues compared with non-tumor tissues ($p = 0.016$). Moreover, overexpression of RPL19 predicted a poor prognosis in hepatocellular carcinoma ($p < 0.0007$). Then, enrichment analysis revealed that cell cycle pathways were significantly enriched, and bile acid metabolism-related pathways were significantly down-regulated when RPL19 was highly expressed. Furthermore, immune infiltration analysis showed that immune response was suppressed.

Conclusion: Our study demonstrates that RPL19 may play an important role in promoting tumor progression and is correlated with a poor prognosis in HCC. RPL19 may serve as a promising biomarker and therapeutic target for the precise diagnosis and treatment of HCC in the future.

Keywords: hepatocellular carcinoma, ribosomal protein L19, weighted gene co-expression network analysis, prognostic biomarker, immune infiltration

INTRODUCTION

Liver cancer is one of the leading causes of global disease burden worldwide, with 42,810 new cases and 30,160 deaths in 2020 (Yu and Schwabe, 2017; Siegel et al., 2020). Hepatocellular carcinoma (HCC) is the most frequent and common type of primary liver cancer and is attributed mainly to the progression of chronic liver disease. Most HCC patients are diagnosed in the advanced stage, and it has been reported that the 5-year recurrence rate is more than 70% (Rahbari et al., 2011). In view of the high incidence and mortality of HCC, it is imperative to find a novel biomarker for diagnosis, prognosis and treatment to improve the patient survival rate.

With the development of high-throughput research methods, precious resources for the analysis of whole-genome co-expression networks and screening of tumor biomarkers associated with prognosis and phenotypes have been provided by a large public transcriptome database. Weighted gene co-expression network analysis (WGCNA) is suitable for multisample complex data analysis and can be used to analyze the relationship between gene clusters and sample phenotypes and the networks between genes in gene sets to identify key transition genes (Panwar et al., 2021). Currently, systematic biological analysis has been widely used to identify diagnostic and prognostic markers and therapeutic targets. For instance, two modules and 10 hub genes identified by Zhang et al. (2018) were related to the tumorigenesis of oral squamous cell carcinoma. Two cervical squamous cell carcinoma-related hub modules and 116 hub genes were identified by the WGCNA method (Liu et al., 2019). Ribosomal protein L19 (RPL19) as a hub gene was identified in HCC by WGCNA in this study. RPL19 is a member of the ribosomal protein family that assembles to form small and large ribosomal subunits. RPL19 has been reported as a biomarker for many cancers (Dressman et al., 2003; Bee et al., 2006; Huang et al., 2008). However, the diagnostic, prognostic and therapeutic value of RPL19 in HCC has not been investigated.

In this study, WGCNA was conducted based on the GSE39791 dataset, which included 144 HCC and paracancerous tissues. After screening, 54 pairs of HCC and paracancerous tissues were selected to identify 17 co-expression modules and four hub genes (RPS12, RPL19, RPL35A, and RPL27A). Then, we screened the above four genes again in The Cancer Genome Atlas (TCGA) and Gene Expression Omnibus (GEO) databases. Subsequently, we validated RPL19 in an HCC tissue microarray. RPL19 was speculated to be a prognostic biomarker and promote tumor progression in HCC.

MATERIALS AND METHODS

Datasets

The study design is shown in a flow diagram (**Figure 1**). GSE39791 tissue chip data for 144 cancer samples (72 pairs of HCC and paracancerous samples paired one by one) were downloaded from the GEO database[1], and corresponding sample information was used to conduct WGCNA (Kim et al., 2014). Then, to verify the results of the above analysis, we searched the GEO and TCGA database again. A total of 369 liver cancer data and 50 non-tumor data points were obtained from the TCGA database[2]. We used the GEO to gather and analyze 11 liver cancer mRNA microarray datasets. BRB-array tools were used to determine the differentially expressed genes between HCC tissues and normal liver tissues in each dataset. Detailed information is shown in **Table 1**. The human protein–protein interactions (PPI) were compiled from the Human Integrated Protein–Protein Interaction rEference (HIPPIE) database[3] (Misselbeck et al., 2019).

Construction of the Co-expression Network

Weighted gene co-expression network analysis is a systematic biology method that uses gene expression data to construct a scale-free network. WGCNA analyzes thousands of genes with the greatest changes instead of genes that are differentially expressed, and at the same time it converts the associations between thousands of genes and phenotypes into associations between several gene sets and phenotypes, eliminating the problem of multiple hypothesis testing and correction. First, we selected the expression data of genes that changed in each sample (seed genes) and used the R software package WGCNA to construct a weighted gene co-expression network. We calculated the coefficient of variation (CV) for each gene and chose 3.6 as the cut-off value to identify the differentially expressed genes (DEGs). Then, a soft threshold of $\beta = 6$ was chosen to ensure that the co-expression network was a scale-free distribution. And we screened the co-expression module. Next, the expression matrix was converted to an adjacency matrix and then to a topological matrix. Based on TOM, clustering was accomplished by using the average linkage algorithm. In accordance with the dynamic hybrid tree cutting algorithm, the minimum number of genes

[1]http://www.ncbi.nlm.nih.gov/geo/

[2]https://tcga-data.nci.nih.gov/tcga/

[3]http://cbdm.mdc-berlin.de/tools/hippie/hippie_current.txt

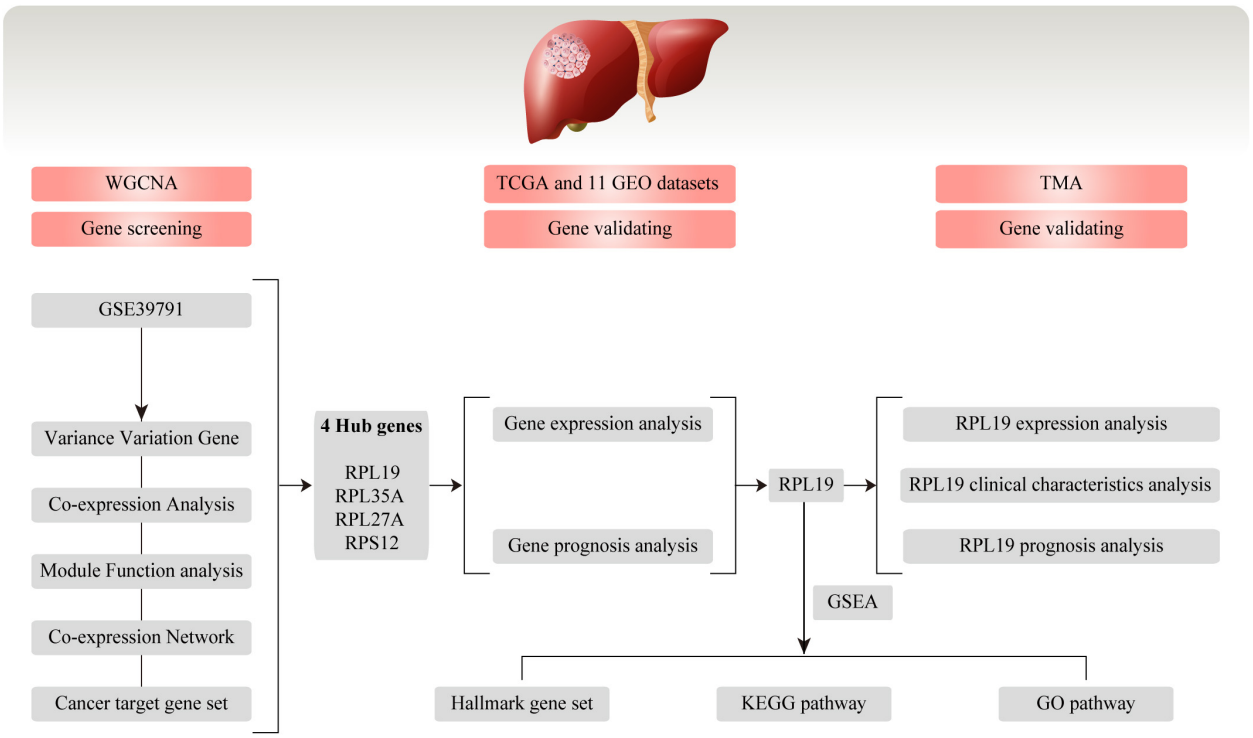

FIGURE 1 | Flow chart for this study. In this study, we conducted WGCNA and screened four hub genes (RPL19, RPL35A, RPL27A, and RPS12) based on the GEO database GSE39791. Then, the four hub genes were validated in TCGA database and 11 GEO datasets. Moreover, we chose RPL19 as a key gene and validated it in the TMA. WGCNA, weighted gene co-expression network analysis; GEO, Gene Expression Omnibus; TCGA, The Cancer Genome Atlas; TMA, tissue microarray; HCC, hepatocellular carcinoma; GSEA, gene set enrichment analysis; KEGG, Kyoto Encyclopedia of Genes and Genomes; GO, Gene Ontology.

(lncRNAs) in the network module was set to 30. We calculated the eigengenes of each module, conducted cluster analysis on the modules, merged the close modules into new modules and set the height = 0.25. The higher the correlation coefficient is, the more important the module. According to the expression relationship of the genes in each co-expression module, we chose the co-expression pairs whose co-expression weights were larger than 0.1 as the edges of the final co-expression network.

Tissue Samples

The tissue microarray (TMA) from Asians containing 90 normal liver specimens and 90 HCC specimens (HLiv-HCC180Sur-15) from cancer-adjacent tissues was purchased from Shanghai Outdo Biotech Co., Ltd. We further validated RPL19 expression and its prognostic value in HCC by TMA. None prior radiotherapy, immunotherapy or chemotherapy were conducted on the patients whose samples were included in the TMA before surgery. This study was approved by the Ethics Committee of The First Affiliated Hospital of Zhengzhou University, Zhengzhou, China.

Immunohistochemistry (IHC) Staining

Immunohistochemistry staining was carried out as described previously (Cui et al., 2019). According to the Remmele scoring system (Remmele et al., 1986), four fields of view were randomly selected under low and high power, 100 cells were counted in each field, and the percentage of RPL19 cytoplasmic staining in each field of power was calculated as a percentage of positive cells. Two experienced pathologists separately evaluated the immunostained samples. The results were divided into four groups: score 1, <25%; score 2, 25%∼50%; score 3, 50%∼75%;

TABLE 1 | HCC expression profile cohorts used in this study.

Cohort ID	Platforms	HCC tissue	Paracancerous tissue	Year	Country
TCGA	Illumina	369	50	2009	United States
GSE14520	Affymetrix	225	220	2010	United States
GSE39791	Illumina	72	72	2014	United States
GSE76297	Affymetrix	153	151	2017	United States
GSE54236	Agilent	81	80	2014	Italy
GSE62232	Affymetrix	81	10	2014	France
E	Affymetrix	95	39	2014	Taiwan
GSE60502	Affymetrix	18	18	2015	Taiwan
GSE57957	Illumina	39	39	2014	Singapore
GSE76427	Illumina	115	52	2017	Singapore
e	Affymetrix	60	65	2016	Switzerland
GSE102083	Affymetrix	156	105	2018	Japan
Total		1464	901		

HCC, hepatocellular carcinoma; TCGA, The Cancer Genome Atlas.

and score 4, >75%. Scores of 1 and 2 were defined as low expression, and scores of 3 and 4 were defined as high expression.

Biological Functional Analysis

The Metascape software[4] was used to analyze the functional gene clustering. The Kyoto Encyclopedia of Genes and Genomes (KEGG) database[5], Gene Ontology (GO) gene sets[6] and Hallmark gene sets[7] were used to conduct gene set enrichment analysis (GSEA).

Single-Sample Gene Set Enrichment Analysis (ssGSEA)

The ssGSEA in R package gsva was used to quantify the infiltration levels of the immune cell types. SsGSEA applies gene signatures expressed by immune cell populations to individual cancer samples. We used the deconvolution approach to analyze the immune cells involved innate immunity and adaptive immunity.

Statistical Analysis

All statistical tests and graphing were performed using R software (version 3.4.3)[8] and GraphPad Prism 7.0 (GraphPad Software, San Diego, United States). Differences between two groups were analyzed by Student's *t*-test. Clinicopathologic variables were analyzed by chi-square tests. The overall survival (OS), relapse-free survival (RFS), and progress-free survival (PFS) of HCC patients were calculated with Kaplan–Meier curves and log-rank tests. GSEA was used to determine which gene sets were associated with the expression of hub genes in datasets. $P < 0.05$ was considered to be statistically significant.

RESULTS

Construction of the Weighted Co-expression Network

We downloaded the raw data of GSE39791, which includes 144 HCC and paracancerous tissues, to construct the gene co-expression networks. Results of the cluster analysis of the correlation between samples are shown in **Figure 2**. However, it can be clearly seen that the correlations between HCC samples can be divided into two groups (**Figure 2A**), and the intragroup correlation was high, which showed that these samples had some heterogeneity. The paracancerous tissue samples could be divided into three groups because two samples had weak correlations (**Figure 2B**). We chose the group with the highest correlation as the datasets for this study. Given that the cancer and paracancerous samples were paired, we ultimately selected 54 pairs of samples. A total of 31,334 genes were obtained (**Supplementary Table 1**). Then, 7,814 DEGs were identified (**Supplementary Table 2**).

We chose $\beta = 6$ to ensure that the co-expression network was scale free (**Figures 2C,D**). Then, a total of 17 modules were obtained (**Figure 3A**). The gene statistics in each module are shown in **Supplementary Table 3**. Overall, 7814 genes were allocated into 17 modules (**Supplementary Table 4**), and the gray module included all the genes that could not be clustered. The Pearson correlation coefficients between each module eigengene (ME) and sample trait were calculated (**Figure 3B**). We can conclude that these three modules (green, blue and purple) are the most relevant to HCC samples. In addition, we used the R package clusterProfiler to conduct the KEGG enrichment analysis and GO enrichment analysis of 17 modules. The results showed that 11 modules were significantly enriched in 121 KEGG pathways (**Supplementary Table 5** and **Supplementary Figure 1**). The green module was enriched in 6 KEGG pathways, including 2 cancer-related pathways (DNA replication and the cell cycle). Additionally, the blue module was enriched in ribosomes, RNA transport and necroptosis, which are closely related to tumorigenesis and progression. These results imply that both the green and blue modules are closely related to tumorigenesis and progression. The co-expression network contained a total of three gene modules, and their distribution is shown in **Supplementary Figure 2** and **Supplementary Tables 6, 7**. As the gene node degree increased, the number of nodes decreased.

Identification of the Four Hub Genes by the Human Protein–Protein Interaction Network

The human PPI network contained 17,381 nodes with 19.6 neighboring nodes on average (**Supplementary Table 8**). Then, all the responsive genes were mapped to the human PPI network. In total, 1148 genes were covered in the PPI network. Among them, 265 interacted with and co-expressed 2.33 neighboring nodes on average (**Figure 3C** and **Supplementary Table 9**). Through topological property and biological enrichment analyses, it was finally determined that the screening threshold was at least 10% of co-expressed genes in the neighboring nodes, and genes whose FDR-corrected *p*-value was less than 0.05 were defined as significantly differentially expressed in the co-expression-interaction gene enrichment analysis. The results are shown in **Table 2**. As shown in the table, four genes, RPL19, RPS12, RPL27A, and RPL35A, were obtained. These four genes are related to ribosomes. According to the literature, RPS12 is a tumor marker for liver cancer (Wang et al., 2009).

Expression, Clinicopathological, and Prognostic Analyses of the Four Hub Genes in the GEO and TCGA Databases

Through the analysis and comparison of 11 HCC datasets in the GEO database, we found that the expression levels of RPL19 were significantly higher in HCC tissues than in paracancerous tissues in 10 datasets ($P < 0.05$). Moreover, RPL27A was markedly increased in eight datasets, and RPL35A and RPS12 were markedly increased in eight datasets (**Figures 4A–D**). In addition, we compared 369 liver cancer samples and 50 paracancerous

[4]http://metascape.org
[5]https://www.kegg.jp/
[6]http://geneontology.org/
[7]http://www.gsea-msigdb.org/gsea/msigdb/genesets.jsp?collection=H
[8]www.r-project.org

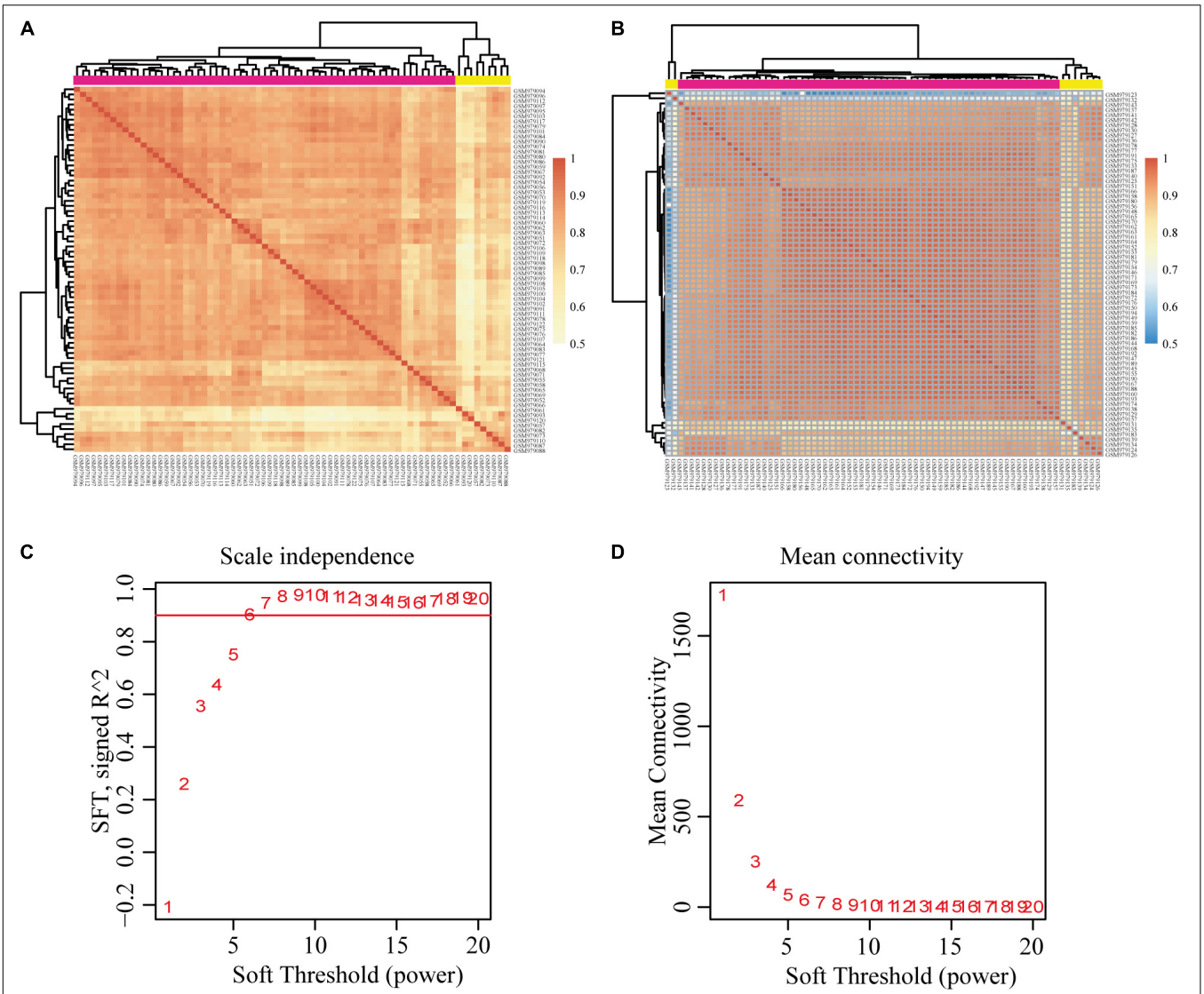

FIGURE 2 | Correlation analysis of each sample and construction of the weighted gene co-expression network based on GEO database GSE39791. **(A)** Correlation between HCC samples. **(B)** Correlation between paracancerous samples. **(C,D)** Analysis of network topology for various soft-thresholding powers. Pearson's correlation test was used to assess the correlation between samples. HCC, hepatocellular carcinoma; GEO, Gene Expression Omnibus.

samples in the TCGA database. The results showed that the expression levels of the four hub genes were significantly higher in HCC tissues than in paracancerous tissues ($P < 0.0001$). The expression levels of the four hub genes in different stages of liver disease are shown in **Supplementary Figure 3**. In addition, the relationship between different expression levels of RPL19, RPL27A, RPL35A, and RPS12 and the clinical prognosis of patients was compared through survival analysis. The OS and relapse-free survival (RFS) of HCC patients with high expression of the four hub genes were significantly shorter than those with low expression (**Figures 4E–H**). Among the HCC patients with TNM stage I∼II disease, OS and RFS were significantly shorter in those with high expression of the four hub genes than in those with low expression ($P < 0.0001$), and the same results were obtained from HCC patients with TNM stage III∼IV disease ($P < 0.0001$) (**Supplementary Figure 4**). Then, we investigated the expression levels of the four hub genes in different AJCC stages of HCC. The expression levels of the four hub genes were significantly higher in stages I, II, and III than in stage 0 ($P < 0.01$) (**Figures 4I–L**). The expression changes in these four genes in stages I, II, and III were not significantly different ($P > 0.05$), indicating that these four genes can be used as important molecular biomarkers for the early diagnosis of HCC. These four genes can also be used as prognostic biomarkers according to the results of the subsistence analysis.

From the above results, at the expression level of the four genes, we found that RPL19 has the most significant difference in the gene expression level between HCC and paracancerous tissues. Compared with the other three genes, the expression level of RPL19 was significantly different in the most GEO

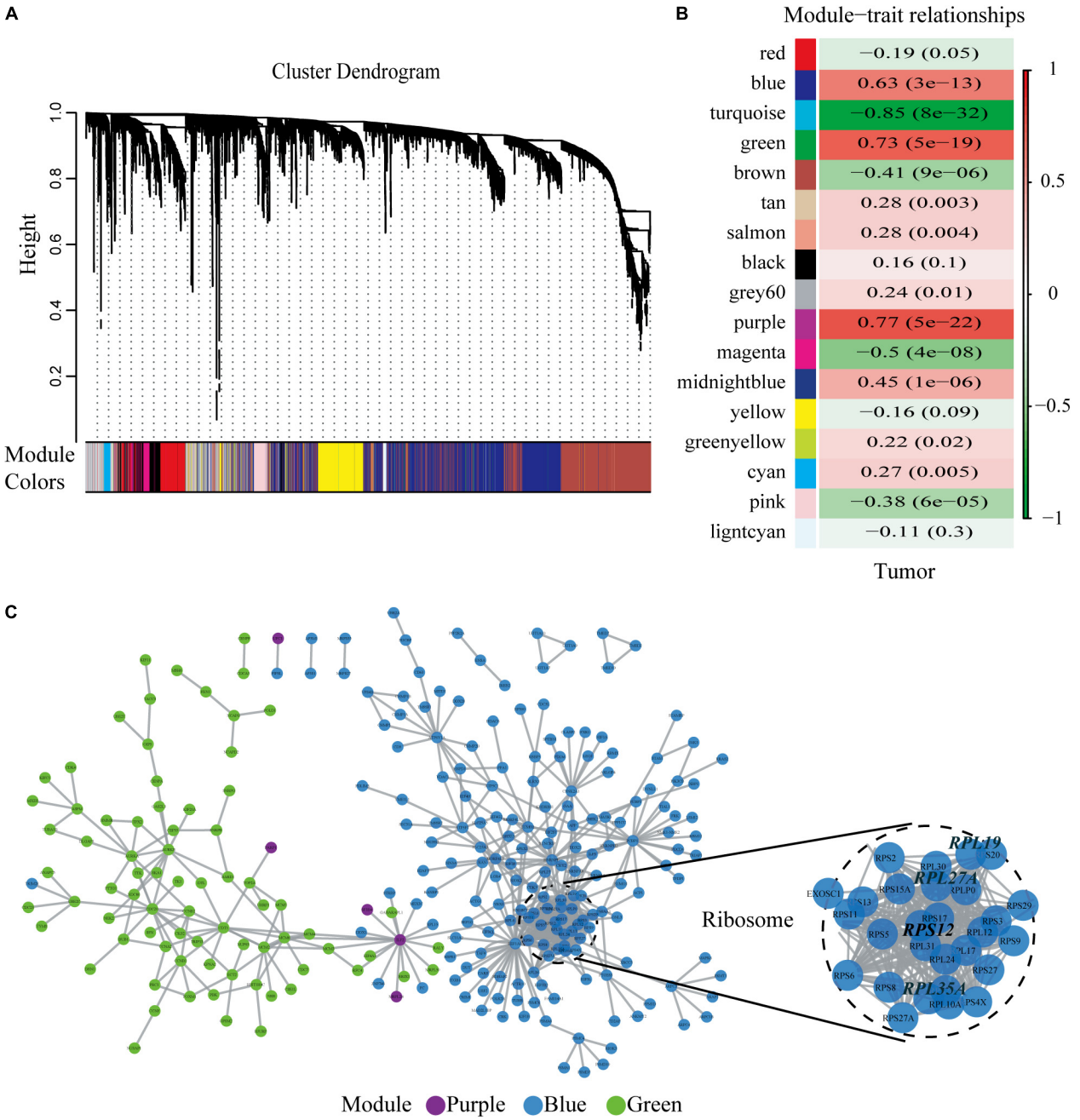

FIGURE 3 | Selected hub modules and the human PPI network. **(A)** Gene dendrogram and module colors. **(B)** Relationship between modules and traits. The figure showed the correlation coefficients and the *P*-values. Red meant positive correlation, while green meant negative correlation. **(C)** Human PPI network was conducted based on the three hub modules. PPI, protein–protein interaction.

data sets. Moreover, the difference in the expression level of RPL19 between HCC and paracancerous tissues has the largest fold change value in the TCGA database. Therefore, judging from the expression levels of the four genes, we thought it was more meaningful to choose RPL19 for further research. Furthermore, at the protein level of the four molecules, we searched the Human Protein Atlas database and found that RPL19 was highly expressed in HCC tissues based on the staining intensity. However, the other three molecules were moderately expressed, lowly expressed or not expressed in HCC tissues. Therefore, judging from the protein level of the four molecules, we thought it was more meaningful to choose RPL19 for further research. At last, we focused on the functions of the four genes. We found that RPL19 served as a biomarker and was involved in the progression of multiple tumors except HCC. In summary, we comprehensively considered the expression level, protein level,

TABLE 2 | Screened cancer-specific genes.

Gene symbol	Number of co-expression neighborhood gene	Number of neighborhood gene	Number of co-expression gene	Number of network gene	Co-expression neighborhood gene per	Fisher's exact test *p*-value	FDR
RPL19	34	158	1148	17381	0.177083	1.18E−07	0.000137
RPS12	26	115	1148	17381	0.184397	1.61E−06	0.00185
RPL27A	29	145	1148	17381	0.166667	3.51E−06	0.004005
RPL35A	20	86	1148	17381	0.188679	1.76E−05	0.01978

FDR, false discovery rate.

and gene function of the four genes. Finally, we chose RPL19 for further research in HCC.

RPL19 Is Closely Related to the Tumor Progress and the Poor Prognosis of HCC

The above results indicated that the four hub genes (RPL19, RPL27A, RPL35A, and RPS12) are closely related to the clinical prognosis of HCC. Through preliminary experiments and a literature search, we ultimately chose RPL19 for further research. According to the IHC staining intensity, the expression of the RPL19 protein in tumor tissues was significantly higher than that in paracancerous tissues ($P = 0.016$) (**Figures 5A–C**). The different levels of staining intensity are shown in **Figure 5B**. Furthermore, RPL19 expression was significantly positively related to alpha fetoprotein (AFP) and potentially positively related to the TNM stage in patients (**Table 3**). Moreover, the expression level of the RPL19 protein increased significantly with progression from TNM stage I to III ($P = 0.046$) (**Figure 5D**). Kaplan-Meier analysis also showed that the OS of HCC patients with low RPL19 expression was significantly longer than that of patients with high RPL19 expression ($P = 0.0007$) (**Figure 5E**). Finally, univariate and multivariate analyses demonstrated that, in addition to AFP and TNM stage, RPL19 might also be an independent prognostic factor for HCC patients (**Table 4**). The above results once again suggest that the expression level of RPL19 is upregulated in HCC tissues and closely related to the clinical prognosis of patients with liver cancer.

Functional Annotation and Immune Infiltration Analysis of RPL19

To further elucidate the mechanism by which RPL19 promotes the progression of HCC, we annotated the biological processes of RPL19 and conducted pathway analysis through Metascape. Metascape enrichment analysis revealed that "ribosome biogenesis," "maturation of rRNA," "TNF-alpha/NF-kappa B signaling pathway," "negative regulation of ubiquitin ligase activity," and "rRNA modification in the nucleus and cytosol" were enriched in biological processes and pathways that might be highly correlated with the malignant progression of HCC. **Figure 6A** showed the top 16 significantly enriched biological processes. Hallmark pathway analysis further revealed that "bile acid metabolism" and "fatty acid metabolism" were suppressed and that the "G2M checkpoint" was activated (**Figure 6B**). Then, gene set enrichment analysis (GSEA) was conducted to determine the hallmark pathways. The results indicated that cell cycle pathways were significantly enriched, and bile acid metabolism-related pathways were significantly downregulated when RPL19 was highly expressed (**Figures 6C,D**). In addition, GSEA was performed to investigate the enriched KEGG pathways. We found that "DNA replication" and "cell cycle" were significantly enriched and "bile secretion" was significantly downregulated (**Figures 6E–G**). Moreover, GSEA was performed to investigate the enriched GO pathways. The results showed that the mitotic cell cycle checkpoint pathway was enriched and that the bile acid transport and metabolic process pathway was downregulated (**Figures 6H–J**). The results showed similar pathways among the three enrichment analyses and indicate that RPL19 is associated with the tumorigenesis and progression of HCC. The immune infiltration analysis showed that activated dendritic cells (aDC), eosinophils, macrophages, natural killer cells (NK cells), mast cells, cytotoxic cells, B cells, regulatory cells (Tregs), Th17 cells, central memory T cell (Tcm), dendritic cells (DC), and neutrophils were negatively correlated with the expression of RPL19. While NK CD56bright cells were positively correlated with the expression of RPL19 (**Figures 7A–F**). To further assess the clinical impact of RPL19, the effect of immune infiltration on survival was analyzed (**Supplementary Figures 5, 6**). Most immune cells were protective factors except T helper cells and Th2 cells (**Figure 7G**). And the immune infiltration was significantly suppressed in HCC with high expression of RPL19.

DISCUSSION

Because of the role of genetic factors in the occurrence, development, progression and prognosis of HCC, we can study the functions of genes at the whole genome level through microarrays and high-throughput sequencing (Byron et al., 2016). As a systematic biological method used to describe how clinical features are related to genes, in this study, WGCNA was used to study gene co-expression in HCC and normal tissues. WGCNA divided genes into multiple modules by analyzing the relationship between genes. Then, correlation analysis between these modules and different phenotypes was used to determine the molecular characteristics of the specific phenotype. To date, WGCNA has been used to explore hub genes and tumor biomarkers of many cancers, such as bladder cancer (Jiang et al., 2020), prostate cancer (Wei et al., 2020), oral squamous cell

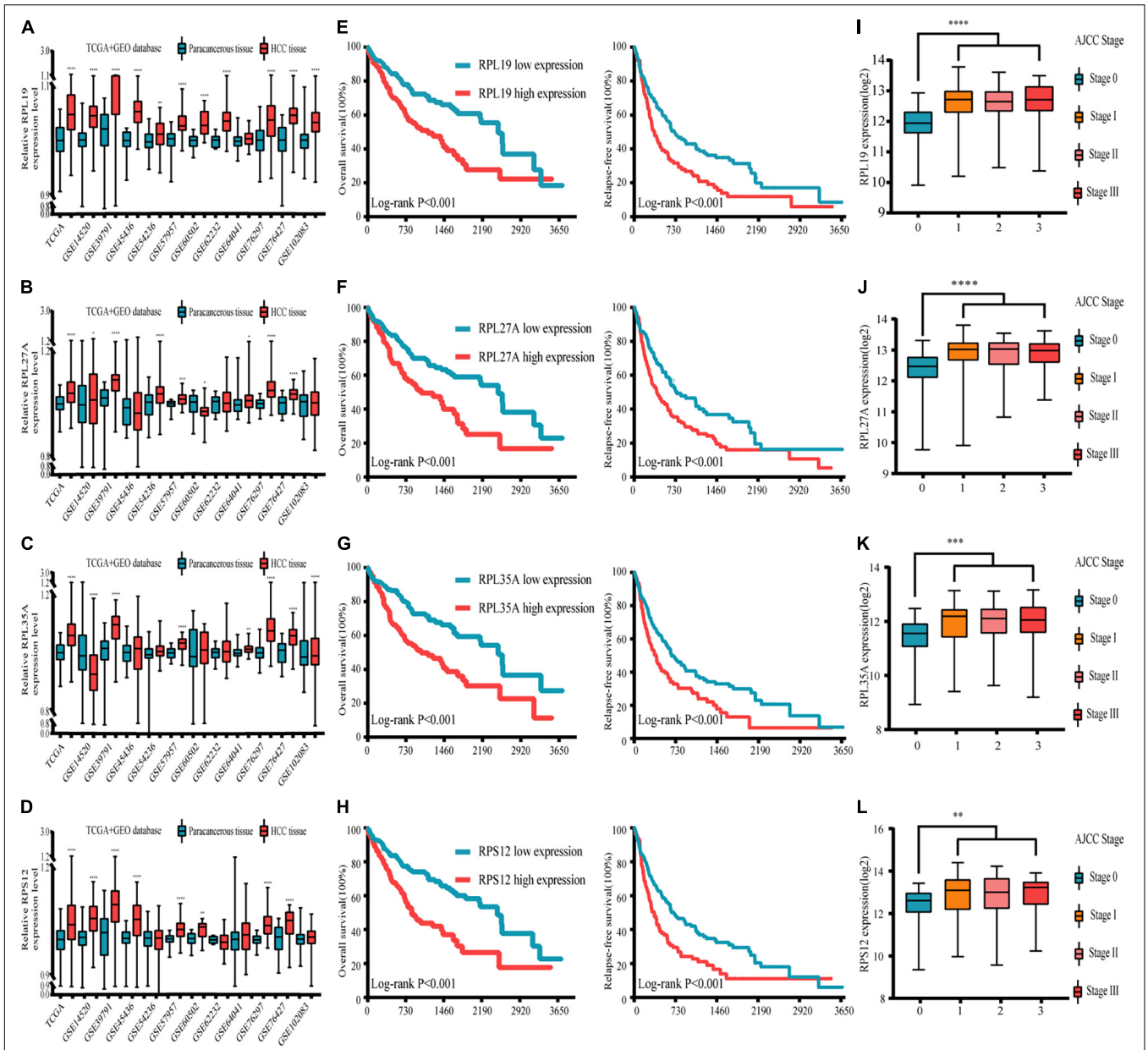

FIGURE 4 | Expression, clinicopathological and prognostic analyses of the four hub genes in the GEO and TCGA databases. **(A–D)** Expression of the four hub genes in the GEO and TCGA databases. **(E–H)** Relationship between the expression levels of the four hub genes and the OS and RFS of HCC patients. **(I–L)** Expression levels of the four hub genes in different AJCC stages of HCC. TCGA database and 11 GEO datasets (including GSE14520, GSE39791, GSE45436, GSE54236, GSE57957, GSE60502, GSE62232, GSE64041, GSE76297, GSE76427, and GSE102083) were used for analysis in this section. Differences between two groups were analyzed by Student's *t*-test. The OS and RFS of HCC patients were calculated with Kaplan–Meier curves. GEO, Gene Expression Omnibus; TCGA, The Cancer Genome Atlas; OS, overall survival; RFS, relapse-free survival; HCC, hepatocellular carcinoma; GSEA, gene set enrichment analysis. $^{*}P < 0.05$, $^{**}P < 0.01$, $^{***}P < 0.001$, $^{****}P < 0.0001$.

carcinoma (Dai et al., 2020) and pancreatic cancer (Wang et al., 2020). In regard to HCC, many studies have been conducted to identify the hub genes correlated with its progression and prognosis. Gu et al. performed WGCNA based on the TCGA database and found two hub modules (turquoise module and blue module) and 13 hub genes (SNRPD2, PRR11, SKA3, etc.) that have a high correlation with progression and prognosis in HCC (Gu et al., 2020). They chose the GEO dataset GSE6764 to validate these genes. Moreover, they conducted real-time PCR to figure out the expression difference in HCC and paracancerous tissues. Li et al. (2020) performed WGCNA based on the GEO dataset GSE54238 and screened four hub genes (TDRKH, TARBP1, STK39, and SOX4) that were correlated with immune infiltration and found that these four genes had certain diagnostic value

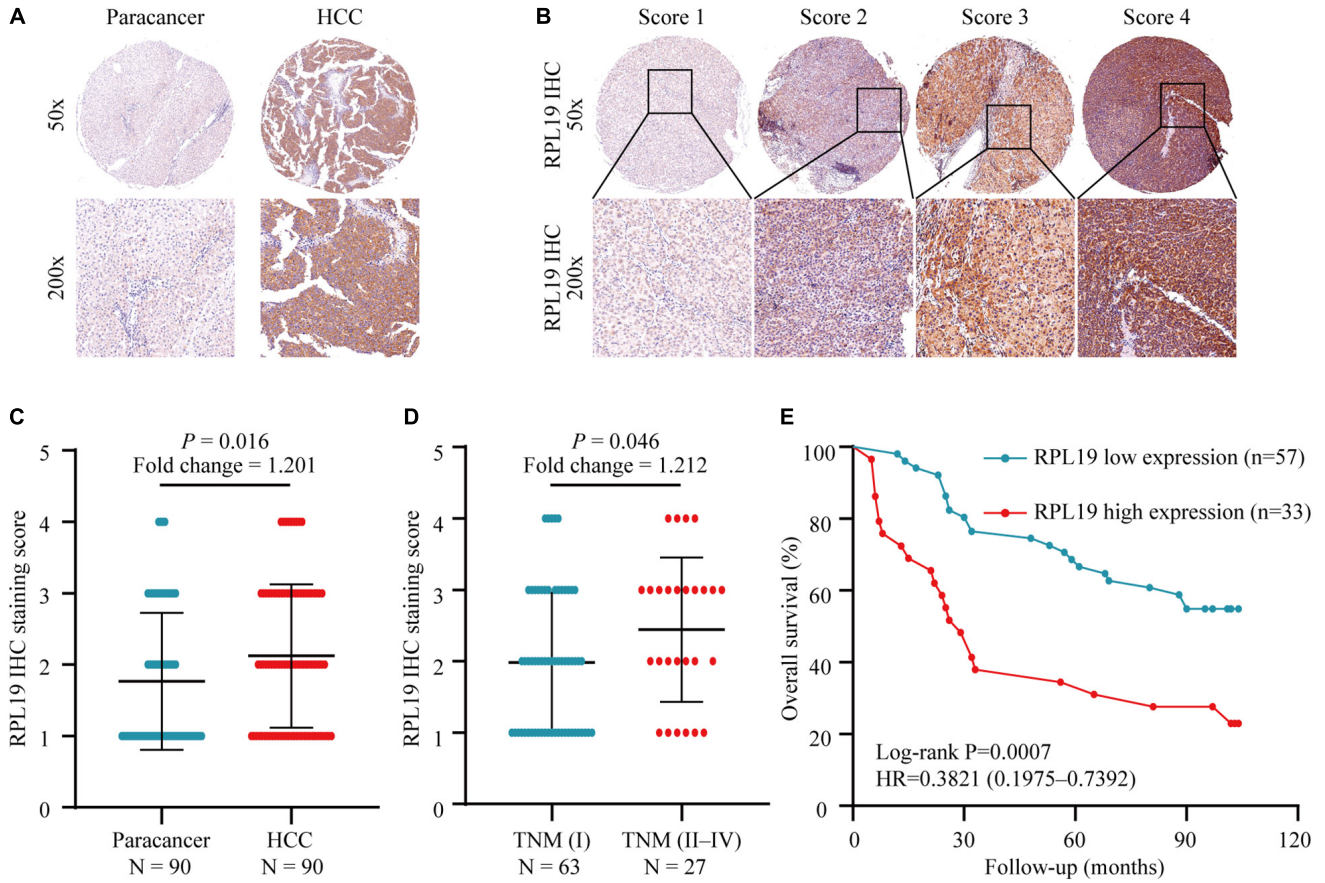

FIGURE 5 | Relationship between the expression of RPL19 in hepatocellular carcinoma and clinical prognosis. **(A)** RPL19 expression was higher in HCC patient tumor tissues than in paired paracancerous tissues. **(B)** IHC analysis of RPL19 expression in the TMA. **(C)** Expression of the RPL19 protein in the TMA in HCC and paracancerous tissues. **(D)** Expression of the RPL19 protein in the TMA in different TNM stages. **(E)** Relationship between the expression of the RPL19 protein and patient OS in the TMA. Differences between two groups were analyzed by Student's *t*-test. The OS of HCC patients were calculated with Kaplan–Meier curves. TMA, tissue microarray; IHC, immunohistochemistry; HCC, hepatocellular carcinoma; OS, overall survival.

for HCC. The TCGA database was chosen to validate these genes. Previous studies have shown that 10 genes (CD8A, GMPS, STAT3, ERBB2, ACACA, ALB, EGFR, TGFB1, KRAS, and BCL2) are involved in multiple pathways, including cell adhesion, migration, locomotion, and differentiation, in the occurrence and progression of HCC (Zhang et al., 2017). Research on multiple different databases help us to understand the mechanism of the occurrence and development of HCC more comprehensively and guide clinical treatment.

In this study, we extracted co-expression networks of groups of genes from GSE39791 to conduct WGCNA and obtained 17 co-expression modules. Through further analysis, we found that three modules (green, blue, and purple) were most relevant to cancer samples. The green and blue modules were involved in multiple cancer-related KEGG pathways. We ultimately identified four genes, RPL19, RPS12, RPL35A, and RPL27A, and all four genes are related to ribosomes and are highly expressed in HCC tissues. The high expression of the four genes was related to the poor prognosis of patients. In addition, we identified the enrichment pathways based on the high expression of RPL19.

The four hub genes we discovered have been studied in multiple tumors. RPL19, which is a tumor-specific antigen of lung adenocarcinoma (Kuroda et al., 2010), can also be used as a prognostic biomarker for prostate cancer (Bee et al., 2006), colorectal cancer (Huang et al., 2008), and diffuse large B-cell lymphoma (Yan et al., 2019). One study (Bee et al., 2006) proposed that the expression of RPL19 in malignant prostate cancer cells was significantly higher than that in prostate cells. The degree of RPL19 staining in cancer tissues was significantly higher than that in normal prostate tissues and benign prostatic hyperplasia tissues, and the survival time of patients with high RPL19 expression was shortened, suggesting that RPL19 could be used as a biomarker for the diagnosis and prognosis of prostate cancer. Another study showed that the expression of cytokeratin 19 (CK19) and RPL19 in the stool of patients with advanced colorectal cancer was significantly increased. The simultaneous detection of two markers could better identify high-risk populations who are prone to metastasis (Huang et al., 2008). It was also found in lung cancer that the level of RPL19 mRNA expression in normal lung tissues was lower than that in

TABLE 3 | Relationship between RPL19 expression and the clinicopathological features of hepatocellular carcinoma patients.

Clinicopathological feature		No. of patients (%)	RPL19 expression level		*P-value*
			Low	High	
Age (years)	≤50	40	25	15	0.883
	>50	50	32	18	
Sex	Female	10	4	6	0.104
	Male	80	53	27	
TNM	I	63	44	19	0.050*
	II-IV	27	13	14	
Tumor size	≤3 cm	36	23	13	0.929
	>3 cm	54	34	20	
AFP	≤300 μg/L	48	36	12	0.014*
	>300 μg/L	42	21	21	

*$P < 0.05$.
TNM, tumor-node-metastasis; HR, hazard ratio; CI, confidential interval; RPL19, ribosomal protein L19; AFP, alpha fetoprotein.

TABLE 4 | Univariate and multivariate analyses of the overall survival of hepatocellular carcinoma patients.

Clinicopathological feature	Univariate analysis			Multivariate analysis		
	HR	95% (CI)	*P*-value	HR	95% (CI)	*P*-value
Age (years)	1.018	0.987–1.049	0.255			
Sex	1.472	0.455–4.754	0.519			
TNM stage	1.707	1.039–2.807	0.035*			
Tumor size	1.082	0.982–1.193	0.112			
AFP	1.377	1.092–1.736	0.007**			
RPL19 expression	1.921	1.39–2.656	<0.001**	1.693	1.189–2.411	0.003**

*$P < 0.05$; **$P < 0.01$.
TNM, tumor-node-metastasis; HR, hazard ratio; CI, confidential interval; RPL19, ribosomal protein L19; AFP, alpha fetoprotein.

lung cancer tissues (Kuroda et al., 2010), and the overexpression RPL19 was positively correlated with interferon IFN-γ. The synthesis of cyclin D1 and D3 decreased after RPL19 expression was inhibited. Therefore, the decrease in the proliferation of lung cancer cell lines caused by RPL19 knockdown may occur through inhibition of the cell cycle (Kuroda et al., 2010). We conducted further studies on RPL19 and obtained consistent results with the bioinformatics analysis on the TMA. RPL27A is a tumor biomarker for colorectal cancer (Yajima et al., 2007). High expression of the RPL27A gene will increase the risk of colorectal cancer (Takemasa et al., 2012). RPL27A was also identified as a biomarker for squamous cervical cancer (Fjeldbo et al., 2016). The RPL35A gene is located at chromosome 3q29-qter (Colombo et al., 1996), and almost all studies have suggested that Diamond-Blackfan anemia is caused by deletion of the RPL35A gene (Farrar et al., 2008, 2011; Gianferante et al., 2020). Finally, the RPS12 gene has been shown to be related to the biological functions of various plants (Lee et al., 2019) and insects (Ji et al., 2019; Kirby and Koslowsky, 2020). Studies have shown that RPS12 gene deletion is associated with diffuse large B-cell lymphoma (Derenzini et al., 2019). The RPS12 gene has been demonstrated to be a hypoxia-related gene, and high expression of the RPS12 gene increases the risk of gastric cancer (Chen et al., 2013), squamous cell carcinoma (Fjeldbo et al., 2016) and HCC (Wang et al., 2009).

Ribosomal proteins are the main component of ribosomes and play an important role in protein biosynthesis in cells. Ribosomes participate in DNA repair, cell development regulation and cell differentiation (Petibon et al., 2021). In addition, the dysregulation of RPs affects the progression and prognosis of multiple diseases (Bolze et al., 2013; Ebright et al., 2020). Moreover, there are many studies on the relationship between ribosomal proteins and HCC. Researchers analyzed HCC cell lines and tissue samples and found that the expression levels of RPS3A in HCC cell lines and tissues were higher than those in normal liver cells and adjacent tumor-free tissues, and patients with high RPS3A expression had shorter OS and RFS than patients with low RPS3A expression (Zhou et al., 2020c). Guo et al. (2018) proposed that ribosomal protein S15a promotes tumor angiogenesis by enhancing Wnt/β-catenin-induced FGF18 expression in HCC. It has been reported that RPS11 is highly expressed in liver cancer tissues, and its high expression indicates a poor prognosis (Zhou et al., 2020b). On the other hand, studies (Chen et al., 2020; Zhou et al., 2020a) have shown that ribosomal proteins can be used as intermediate targets to inhibit the progression of HCC. Therefore, in the future, ribosomal proteins may become important targets in the diagnosis, treatment and prognosis of HCC.

Through the functional annotation and enrichment pathway analysis of RPL19, we found that high RPL19 expression suppressed bile acid metabolism and activated the cell cycle. Bile acids are produced in the liver and metabolized by enzymes derived from gut bacteria. They are essential for maintaining healthy gut microbiota, balancing lipid and carbohydrate metabolism, insulin sensitivity and innate immunity (Li et al., 2017). Increasing evidence has shown that bile acids play a vital role in the occurrence and progression of HCC (Jia et al., 2018). Studies have shown that the inhibition of bile acid metabolism can lead to cholestasis and increase the risk of HCC (Knisely et al., 2006). On the other hand, ursodeoxycholic acid can prevent liver cholestasis, thereby exerting its hepatoprotective effect (Beuers et al., 2015). Bioinformatic analysis indicated that high DDX11 expression was closely related to the G2-M phase transition of the cell cycle and DNA replication. Uncontrolled excessive proliferation is one of the main characteristics of tumor cells. Multiple studies have shown that the cell cycle pathway of liver cancer cells is significantly enhanced (Rebouissou and Nault, 2020), and the progression of liver cancer can be inhibited by inhibiting the cell cycle (Lee et al., 2018). Moreover, the immune infiltration analysis showed that the immune infiltration was significantly suppressed in HCC with high expression of RPL19. Ma et al. (2020) found that the expression of Aurora kinase A and ninein-interacting protein (AUNIP) was positively correlated with the degree of infiltration of dendritic cells, macrophages, neutrophils, CD8 + T cells,

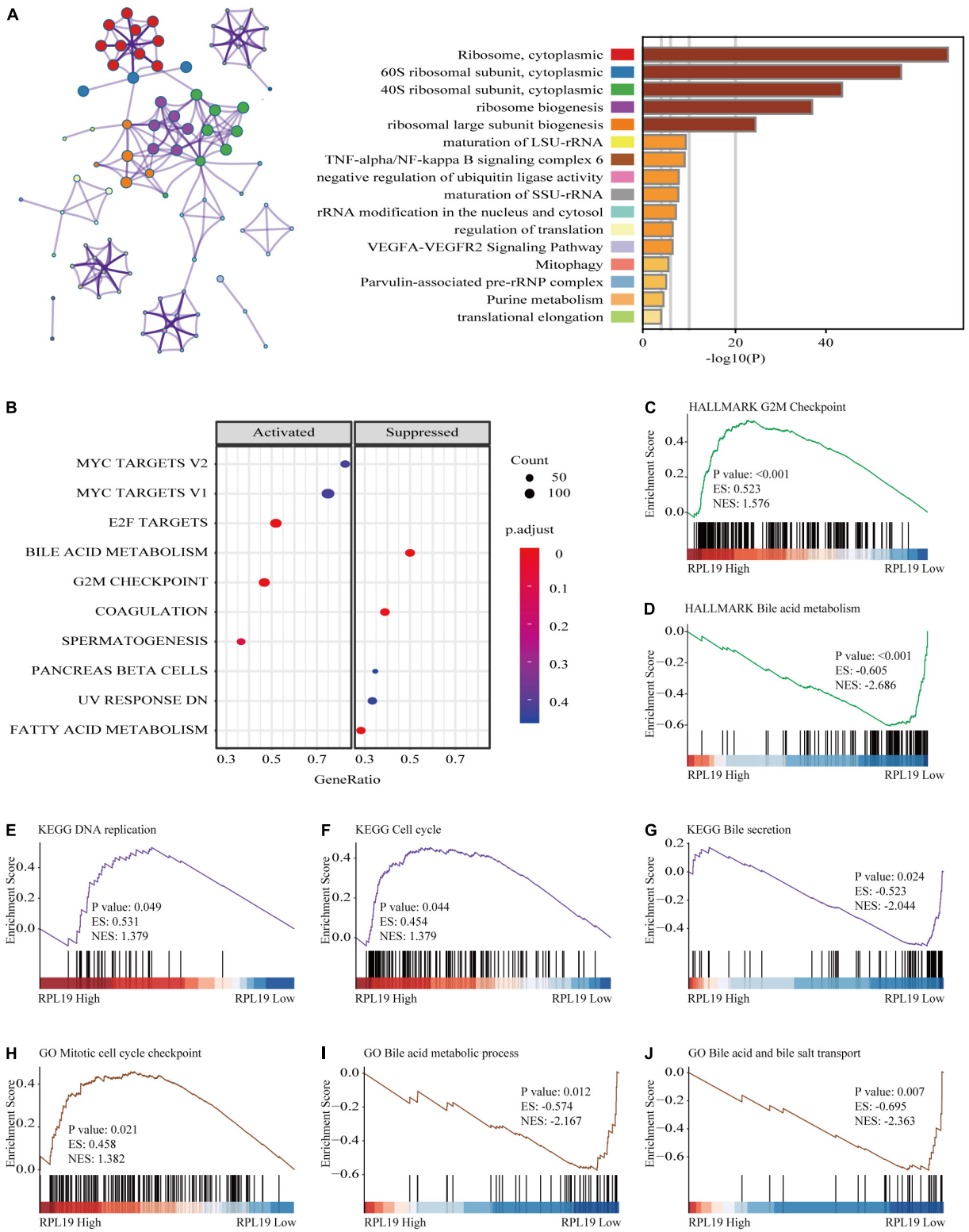

FIGURE 6 | Functional annotation of RPL19. **(A)** Network and bar chart of 16 significantly enriched biological processes in HCC patients with high RPL19 expression. Each enriched node is presented in a different color. **(B)** The suppressed and activated hallmark pathways. **(C,D)** GSEA was conducted to determine the hallmark pathways. **(E–G)** GSEA was conducted to determine the KEGG pathways. **(H–J)** GSEA was conducted to determine the GO pathways. In this section, KEGG, HALLMARK, and GO database were used for analysis. GSEA, gene set enrichment analysis. KEGG, Kyoto Encyclopedia of Genes and Genomes; GO, Gene Ontology.

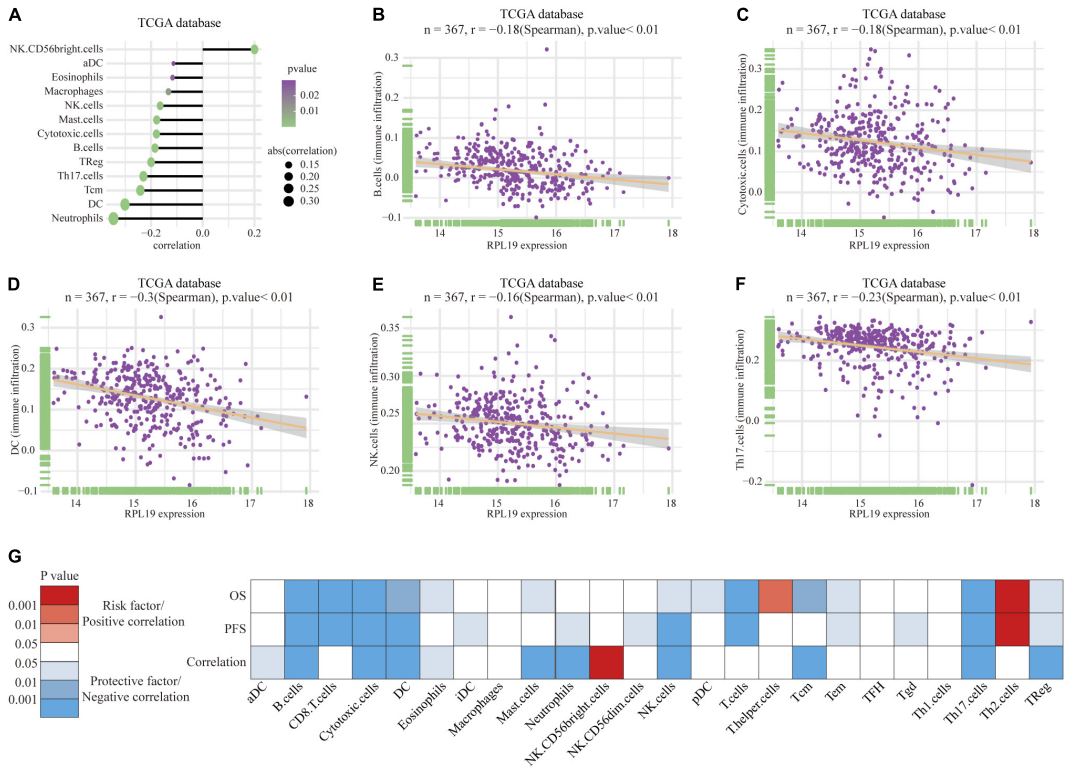

FIGURE 7 | Immune infiltration analysis of RPL19. **(A–F)** Correlation between immune cells and the expression of RPL19, including B cells, Cytotoxic cells, DC, NK cells, and Th17 cells. **(G)** The heatmap of the correlation between OS, PFS and the expression of RPL19. In this section, TCGA database was used for analysis. Spearman's correlation test was used to evaluate the correlation between the expression level of RPL19 and immune cells. DC, dendritic cells; NK cells, natural killer cells; OS, overall survival; PFS, progress free survival.

CD4 + T cells and B cells in HCC. Subsequent study showed that TANK-binding kinase 1 (TBK1) was a potential target for HCC by enhancing tumor immune infiltration (Jiang et al., 2021).

We acknowledge that there were some limitations and shortcomings to this study. First, WGCNA is based on highly correlated key modules to conduct the analysis, some key genes with low correlation may be missed. In addition, in this study we chose three hub modules with the highest correlation coefficient and positive correlation for model construction. In the process, we missed some highly negatively correlated modules (such as turquoise model in **Figure 3**). In the future research, we need to pay attention to the genes in these modules. Second, in this study, we identified four hub genes through WGCNA. We comprehensively considered the expression level, protein level, and gene function of the four genes. Only RPL19 has been validated in this study, the functions of the other three molecules (RPL35A, RPL27A, and RPS12) need further studies. Third, we only analyzed the relationship between the expression and clinical features but did not verify these findings through in vivo and in vitro experiments. Finally, we only explored the underlying mechanism based on bioinformatic prediction. The molecular mechanism of up-regulated RPL19 promoting the progression of HCC remains a subject for further study.

CONCLUSION

In conclusion, WGCNA was used to construct a co-expression gene network and revealed four hub genes (RPL19, RPL35A, RPL27A, and RPS12) that were highly expressed in HCC and whose expression were negatively correlated with HCC prognosis. Then, the effect of high RPL19 expression on the prognosis of HCC was verified through a TMA. Enrichment analysis revealed that cell cycle pathways were significantly enriched, and bile acid metabolism-related pathways were significantly down-regulated when RPL19 was highly expressed. The immune infiltration analysis showed that the immune infiltration was significantly suppressed in HCC with high expression of RPL19. As a result, RPL19 may be a molecular biomarker and drug target for the early diagnosis and prognosis of HCC. However, the mechanism by which RPL19 promotes the occurrence and development of HCC through the above pathways is still unknown, which is our next key research direction.

DATA AVAILABILITY STATEMENT

The datasets presented in this study can be found in online repositories. The names of the repository/repositories

and accession number(s) can be found in the article/ **Supplementary Material**.

ETHICS STATEMENT

The studies involving human participants were reviewed and approved by Institutional Review Board of The First Affiliated Hospital of Zhengzhou University. The patients/participants provided their written informed consent to participate in this study.

AUTHOR CONTRIBUTIONS

ZY and ZR designed the study. BR, JL, and TR provided equal contributions to the research design, data analysis, and article writing. JY, GZ, LL, HW, and MH revised the manuscript. All authors contributed to the article and approved the submitted version.

FUNDING

This study was supported by the China Postdoctoral Science Foundation (2020T130609 and 2020T130109ZX), National Natural Science Foundation of China (U2004121, 82070643, and U1904164), and Key Scientific Research Projects of Higher Education Institutions in Henan Province (20A320056).

SUPPLEMENTARY MATERIAL

The Supplementary Material for this article can be found online at: https://www.frontiersin.org/articles/10.3389/fcell.2021.686547/full#supplementary-material

Supplementary Figure 1 | The 11 modules were enriched in 121 KEGG pathways. KEGG, Kyoto Encyclopedia of Genes and Genomes.

Supplementary Figure 2 | Distribution of the co-expression network degree.

Supplementary Figure 3 | Expression levels of the four hub genes in different stages of liver disease. **(A)** Expression level of RPL19 in different stages of liver diseases. **(B)** Expression level of RPL27A in different stages of liver diseases. **(C)** Expression level of RPL35A in different stages of liver diseases. **(D)** Expression level of RPS12 in different stages of liver diseases. $^{*}P < 0.05$, $^{**}P < 0.01$.

Supplementary Figure 4 | Relationship between the expression levels of the four hub genes and the prognosis of HCC patients with different TNM stages. **(A)** Relationship between RPL19 expression and the OS and RFS of HCC patients according to TNM stage (stages I∼II and III∼IV). **(B)** Relationship between RPL27A expression and the OS and RFS of HCC patients according to TNM stage (stages I∼II and III∼IV). **(C)** Relationship between RPL35A expression and the OS and RFS of HCC patients according to TNM stage (stages I∼II and III∼IV). **(D)** Relationship between RPS12 expression and the OS and RFS of HCC patients according to TNM stage (stages I∼II and III∼IV). OS, overall survival. RFS, relapse-free survival.

Supplementary Figure 5 | Overall survival curves of the immune infiltrating cells in HCC. Kaplan-Meier analysis showing the correlation between the immune cells scores and the OS of HCC patients. OS, overall survival.

Supplementary Figure 6 | Progression free survival curves of the immune infiltrating cells in HCC. Kaplan-Meier analysis showing the correlation between the immune cells scores and the PFS of HCC patients. PFS, progress free survival.

Supplementary Table 1 | All 31,334 genes identified.

Supplementary Table 2 | All 7,814 DEGs.

Supplementary Table 3 | Statistical results of genes corresponding to each module.

Supplementary Table 4 | Distribution of 7,814 selected genes in the different modules.

Supplementary Table 5 | Eleven modules were enriched in 121 KEGG pathways.

Supplementary Table 6 | All genes whose co-expression values were greater than 0.1.

Supplementary Table 7 | Eleven modules were enriched in 121 KEGG pathways.

Supplementary Table 8 | Human PPI data from the HIPPIE database.

Supplementary Table 9 | Human PPI network.

REFERENCES

Bee, A., Ke, Y., Forootan, S., Lin, K., Beesley, C., Forrest, S. E., et al. (2006). Ribosomal protein l19 is a prognostic marker for human prostate cancer. *Clin. Cancer Res.* 12(7 Pt. 1), 2061–2065. doi: 10.1158/1078-0432.CCR-05-2445

Beuers, U., Trauner, M., Jansen, P., and Poupon, R. (2015). New paradigms in the treatment of hepatic cholestasis: from UDCA to FXR, PXR and beyond. *J. Hepatol.* 62(1 Suppl.), S25–S37. doi: 10.1016/j.jhep.2015.02.023

Bolze, A., Mahlaoui, N., Byun, M., Turner, B., Trede, N., Ellis, S. R., et al. (2013). Ribosomal protein SA haploinsufficiency in humans with isolated congenital asplenia. *Science (New York N. Y.)* 340, 976–978. doi: 10.1126/science.1234864

Byron, S. A., Van Keuren-Jensen, K. R., Engelthaler, D. M., Carpten, J. D., and Craig, D. W. (2016). Translating RNA sequencing into clinical diagnostics: opportunities and challenges. *Nat. Rev. Genet.* 17, 257–271. doi: 10.1038/nrg.2016.10

Chen, D., Zhang, R., Shen, W., Fu, H., Liu, S., Sun, K., et al. (2013). RPS12-specific shRNA inhibits the proliferation, migration of BGC823 gastric cancer cells with S100A4 as a downstream effector. *Int. J. Oncol.* 42, 1763–1769. doi: 10.3892/ijo.2013.1872

Chen, M., Wang, D., Liu, J., Zhou, Z., Ding, Z., Liu, L., et al. (2020). MicroRNA-587 functions as a tumor suppressor in hepatocellular carcinoma by targeting ribosomal protein SA. *Biomed. Res. Int.* 2020:3280530. doi: 10.1155/2020/3280530

Colombo, P., Read, M., and Fried, M. (1996). The human L35a ribosomal protein (RPL35A) gene is located at chromosome band 3q29-qter. *Genomics* 32, 148–150. doi: 10.1006/geno.1996.0093

Cui, X., Liu, X., Han, Q., Zhu, J., Li, J., Ren, Z., et al. (2019). DPEP1 is a direct target of miR-193a-5p and promotes hepatoblastoma progression by PI3K/Akt/mTOR pathway. *Cell Death Dis.* 10:701. doi: 10.1038/s41419-019-1943-0

Dai, Y., Lv, Q., Qi, T., Qu, J., Ni, H., Liao, Y., et al. (2020). Identification of hub methylated-CpG sites and associated genes in oral squamous cell carcinoma. *Cancer Med.* 9, 3174–3187. doi: 10.1002/cam4.2969

Derenzini, E., Agostinelli, C., Rossi, A., Rossi, M., Scellato, F., Melle, F., et al. (2019). Genomic alterations of ribosomal protein genes in diffuse large B cell lymphoma. *Br. J. Haematol.* 185, 330–334. doi: 10.1111/bjh.15442

Dressman, M. A., Baras, A., Malinowski, R., Alvis, L. B., Kwon, I., Walz, T. M., et al. (2003). Gene expression profiling detects gene amplification and differentiates tumor types in breast cancer. *Cancer Res.* 63, 2194–2199.

Ebright, R. Y., Lee, S., Wittner, B. S., Niederhoffer, K. L., Nicholson, B. T., Bardia, A., et al. (2020). Deregulation of ribosomal protein expression and translation promotes breast cancer metastasis. *Science (New York N. Y.)* 367, 1468–1473. doi: 10.1126/science.aay0939

Farrar, J. E., Nater, M., Caywood, E., McDevitt, M. A., Kowalski, J., Takemoto, C. M., et al. (2008). Abnormalities of the large ribosomal subunit protein, Rpl35a, in Diamond-Blackfan anemia. *Blood* 112, 1582–1592. doi: 10.1182/blood-2008-02-140012

Farrar, J. E., Vlachos, A., Atsidaftos, E., Carlson-Donohoe, H., Markello, T. C., Arceci, R. J., et al. (2011). Ribosomal protein gene deletions in Diamond-Blackfan anemia. *Blood* 118, 6943–6951. doi: 10.1182/blood-2011-08-375170

Fjeldbo, C. S., Aarnes, E. K., Malinen, E., Kristensen, G. B., and Lyng, H. (2016). Identification and validation of reference genes for RT-qPCR studies of hypoxia in squamous cervical cancer patients. *PLoS One* 11:e0156259. doi: 10.1371/journal.pone.0156259

Gianferante, D. M., Wlodarski, M. W., Atsidaftos, E., Da Costa, L., Delaporta, P., Farrar, J. E., et al. (2020). Genotype-phenotype association and variant characterization in Diamond-Blackfan anemia caused by pathogenic variants in RPL35A. *Haematologica* 106, 1303–1310. doi: 10.3324/haematol.2020.246629

Gu, Y., Li, J., Guo, D., Chen, B., Liu, P., Xiao, Y., et al. (2020). Identification of 13 key genes correlated with progression and prognosis in hepatocellular carcinoma by weighted gene Co-expression network analysis. *Front. Genet.* 11:153. doi: 10.3389/fgene.2020.00153

Guo, P., Wang, Y., Dai, C., Tao, C., Wu, F., Xie, X., et al. (2018). Ribosomal protein S15a promotes tumor angiogenesis via enhancing Wnt/beta-catenin-induced FGF18 expression in hepatocellular carcinoma. *Oncogene* 37, 1220–1236. doi: 10.1038/s41388-017-0017-y

Huang, C. J., Chien, C. C., Yang, S. H., Chang, C. C., Sun, H. L., Cheng, Y. C., et al. (2008). Faecal ribosomal protein L19 is a genetic prognostic factor for survival in colorectal cancer. *J. Cell. Mol. Med.* 12, 1936–1943. doi: 10.1111/j.1582-4934.2008.00253.x

Ji, Z., Kiparaki, M., Folgado, V., Kumar, A., Blanco, J., Rimesso, G., et al. (2019). *Drosophila* RpS12 controls translation, growth, and cell competition through Xrp1. *PLoS Genet.* 15:e1008513. doi: 10.1371/journal.pgen.1008513

Jia, W., Xie, G., and Jia, W. (2018). Bile acid-microbiota crosstalk in gastrointestinal inflammation and carcinogenesis. *Nat. Rev. Gastroenterol. Hepatol.* 15, 111–128. doi: 10.1038/nrgastro.2017.119

Jiang, J., Bi, Y., Liu, X. P., Yu, D., Yan, X., Yao, J., et al. (2020). To construct a ceRNA regulatory network as prognostic biomarkers for bladder cancer. *J. Cell. Mol. Med.* 24, 5375–5386. doi: 10.1111/jcmm.15193

Jiang, Y., Chen, S., Li, Q., Liang, J., Lin, W., Li, J., et al. (2021). TANK-binding kinase 1 (TBK1) serves as a potential target for hepatocellular carcinoma by enhancing tumor immune infiltration. *Front. Immunol.* 12:612139. doi: 10.3389/fimmu.2021.612139

Kim, J. H., Sohn, B. H., Lee, H. S., Kim, S. B., Yoo, J. E., Park, Y. Y., et al. (2014). Genomic predictors for recurrence patterns of hepatocellular carcinoma: model derivation and validation. *PLoS Med.* 11:e1001770. doi: 10.1371/journal.pmed.1001770

Kirby, L. E., and Koslowsky, D. (2020). Cell-line specific RNA editing patterns in *Trypanosoma brucei* suggest a unique mechanism to generate protein variation in a system intolerant to genetic mutations. *Nucleic Acids Res* 48, 1479–1493. doi: 10.1093/nar/gkz1131

Knisely, A. S., Strautnieks, S. S., Meier, Y., Stieger, B., Byrne, J. A., Portmann, B. C., et al. (2006). Hepatocellular carcinoma in ten children under five years of age with bile salt export pump deficiency. *Hepatology* 44, 478–486. doi: 10.1002/hep.21287

Kuroda, K., Takenoyama, M., Baba, T., Shigematsu, Y., Shiota, H., Ichiki, Y., et al. (2010). Identification of ribosomal protein L19 as a novel tumor antigen recognized by autologous cytotoxic T lymphocytes in lung adenocarcinoma. *Cancer Sci.* 101, 46–53. doi: 10.1111/j.1349-7006.2009.01351.x

Lee, D., Jang, M. K., Seo, J. H., Ryu, S. H., Kim, J. A., and Chung, Y. H. (2018). ARD1/NAA10 in hepatocellular carcinoma: pathways and clinical implications. *Exp. Mol. Med.* 50, 1–12. doi: 10.1038/s12276-018-0106-1

Lee, K., Park, S. J., Colas des Francs-Small, C., Whitby, M., Small, I., and Kang, H. (2019). The coordinated action of PPR4 and EMB2654 on each intron half mediates trans-splicing of rps12 transcripts in plant chloroplasts. *Plant J.* 100, 1193–1207. doi: 10.1111/tpj.14509

Li, J., Wang, X., Yang, J., Zhao, S., Liu, T., and Wang, L. (2020). Identification of hub genes in hepatocellular carcinoma related to progression and prognosis by weighted gene Co-expression network analysis. *Med. Sci. Monit.* 26:e920854. doi: 10.12659/MSM.920854

Li, M., Cai, S. Y., and Boyer, J. L. (2017). Mechanisms of bile acid mediated inflammation in the liver. *Mol. Aspects Med.* 56, 45–53. doi: 10.1016/j.mam.2017.06.001

Liu, J., Nie, S., Gao, M., Jiang, Y., Wan, Y., Ma, X., et al. (2019). Identification of EPHX2 and RMI2 as two novel key genes in cervical squamous cell carcinoma by an integrated bioinformatic analysis. *J. Cell. Physiol.* 234, 21260–21273. doi: 10.1002/jcp.28731

Ma, C., Kang, W., Yu, L., Yang, Z., and Ding, T. (2020). AUNIP expression is correlated with immune infiltration and is a candidate diagnostic and prognostic biomarker for hepatocellular carcinoma and lung adenocarcinoma. *Front. Oncol.* 10:590006. doi: 10.3389/fonc.2020.590006

Misselbeck, K., Parolo, S., Lorenzini, F., Savoca, V., Leonardelli, L., Bora, P., et al. (2019). A network-based approach to identify deregulated pathways and drug effects in metabolic syndrome. *Nat. Commun.* 10:5215. doi: 10.1038/s41467-019-13208-z

Panwar, B., Schmiedel, B. J., Liang, S., White, B., Rodriguez, E., Kalunian, K., et al. (2021). Multi-cell type gene coexpression network analysis reveals coordinated interferon response and cross-cell type correlations in systemic lupus erythematosus. *Genome Res.* 31, 659–676. doi: 10.1101/gr.265249.120

Petibon, C., Malik Ghulam, M., Catala, M., and Abou Elela, S. (2021). Regulation of ribosomal protein genes: an ordered anarchy. *Wiley Interdiscip. Rev. RNA* 12:e1632. doi: 10.1002/wrna.1632

Rahbari, N. N., Mehrabi, A., Mollberg, N. M., Muller, S. A., Koch, M., Buchler, M. W., et al. (2011). Hepatocellular carcinoma: current management and perspectives for the future. *Ann. Surg.* 253, 453–469. doi: 10.1097/SLA.0b013e31820d944f

Rebouissou, S., and Nault, J. C. (2020). Advances in molecular classification and precision oncology in hepatocellular carcinoma. *J. Hepatol.* 72, 215–229. doi: 10.1016/j.jhep.2019.08.017

Remmele, W., Hildebrand, U., Hienz, H. A., Klein, P. J., Vierbuchen, M., Behnken, L. J., et al. (1986). Comparative histological, histochemical, immunohistochemical and biochemical studies on oestrogen receptors, lectin receptors, and Barr bodies in human breast cancer. *Virchows Arch. A Pathol. Anat. Histopathol.* 409, 127–147. doi: 10.1007/BF00708323

Siegel, R. L., Miller, K. D., and Jemal, A. (2020). Cancer statistics, 2020. *CA Cancer J. Clin.* 70, 7–30. doi: 10.3322/caac.21590

Takemasa, I., Kittaka, N., Hitora, T., Watanabe, M., Matsuo, E., Mizushima, T., et al. (2012). Potential biological insights revealed by an integrated assessment of proteomic and transcriptomic data in human colorectal cancer. *Int. J. Oncol.* 40, 551–559. doi: 10.3892/ijo.2011.1244

Wang, F., Kuang, Y., Salem, N., Anderson, P. W., and Lee, Z. (2009). Cross-species hybridization of woodchuck hepatitis viral infection-induced woodchuck hepatocellular carcinoma using human, rat and mouse oligonucleotide microarrays. *J. Gastroenterol. Hepatol.* 24, 605–617. doi: 10.1111/j.1440-1746.2008.05581.x

Wang, W., Xing, H., Huang, C., Pan, H., and Li, D. (2020). Identification of pancreatic cancer type related factors by weighted gene Co-expression network analysis. *Med. Oncol.* 37:33. doi: 10.1007/s12032-020-1339-0

Wei, J., Yin, Y., Deng, Q., Zhou, J., Wang, Y., Yin, G., et al. (2020). Integrative analysis of MicroRNA and gene interactions for revealing candidate signatures in prostate cancer. *Front. Genet.* 11:176. doi: 10.3389/fgene.2020.00176

Yajima, S., Ishii, M., Matsushita, H., Aoyagi, K., Yoshimatsu, K., Kaneko, H., et al. (2007). Expression profiling of fecal colonocytes for RNA-based screening of colorectal cancer. *Int. J. Oncol.* 31, 1029–1037.

Yan, W., Li, S. X., Gao, H., and Yang, W. (2019). Identification of B-cell translocation gene 1-controlled gene networks in diffuse large B-cell lymphoma:

a study based on bioinformatics analysis. *Oncol. Lett.* 17, 2825–2835. doi: 10.3892/ol.2019.9900

Yu, L. X., and Schwabe, R. F. (2017). The gut microbiome and liver cancer: mechanisms and clinical translation. *Nat. Rev. Gastroenterol. Hepatol.* 14, 527–539. doi: 10.1038/nrgastro.2017.72

Zhang, C., Peng, L., Zhang, Y., Liu, Z., Li, W., Chen, S., et al. (2017). The identification of key genes and pathways in hepatocellular carcinoma by bioinformatics analysis of high-throughput data. *Med. Oncol.* 34:101. doi: 10.1007/s12032-017-0963-9

Zhang, X., Feng, H., Li, Z., Li, D., Liu, S., Huang, H., et al. (2018). Application of weighted gene co-expression network analysis to identify key modules and hub genes in oral squamous cell carcinoma tumorigenesis. *Onco Targets Ther.* 11, 6001–6021. doi: 10.2147/OTT.S171791

Zhou, C., Liu, C., Liu, W., Chen, W., Yin, Y., Li, C. W., et al. (2020a). SLFN11 inhibits hepatocellular carcinoma tumorigenesis and metastasis by targeting RPS4X via mTOR pathway. *Theranostics* 10, 4627–4643. doi: 10.7150/thno.42869

Zhou, C., Sun, J., Zheng, Z., Weng, J., Atyah, M., Zhou, Q., et al. (2020b). High RPS11 level in hepatocellular carcinoma associates with poor prognosis after curative resection. *Ann. Transl. Med.* 8:466. doi: 10.21037/atm.2020.03.92

Zhou, C., Weng, J., Liu, C., Zhou, Q., Chen, W., Hsu, J. L., et al. (2020c). High RPS3A expression correlates with low tumor immune cell infiltration and unfavorable prognosis in hepatocellular carcinoma patients. *Am. J. Cancer Res.* 10, 2768–2784.

Conflict of Interest: The authors declare that the research was conducted in the absence of any commercial or financial relationships that could be construed as a potential conflict of interest.

frontiers in Cell and Developmental Biology

ORIGINAL RESEARCH
published: 05 August 2021
doi: 10.3389/fcell.2021.681529

Long Non-coding RNA TMEM220-AS1 Suppressed Hepatocellular Carcinoma by Regulating the miR-484/MAGI1 Axis as a Competing Endogenous RNA

Cong Cao[1†], Jun Li[1†], Guangzhi Li[1†], Gaoyu Hu[2], Zhihua Deng[2], Bing Huang[1], Jing Yang[1], Jiequn Li[3,4] and Song Cao[5*]*

[1] Department of General Practice, The Affiliated Hospital of Youjiang Medical University for Nationalities, Baise, China, [2] Department of Gastroenterology, The Affiliated Hospital of Youjiang Medical University for Nationalities, Baise, China, [3] Department of Liver Transplantation, Second Xiangya Hospital, Central South University, Changsha, China, [4] Transplant Medical Research Center, The Second Affiliated Hospital of Guangxi Medical University, Nanning, China, [5] Department of Liver Transplantation, The Second Affiliated Hospital of Guangxi Medical University, Nanning, China

Long non-coding RNAs (lncRNAs) have a considerable regulatory influence on multiple biological processes. Nevertheless, the role of TMEM220-AS1 in hepatocellular carcinoma (HCC) remains unclear. We used The Cancer Genome Atlas (TCGA) database to analyze the differentially expressed lncRNAs. qRT-PCR was used to verify the results for a large population. The *in vitro* effects of TMEM220-AS1 on HCC cells were determined using Cell Counting Kit-8 (CCK-8), 5-ethynyl-2'-deoxyuridine (EdU), flow cytometry, and Transwell assays in HCC cells. We used qRT-PCR and western blotting to identify the epithelial-mesenchymal transition (EMT). Moreover, we performed bioinformatics analysis, western blotting, dual luciferase reporter gene assay, RNA pull-down, and RNA binding protein immunoprecipitation (RIP) to investigate the underlying molecular mechanisms of TMEM220-AS1 function. Finally, the function of TMEM220-AS1 was verified *in vivo*. The results showed that TMEM220-AS1 was expressed at considerably low levels in HCC. It was demonstrated that malignant phenotypes and EMT of HCC cells were promoted by the knock down of TMEM220-AS1 both *in vivo* and *in vitro*. TMEM220-AS1, which was detected primarily in the cytoplasm, functioned as an miRNA sponge to bind miR-484 and promote the level of membrane-associated guanylate kinase, WW, and PDZ domain containing 1 (*MAGI1*), thereby curbing the malignant phenotypes of HCC cells. In conclusion, low levels of TMEM220-AS1 promote proliferation and metastasis through the miR-484/*MAGI1* axis in HCC.

Keywords: hepatocellular carcinoma, long non-coding RNA, TMEM220-AS1, cell invasion, epithelial-mesenchymal transition

OPEN ACCESS

Edited by:
Xiaochen Wang, University of Texas Southwestern Medical Center, United States

Reviewed by:
Jin Zhou, University of Texas Southwestern Medical Center, United States
Yanhong Zhang, Brigham and Women's Hospital and Harvard Medical School, United States

****Correspondence:***
Song Cao
13877189102@163.com
Jiequn Li
leejiequn@csu.edu.cn

† These authors have contributed equally to this work

Specialty section:
This article was submitted to Molecular and Cellular Oncology, a section of the journal Frontiers in Cell and Developmental Biology

Received: *16 March 2021*
Accepted: *24 June 2021*
Published: *05 August 2021*

Citation:
Cao C, Li J, Li G, Hu G, Deng Z, Huang B, Yang J, Li J and Cao S (2021) Long Non-coding RNA TMEM220-AS1 Suppressed Hepatocellular Carcinoma by Regulating the miR-484/MAGI1 Axis as a Competing Endogenous RNA. Front. Cell Dev. Biol. 9:681529. doi: 10.3389/fcell.2021.681529

INTRODUCTION

As the sixth most frequently occurring cancer worldwide, liver cancer is the third leading cause of cancer-related deaths, globally (Nakagawa et al., 2019; Anwanwan et al., 2020; Rahmani et al., 2020). Among all primary liver cancers, hepatocellular carcinoma (HCC) is the most frequent, accounting for 80–90% of all cases (Ringelhan et al., 2017). HCC, which is one of the most aggressive and resistant cancers, has a poor prognosis (Gailhouste et al., 2018). In the United States and many other countries, the morbidity of HCC has doubled over the past two decades. Annually, the number of patients diagnosed with HCC is almost 800,000 worldwide, with approximately 750,000 causalities (Ryerson et al., 2016; Momin et al., 2017). Chronic hepatitis B and C viral infections are the most common risk factors and are responsible for approximately 75% of HCCs, leading to a twenty-fold increase in the development of HCCs (Ryerson et al., 2016). Other major risk factors include non-alcoholic fatty liver disease (NAFLD), aflatoxin B1 (AFB1) exposure obesity, and chronic alcohol consumption (Kim et al., 2014). However, the molecular mechanisms involved in the pathogenesis of HCC are still under intense investigation.

Recently, increasing evidence has identified lncRNAs as vital regulators in numerous cancers, including HCC (Chi et al., 2020; Zhou et al., 2020). Abnormal lncRNA expression exerts a considerable influence on cancer progression and carcinogenesis through several mechanisms (Lian et al., 2018; Tichon et al., 2018). For instance, LINC00346 modulates the CDK1/CCNB1 axis, consequently regulating the development of HCC and serving as a competing endogenous RNA (Jin et al., 2020). In HCC, LINC00160 mediates drug resistance and autophagy through the microRNA-132/PIK3R3 axis (Zhang et al., 2020). By modifying the genomic methylation profiles, LINC00662 can promote the progression of HCC progression (Guo et al., 2020).

We used TCGA database to analyze the differentially expressed lncRNAs and found that TMEM220-AS1 was poorly expressed in HCC; however, it is unclear whether TMEM220-AS1 is correlated with the development of HCC. To determine this, we assessed the function of TMEM220-AS1 in HCC by performing a large sample validation in a population, followed by a series of cell function tests, dual luciferase reporter gene assay, bioinformatics analysis, western blotting, and RNA binding protein immunoprecipitation (RIP) to explore the underlying molecular mechanisms of TMEM220-AS1 function. We verified that TMEM220-AS1 is a novel tumor suppressor that regulates HCC through the miR-484/*MAGI1* axis.

MATERIALS AND METHODS

Collection of Clinical Samples

From 2016 to 2018, 50 paired fresh liver tumor and adjacent normal tissues were harvested at The Affiliated Hospital of Youjiang Medical University for Nationalities. We snap-freezed these tissues at −80°C. All included subjects offered an informed consent and the research got approval from the Institutional Review Board of The Affiliated Hospital of Youjiang Medical University for Nationalities.

Cell Culture

HB611, HHCC, H-97, HuH-7, Li-7, and LO2 cell lines were acquired from the American Type Culture Collection (ATCC, Manassas, VA, United States) and the Cell Bank of the Chinese Academy of Sciences (Shanghai, China). Human immortalized liver LO2 cells were cultured in Dulbecco's modified Eagle's medium (DMEM; Gibco, United States). We cultured HCC cells in DMEM with high glucose concentration (25 mM), 1% penicillin-streptomycin, and 10% fetal bovine serum (FBS), and maintained them in a 5% CO_2 humidified incubator.

Cell Transfection

We purchased plasmid vector PLKO.1-puro from BioVector NTCC Inc., Guangzhou, China. Through chemical synthesis, we designed the related TMEM220-AS1 and *MAGI1* short hairpin RNA (shRNA) sequences (**Table 1**) and the negative control. These synthesis-related sequences were inserted into the PLKO.1-puro vector. We purchased microRNA mimics and their inhibitors from RIBOBIO, Guangzhou, China. Cells were cultured for 24 h before transfection. We then transiently transfected the cells with the corresponding vector, using Lipofectamine 3000 Transfection Reagent (Invitrogen, Carlsbad,

TABLE 1 | qRT-PCR or shRNAs related sequences.

Name		Sequence
TMEM220-AS1	Forward	5′-AGCTTCCACTCTTGTCTCCC-3′
	Reverse	5′-TGAGCAGTGATGGAGCAGAA -3′
miR-484	Forward	5′-ACACTCCAGCTGGGUAGCCCU CCCCUGACU-3′
	Reverse	5′-CTCAACTGGTGTCGTGGAGTCG GCAATTCAGTTGAGAGTCCGAG-3′
MAGI1	Forward	5′-GAACAAGGACCTGCGACATTT -3′
	Reverse	5′-ACAGCATGGCGGTAAAGGTTA -3′
E-cadherin	Forward	5′- GCTGGACCGAGAGAGTTTCC -3′
	Reverse	5′- CAAAATCCAAGCCCGTGGTG -3′
Vimentin	Forward	5′- CGGGAGAAATTGCAGGAGGA -3′
	Reverse	5′-AAGGTCAAGACGTGCCAGAG-3′
Snail	Forward	5′-TCGGAAGCCTAACTACAGCGA-3′
	Reverse	5′-AGATGAGCATTGGCAGCGAG-3′
TMEM220-AS1 shRNA #1	Forward	5′- GATCCCCTGTAATCCCAGCTACT CAGCTTCCTGTCACTGAGTAGCTGG GATTACATTTTTGGAAA-3′
	Reverse	5′- AGCTTTTCCAAAAATGTAATCCCA GCTACTCAGTGACAGGAAGCTGAGT AGCTGGGATTACAGGG-3′
TMEM220-AS1 shRNA #2	Forward	5′- GATCCCCTGGTGAAACCCCGTA TCTCCTTCCTGTCAGAGATACGGG GTTTCACCATTTTTGGAAA-3′
	Reverse	5′- AGCTTTTCCAAAAATGGTGAAACC CCGTATCTCTGACAGGAAGGAGATAC GGGGTTTCACCAGGG-3′

CA, United States) as per the manufacturer's instructions. We harvested cells that were transfected with the corresponding vector and performed quantitative real-time polymerase chain reaction (qRT-PCR) after 48 h. Each experiment was performed in triplicate.

RNA Isolation and qRT-PCR

Total RNA was extracted from cell samples using TRIzol reagent (Invitrogen). Referring to the manufacturer's instructions, RNA was reverse transcribed using the PrimerScript RT-PCR kit (Takara). RNA levels were determined using qRT-PCR analysis using the TaqMan MicroRNA Assay Kit (Applied Biosystems). We measured the relative levels of the predicted targets in triplicate on an ABI 7500 real-time PCR machine (Applied Biosystems). U6 or β-actin was used as a reference gene to normalize the expression levels of miRNAs or mRNAs. The delta Ct method was used to calculate the relative expression. The primers used in this study are shown in **Table 1**.

Cell Proliferation, Invasion, Cycle, and Apoptosis Detection

These methods are shown in **Supplementary Methods**.

Western Blotting

Total cell lysates were prepared in 1 × sodium dodecyl sulfate buffer. Next, the proteins were separated by sodium dodecyl sulfate-polyacrylamide gel electrophoresis, and total proteins were transferred onto nitrocellulose membranes. Then, with 5% non-fat milk, the membrane was blocked and incubated with primary antibodies at 4°C overnight. After incubation with antibodies specific for β-actin (ab8227, Abcam, Hong Kong, China), MAGI1 (55048-1-AP, WUHAN SANYING, Wuhan, China), E-cadherin (ab227639), vimentin (ab92547), and snail (ab216347), the membrane was incubated with goat anti-rabbit secondary antibody (ab7090) and visualized via enhanced chemiluminescence. Each experiment was performed in triplicate.

RNA Fluorescent *in situ* Hybridization (FISH)

The FISH assay was implemented using Ribo^{TM} Fluorescent *in situ* Hybridization Kit (Ribobio Company, China). The TMEM220-AS1 probe was labeled with FITC fluorescent dye, and the design and synthesis were implemented by Ribobio Company. RNA FISH was performed using a fluorescent *in situ* hybridization kit (RiboBio) following the manufacturer's instructions. Fluorescence was detected using a confocal laser scanning microscope (Leica, Germany).

RIP Assay

Following the product specifications, we adopted the EZ-magna RIP kit (Millipore, United States) to perform the RIP assay. HB611 and HuH-7 cells were collected and lysed in a full RIP lysis buffer. Cell extracts were incubated with RIP buffer containing magnetic beads conjugated to human AGO2 antibodies (ab32381, Abcam, Cambridge, United Kingdom); we used the IgG antibody (ab6702, Abcam) as control. Samples were incubated with protease K, and oscillated to digest the protein and isolate the immunoprecipitated RNA. Using a NanoDrop spectrophotometer, we measured the concentration of RNA and performed real-time PCR analysis using the purified RNA.

Dual Luciferase Reporter Gene Assay

First, we manufactured TMEM220-AS1 Wt and *MAGI1* Wt. In brief, TMEM220-AS1 and *MAGI1* fragments containing miR-484 binding sites were amplified using PCR and cloned downstream of the luciferase reporter gene in the pmirGLO vector, which were named TMEM220-AS1 Wt and *MAGI1* Wt. Using the Quickchange XL Site-Directed Mutagenesis Kit (Stratagene), we generated TMEM220-AS1 Mut and *MAGI1* Mut (mutations within the binding sites). MiR-NC and miR-484 mimic were co-transfected with TMEM220-AS1 Wt or TMEM220-AS1 Mut and *MAGI1* Wt or *MAGI1* Mut, respectively, into HEK293T cells. Cells were harvested 48 h after transfection and the Dual-Luciferase Reporter Assay System (Promega, Madison, WI, United States) was used to perform the luciferase assay.

Immunochemistry

To detect Ki-67 staining in tumor tissue samples, sections of 5 μm were cut. After dewaxing and hydration, the slides were rinsed in PBS, followed by boiling in 10 mM sodium citrate at pH 6. Then, the slides were incubated in 3% H_2O_2 for 25 min to remove horseradish peroxidase. The slides were blocked with 10% BSA after washing thrice with 1 × PBS, followed by incubation with primary anti-Ki-67 antibody (ab92742) at 4°C overnight. The slides were incubated with a secondary antibody labeled with HRP (rabbit) at room temperature for 45 min and with 3,3-diaminobenzidine tetrahydrochloride (DAB), and the immunoreactivity was visualized the next day. Finally, the slides were dehydrated and mounted with neutral gum.

Tumor Xenograft Implantation in Nude Mice

Six-week-old nude mice were randomly divided into two groups (three mice per group), and cultured with continuous access to sterile food and water in pathogen-free sterile conditions. For transfections, cells at 60–80% confluence were infected with 1×10^6 recombinant lentivirus-transducing units and 6 μg/mL Polybrene (Sigma). Stably transfected cells were selected using 2 μg/mL puromycin treatment for 2 weeks. Stably transfected cells were selected for subsequent assays via flow cytometry. Lentivirus used in this study was purchased from GenePharma (Shanghai, China). To establish the HCC xenograft model, we subcutaneously injected 5×10^6 HB611 cells stably transfected with *MAGI1* overexpression vectors or TMEM220-AS1 overexpression vectors into nude mice. Tumor growth was monitored weekly and calculated as follows: volume = (length) × $(\text{width})^2/2$. The study was approved by the Ethics Committee of The Affiliated Hospital of Youjiang Medical University for Nationalities, and experiments were performed following the NIH guidelines on animal welfare.

Lung Metastasis Assay

Briefly, 1×10^6 HB611 cells in 30 μL of 30% Matrigel were injected intravenously through the tail vein of nude mice. After

6 weeks, the mice were sacrificed, and metastatic nodules in each lung were analyzed. All animal experiments were performed according to the protocols approved by the Animal Experimental Ethics Committee of The Affiliated Hospital of Youjiang Medical University for Nationalities.

Statistical Analysis

For normally distributed data with equal variance, the difference was evaluated using a two-tailed Student's *t*-tests (two-group comparisons) or ANOVA, followed by the Bonferroni's *post hoc* test (multigroup comparisons). For non-normally distributed data or data with unequal variances, the difference was evaluated using a non-parametric Mann–Whitney *U*-test (two-group comparisons) or the Kruskal–Wallis test followed by the Bonferroni's *post hoc* test (multigroup comparisons). $P < 0.05$ determined statistical significance. All tests were performed using SPSS (version 22.0, SPSS, Chicago, IL, United States).

RESULTS

Low Level of TMEM220-AS1 in HCC Tissues and Cell Lines

Through analysis of the TCGA database, we found that TMEM220-AS1 was remarkably lower in HCC tissues than that in normal tissues (**Figure 1A**). Second, the expression level of TMEM220-AS1 in periods III and IV was lower than that in periods I and II (**Figure 1B**). TMEM220-AS1 expression levels in the tissues that were dead were lower than those in the tissues that were alive (**Figure 1C**). We verified this result in 50 HCC tissues and adjacent non-tumorous tissues. As revealed by qRT-PCR assays, TMEM220-AS1 levels were remarkably lower in HCC tissues than those in paired adjacent normal liver tissues (**Figure 1D**). We detected the mRNA level of TMEM220-AS1 in six cell lines, including one normal cell line (LO2) and five HCC cell lines (HB611, HHCC, H-97, HuH-7, and Li-7). Similarly, TMEM220-AS1 was found to be expressed at low levels in HCC cell lines compared to those in LO2 cells (**Figure 1E**). Among the HCC cell lines, the expression level of TMEM220-AS1 was the highest in HuH-7 cells and the lowest in HB611 cells. Therefore, HuH-7 and HB611 cell lines were used as cell models in subsequent studies. Data from TCGA database showed that the overall survival rate of patients with low TMEM220-AS1 levels was lower than that of patients with high TMEM220-AS1 levels (**Figure 1F**).

TMEM220-AS1 Inhibits Proliferation and Cell Cycle of HCC Cells, and Promotes Cell Apoptosis of HCC Cells

Two shRNAs targeting different sites of TMEM220-AS1 mRNA were used to knockdown TMEM220-AS1 in HuH-7 cells (**Figure 2A**). Using a TMEM220-AS1-overexpressing vector, we overexpressed TMEM220-AS1 in HB611 cells (**Figure 2A**). CCK-8 demonstrated that TMEM220-AS1

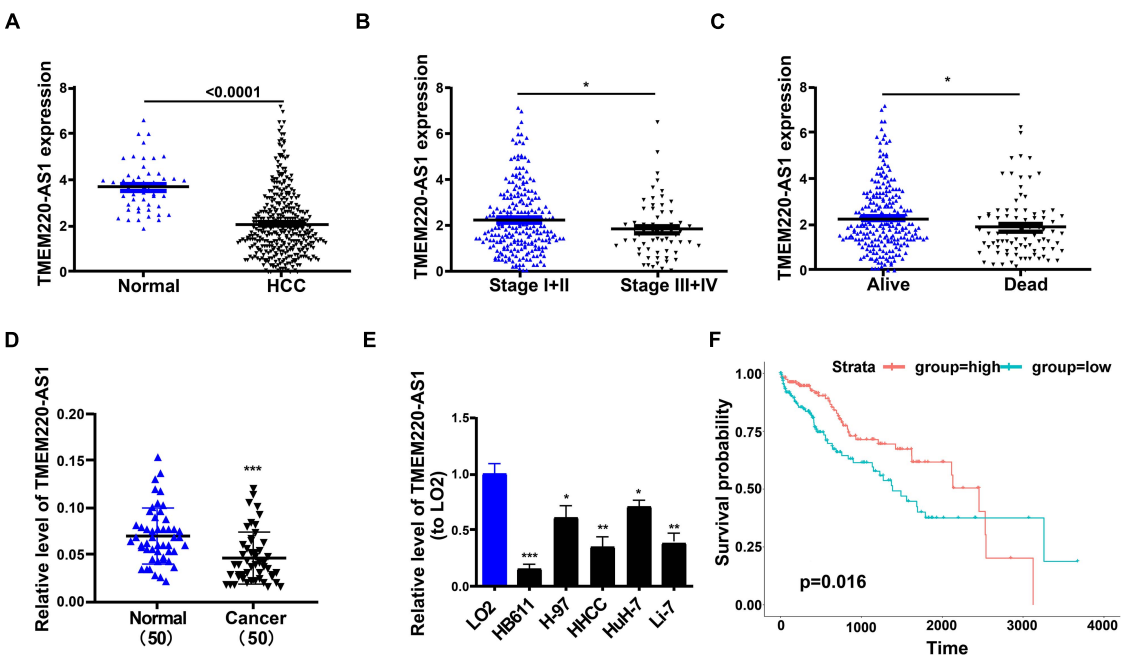

FIGURE 1 | Low level of TMEM220-AS1 in HCC tissues and cell lines. **(A)** TME M220-AS1 expression in HCC samples and normal samples, from TCGA database. **(B)** TMEM220-AS1 expression in stage I + II and stage III + IV, from TCGA database. **(C)** TMEM220-AS1 expression in alive samples and dead samples, from TCGA database. **(D)** TMEM220-AS1 expression in HCC tissues and paired adjacent normal tissues was analyzed by qRT-PCR. **(E)** TMEM220-AS1 expression in HCC cell lines and LO2 cell line was analyzed by qRT-PCR. **(F)** Kaplan-Meier curves of overall survival (OS) from TCGA database. Data represent the mean ± SD; $^{*}P < 0.05$, $^{**}P < 0.01$, $^{***}P < 0.001$.

knockdown remarkably promoted proliferation in HuH-7 cells, and overexpression of TMEM220-AS1 remarkably suppressed proliferation in HB61 cells (**Figure 2B**). Similar promotional effects of TMEM220-AS1 on HCC proliferation were also demonstrated by EdU assays (**Figure 2C**). The proportion of cells in the S phase increased when transfected with the TMEM220-AS1 shRNA, while it was decreased by TMEM220-AS1 overexpression (**Figure 2D**). Additionally, TMEM220-AS1 elevated the apoptotic rate of HB611 cells, while TMEM220-AS1 knockdown remarkably suppressed the apoptosis of HuH-7 cells (**Figure 2E**).

TMEM220-AS1 Inhibits Cell Invasion and EMT of HCC Cells

Next, we investigated whether TMEM220-AS1 regulates the invasion of HCC cells. Using the Transwell assay, the invasive ability of HCC cells was identified. Inhibited cell invasion was observed in HB611 cells transfected with the TMEM220-AS1-overexpressing vector. In contrast, TMEM220-AS1 knockdown increased cell invasion (**Figure 3A**). We also explored whether TMEM220-AS1 regulates the EMT of HCC cells. We used qRT-PCR and western blotting to observe the expression of EMT markers. E-cadherin expression was decreased while Snail

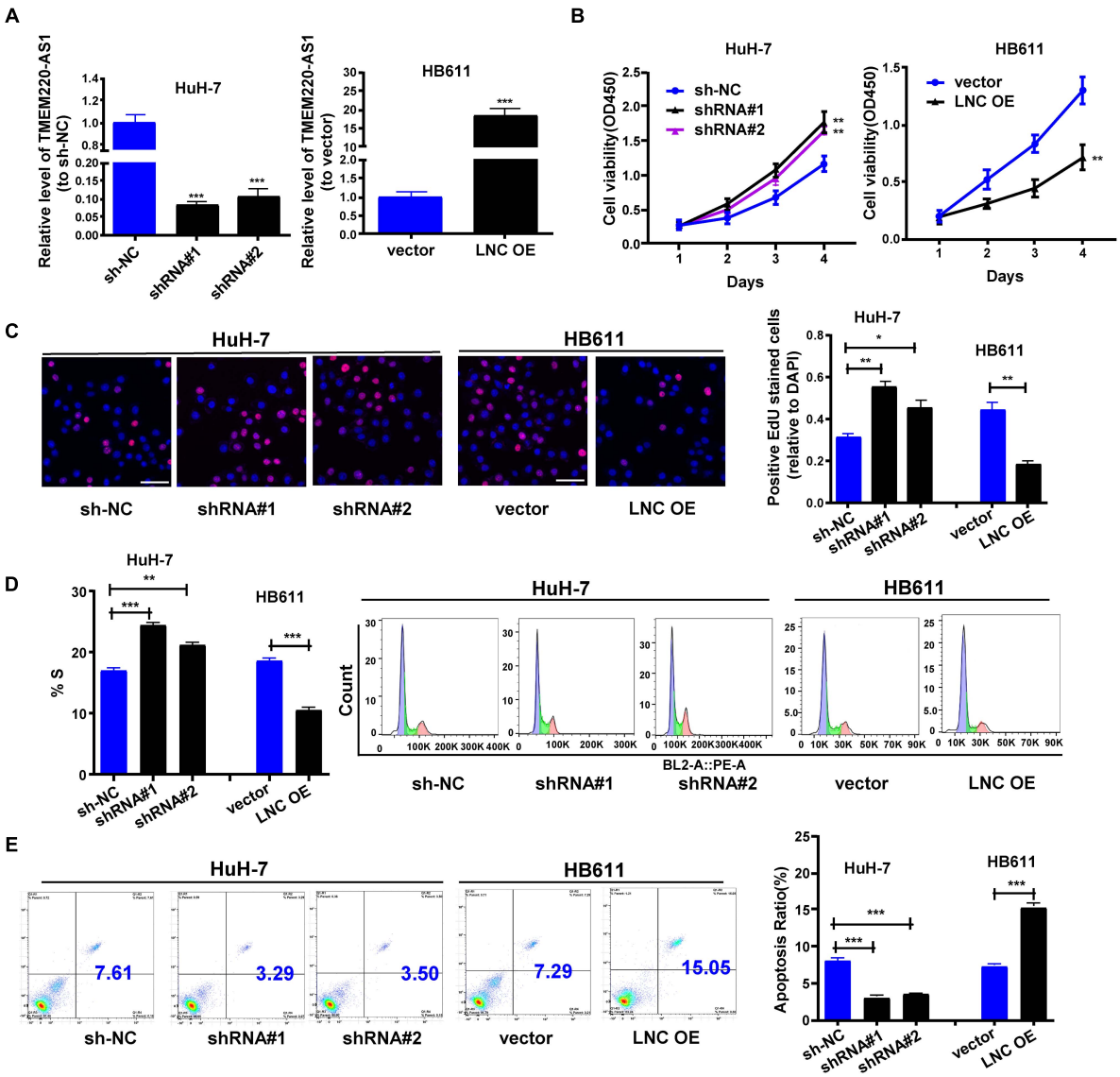

FIGURE 2 | TMEM220-AS1 inhibits the proliferation and cell cycle of HCC cells, but promotes the cell apoptosis of HCC cells. **(A)** Transfection efficiency of sh-TMEM220-AS1#1 (shRNA#1), sh-TMEM220-AS1#2 (shRNA#2) and TMEM220-AS1-overexpressing vector (LNC OE). **(B)** Cell viability was analyzed by **(B)** CCK-8 assay and **(C)** EdU assay (bar = 50 μm). **(D)** Cell cycle. **(E)** Cell apoptosis. Data were presented as represent the mean ± SD of 3 independent experiments; $^{*}P < 0.05$, $^{**}P < 0.01$, $^{***}P < 0.001$.

and vimentin expression was increased by TMEM220-AS1 knockdown in HCC cells (**Figures 3B,C**).

TMEM220-AS1 Interacted With miR-484 in a Direct Manner

The biological effects and potential molecular roles of lncRNAs are closely associated with their subcellular localization (Wen et al., 2018). We performed a nucleocytoplasmic separation experiment to determine the subcellular distribution of TMEM220-AS1. It was found that most TMEM220-AS1 was concentrated in the cytoplasm, with a minority in the nucleus (**Figure 4A**). Moreover, this was confirmed by the RNA-FISH assay (**Figure 4B**). To uncover the underlying mechanisms of TMEM220-AS1 function, we searched for potential targets using the LncBase Experimental v.2. Fourteen miRNAs (hsa-miR-6825-5p, hsa-miR-4776-3p, hsa-miR-3064-5p, hsa-miR-6825-5p, hsa-miR-4515, hsa-miR-877-3p, hsa-miR-6504-5p, hsa-miR-1236-3p, hsa-miR-4695-5p, hsa-miR-1276, hsa-miR-185-3p, hsa-miR-670-3p, hsa-miR-6799-5p, and hsa-miR-484) with a score greater than 0.85 were selected as potential research objects. The results of the RNA pull-down assay with biotin-labeled TMEM220-AS1 in HuH-7 cells showed that hsa-miR-4776-3p, hsa-miR-6825-5p, hsa-miR-6504-5p, hsa-miR-185-3p, and hsa-miR-484 could be pulled down by TMEM220-AS1 (**Figure 4C**). Then, we silenced the expression of TMEM220-AS1 in HuH-7 and HB611 cells; only miR-484 was remarkably upregulated (**Figure 4D**). Therefore, we chosen miR-484 as the study subject. To further identify whether miR-484 could interact with TMEM220-AS1 directly, we conducted dual luciferase reporter and RIP assays. The binding sites of wild-type (TMEM220-AS1 Wt) and mutant-type (TMEM220-AS1 Mut) are shown in **Figure 4E**. Dual luciferase reporter assays in HEK293T cells demonstrated that luciferase activity was remarkably reduced by co-transfection with TMEM220-AS1 Wt and miR-484 mimics (**Figure 4F**). Using the RIP assay, we further validated the interaction between miR-484 and TMEM220-AS1. We found that both TMEM220-AS1 and miR-484 were enriched in AGO2-containing miRNA ribonucleoprotein complexes (**Figure 4G**). Consistently, both TCGA database and our dataset showed that miR-484 expression in HCC tumor samples was higher than that in negative control samples (**Figures 4H,I**). Moreover, TMEM220-AS1 expression levels were negatively correlated with miR-484 expression in HCC samples, both in the TCGA database and our dataset (**Figures 4J,K**). Taken together, the above results proved that TMEM220-AS1 was targeted by miR-484.

TMEM220-AS1 Regulates the miR-484 Target Gene, MAGI1

Target genes of miR-484 were screened out through MIRDB, and the top five mRNAs (*MAGI1*, *TNRC6C*, *HOXA5*, *PTPRE*, and *ACVR1B*) according to their scores were selected as potential research subjects. Only *MAGI1* expression was inhibited by miR-484 overexpression in HCC cells (**Figure 5A**). In addition, studies have shown that *MAGI1* inhibits cancer cell migration and invasion in HCC (Zhang and Wang, 2011; Zhang et al., 2012). Therefore, we chose *MAGI1* as the study object. We showed the binding sites of wild-type (*MAGI1* Wt) and mutant-type (*MAGI1* Mut) (**Figure 5B**). Dual luciferase reporter assays demonstrated that luciferase activity was remarkably reduced by

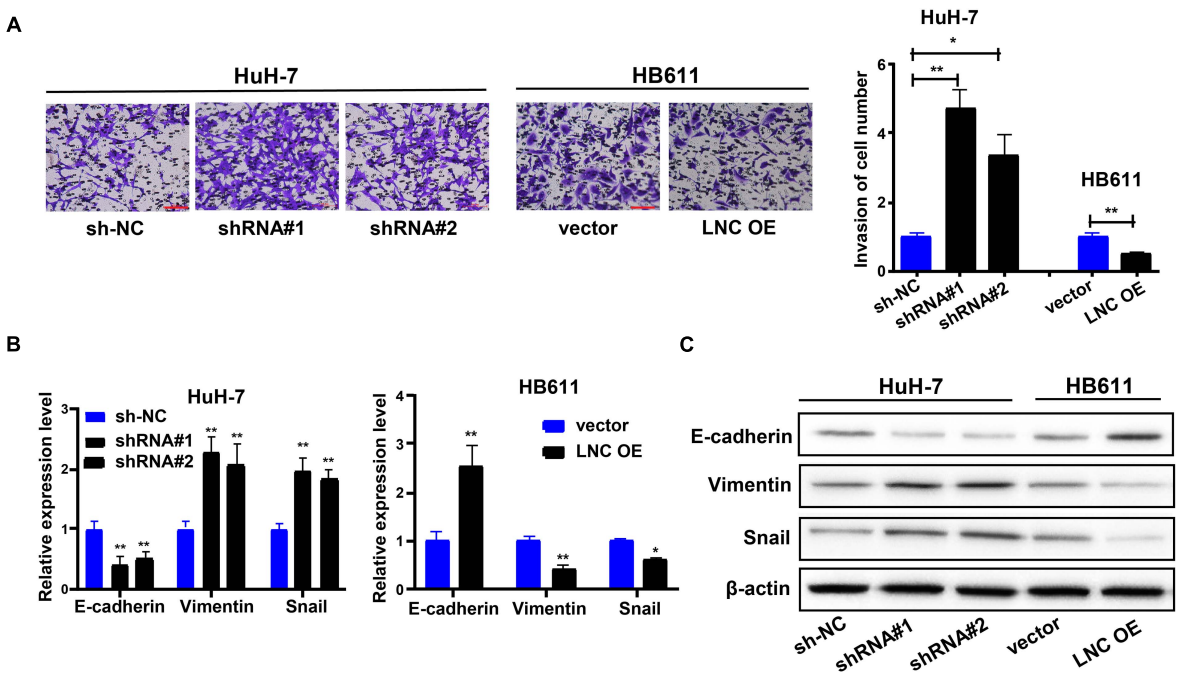

FIGURE 3 | TMEM220-AS1 inhibits the cell invasion and EMT of HCC cells. **(A)** Cell invasion was determined using Transwell assay (bar = 100 μm). **(B,C)** The expression of EMT markers were determined using qRT-PCR and western blot assay. Data were presented as represent the mean ± SD of 3 independent experiments; *$P < 0.05$, **$P < 0.01$.

MAGI1 Wt and miR-484 mimic co-transfection (**Figure 5C**). Both the TCGA database and our dataset showed that *MAGI1* gene expression in HCC samples was lower than that in negative control samples (**Figures 5D,G**). Moreover, *MAGI1* expression levels were negatively correlated with miR-484 expression in HCC samples (**Figures 5E,H**), but it was positively correlated with TMEM220-AS1 expression in HCC samples, according to the TCGA database and our dataset (**Figures 5F,I**). Altogether, *MAGI1* was indicated to be a target gene of miR-484.

Next, we used western blotting to investigate whether TMEM220-AS1 can modulate the expression of MAGI1 in HCC cells via miR-484. The results showed that MAGI1 expression levels were inhibited by sh-TMEM220-AS1 and miR-484 mimics (**Figures 5J,K**). MAGI1 expression was promoted

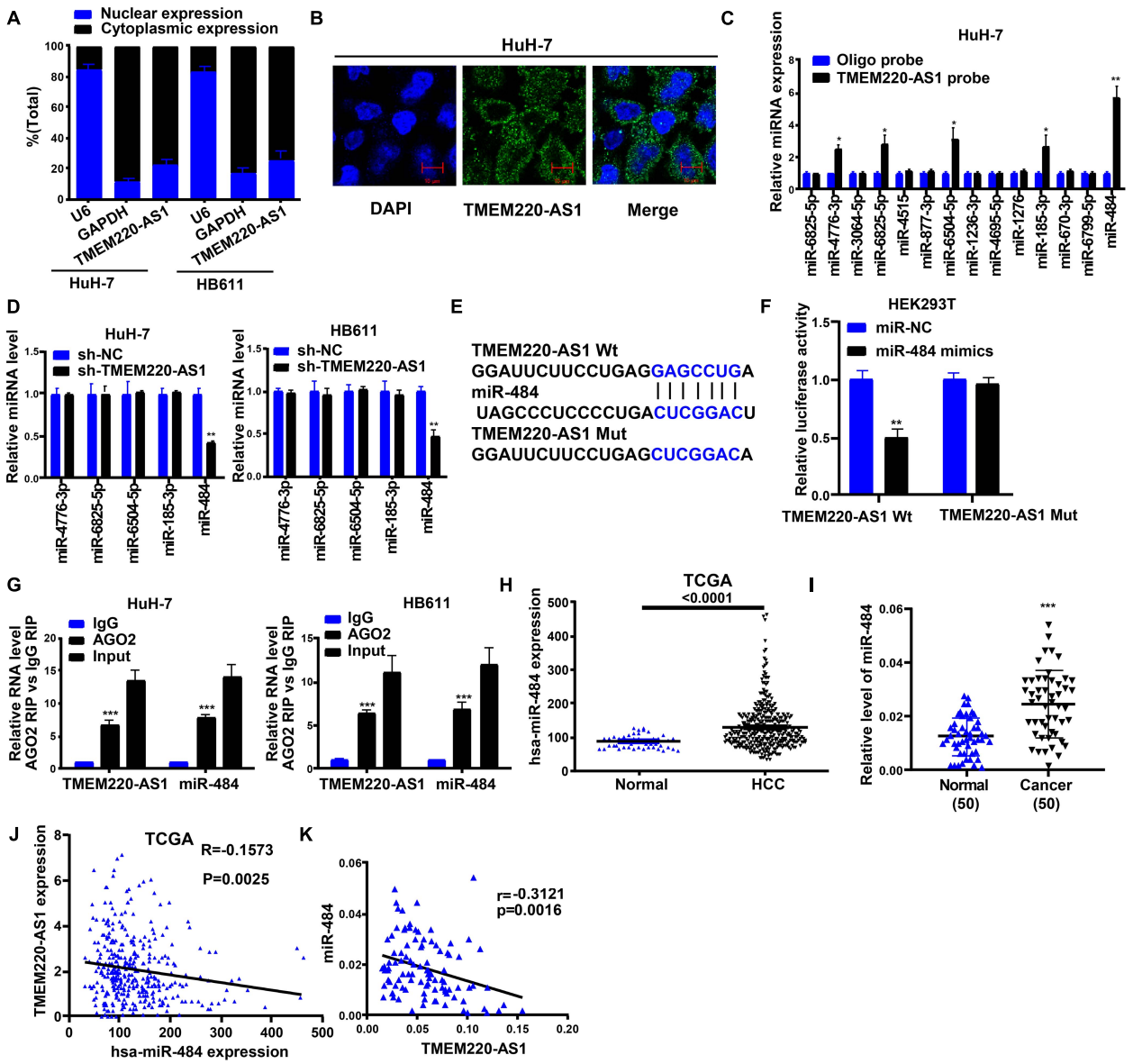

FIGURE 4 | TMEM220-AS1 is targeted by miR-484. **(A,B)** Localization of TMEM220-AS1 by nucleocytoplasmic separation experiment and RNA-FISH in HCC cells (bar = 10 μm). **(C)** The relative expression of candidate miRNAs which could potentially bind to TMEM220-AS1 were quantified by qRT-PCR after the biotinylated-TMEM220-AS1 pull-down assays in HuH-7 cells. **(D)** The levels of miRNAs after TMEM220-AS1 cutdown were tested by qRT-PCR. **(E)** Putative miR-484 binding sequence and mutation sequence of TMEM220-AS1 mRNA were as shown. **(F)** Dual luciferase reporter assays were used to confirm the direct target between TMEM220-AS1 and miR-484. **(G)** RIP assay was used to detect whether miR-484 could bind with TMEM220-AS1. **(H)** miR-484 expression in HCC samples and normal samples, from TCGA database. **(I)** The correlation analysis between miR-484 expression and TMEM220-AS1 expression in HCC samples and normal samples, from TCGA database. **(J)** miR-484 expression in HCC tumor tissues and adjacent non-tumorous tissues. **(K)** The correlation analysis between miR-484 expression and TMEM220-AS1 expression in HCC tumor tissues and adjacent non-tumorous tissues, from our dataset. Data were presented as represent the mean ± SD; $^{*}P < 0.05$, $^{**}P < 0.01$, $^{***}P < 0.001$.

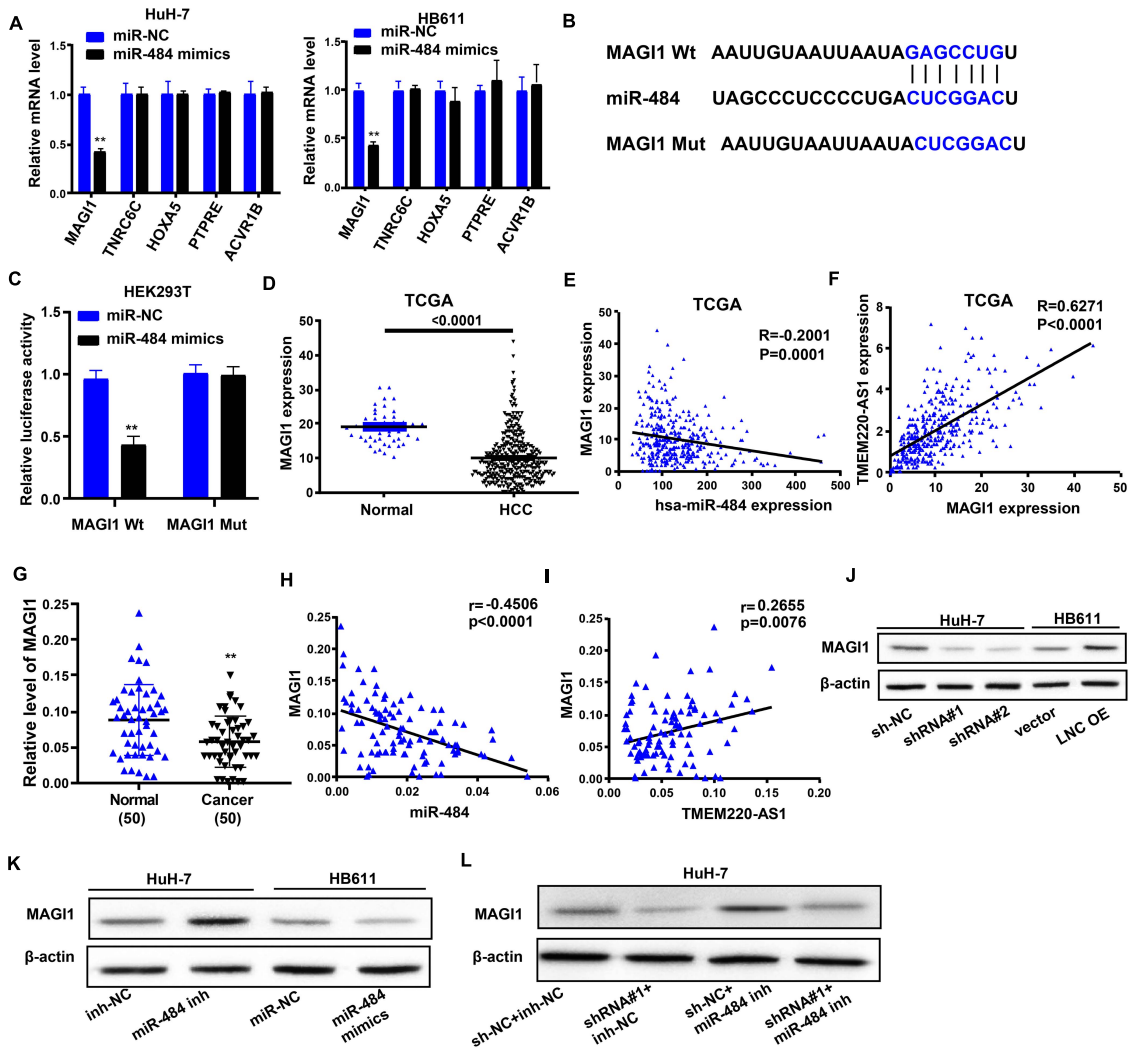

FIGURE 5 | TMEM220-AS1 regulates the miR-484 target gene, *MAGI1*. **(A)** The levels of mRNAs after miR-484 cutdown were tested by qRT-PCR. **(B)** Putative miR-484 binding sequence and mutation sequence of *MAGI1* mRNA were as shown. **(C)** Dual luciferase reporter assays were used to confirm the direct target between *MAGI1* and miR-484. **(D)** *MAGI1* gene expression in HCC samples and normal samples, from TCGA database. **(E)** The correlation analysis between miR-484 expression and *MAGI1* expression in HCC samples and normal samples, from TCGA database. **(F)** The correlation analysis between TMEM220-AS1 expression and *MAGI1* expression in HCC samples and normal samples, from TCGA database. **(G)** *MAGI1* gene expression in HCC tissues and paired adjacent normal tissues, from our dataset. **(H)** The correlation analysis between miR-484 expression and *MAGI1* expression in HCC tissues and paired adjacent normal tissues, from our dataset. **(I)** The correlation analysis between TMEM220-AS1 expression and *MAGI1* expression in HCC tissues and paired adjacent normal tissues, from our dataset. **(J–L)** The level of MAGI1 was detected by western blot assay. Data were presented as represent the mean ± SD; $^{**}P < 0.01$.

by TMEM220-AS1 overexpression and miR-484 inhibitor (**Figures 5J,K**). Knockdown of miR-484 partially reversed MAGI1 inhibition due to the silencing of TMEM220-AS1 in HuH-7 cells (**Figure 5L**). The results indicated that TMEM220-AS1 modulated MAGI1 expression in an miR-484-dependent manner in HCC cells. The transfection efficiency of miR-484 inhibitor and miR-484 mimics is shown in **Supplementary Figures 1A,B**.

MAGI1 Inhibited the Proliferation, Invasion, and Tumor Formation of HCC

To investigate the role of *MAGI1* in HCC, we used *MAGI1* shRNA to silence the expression of *MAGI1* in the HuH-7 cell line (**Supplementary Figure 1C**), and *MAGI1* overexpression vectors were used to increase the expression of *MAGI1* in the HB611 cell line (**Supplementary Figure 1D**). CCK-8 assays demonstrated that *MAGI1* knockdown inhibited HuH-7 cell growth, and *MAGI1* overexpression promoted HB611 cell growth (**Figure 6A**). Similarly, *MAGI1* knockdown inhibited the invasion of HuH-7 cells, and *MAGI1* overexpression promoted the invasion of HB611 cells (**Figure 6B**). *In vivo*, HB611 cells transfected with *MAGI1* overexpression vectors were subcutaneously injected into nude mice. The tumor lumps are shown in **Figure 6C**. The tumor volumes (**Figure 6D**) and weights (**Figure 6E**) in *MAGI1* overexpression group were clearly inhibited compared to those in the vector group.

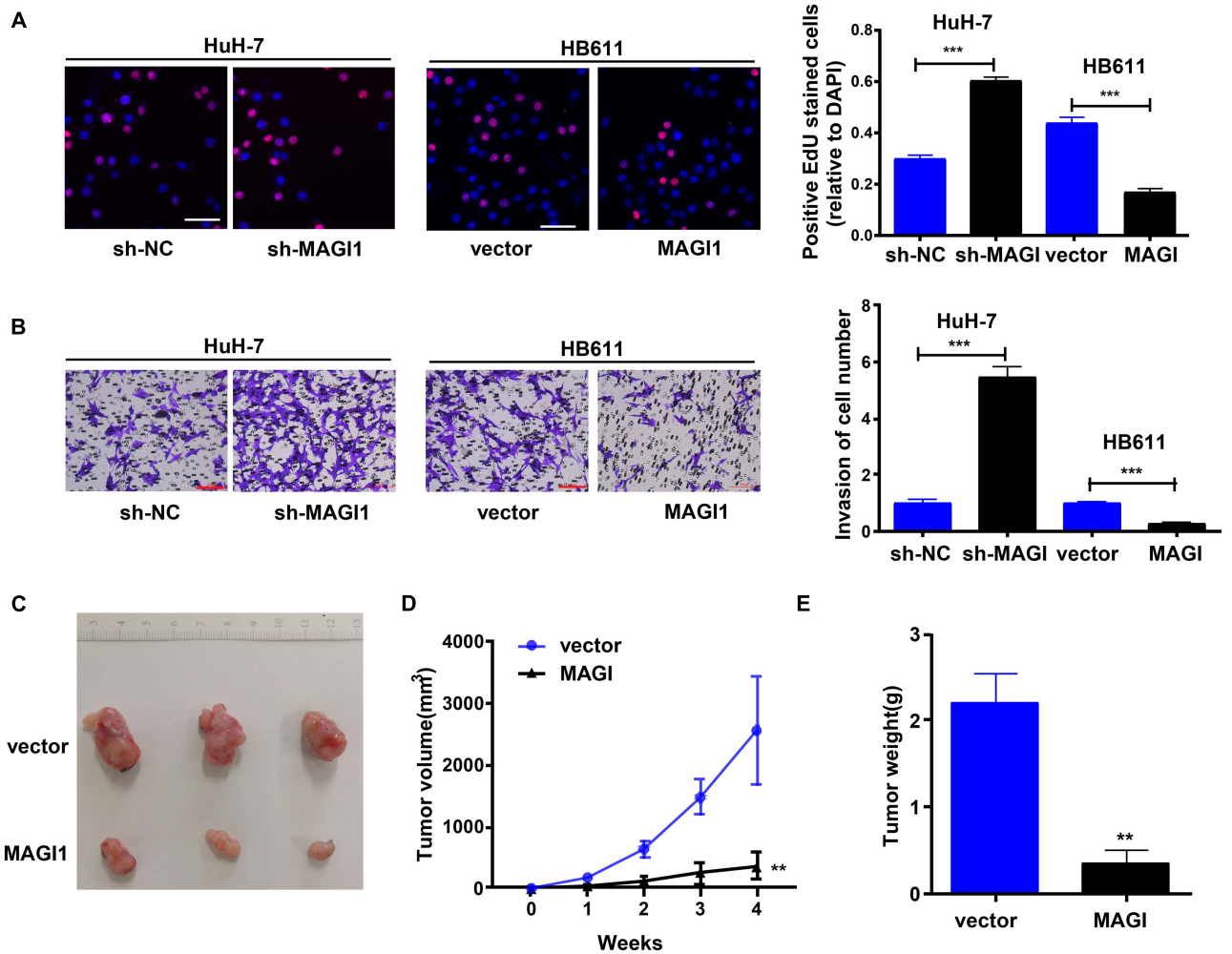

FIGURE 6 | *MAGI1* inhibited the proliferation, invasion, and tumor formation of HCC. **(A)** Cell viability was analyzed by EdU assay (bar = 50 μm). **(B)** Transwell assays were used to determine the invasion of HCC cells (bar = 100 μm). **(C)** Representative image of tumors formed in nude mice from empty vector and *MAGI1* overexpression vector groups. **(D)** Tumor volume and **(E)** weight data of indicated orthotopic xenografts. $^{**}P < 0.01$, $^{***}P < 0.001$.

TMEM220-AS1/miR-484 Axis Regulates Behaviors of HCC Cells

Subsequently, we explored the effect of the TMEM220-AS1/miR-484 axis on HCC. We transfected HuH-7 cells and divided them into sh-NC + inh-NC, sh-TMEM220-AS1#1 (shRNA#1) + inh-NC group, sh-NC + miR-484 inh group, and sh-TMEM220-AS1#1 (shRNA#1) + miR-484 inh group. First, the EdU assay showed that cell proliferation was increased by silencing TMEM220-AS1, but it was decreased by miR-484 inhibitor, and miR-484 inhibitor treatment reversed the promoting effect of TMEM220-AS1 silencing on cell proliferation (**Figure 7A**). Next, the proportion of cells in the S-phase was increased by silencing TMEM220-AS1, while miR-484 inhibitor decreased the proportion of cells in S-phase. The effect of TMEM220-AS1 shRNA on the cell cycle was reversed by co-transfection with the miR-484 inhibitor (**Figure 7B**). In addition, the miR-484 inhibitor promoted cell apoptosis. Knockdown of TMEM220-AS1 downregulated cell apoptosis, but the effect of TMEM220-AS1 knockdown on cell apoptosis could be reversed by co-transfection with miR-484 inhibitor (**Figure 7C**). Finally, cell invasion was increased by silencing TMEM220-AS1; however, it was decreased by the miR-484 inhibitor. Moreover, miR-484 inhibitor treatment reversed the effect of TMEM220-AS1 silencing on cell invasion (**Figure 7D**).

TMEM220-AS1 Overexpression Limited the Growth and Metastasis of HCC *in vivo*

We generated xenograft models to verify the findings in this study. HB611 cells transfected with TMEM220-AS1 overexpression vectors were subcutaneously or intravenously injected into nude mice. The results showed that TMEM220-AS1 overexpression greatly limited tumor proliferation *in vivo* (**Figures 8A–C**). The tumors collected from the mice are shown in **Figure 8A**. Tumor growth in the vector group was faster than that in the TMEM220-AS1 overexpression

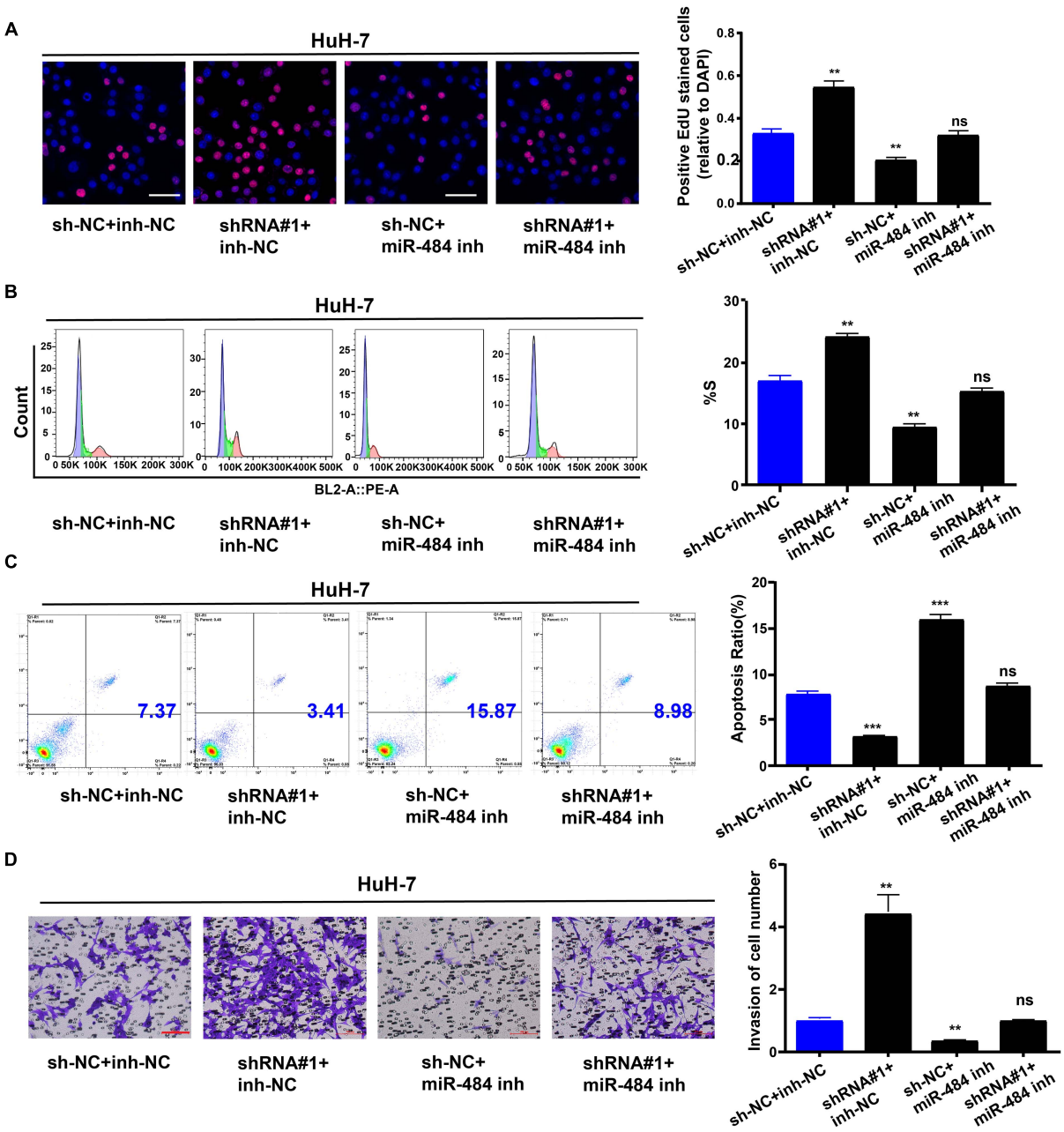

FIGURE 7 | TMEM220-AS1/miR-484 axis regulates behaviors of HCC cells. **(A)** EdU assays were used to determine the cell proliferation ability of HuH-7 cells. **(B)** Cell cycle (bar = 50 μm). **(C)** Cell apoptosis. **(D)** Cell invasion (bar = 100 μm). Data were presented as represent the mean ± SD of 3 independent experiments; $^{**}P < 0.01$, $^{***}P < 0.001$, ns, no significance.

group, both in volume and weight (**Figures 8B,C**). qRT-PCR and western blotting indicated that upregulation of TMEM220-AS1 increased the expression of MAGI1 and E-cadherin, but inhibited vimentin and Snail *in vivo* (**Figures 8D,E**). Immunohistochemistry also showed that TMEM220-AS1 promoted MAGI1 expression, but decreased Ki-67 expression in xenograft tumor tissues (**Figure 8F**). Moreover, TMEM220-AS1 overexpression in pulmonary metastasis models greatly decreased the incidence of pulmonary metastasis (**Figure 8G**). Thus, TMEM220-AS1 inhibits HCC growth and metastasis *in vivo*.

DISCUSSION

HCC is a frequently detected malignant tumor of the digestive system, and its occurrence is associated with the unrestricted proliferation of hepatocytes (Jin et al., 2018). Therefore, any

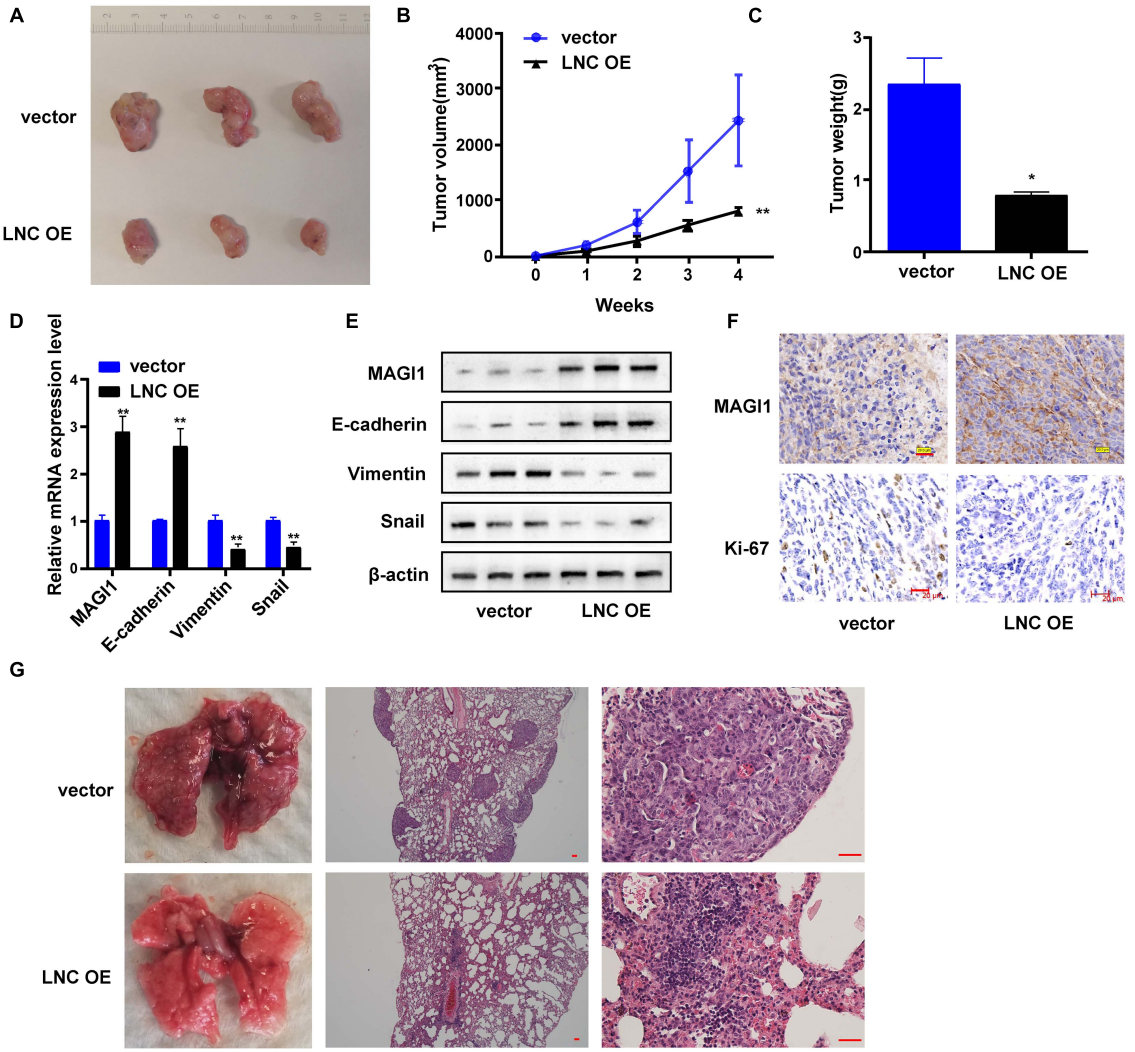

FIGURE 8 | TMEM220-AS1 overexpression limited the growth and metastasis of HCC *in vivo*. **(A)** Representative images of tumors from indicated orthotopic xenografts. **(B)** Tumor volume and **(C)** weight data of indicated orthotopic xenografts. **(D,E)** mRNA and protein expression levels of MAGI1 and EMT-related markers after TMEM220-AS1 overexpression. **(F)** The expression level of MEGI1 and Ki-67 determined using immunohistochemistry (bar = 20 μm). **(G)** Representative images of lung metastases of indicated orthotopic xenografts (bar = 50 μm). Data were presented as represent the mean ± SD; $^{*}P < 0.05$, $^{**}P < 0.01$.

cause of hepatocyte proliferation may lead to HCC. In recent years, lncRNAs have become a focus of tumor-related research, and there is much evidence that they can participate in the modulation of cancer cell migration, proliferation, and apoptosis (Chen et al., 2020; Nekvindova et al., 2020; Shang et al., 2020; Wang et al., 2020). In this study, TMEM220-AS1 was selected by analyzing TCGA database, which was poorly expressed in HCC samples and was associated with clinical staging and survival prognosis. Then, we verified the low expression of TMEM220-AS1 in a large population-based sample (n = 50), and the results of subsequent cell function experiments showed that the downregulation of TMEM220-AS1 promoted cell proliferation, cell cycle, invasion, and EMT process, while cell apoptosis was inhibited. Next, we studied the specific mechanism of TMEM220-AS1 in HCC.

It has been shown that lncRNAs can interact with miRNAs and regulate target mRNAs (Bo et al., 2020; Lyu et al., 2020). For example, AGAP2-AS1 promotes ANXA11 expression by sponging miR-16-5p and promotes proliferation and metastasis in HCC (Liu et al., 2019). Another study showed that the growth and epithelial-to-mesenchymal transition phenotype was regulated by the LINC01287/miR-298/STAT3 feedback loop in HCC cells (Mo et al., 2018). In addition, the migration and invasion of HCC cells were promoted by the lncRNA n335586/miR-924/CKMT1A axis (Fan et al., 2018). In our study, LncBase Experimental v.2 was used to predict miRNAs that might bind to TMEM220-AS1, and RNA pull-down, interference experiments with TMEM220-AS1, dual luciferase reporter assay, RIP, and qRT-PCR results indicated that TMEM220-AS1 acts as a molecular sponge for miR-484. Moreover, miR-484 has

been reported to promote non-small cell lung cancer (Li et al., 2017) and HCC (Qiu et al., 2019) progression. Subsequent results also confirmed that miR-484 inhibitor curbed the invasion, proliferation, and cell cycle of HuH-7 cells and promoted the apoptosis of HuH-7 cells. Moreover, miR-484 inhibitor can partially reverse the effects of TMEM220-AS1 shRNA on the proliferation, invasion, cell cycle, and apoptosis of HCC cells.

The downstream target genes of miR-484 were predicted using MIRDB. The top five mRNAs (*MAGI1*, *TNRC6C*, *HOXA5*, *PTPRE*, and *ACVR1B*) according to their scores were selected as potential research subjects. Only *MAGI1* expression was inhibited by miR-484 overexpression in HCC cells. A dual luciferase reporter assay was performed to confirm the binding relationship between miR-484 and *MAGI1*. Some studies have indicated that in estrogen receptor-positive breast cancer, *MAGI1* is a new potential tumor suppressor gene (Alday-Parejo et al., 2020). Via the Wnt/β-Catenin and PTEN/AKT signaling pathways, *MAGI1* silencing inhibits apoptosis of glioma cells and promotes proliferation (Lu et al., 2019). Moreover, by regulating PTEN, *MAGI1* curbed the invasion and migration of HCC (Zhang and Wang, 2011). In summary, our study confirmed that *MAGI1* was the downstream target gene of miR-484, and TMEM220-AS1 released *MAGI1* through competitive binding of miR-484. *MAGI1* inhibited the proliferation, invasion, and tumor formation of HCC.

This research has several limitations. First, U6 and GAPDH (or 18S) should be added as controls in RNA-FISH assay. Second, it's better to measure EMT-related proteins in lung metastasis by Immunochemistry or Immunofluorescence.

CONCLUSION

In conclusion, TMEM220-AS1 acts as a tumor suppressor that inhibits HCC cell proliferation and metastasis, while promoting apoptosis through the miR-484/*MAGI1* axis.

DATA AVAILABILITY STATEMENT

The original contributions presented in the study are included in the article/**Supplementary Material**, further inquiries can be directed to the corresponding author/s.

ETHICS STATEMENT

The studies involving human participants were reviewed and approved by the Affiliated Hospital of Youjiang Medical University for Nationalities. The patients/participants provided their written informed consent to participate in this study. The animal study was reviewed and approved by the Affiliated Hospital of Youjiang Medical University for Nationalities. Written informed consent was obtained from the individual(s) for the publication of any potentially identifiable images or data included in this article.

AUTHOR CONTRIBUTIONS

SC and JQL designed and supervised the study. CC, JL, and GL performed the experiments. GH and ZD collected and analyzed the data. BH and JY supported administration, technique and materials. CC prepared the manuscript. SC revised the manuscript. All authors read and approved the final manuscript.

FUNDING

This study was supported by the National Natural Science Foundation of Guangxi Province (No. 2020JJA140192), the Young and middle-aged teachers' basic scientific research ability improvement project in Guangxi Colleges and Universities (No. 2020KY13020), the Innovation Project of GuangXi Graduate Education (No. JGY2020166), the National Natural Science Foundation of China (No. 82070679), and Hunan Province Science and Technology Grant (No. 2019GK5010).

SUPPLEMENTARY MATERIAL

The Supplementary Material for this article can be found online at: https://www.frontiersin.org/articles/10.3389/fcell.2021.681529/full#supplementary-material

REFERENCES

Alday-Parejo, B., Richard, F., Worthmuller, J., Rau, T., Galvan, J. A., Desmedt, C., et al. (2020). MAGI1, a new potential tumor suppressor gene in estrogen receptor positive Breast Cancer. *Cancers* 12:223. doi: 10.3390/cancers12010223

Anwanwan, D., Singh, S. K., Singh, S., Saikam, V., and Singh, R. (2020). Challenges in liver cancer and possible treatment approaches. *Biochim. Biophys. Acta Rev. Cancer* 1873:188314. doi: 10.1016/j.bbcan.2019.188314

Bo, H., Liu, Z., Zhu, F., Zhou, D., Tan, Y., Zhu, W., et al. (2020). Long noncoding RNAs expression profile and long noncoding RNA-mediated competing endogenous RNA network in nonobstructive azoospermia patients. *Epigenomics* 12, 673–684. doi: 10.2217/epi-2020-0008

Chen, Z., Pan, T., Jiang, D., Jin, L., Geng, Y., Feng, X., et al. (2020). The lncRNA-GAS5/miR-221-3p/DKK2 Axis modulates ABCB1-Mediated adriamycin resistance of Breast Cancer via the Wnt/beta-Catenin Signaling Pathway. *Mol. Ther. Nucleic Acids* 19, 1434–1448. doi: 10.1016/j.omtn.2020.01.030

Chi, Y., Gong, Z., Xin, H., Wang, Z., and Liu, Z. (2020). Long noncoding RNA lncARSR promotes nonalcoholic fatty liver disease and hepatocellular carcinoma by promoting YAP1 and activating the IRS2/AKT pathway. *J. Transl. Med.* 18:126. doi: 10.1186/s12967-020-02225-y

Fan, H., Lv, P., Mu, T., Zhao, X., Liu, Y., Feng, Y., et al. (2018). LncRNA n335586/miR-924/CKMT1A axis contributes to cell migration and invasion in hepatocellular carcinoma cells. *Cancer Lett.* 429, 89–99. doi: 10.1016/j.canlet.2018.05.010

Gailhouste, L., Liew, L. C., Yasukawa, K., Hatada, I., Tanaka, Y., Nakagama, H., et al. (2018). Differentiation therapy by epigenetic reconditioning exerts antitumor

effects on Liver Cancer Cells. *Mol. Ther.* 26, 1840–1854. doi: 10.1016/j.ymthe.2018.04.018

Guo, T., Gong, C., Wu, P., Battaglia-Hsu, S. F., Feng, J., Liu, P., et al. (2020). LINC00662 promotes hepatocellular carcinoma progression via altering genomic methylation profiles. *Cell Death Differ.* 27, 2191–2205. doi: 10.1038/s41418-020-0494-3

Jin, J., Xu, H., Li, W., Xu, X., Liu, H., and Wei, F. (2020). LINC00346 acts as a competing endogenous RNA regulating development of hepatocellular carcinoma via modulating CDK1/CCNB1 Axis. *Front. Bioeng. Biotechnol.* 8:54. doi: 10.3389/fbioe.2020.00054

Jin, L., He, Y., Tang, S., and Huang, S. (2018). LncRNA GHET1 predicts poor prognosis in hepatocellular carcinoma and promotes cell proliferation by silencing KLF2. *J. Cell Physiol.* 233, 4726–4734. doi: 10.1002/jcp.26257

Kim, Y., Ejaz, A., Tayal, A., Spolverato, G., Bridges, J. F., Anders, R. A., et al. (2014). Temporal trends in population-based death rates associated with chronic liver disease and liver cancer in the United States over the last 30 years. *Cancer* 120, 3058–3065. doi: 10.1002/cncr.28843

Li, T., Ding, Z. L., Zheng, Y. L., and Wang, W. (2017). MiR-484 promotes non-small-cell lung cancer (NSCLC) progression through inhibiting Apaf-1 associated with the suppression of apoptosis. *Biomed. Pharmacother.* 96, 153–164. doi: 10.1016/j.biopha.2017.09.102

Lian, Y., Xiong, F., Yang, L., Bo, H., Gong, Z., Wang, Y., et al. (2018). Long noncoding RNA AFAP1-AS1 acts as a competing endogenous RNA of miR-423-5p to facilitate nasopharyngeal carcinoma metastasis through regulating the Rho/Rac pathway. *J. Exp. Clin. Cancer Res.* 37:253. doi: 10.1186/s13046-018-0918-9

Liu, Z., Wang, Y., Wang, L., Yao, B., Sun, L., Liu, R., et al. (2019). Long non-coding RNA AGAP2-AS1, functioning as a competitive endogenous RNA, upregulates ANXA11 expression by sponging miR-16-5p and promotes proliferation and metastasis in hepatocellular carcinoma. *J. Exp. Clin. Cancer Res.* 38:194. doi: 10.1186/s13046-019-1188-x

Lu, Y., Sun, W., Zhang, L., and Li, J. (2019). Silencing Of magi1 promotes the proliferation and inhibits apoptosis of glioma cells Via The Wnt/beta-Catenin And PTEN/AKT signaling pathways. *Onco Targets Ther.* 12, 9639–9650. doi: 10.2147/OTT.S215400

Lyu, K., Li, Y., Xu, Y., Yue, H., Wen, Y., Liu, T., et al. (2020). Using RNA sequencing to identify a putative lncRNA-associated ceRNA network in laryngeal squamous cell carcinoma. *RNA Biol.* 17, 977–989. doi: 10.1080/15476286.2020.1741282

Mo, Y., He, L., Lai, Z., Wan, Z., Chen, Q., Pan, S., et al. (2018). LINC01287/miR-298/STAT3 feedback loop regulates growth and the epithelial-to-mesenchymal transition phenotype in hepatocellular carcinoma cells. *J Exp. Clin. Cancer Res.* 37:149. doi: 10.1186/s13046-018-0831-2

Momin, B. R., Pinheiro, P. S., Carreira, H., Li, C., and Weir, H. K. (2017). Liver cancer survival in the United States by race and stage (2001-2009): findings from the CONCORD-2 study. *Cancer* 123(Suppl. 24), 5059–5078. doi: 10.1002/cncr.30820

Nakagawa, H., Fujita, M., and Fujimoto, A. (2019). Genome sequencing analysis of liver cancer for precision medicine. *Semin. Cancer Biol.* 55, 120–127. doi: 10.1016/j.semcancer.2018.03.004

Nekvindova, J., Mrkvicova, A., Zubanova, V., Vaculova, A. H., Anzenbacher, P., Soucek, P., et al. (2020). Hepatocellular carcinoma: gene expression profiling and regulation of xenobiotic-metabolizing cytochromes P450. *Biochem. Pharmacol.* 117:113912. doi: 10.1016/j.bcp.2020.113912

Qiu, L., Huang, Y., Li, Z., Dong, X., Chen, G., Xu, H., et al. (2019). Circular RNA profiling identifies circADAMTS13 as a miR-484 sponge which suppresses cell proliferation in hepatocellular carcinoma. *Mol. Oncol.* 13, 441–455. doi: 10.1002/1878-0261.12424

Rahmani, J., Kord Varkaneh, H., Kontogiannis, V., Ryan, P. M., Bawadi, H., Fatahi, S., et al. (2020). Waist circumference and risk of liver cancer: a systematic review and meta-analysis of over 2 million cohort study participants. *Liver Cancer* 9, 6–14. doi: 10.1159/000502478

Ringelhan, M., McKeating, J. A., and Protzer, U. (2017). Viral hepatitis and liver cancer. *Philos. Trans. R. Soc. Lond. B Biol. Sci.* 372:20160274. doi: 10.1098/rstb.2016.0274

Ryerson, A. B., Eheman, C. R., Altekruse, S. F., Ward, J. W., Jemal, A., Sherman, R. L., et al. (2016). Annual Report to the nation on the Status of Cancer, 1975-2012, featuring the increasing incidence of liver cancer. *Cancer* 122, 1312–1337. doi: 10.1002/cncr.29936

Shang, R., Wang, M., Dai, B., Du, J., Wang, J., Liu, Z., et al. (2020). Long noncoding RNA SLC2A1-AS1 regulates aerobic glycolysis and progression in hepatocellular carcinoma via inhibiting the STAT3/FOXM1/GLUT1 pathway. *Mol. Oncol.* 14, 1381–1396. doi: 10.1002/1878-0261.12666

Tichon, A., Perry, R. B., Stojic, L., and Ulitsky, I. (2018). SAM68 is required for regulation of Pumilio by the NORAD long noncoding RNA. *Genes Dev.* 32, 70–78. doi: 10.1101/gad.309138.117

Wang, J., Ding, W., Xu, Y., Tao, E., Mo, M., Xu, W., et al. (2020). Long non-coding RNA RHPN1-AS1 promotes tumorigenesis and metastasis of ovarian cancer by acting as a ceRNA against miR-596 and upregulating LETM1. *Aging* 12, 4558–4572. doi: 10.18632/aging.102911

Wen, X., Gao, L., Guo, X., Li, X., Huang, X., Wang, Y., et al. (2018). lncSLdb: a resource for long non-coding RNA subcellular localization. *Database* 2018, 1–6. doi: 10.1093/database/bay085

Zhang, G., Liu, T., and Wang, Z. (2012). Downregulation of MAGI1 associates with poor prognosis of hepatocellular carcinoma. *J. Invest. Surg.* 25, 93–99. doi: 10.3109/08941939.2011.606875

Zhang, G., and Wang, Z. (2011). MAGI1 inhibits cancer cell migration and invasion of hepatocellular carcinoma via regulating PTEN. *Zhong Nan Da Xue Xue Bao Yi Xue Ban* 36, 381–385. doi: 10.3969/j.issn.1672-7347.2011.05.002

Zhang, W., Liu, Y., Fu, Y., Han, W., Xu, H., Wen, L., et al. (2020). Long non-coding RNA LINC00160 functions as a decoy of microRNA-132 to mediate autophagy and drug resistance in hepatocellular carcinoma via inhibition of PIK3R3. *Cancer Lett.* 478, 22–33. doi: 10.1016/j.canlet.2020.02.014

Zhou, Y., Huang, Y., Hu, K., Zhang, Z., Yang, J., and Wang, Z. (2020). HIF1A activates the transcription of lncRNA RAET1K to modulate hypoxia-induced glycolysis in hepatocellular carcinoma cells via miR-100-5p. *Cell Death Dis.* 11:176. doi: 10.1038/s41419-020-2366-7

Conflict of Interest: The authors declare that the research was conducted in the absence of any commercial or financial relationships that could be construed as a potential conflict of interest.

Publisher's Note: All claims expressed in this article are solely those of the authors and do not necessarily represent those of their affiliated organizations, or those of the publisher, the editors and the reviewers. Any product that may be evaluated in this article, or claim that may be made by its manufacturer, is not guaranteed or endorsed by the publisher.

frontiers in Cell and Developmental Biology

ORIGINAL RESEARCH
published: 24 August 2021
doi: 10.3389/fcell.2021.678670

Cancer-Associated Fibroblasts Promote Vascular Invasion of Hepatocellular Carcinoma via Downregulating Decorin-integrin β1 Signaling

Xiaobo Zheng[1†], Peng Wang[1†], Li Li[2], Jing Yu[1], Chune Yu[1], Liangliang Xu[1], Lian Li[1], Fuzhen Dai[3], Lei Feng[4], Hong Zou[1,5], Xiaobo Chen[6], Ming Zhang[1,7] and Mingqing Xu[1,6]*

[1] Department of Liver Surgery, West China Hospital, Sichuan University, Chengdu, China, [2] Institute of Clinical Pathology, West China Hospital of Sichuan University, Chengdu, China, [3] Department of General Surgery, The First People's Hospital of Longquanyi District, Chengdu, China, [4] Department of Biliary Surgery, West China Hospital, Sichuan University, Chengdu, China, [5] General Surgery Center of PLA, General Hospital of Western Theater Command, Chengdu, China, [6] Department of Hepatopancreatobiliary Surgery, Meishan City People's Hospital, Meishan Hospital of West China Hospital, Sichuan University, Meishan, China, [7] Department of General Surgery, Mianzhu Hospital of West China hospital, Sichuan University, Mianzhu, China

Hepatocellular carcinoma (HCC) is a common malignancy worldwide, and the high ratio of recurrence and metastasis remains the main cause of its poor prognosis. Vascular invasion of HCC includes microvascular invasion (MVI) and portal vein tumor thrombosis (PVTT) and is regarded as a common roadmap of intrahepatic metastasis in HCC. However, the molecular mechanism underlying vascular invasion of HCC is largely unknown. Here, we analyzed the transcriptomes of primary tumors, PVTT tissues, and tumor tissues with or without MVI. We found that extracellular matrix-related pathways were involved in vascular invasion of HCC and that decorin secreted by cancer-associated fibroblasts was gradually downregulated from normal to tumor tissues and more so in PVTT tissues. We also established that low-level decorin expression is an independent risk factor for MVI and it is associated with a poor prognosis. Decorin downregulated integrin β1 and consequently inhibited HCC cell invasion and migration *in vitro*. Co-staining DCN and integrin β1 revealed that DCN dynamically regulated integrin β1 protein expression. Integrin β1 knockdown significantly inhibited HCC invasion and migration, and decorin combined with such knockdown synergistically augmented the anti-metastatic effects. Co-IP assay confirmed the direct interaction of decorin with integrin β1. Our findings showed that targeting cancer-associated fibroblast-related decorin is not only a promising strategy for inhibiting HCC vascular invasion and metastasis but also provides insight into the clinical treatment of patients with PVTT.

Keywords: hepatocellular carcinoma, vascular invasion, portal vein tumor thrombosis, cancer-associated fibroblasts, tumor microenvironment, decorin-integrin β1 signaling

OPEN ACCESS

Edited by:
Jiang Chen,
Zhejiang University, China

Reviewed by:
Wanessa Altei,
Federal University of Sao Carlos, Brazil
Haiwei Mou,
Cold Spring Harbor Laboratory, United States

****Correspondence:***
Mingqing Xu
xumingqing0018@163.com

† These authors have contributed equally to this work

Specialty section:
This article was submitted to Molecular and Cellular Oncology, a section of the journal Frontiers in Cell and Developmental Biology

Received: *10 March 2021*
Accepted: *10 May 2021*
Published: *24 August 2021*

Citation:
Zheng X, Wang P, Li L, Yu J, Yu C, Xu L, Li L, Dai F, Feng L, Zou H, Chen X, Zhang M and Xu M (2021) Cancer-Associated Fibroblasts Promote Vascular Invasion of Hepatocellular Carcinoma via Downregulating Decorin-integrin β1 Signaling. Front. Cell Dev. Biol. 9:678670. doi: 10.3389/fcell.2021.678670

INTRODUCTION

Hepatocellular carcinoma (HCC) is a common malignancy worldwide and the fourth leading cause of cancer-related death (Bray et al., 2018). High rates of recurrence and metastasis, even after systemic treatment, comprise the main causes of a poor prognosis for patients with HCC (Forner et al., 2018). Intrahepatic metastasis derived from vascular invasion (VI) of HCC, accounts for 90% of metastases and is the primary profile of HCC metastasis (Tabrizian et al., 2015). Vascular invasion is a process of intrahepatic dissemination in which aggressive tumor cells invade blood vessels and spread to distant organs. Vascular invasion is a common phenomenon in HCC, and microvascular invasion (MVI) and portal vein tumor thrombosis (PVTT) are found in 44.0–62.2% of patients with HCC at autopsy (Lu J. et al., 2019). Vascular invasion has been regarded as an independent risk factor for a poor prognosis (Renne et al., 2020). The median overall survival (OS) of untreated patients who have HCC with PVTT is ∼ 4 months (Roayaie et al., 2009). The clinical management of such patients has been intensively investigated, and guidelines for surgical and palliative therapy have been established (Lu J. et al., 2019; Wei et al., 2019; Zhang et al., 2019). Because the mechanism of VI in HCC is not well understood, clinical treatment remains challenging. Biomarkers such as circular RNA (Fransvea et al., 2009) and imaging methods (Huang et al., 2020) have recently been applied to predict MVI, and VI in HCC has been analyzed by multi-omics (Zhang et al., 2015; Yang et al., 2017; Sulaiman et al., 2019). However, the fundamental molecular mechanism underlying VI in HCC remains largely unknown.

Tumors comprise a complex ecosystem that includes the tumor microenvironment (TME) immune cells, fibroblasts, and endothelial cells (Hernandez-Gea et al., 2013; Fu et al., 2019; Lu C. et al., 2019; Craig and von Felden, 2020). Encouraging results from recent clinical trials of therapy with immune checkpoint inhibitors have encouraged research focus on the TME (Le et al., 2015; Finn et al., 2020). Fibroblasts are a central component of the TME, and cancer-associated fibroblasts (CAFs) are involved in tumor carcinogenesis and progression. CAFs regulate tumor-initiating cell plasticity in HCC through c-Met/FRA1/HEY1 signaling (Lau et al., 2016). Peri-tumor-associated fibroblasts promote intrahepatic HCC metastasis by recruiting cancer stem cells (Jiang et al., 2017), and targeting CAFs has generated encouraging results as HCC anti-tumor therapy (Kubo et al., 2016; Lau et al., 2016; Jiang et al., 2017). However, how CAFs mediate VI to promote HCC metastasis remains poorly understood.

Decorin (DCN) is a prototypical small leucine-rich proteoglycan and important component of the cellular microenvironment or extracellular matrix (ECM) (Feugaing et al., 2013). The *DCN* gene is a marker of fibroblasts and is most commonly distributed in fibroblasts (Neill et al., 2016). Its interactions with matrix and cell membrane components have been implicated in many physiological and pathophysiological processes, including matrix organization, signal transduction, wound healing, cell migration, inhibition of metastasis, and angiogenesis (Järveläinen et al., 2015). Decorin binds with high affinity to various receptor tyrosine kinases including Met, EGFR, IGF-IR, PDGFR, and VEGFR2, to induce a multitude of oncosuppressive functions, including the inhibition of tumor growth and progression (Bi et al., 2008; Horváth et al., 2014). Decorin also acts as a pro-inflammatory agent by modulating macrophage function and cytokine secretion (Jármay et al., 2000). Therefore, DCN is an ideal therapeutic candidate for controlling solid malignancies. However, how DCN regulates VI in HCC remains unclear.

We analyzed the transcriptomes of primary tumor and PVTT tissues from patients with HCC, as well as tumor tissues with or without MVI. We established that ECM-related pathways mediated VI by HCC, and that DCN gradually became downregulated from normal to tumor and further in PVTT tissues. We found that DCN was mainly expressed in fibroblasts, indicating that these cells promoted VI by HCC by regulating DCN secretion. We also found that DCN expression in tumor tissues was associated with MVI, and that low DCN expression was associated with a poor prognosis. Decorin inhibited the invasion and migration of HCC by downregulating integrin β1 *in vitro*.

MATERIALS AND METHODS

Data Acquisition

We obtained data about patients with HCC tumors, PVTT tissues, and mRNA sequences from GSE77509 in the Gene Expression Omnibus (GEO) database. The HCC tumor tissues with MVI and without the MVI mRNA sequencing set and patient personal information and clinical pathological features were obtained from The Cancer Genome Atlas (TCGA) database[1]. For further verification, we downloaded independent microarray datasets (GSE69164, GSE74656) from GEO. According to the publication guidelines, the datasets can be used for publication without restriction or limitation[2,3].

Patients and Specimens

Paired normal, tumor and PVTT tissues were collected from patients with HCC at West China Hospital, Sichuan University, Chengdu, China. Detailed clinicopathological parameters for each patient were extracted from the digital health care system of West China Hospital. The Biomedical Ethics Committee of West China Hospital approved the study protocols, and all patients signed written, informed consent forms.

Cell Culture

We maintained the HCCLM3, HEK293T, and Hep3B cells (Cell Bank of Type Culture Collection, Chinese Academy of Sciences, Shanghai, China) maintained in Dulbecco's modified Eagle medium (DMEM)/high glucose medium (Hyclone, Logan, UT, United States) supplemented with 10% fetal bovine serum (FBS) (PAN-Biotek, Aidenbach, Bavaria) and 1% penicillin-streptomycin (Hyclone) at 37℃ in a humidified 5% CO_2 atmosphere. The authenticity of the cell line was verified by DNA

[1]http://www.cbioportal.org/

[2]https://cancergenome.nih.gov/publications/publicationguidelines

[3]https://www.ncbi.nlm.nih.gov/geo/info/disclaimer.html

fingerprinting before use. We explored the function of 1 and 4 μg/mL of polypeptide DCN (R&D Systems, Minneapolis, MN, United States) in HCC HCCLM3 and Hep3B cells *in vitro* in the above medium. Blank medium was the control.

RNA Extraction and Quantitative Real-Time PCR (qRT-PCR)

Total RNA was extracted from each specimen using Trizol (Invitrogen, Carlsbad, CA, United States) as described by the manufacturer. The concentration and quality of RNA were assessed by measuring absorbance ratios of A260/A280 and A260/A280 using a ScanDrop Nuclear Acid Analyzer (Analytik Jena GmbH, Jena, Germany). Complementary DNAs (cDNAs) were generated using Reverse Transcription System Kits (Vazyme Biotech Co., Ltd., Nanjing, China), and amplified by qRT-PCR in triplicate using Maxima SYBR Green qPCR Master Mix (Vazyme) on a CFX connect real-time system (Bio-Rad, Hercules, CA, United States) as described by the manufacturer. The glyceraldehyde 3-phosphate dehydrogenase (GAPDH) gene was the internal control for each gene. Relative expression levels of each gene were calculated using the $2^{-\Delta\Delta Ct}$ method. We determined ΔCt by subtracting the Ct of GAPDH mRNA from that of each gene. **Table 1** shows the qRT-PCR primers.

Integrin β1 Lentivirus shRNA Constructs

The core sequence for constructing an shRNA plasmid targeting integrin β1 was 5′- GCCTTGCATTACTGCTGATAT-3′. Lentivirus preparations were produced by co-transfecting the helper virus packaging plasmids pMD2.G, psPAX2, and pLKO.1 puro (empty vector or containing shRNA) into HEK293T cells. Supernatants containing viruses were collected after 48-h incubation.

Protein Isolation and Western Blotting

Total protein was lysed in RIPA buffer (Beyotime Biotechnology, Shanghai, China) containing 1% protease inhibitor (Cell Signaling Technology, Danvers, MA, United States). Proteins in lysates were quantified using Pierce bicinchoninic acid (BCA) protein assay kits (Beyotime Biotechnology), and then 30 μg were separated by 10% SDS-PAGE and transferred to polyvinylidene fluoride (PVDF) membranes. Non-specific protein binding was blocked with 5% non-fat dry milk in Tris buffered saline-Tween (TBST) for at least 1 h, then the membranes were incubated at 4°C overnight with the following primary antibodies diluted 1:1,000 unless otherwise stated: DCN (ab175404), integrin α1 (ab243032), integrin α3 (ab242196), integrin α11 (ab198826, 1:800 dilution; all from Abcam, Cambridge, United Kingdom), vimentin (5741S), N-cadherin (13116S), β-catenin (8480S), E-cadherin (3195S), HER2/ErbB2 (4290S), integrin β5 (3629S), integrin β1 (34971S; all from Cell Signaling Technology), TGF beta-1 (MA5-16949), and TGF beta-2 (710276; diluted 1:750, both from Thermo Fisher Scientific Inc., Waltham, MA, United States), MMP2 (10373-2-AP undiluted; Proteintech, Group Inc., Rosemont, IL, United States) and GAPDH (200306-7E4 diluted 1:2,000; Zen BioScience, China). The membranes were then incubated with secondary antibody diluted 1:5,000 (Zenbio, Chengdu, China) at 37°C for 1 h and immersed in SuperSignal West Femto Agent (Millipore Sigma Co., Ltd., Burlington, MA, United States). Protein signals were detected by the Chemical Mp Imaging System (Bio-Rad) and proteins were quantified using ImageJ. The internal reference was GAPDH.

Immunofluorescence Assays

Normal, tumor, and PVTT tissues were fixed in 4% paraformaldehyde, embedded in paraffin, and cut into 4-μm sections. After three washes with PBS, non-specific protein binding was blocked with 5% bovine serum albumin (BSA) at room temperature for 1 h. The sections were incubated at 4°C overnight with anti-DCN diluted 1:200, and anti-E-cadherin, anti-αSMA, and anti-integrin β1 all diluted 1:100. The sections were incubated on the following day with a 1:500-diluted secondary antibody labeled with a fluorescent dye (Life Technologies Corporation, Carlsbad, CA, United States) at 37°C for 40 min and stained with DAPI for 10 min at room temperature. Stained cells were visualized by fluorescence microscopy (Leica, Mannheim, Germany) or Nikon N-STORM confocal microscopy (Nikon Corp., Tokyo, Japan).

Immunoprecipitation (IP)

Cells on ice were lysed using a buffer provided with Co-IP kits containing protease inhibitors (abs955; Absin Bioscience Inc., Shanghai, China), as described by the manufacturer. Lysates were centrifuged at 14,000 × g at 4°C for 10 min, and then the soluble fraction was clarified by incubation with protein

TABLE 1 | Primers used in our study.

Primer name	Forward	Reverse
DCN	CAGTGTTCTGATTTGGGTCT	CCATCTTTGATTTCGGTTAT
COL1A1	GAGGGCCAAGACGAAGACATC	CAGATCACGTCATCGCACAAC
COL3A1	GGAGCTGGCTACTTCTCGC	GGGAACATCCTCCTTCAACAG
COL4A1	GGGATGCTGTTGAAAGGTGAA	GGTGGTCCGGTAAATCCTGG
Fibronectin 1	GAGAATAAGCTGTACCATCGCAA	CGACCACATAGGAAGTCCCAG
Integrin α5	GCCTGTGGAGTACAAGTCCTT	AATTCGGGTGAAGTTATCTGTGG
Integrin β3	AGTAACCTGCGGATTGGCTTC	GTCACCTGGTCAGTTAGCGT
GAPDH	ACTCCTCCACCTTTGACGC	GCTGTAGCCAAATTCGTTGTC

qPCR quantitative polymerase chain reaction, DCN decorin.

A/G agarose beads. Proteins in the cleared supernatant were immunoprecipitated using the indicated primary antibodies at 4°C overnight, then incubated with Protein A/G beads at 4°C for 12 h. The immunoprecipitated complexes were rinsed and western blotted. The positive control was Input.

Wound Healing Assays

Cells cultured in 6-well plates were scratched using a sterilized pipet tip, gently rinsed with PBS, then in DMEM/high glucose medium containing 0.5% FBS and 1% penicillin/streptomycin. Images were acquired using an Olympus digital camera every 24 h.

Transwell Assays

Cells were suspended in 300 μL of serum-free DMEM medium, and placed in the upper chamber of 24-well Transwell chambers (MilliporeSigma Co., Ltd., Burlington, MA, United States) coated with Matrigel with 8-μm pores (BD Biosciences, San Jose, CA, United States). Chemoattractant medium containing 10% FBS was placed in the lower chamber. Cells that did not penetrate the matrix after 48 h were removed. The inserts were then visualized by staining with 0.2% crystal violet and counted using an inverted microscope.

Statistical Analysis

Data were statistically analyzed using GraphPad Prism 8 (GraphPad Software, San Diego, CA, United States) and SPSS version 25.0 (IBM Inc., Armonk, NY, United States). Normally distributed data are presented as means ± standard deviation (SD). If the 95% confidence interval (CI) did not include the value 1, then values with $P < 0.05$ were considered statistically significant. Differences between datasets were assessed using one-way ANOVA and two-tailed Student *t*-tests. The cut-off value was the median expression of DCN. Risk factors associated with MVI were identified by univariate and multivariate binary logistic regression analyses. Kaplan-Meier survival curves were plotted and survival was compared using log-rank tests.

RESULTS

Pathways Associated With ECM Are Involved in VI by HCC

We analyzed changes in the transcriptomes of malignant cells during VI to understand the molecular mechanism of VI by HCC. Clinical samples of PVTT are available as this is a common stage of macrovascular invasion by HCC. Therefore, we compared the transcriptome of primary tumor samples with that of PVTT tissues. We reanalyzed the RNA-seq data of 20-paired primary tumor and PVTT tissues from the GEO GSE77509 datasets. Transcript profiles varied between primary tumor and PVTT tissues, and numerous differentially expressed genes (DEGs) were identified between these tissues (**Figure 1A**). We analyzed Gene Ontology (GO)/Kyoto Encyclopedia of Genes and Genomes (KEGG) enrichment of these DEGs to identify which molecular signatures were enriched. The significantly enriched ECM-related pathways were cytokine-cytokine receptor interaction, ECM organization, regulation of integrin activation, and collagen fibril organization (**Figure 1B**). The ECM-related genes, *DCN*, *COL11A1*, *LAMC3*, and *COL25A1*, were also significantly downregulated in PVTT, compared with primary tumor tissues (**Figure 1C**), indicating that the ECM is involved in macrovascular invasion by HCC.

To confirm that the ECM is involved in the formation of MVI, we compared transcriptomic alterations between tumor tissues with and without MVI derived from patients with TNM stage I HCC from TCGA. The DEGs that were significantly upregulated in the group with MVI compared with the group without MVI were not exclusively upregulated in PVTT tissues, possibly because of the high degree of tumor heterogeneity among patients (**Figure 1D**). Notably, the expression of DEGs that were significantly downregulated in the group with MVI relative to that without MVI was consistently lower across patients with MVI. These findings indicated that these genes play fundamental roles in regulating MVI development (**Figure 1D**). The downregulated genes in the MVI group were significantly enriched in ECM-related pathways (**Figure 1E**), which agreed with the dysregulated pathways between the primary tumor and PVTT samples (**Figure 1B**). Similarly, the ECM-related genes *BMP7*, *COL2A1*, *COL22A1*, and *COL28A1*, were significantly downregulated in the group with MVI (**Figure 1F**). Collectively, these results indicated that the downregulation of ECM-related pathways is an important molecular event mediating the entire process of VI, from MVI to macrovascular invasion.

Downregulation of DCN Secreted by CAFs Facilitated VI by HCC

We analyzed DEGs that were involved in the ECM pathway to identify potential molecules that downregulate ECM pathways and promote VI by HCC. We analyzed intersects of the DEGs enriched in the ECM pathway (**Figures 1B,E**) between GSE77509 and TCGA cohorts to identify common dysregulated genes. A Venn diagram revealed that the ECM-related genes, *DCN*, *TMEM100*, *COL25A1*, *LAM2*, *TPSAB1*, and *CXCL14*, were simultaneously dysregulated in both cohorts (**Figure 2A**). To confirm the recurrent downregulation of these genes during VI by HCC, we analyzed the mRNA expression levels of these genes in normal, tumor, and PVTT tissues from internal and external cohorts. We found that DCN gradually decreased during progress from normal to primary tumor and metastatic tissues from the public GSE69164 dataset and in our cohort (**Figures 2B,D**). The expression of DCN was significantly downregulated in PVTT, compared with normal tissues in the public GSE74656 dataset. Although less DCN was expressed in PVTT, than in tumor tissues in GSE74656, the values did not reach statistical significance because of the small sample size (**Figure 2C**). These results confirmed that DCN expression was downregulated in tumor tissues and further downregulated in PVTT tissues at the mRNA

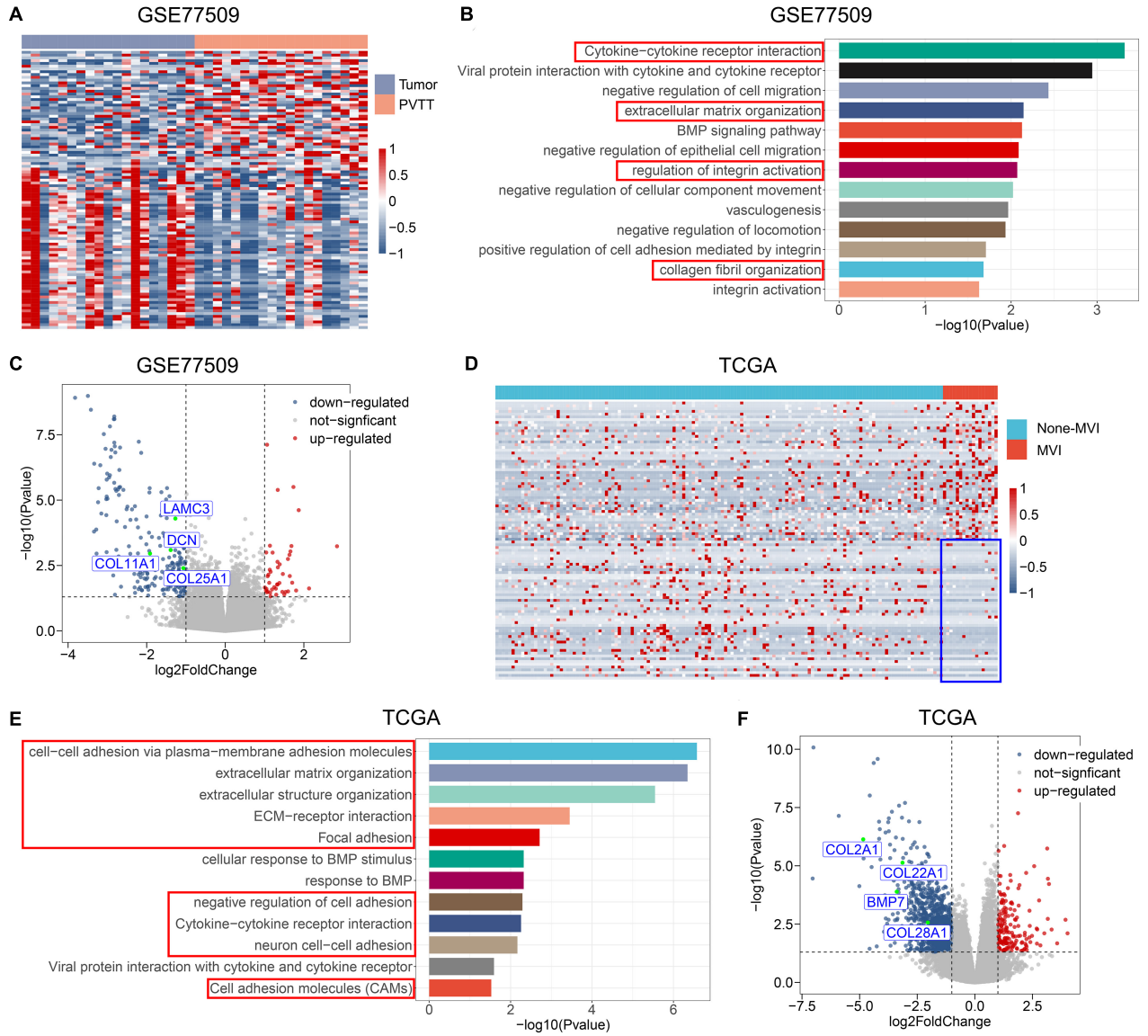

FIGURE 1 | ECM-related pathways and genes are involved in vascular invasion of HCC. **(A)** Heatmap of top 20 DEGs between tumor tissues and PVTT tissues from public dataset GSE77509; the colors represent Z-Score of log-normalized data. **(B)** The significantly altered molecular pathways between tumor tissues and PVTT tissues from public dataset GSE77509. Red frame indicates ECM-related pathways. **(C)** Volcano plot of DEGs in tumor tissues and PVTT tissues from public dataset GSE77509; multiple ECM-associated genes are shown. **(D)** Heatmap of top 20 DEGs between none-MVI tumor tissues and MVI tumor tissues from TCGA; the colors represent Z-Score of log-normalized data. Blue frame indicates consistent lower expression of top 20 downregulated genes in MVI group across patients. **(E)** The significantly altered molecular pathways between none-MVI tumor tissues and MVI tumor tissues from TCGA. Red frame indicates ECM-related pathways. **(F)** Volcano plot of DEGs in none-MVI tumor tissues and MVI tumor tissues from TCGA, and multiple ECM-associated genes are represented. MVI, microvascular invasion; TCGA, The Cancer Genome Atlas.

level, suggesting that DCN plays anti-tumorigenic and anti-metastatic roles.

We then analyzed DCN expression at the protein level in clinical tissues from our cohort. Immunoblotting findings showed that DCN gradually decreased from normal tissue adjacent to tumors, to primary tumors and more so in PVTT tissues (**Figure 2E** and **Supplementary Figure 1**). To confirm the subcellular location of DCN, we immunohistochemically co-stained E-cadherin with DCN and alpha-smooth muscle actin (a-SMA) in formalin-fixed paraffin-embedded samples. a-SMA is considered as the main marker of fibroblasts in numerous cancers (Lau et al., 2016; Jiang et al., 2017). The finding that DCN co-localized with a-SMA but not E-cadherin indicated that DCN is preferentially expressed in fibroblasts and not in epithelial cells (**Figures 2F,G**). This was consistent with the finding that DCN secreted by fibroblasts is a matrix-mediating agent in cancer development (Neill et al., 2016). In addition, DCN was gradually downregulated from normal

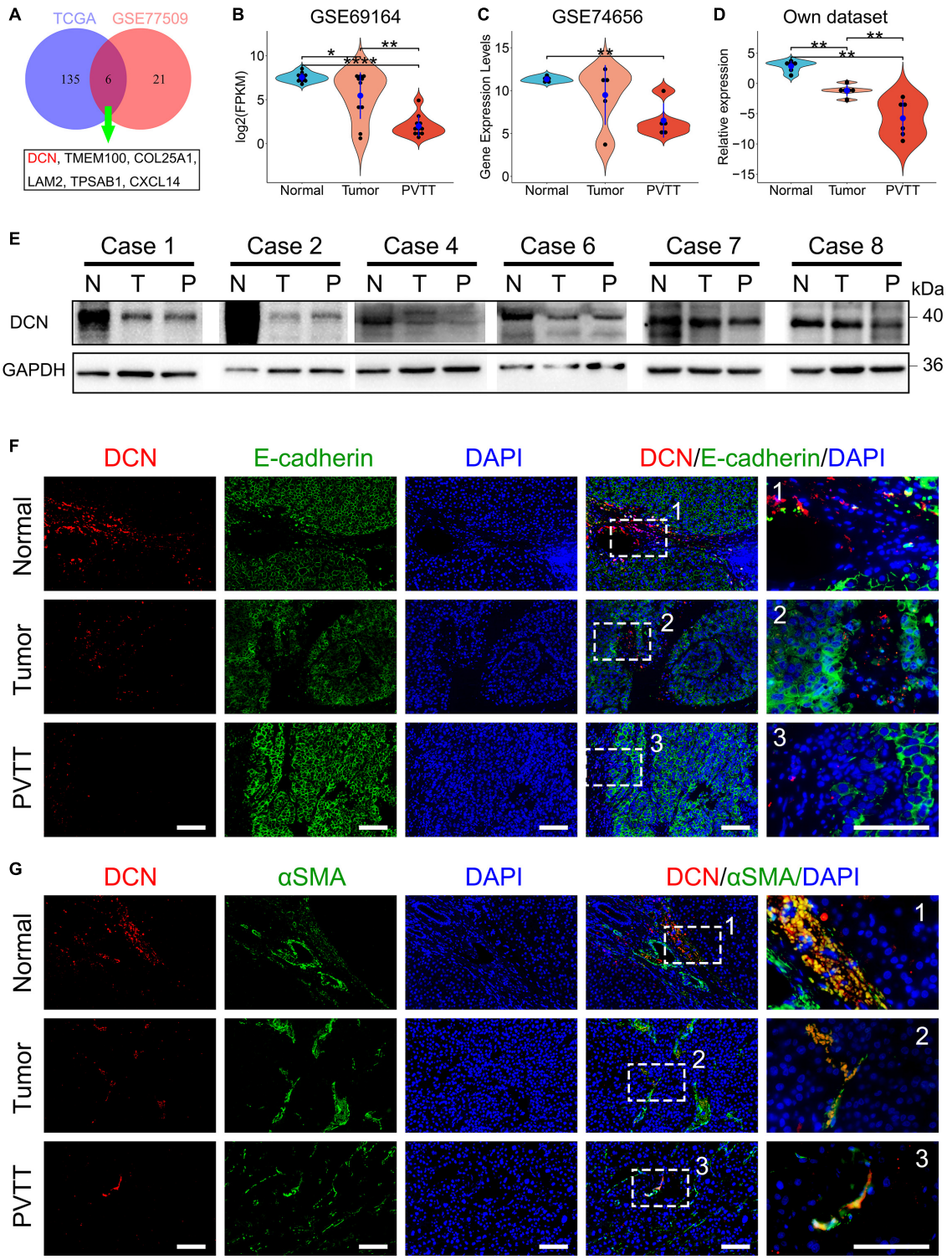

FIGURE 2 | DCN secreted by CAFs is gradually downregulated during HCC progression. **(A)** Venn diagram of DEGs enriched in ECM-related pathways between public dataset GSE77509 and TCGA. **(B–D)** Relative mRNA expression of DCN among normal tissue, tumor tissue, and PVTT tissue in the GEO datasets GSE69164 **(B)**, GSE74656 **(C)**, and our dataset **(D)**. **(E)** DCN protein expression in normal tissue (N), tumor tissue (T), and PVTT (P) tissue as obtained by immunoblot analysis. **(F,G)** Co-immunofluorescence staining of DCN with E-cadherin **(F)** and DCN with α-SMA **(G)** was performed in normal tissue, tumor tissue, and PVTT tissue. Scale bar, 100 μm. α-SMA, alpha-smooth muscle actin; PVTT, portal vein tumor thrombosis. TCGA, The Cancer Genome Atlas. Data presented as mean ± SEM. $^{*}P < 0.05$, $^{**}P < 0.01$, and $^{****}P < 0.0001$, Student's *t*-test.

fibroblasts to primary tumor-associated fibroblasts and further in PVTT-associated fibroblasts (**Figure 2G**). These results indicated that downregulating DCN secreted by fibroblasts promotes VI of HCC.

Low DCN Expression Is Associated With MVI Occurrence and Poor Prognosis

We analyzed correlations between DCN mRNA expression in HCC tumor tissues and clinical pathological characteristics to determine the clinical importance of DCN expression. Tumor DCN levels in our dataset significantly differed only between subgroups of patients divided by MVI status (yes or no, $p = 0.048$; **Table 2**). We explored potential risk factors for MVI to confirm this correlation between DCN expression and MVI. Univariate analysis revealed that various characteristics, including age (<60 years), Ishak grade (≥6), incomplete tumor capsule, and low tumor DCN expression, were risk factors for MVI (**Table 3**). Moreover, multivariate logistic models showed that low tumor DCN expression was an independent risk factor for MVI. Kaplan-Meier findings significantly associated decreased DCN expression with shorter disease-free survival in both the TCGA and our dataset (**Figures 3A,B**). These results agreed with the reduced DCN levels that were associated with MVI. This might be because a lower abundance of DCN facilitates the development of VI, which accelerates tumor recurrence and metastasis. In addition, Kaplan-Meier analysis significantly associated decreased DCN expression with shorter OS in the TCGA dataset (**Figure 3C**). Similarly, low DCN expression positively correlated with poor OS in our dataset, although the correlation did not reach statistical significance (**Figure 3D**). Collectively, these results suggested that DCN is involved in the formation of MVI in patients and could serve as a potential prognostic indicator for patients with HCC.

Decorin Inhibited HCC Cell Migration and Invasion *in vitro*

We evaluated the effects of DCN on HCC cell migration and invasion to functionally validate the biological role of DCN in HCC metastasis. Considering that DCN affects tumor cells mainly via extracellular signaling, we added DCN to culture medium as ectopic expression. Notably, adding 1 μg/mL DCN to the culture medium significantly inhibited HCCLM3 and Hep3B cell migration (**Figures 4A,B**) and invasion (**Figures 4C,D**). These results confirmed the anti-metastatic function of DCN in HCC cells.

Decorin Downregulated Integrin β1 Expression in HCC

To explore the downstream targets of DCN involved in inhibiting HCC metastasis, we analyzed proteins related to the epithelial mesenchymal transition (EMT) that are involved in tumor metastasis (Yang et al., 2020). Levels of E-cadherin were high in normal tissues but decreased in tumor and PVTT tissues among our clinical samples. The expression of N-cadherin and vimentin, that are markers of mesenchymal cells, was upregulated in tumor and PVTT tissues (**Supplementary Figures 2A,B**). These results confirmed that tumor cells initiated the EMT to promote tumorigenesis and metastasis. However, N-cadherin, vimentin, and MMP2 expression did not significantly differ between 1 and 4 μg/mL DCN and controls, indicating that the EMT and MMP2

TABLE 2 | Relationship between the expression of decorin in tumor tissues and clinical characteristics of HCC patients.

Clinical parameters	Patient number (total = 73)	log_2DCN relative expression	
		Mean ± SD	*P*-value
Gender			0.085
Female	12	1.10 ± 2.14	
Male	61	2.56 ± 4.22	
Age			0.054
< 60	58	1.91 ± 4.06	
≥ 60	15	3.93 ± 3.28	
AFP			0.626
< 400	40	2.53 ± 4.10	
≥ 400	33	2.07 ± 3.87	
HbsAg			0.293
Positive	70	2.39 ± 4.03	
Negative	3	0.68 ± 2.12	
HBV DNA			0.927
Positive	61	2.37 ± 4.07	
Negative	11	2.25 ± 3.75	
Cirrhosis			0.128
Yes	26	1.34 ± 4.45	
No	41	2.95 ± 3.58	
Tumor number			0.391
Single	49	2.61 ± 3.95	
Multiple	24	1.74 ± 4.06	
Tumor size			0.453
≤ 5	25	2.81 ± 3.99	
> 5	48	2.07 ± 3.99	
BCLC stage			0.497
A + B	49	2.09 ± 3.85	
C	24	2.80 ± 4.26	
Tumor capsule			0.26
Complete	28	1.69 ± 3.97	
Infiltration	42	2.79 ± 3.99	
Satellite lesions			0.594
Yes	13	2.95 ± 4.74	
No	60	2.19 ± 3.83	
GVI			0.878
Yes	21	2.42 ± 4.58	
No	50	2.24 ± 3.81	
MVI			0.048*
Yes	33	1.33 ± 3.35	
No	40	3.14 ± 4.30	
Differentiation			0.719
High + moderate	40	2.48 ± 4.11	
Moderate + low	33	2.14 ± 3.87	

*AFP, alpha feto protein; BCLC, Barcelona-Clinic Liver Cancer; GVI, gross vascular invasion (defined as tumor embolus in first or second branches of portal veins found by preoperative CT or MRI); HBsAg, hepatitis B surface antigen; MVI, microvascular invasion, SD standard deviation. *Statistically significant.*

TABLE 3 | Univariate and multivariate analysis of risk factors of MVI.

Factors	Regression coefficient β	OR (95% CI)	*P*-value
Univariate analysis			
Gender (male vs. female)	−0.331	0.718 (0.480–1.076)	0.108
Age (year ≥ 60 vs. < 60)	−0.981	0.375 (0.147–0.958)	0.040*
Tumor diameter (cm ≥ 5 vs. < 5)	−0.279	0.757 (0.463–1.236)	0.266
Tumor number (multiple vs. single)	0.405	1.500 (0.674–3.339)	0.321
Ishak grade (≥ 6 vs. < 6)	−0.821	0.440 (0.217–0.894)	0.023*
GVI (presence vs. absence)	0.511	1.667 (0.729–3.808)	0.226
Satellite nodules (presence vs. absence)	0.288	1.333 (0.463–3.843)	0.594
Tumor capsule (complete vs. incomplete)	−0.811	0.444 (0.225–0.877)	0.019*
BCLC stage (B + C vs. 0 + A)	0.693	2.000 (0.899–4.452)	0.090
AFP (ng/ml ≥ 400 vs. < 400)	0.095	1.100 (0.600–2.015)	0.758
Edmondson-Steiner grade (I/II vs. III/IV)	−0.463	0.630 (0.343–1.155)	0.135
HBV-DNA (copies ≥ 10^3 vs. < 10^3)	−0.492	0.611 (0.289–1.294)	0.198
HBsAg (positive vs. negative)	−0.340	0.712 (0.467–1.085)	0.114
Tumor DCN expression (high vs. low)	−0.916	0.400(0.215–0.743)	0.004**
Multivariate analysis			
Age (year ≥ 60 vs. **< 60)**	−0.467	0.627 (0.206–1.908)	0.411
Tumor capsule (complete vs. incomplete)	−0.382	0.682 (0.321–1.449)	0.320
Tumor DCN expression (high vs. low)	−0.831	0.436 (0.211–0.900)	0.025*

*Tumor DCN expression is independent risk factors of MVI. OR odds ratio, CI confidence interval, GVI gross vascular invasion, BCLC Barcelona-Clinic Liver Cancer, AFP alpha-fetoprotein, HBV-DNA hepatitis B deoxyribonucleic acid, HBsAg hepatitis B surface antigen, DCN decorin. *A significant correlation was detected at P < 0.05, **P < 0.01.*

are not regulated by DCN (**Supplementary Figures 2C,D**). We then investigated the expression of TGF-β1, TGF-β2, and receptor tyrosine kinases (HER2), which are signaling molecules involved in DCN-mediated tumor carcinogenesis and metastasis (Hildebrand et al., 1994; Goldoni et al., 2008). The expression of HER2, TGF-β1, and TGF-β2 was slightly decreased in the DCN, compared with control HCCLM3 and Hep3B cells (**Supplementary Figures 2E,F**). These results are consistent with those of previous studies (Hildebrand et al., 1994; Goldoni et al., 2008), and validated accuracy of our findings.

Integrins are involved in tumor progression and drug resistance (Hamidi and Ivaska, 2018; Yu et al., 2020). As shown by the transcriptomic results of clinically matched samples from patients who had HCC with PVTT, signals of ECM organization and regulation of integrin activation were enriched during PVTT development (**Figure 1B**). To confirm whether DCN inhibits HCC metastasis through regulating the integrin pathway, we analyzed the expression of integrins α1, α3, α11, β1, and β5 in DCN and control HCCLM3 and Hep3B cells at the protein level. The expression of integrins β1 and α11 was significantly downregulated in response to enhanced DCN expression, whereas that of integrins α1, α3, and β5 was not changed, suggesting that DCN binds to integrin β1 or integrin α11 to inhibit HCC metastasis (**Figure 5A** and **Supplementary Figure 3**). We also analyzed the expression of integrins α5 and β3 at the mRNA level in the DCN and control groups. The expression of integrin α5 was downregulated by upregulated DCN, whereas integrin β3 was upregulated by enhancing DCN expression in HCCLM3 and Hep3B HCC cells (**Figures 5B,C**). The ECM components COL1A1, COL3A1, COL4A1, and fibronectin 1 (FN1), are critical regulators during tumor metastasis, so we examined their expression in the DCN and control cells using qPCR. The upregulation of DCN resulted in downregulated COL1A1, and upregulated FN1 expression (**Supplementary Figure 4**).

To confirm that integrin β1 is a critical factor in VI and HCC metastasis, we analyzed integrin β1 protein expression in clinical samples. We found significantly upregulated integrin β1 protein expression in epithelial cells of primary tumor and PVTT, compared with normal tissues (**Supplementary Figure 5**). More importantly, co-staining DCN and integrin β1 revealed that DCN dynamically regulated integrin β1 protein expression, in that a decrease in DCN was accompanied by integrin β1 upregulation from normal, to primary tumor and PVTT tissues (**Figure 5D**). Collectively, these results suggest that DCN regulates integrin β1 to promote HCC metastasis.

Decorin Plays Anti-metastatic Role in HCC by Binding to Integrin β1

To confirm the pro-metastatic role of integrin β1 in HCC, we evaluated the effects of integrin β1 knockdown on HCCLM3 and Hep3B cell migration and invasion. We downregulated integrin β1 expression in these cell lines using shRNA and confirmed the knockdown by qPCR (**Figures 6A,B**). Notably, integrin β1 knockdown significantly inhibited HCCLM3 and Hep3B cell migration and invasion in Transwell chambers (**Figures 6C,D**). The results of wound healing assays further confirmed that integrin β1 downregulation significantly inhibited HCCLM3 and Hep3B cell migration (**Figures 6E,F**). These results confirmed the pro-metastatic role of integrin β1 in HCC.

To further confirm that DCN downregulates integrin β1 expression to suppress HCC metastasis, we evaluated the effects of simultaneously modulating DCN and integrin β1 expression in HCC cell lines. The combination of DCN and integrin β1 downregulation further inhibited HCCLM3 and Hep3B cell migration and invasion compared with either DCN or integrin β1 downregulation alone (**Figures 7A–D**). The expression of integrin β1 was downregulated in each of

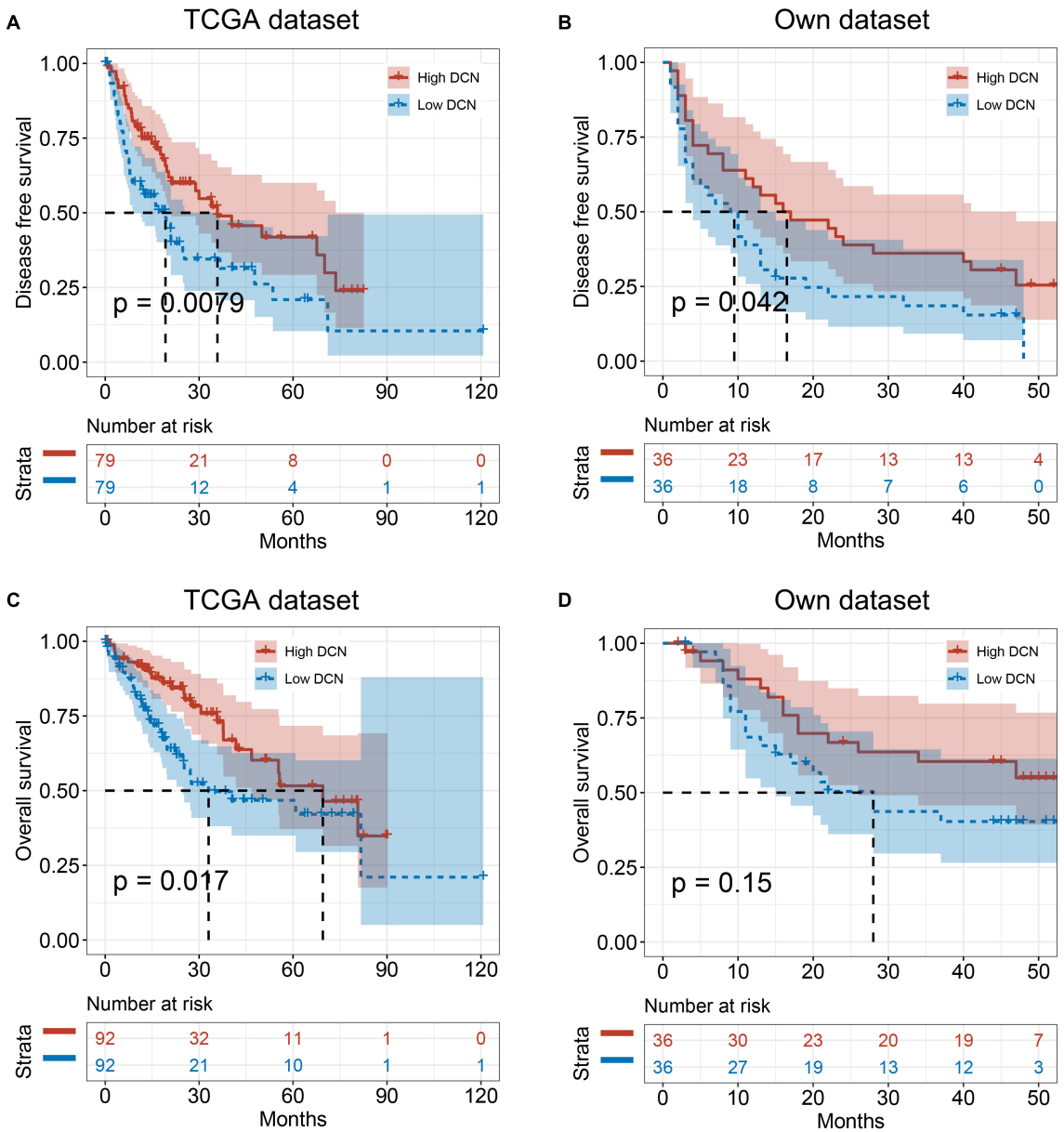

FIGURE 3 | Low DCN expression levels correlate with poor prognosis. **(A,B)** Kaplan–Meier analyses showing the correlations between DCN expression level and disease-free survival of patients with HCC from TCGA database **(A)** and our own dataset **(B)**. **(C,D)** Kaplan–Meier analyses of the correlations between DCN expression level and overall survival of patients with HCC from TCGA database **(C)**, and our own dataset **(D)**. The median expression level was used as the cut-off. Values are expressed as the median with interquartile range. TCGA, The Cancer Genome Atlas.

the DCN and integrin β1 knockdown groups, and further downregulated when DCN was combined with integrin β1 knockdown (**Figure 7E** and **Supplementary Figure 6**). These results suggested that DCN binds residual integrin β1 that was not knocked down by shRNA, thus further downregulating integrin β1 to inhibit HCC metastasis. The results of the Co-IP assays using DCN and integrin β1 antibodies showed that integrin β1 was expressed after conjugation with the DCN antibody, which further confirmed direct interaction between DCN and integrin β1 (**Figure 7F**). Collectively, the combination of DCN and integrin β1 knockdown synergistically augmented the anti-metastatic effects.

DISCUSSION

Hepatocellular carcinoma is difficult to treat; it recurs at a high rate and metastasizes even after radical surgical resection (Liu et al., 2016). The high propensity of HCC for VI is the main cause of high intrahepatic metastasis (Vilarinho et al., 2017).

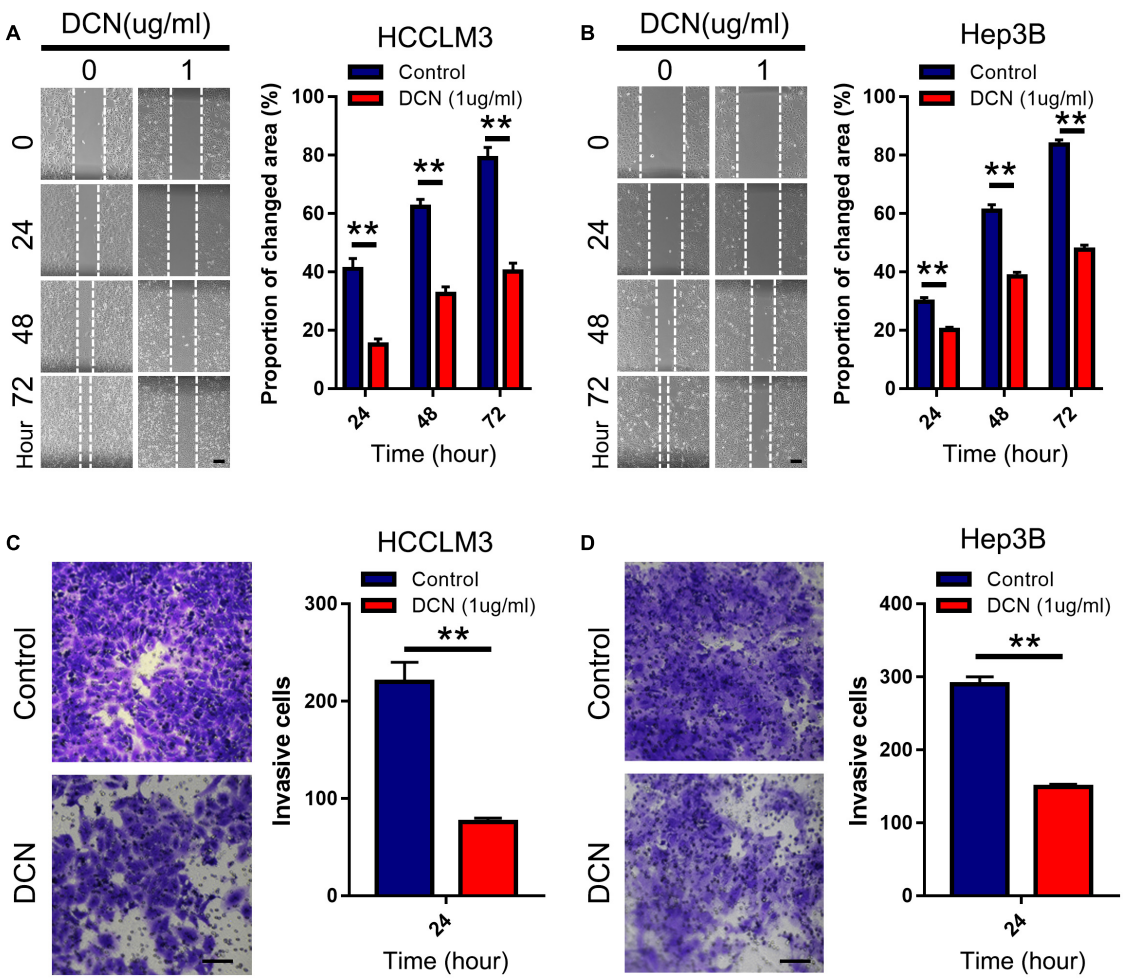

FIGURE 4 | DCN inhibits migration and invasion of HCC cell lines. **(A,B)** Wound-healing assays for HCCLM3 **(A)**, and Hep3B **(B)** cells treated with DCN (1 μg/mL) or the negative control. Scale bars, 200 μm. **(C,D)** Transwell assays for HCCLM3 **(C)**, and Hep3B **(D)** cells treated with DCN(1 μg/mL) or the negative control. Scale bars, 100 μm. Data presented as mean ± SEM. $^{**}P < 0.01$, Student's *t*-test.

Both MVI and PVTT are common in VI by HCC, and have become hotspots in studies of HCC prevention and treatment (Wei et al., 2019; Xu et al., 2019). Although clinical strategies such as single surgery, transarterial chemoembolization, targeted, or combined therapies have been applied in attempts to improve therapeutic effects, the clinical benefit for patients with HCC remains poor. Incremental evidence suggests that MVI and PVTT are predictors of poor prognosis for HCC (Forner et al., 2012). However, little is known about the biological molecular mechanisms underlying the evolution of VI. Determining the fundamental events of VI will provide insight for understanding HCC metastasis.

We analyzed the transcriptome of clinical samples from patients who had HCC with or without VI and found that ECM-related pathways are involved in VI by HCC. In addition, DCN secreted by CAFs was downregulated in VI compared with non-VI tissues. Various cell types in the TME, particularly CAFs, play important roles in regulating tumor carcinogenesis and progression. Whether CAF-mediated VI of HCC promotes metastasis remains poorly understood. Consistent with previous findings (Li et al., 2019), DCN was co-expressed with a-SMA but not with E-cadherin, indicating that it is preferentially expressed in fibroblasts and not in epithelial cells. In addition, DCN was gradually downregulated from normal, to primary tumor tissues and even more so in PVTT tissues. These results indicated that fibroblasts in malignant tissues decreased the secretion of DCN to promote VI by HCC, suggesting an anti-metastatic role for DCN secreted by CAFs in HCC. Moreover, we also showed that low DCN expression was associated with a poor prognosis and MVI development. Collectively, these results indicated that DCN secreted by CAFs functions as a tumor suppressor to inhibit VI of HCC.

We analyzed the effects of elevated DCN concentrations in culture medium of HCC cell tumor phenotypes to functionally validate the anti-metastatic role of DCN. Elevated interstitial concentrations of DCN inhibited HCC cell migration and invasion *in vitro*. Decorin functions in the tumorigenesis of various types of cancer (Ju et al., 2015; Reszegi et al., 2020).

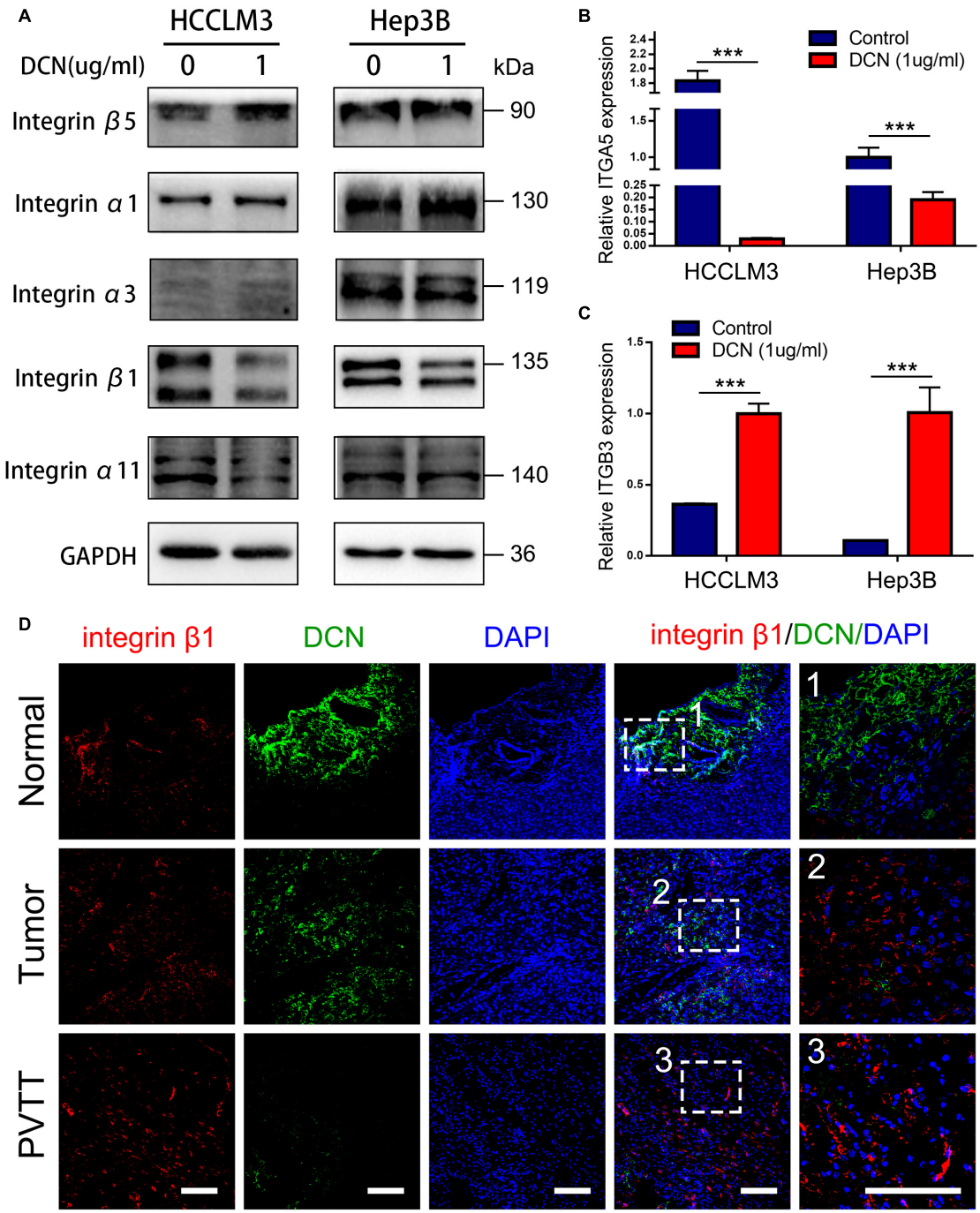

FIGURE 5 | DCN downregulates integrin β1 expression. **(A)** Western blot analysis of integrins expression in HCCLM3 and Hep3B cells treated with DCN (1 μg/mL) or the negative control. **(B)** qPCR analysis of integrin α5 expression in HCCLM3 and Hep3B cells treated with DCN (1 μg/mL) or the negative control. **(C)** qPCR analysis of integrin β3 expression in HCCLM3 and Hep3B cells treated with DCN (1 μg/mL) or the negative control. **(D)** Representative images of integrin β1 and DCN expressions in normal tissue, tumor tissue, and PVTT tissue obtained by co-immunofluorescence staining. Scale bar, 100 μm. ITGA5, integrin α5; ITGB3, integrin β3; PVTT, portal vein tumor thrombosis. Data presented as mean ± SEM. ***$P < 0.001$, Student's *t*-test.

Delivery of the DCN gene reduced tumor formation in a mouse model of hepatocarcinogenesis evoked by thioacetamide. Serum DCN levels might be associated with the physical function and prognosis of patients with HCC (Kawaguchi et al., 2020). Decorin significantly inhibited the growth potential of various hepatoma cell lines (Horváth et al., 2019). Although these studies found that DCN inhibits the development and growth of HCC, the anti-metastatic role of DCN in HCC has not been determined. To our

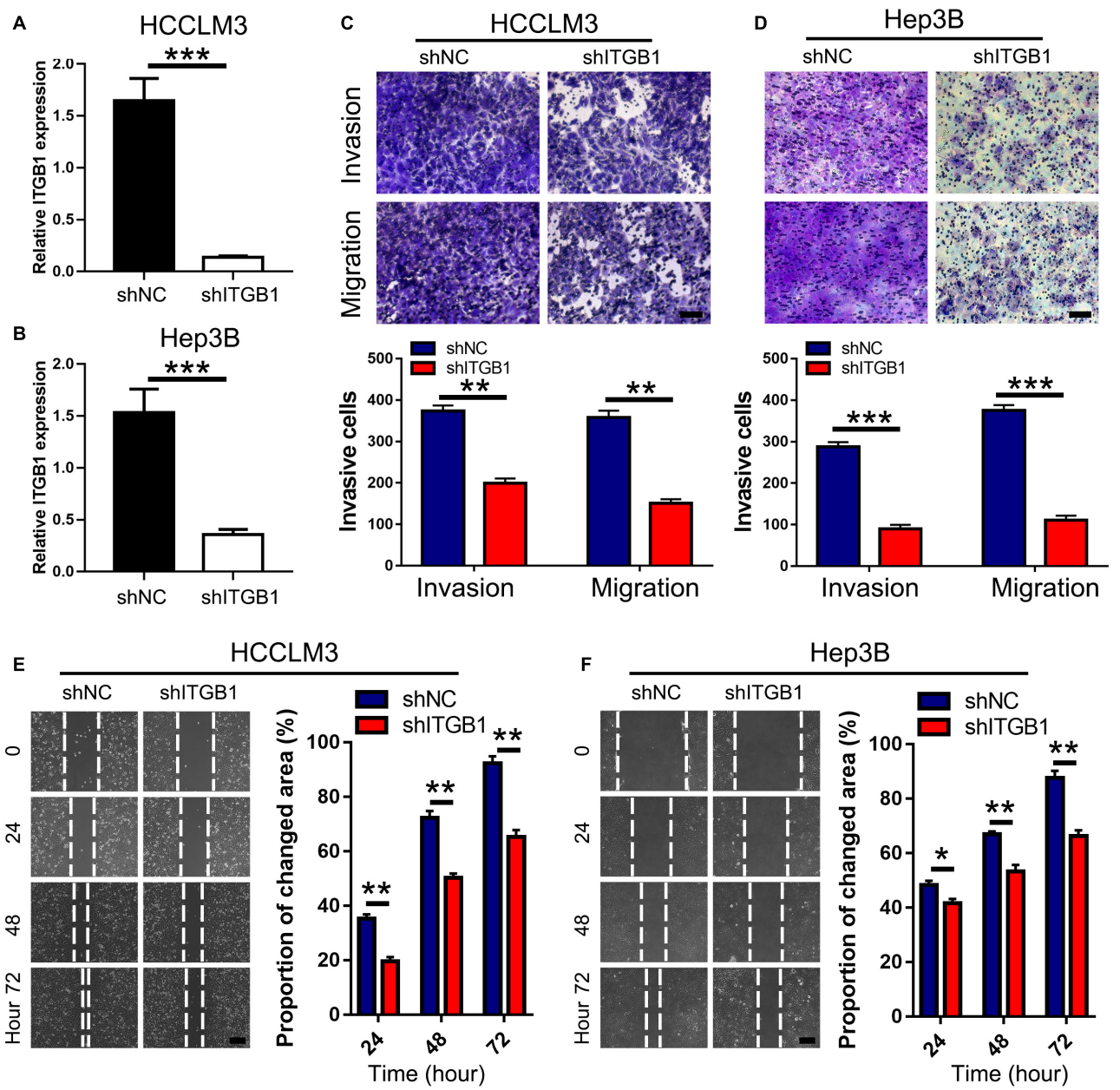

FIGURE 6 | Integrin β1 downregulation inhibits migration and invasion of HCC cell lines. **(A,B)** Results of qRT-PCR validated the integrin β1 knockdown in HCCLM3 **(A)** and Hep3B **(B)** cells. **(C,D)** Transwell assays for HCCLM3 **(C)**, and Hep3B **(D)** cells transfected with integrin β1 specific shRNA or the negative control. Scale bars, 100 μm. **(E,F)** Wound-healing assays for HCCLM3 **(E)**, and Hep3B **(F)** cells transfected with integrin β1 specific shRNA or the negative control. Scale bars, 200 μm. ITGB1, integrin β1. Data presented as mean ± SEM. $^{*}P < 0.05$, $^{**}P < 0.01$, and $^{***}P < 0.001$, Student's *t*-test.

knowledge, this is the first study to show that DCN secreted by CAFs in the TME is involved in VI by HCC.

We examined ECM pathways that related to cancer progression to identify downstream targets of DCN for promoting tumor metastasis. The expression of integrin β1 was downregulated in cells with elevated DCN, indicating that DCN inhibits HCC metastasis by downregulating integrin β1 expression. Integrin β1 plays crucial roles in cell adhesion, migration, invasion, and proliferation. The role of integrin β1 in tumor growth, tumor recurrence, metastasis and drug resistance is important (Barkan and Chambers, 2011). The expression of integrin β1 in epithelial cells was upregulated in PVTT, compared with tumor and normal tissues. Immunohistochemical co-staining DCN and integrin β1 in the same clinical tissue shows that DCN dynamically regulated the protein expression of integrin β1 in terms of a decrease in DCN accompanied by integrin β1 upregulation from normal, to primary tumor, to PVTT tissues. Its knockdown significantly

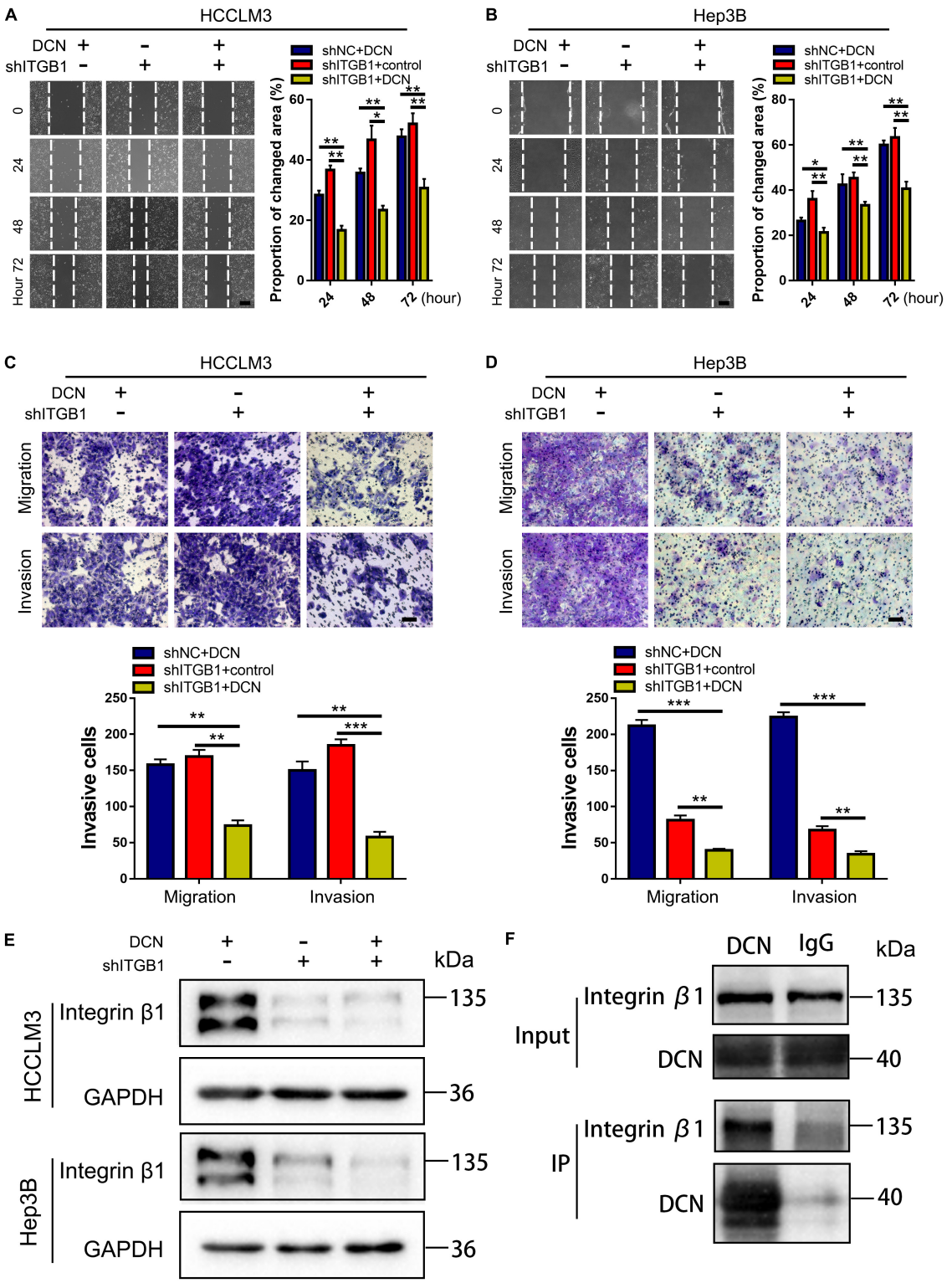

FIGURE 7 | DCN treatment combined with integrin β1 downregulation synergistically inhibits migration and invasion of HCC cell lines. **(A,B)** Wound-healing assays using integrin β1 knocked-down or negative control HCCLM3 **(A)**, and Hep3B **(B)** cells treated with DCN (1 μg/mL) or the negative control. Scale bars, 200 μm. **(C,D)** Transwell assays using integrin β1 knocked-down or negative control HCCLM3 **(C)**, and Hep3B **(D)** cells treated with the addition of DCN (1 μg/mL) or the negative control. **(E)** Western blot analysis of integrin β1 expression using integrin β1 knocked-down or negative control HCCLM3 and Hep3B cells treated with DCN (1 μg/mL) or the negative control. **(F)** Co-IP assay of DCN with integrin β1, as detected by immunoblot analysis. Scale bars, 100 μm. ITGB1, integrin β1. Data presented as mean ± SEM. $^{*}P < 0.05$, $^{**}P < 0.01$, and $^{***}P < 0.001$, Student's *t*-test.

inhibited HCC cell invasion and migration. Moreover, the combination of DCN and integrin β1 knockdown synergistically augmented the anti-metastatic effects. The results of Co-IP assays showed direct interaction between DCN and integrin β1, thus confirming that DCN-integrin β1 signaling inhibited HCC migration and invasion.

We focused on VI by HCC and identified DCN as a new target for inhibiting HCC intrahepatic metastasis. Our finding that decorin was secreted by fibroblasts indicates that our results offer insight into targeting CAFs in the TME that can be applied to strategies for treating patients who have HCC with PVTT.

DATA AVAILABILITY STATEMENT

The original contributions presented in the study are included in the article/**Supplementary Material**, further inquiries can be directed to the corresponding author.

ETHICS STATEMENT

The studies involving human participants were reviewed and approved by Local Ethics Committee of West China Hospital. The patients/participants provided their written informed consent to participate in this study.

AUTHOR CONTRIBUTIONS

MX supervised the project, conceived and designed the experiments, analyzed the data, and wrote the manuscript. XZ and PW performed the experiments, analyzed the data, and wrote the manuscript. LiL analyzed the data of IHC staining. JY performed bioinformatics analysis. CY performed the *in vitro* experiments. LX, LiaL, and XC analyzed the data. FD, LF, HZ, and MZ assisted with the writing. All authors contributed to the article and approved the submitted version.

FUNDING

This work was funded by the Key Technology Research and Development Program of the Sichuan Province (Nos. 2019YFS0208, 2021YFSY0009, and 2021YFS0106), the National Natural Science Foundation of China (No. 81803574), the China Postdoctoral Science Foundation (No. 2019M653430), and the Post-Doctor Research Project, West China Hospital, Sichuan University (Nos. 2018HXBH003 and 2020HXBH076).

ACKNOWLEDGMENTS

We would like to thank and express our heartfelt gratitude to Fei Chen and Chunjuan Bao (Institute of Clinical Pathology, West China Hospital of Sichuan University) who assisted with the immunohistochemical staining experiment. We would like to thank Yan Wang (the Core Facility of West China Hospital of Sichuan University) and Xiaoting Chen (The Animal Laboratory Center of West China Hospital of Sichuan University) for technical assistance.

SUPPLEMENTARY MATERIAL

The Supplementary Material for this article can be found online at: https://www.frontiersin.org/articles/10.3389/fcell.2021.678670/full#supplementary-material

Supplementary Figure 1 | Quantification analysis of DCN expression in normal tissues, tumor tissues and PVTT tissues at protein level.

Supplementary Figure 2 | Explore the downstream targets of DCN involved in inhibiting HCC metastasis.

Supplementary Figure 3 | Quantification of the WB membranes in **Figure 5A**.

Supplementary Figure 4 | Explore ECM components that could be involved in inhibition of HCC metastasis through DCN upregulation.

Supplementary Figure 5 | Expression levels of integrin β1 in clinical matched samples.

Supplementary Figure 6 | Quantification of the WB membranes in **Figure 7E**.

REFERENCES

Barkan, D., and Chambers, A. F. (2011). β1-integrin: a potential therapeutic target in the battle against cancer recurrence. *Clin. Cancer Res.* 17, 7219–7223. doi: 10.1158/1078-0432.CCR-11-0642

Bi, X., Tong, C., Dockendorff, A., Bancroft, L., Gallagher, L., Guzman, G., et al. (2008). Genetic deficiency of decorin causes intestinal tumor formation through disruption of intestinal cell maturation. *Carcinogenesis* 29, 1435–1440. doi: 10.1093/carcin/bgn141

Bray, F., Ferlay, J., Soerjomataram, I., Siegel, R. L., Torre, L. A., and Jemal, A. (2018). Global cancer statistics 2018: GLOBOCAN estimates of incidence and mortality worldwide for 36 cancers in 185 countries. *CA Cancer J. Clin.* 68, 394–424. doi: 10.3322/caac.21492

Craig, A. J., and von Felden, J. (2020). Tumour evolution in hepatocellular carcinoma. *Nat. Rev. Gastroenterol. Hepatol.* 17, 139–152. doi: 10.1038/s41575-019-0229-4

Feugaing, D. D. S., Götte, M., and Viola, M. (2013). More than matrix: the multifaceted role of decorin in cancer. *Eur. J. Cell Biol.* 92, 1–11. doi: 10.1016/j.ejcb.2012.08.004

Finn, R. S., Qin, S., Ikeda, M., Galle, P. R., Ducreux, M., Kim, T. Y., et al. (2020). Atezolizumab plus bevacizumab in unresectable hepatocellular carcinoma. *N. Engl. J. Med.* 382, 1894–1905. doi: 10.1056/NEJMoa1915745

Forner, A., Llovet, J. M., and Bruix, J. (2012). Hepatocellular carcinoma. *Lancet* 379, 1245–1255. doi: 10.1016/s0140-6736(11)61347-0

Forner, A., Reig, M., and Bruix, J. (2018). Hepatocellular carcinoma. *Lancet* 391, 1301–1314. doi: 10.1016/s0140-6736(18)30010-2

Fransvea, E., Mazzocca, A., Antonaci, S., and Giannelli, G. (2009). Targeting transforming growth factor (TGF)-betaRI inhibits activation of beta1 integrin and blocks vascular invasion in hepatocellular carcinoma. *Hepatology* 49, 839–850. doi: 10.1002/hep.22731

Fu, Y., Liu, S., Zeng, S., and Shen, H. (2019). From bench to bed: the tumor immune microenvironment and current immunotherapeutic strategies for hepatocellular carcinoma. *J. Exp. Clin. Cancer Res.* 38:396. doi: 10.1186/s13046-019-1396-4

Goldoni, S., Seidler, D. G., Heath, J., Fassan, M., Baffa, R., Thakur, M. L., et al. (2008). An antimetastatic role for decorin in breast cancer. *Am. J. Pathol.* 173, 844–855. doi: 10.2353/ajpath.2008.080275

Hamidi, H., and Ivaska, J. (2018). Every step of the way: integrins in cancer progression and metastasis. *Nat. Rev. Cancer* 18, 533–548. doi: 10.1038/s41568-018-0038-z

Hernandez-Gea, V., Toffanin, S., Friedman, S. L., and Llovet, J. M. (2013). Role of the microenvironment in the pathogenesis and treatment of hepatocellular carcinoma. *Gastroenterology* 144, 512–527. doi: 10.1053/j.gastro.2013.01.002

Hildebrand, A., Romarís, M., Rasmussen, L. M., Heinegård, D., Twardzik, D. R., Border, W. A., et al. (1994). Interaction of the small interstitial proteoglycans biglycan, decorin and fibromodulin with transforming growth factor beta. *Biochem. J.* 302 (Pt 2), 527–534. doi: 10.1042/bj3020527

Horváth, Z., Kovalszky, I., Fullár, A., Kiss, K., Schaff, Z., Iozzo, R. V., et al. (2014). Decorin deficiency promotes hepatic carcinogenesis. *Matrix Biol.* 35, 194–205. doi: 10.1016/j.matbio.2013.11.004

Horváth, Z., Reszegi, A., Szilák, L., Dankó, T., Kovalszky, I., and Baghy, K. (2019). Tumor-specific inhibitory action of decorin on different hepatoma cell lines. *Cell. Signal.* 62:109354. doi: 10.1016/j.cellsig.2019.109354

Huang, J., Tian, W., Zhang, L., Huang, Q., Lin, S., Ding, Y., et al. (2020). Preoperative prediction power of imaging methods for microvascular invasion in hepatocellular carcinoma: a systemic review and meta-analysis. *Front. Oncol.* 10:887. doi: 10.3389/fonc.2020.00887

Jármay, K., Gallai, M., Karácsony, G., Ozsvár, Z., Schaff, Z., Lonovics, J., et al. (2000). Decorin and actin expression and distribution in patients with chronic hepatitis C following interferon-alfa-2b treatment. *J. Hepatol.* 32, 993–1002. doi: 10.1016/s0168-8278(00)80104-x

Järveläinen, H., Sainio, A., and Wight, T. N. (2015). Pivotal role for decorin in angiogenesis. *Matrix Biol.* 43, 15–26. doi: 10.1016/j.matbio.2015.01.023

Jiang, J., Ye, F., Yang, X., Zong, C., Gao, L., Yang, Y., et al. (2017). Peritumor associated fibroblasts promote intrahepatic metastasis of hepatocellular carcinoma by recruiting cancer stem cells. *Cancer Lett.* 404, 19–28. doi: 10.1016/j.canlet.2017.07.006

Ju, W., Li, S., Wang, Z., Liu, Y., and Wang, D. (2015). Decorin protects human hepatoma HepG2 cells against oxygen-glucose deprivation via modulating autophagy. *Int. J. Clin. Exp. Med.* 8, 13347–13352.

Kawaguchi, T., Yoshio, S., Sakamoto, Y., Hashida, R., Koya, S., Hirota, K., et al. (2020). Impact of decorin on the physical function and prognosis of patients with hepatocellular carcinoma. *J. Clin. Med.* 9:936. doi: 10.3390/jcm9040936

Kubo, N., Araki, K., Kuwano, H., and Shirabe, K. (2016). Cancer-associated fibroblasts in hepatocellular carcinoma. *World J. Gastroenterol.* 22, 6841–6850. doi: 10.3748/wjg.v22.i30.6841

Lau, E. Y., Lo, J., Cheng, B. Y., Ma, M. K., Lee, J. M., Ng, J. K., et al. (2016). Cancer-associated fibroblasts regulate tumor-initiating cell plasticity in hepatocellular carcinoma through c-Met/FRA1/HEY1 signaling. *Cell Rep.* 15, 1175–1189. doi: 10.1016/j.celrep.2016.04.019

Le, D. T., Uram, J. N., Wang, H., Bartlett, B. R., Kemberling, H., Eyring, A. D., et al. (2015). PD-1 blockade in tumors with mismatch-repair deficiency. *N. Engl. J. Med.* 372, 2509–2520. doi: 10.1056/NEJMoa1500596

Li, S., Wang, P., Zhang, G., Ji, J., Lv, T., Wang, X., et al. (2019). The effect of ALA-PDT on reversing the activation of cancer-associated fibroblasts in cutaneous squamous cell carcinoma. *Photodiagnosis Photodyn. Ther.* 27, 234–240. doi: 10.1016/j.pdpdt.2019.05.043

Liu, P. H., Hsu, C. Y., Hsia, C. Y., Lee, Y. H., Su, C. W., Huang, Y. H., et al. (2016). Prognosis of hepatocellular carcinoma: assessment of eleven staging systems. *J. Hepatol.* 64, 601–608. doi: 10.1016/j.jhep.2015.10.029

Lu, C., Rong, D., Zhang, B., Zheng, W., Wang, X., Chen, Z., et al. (2019). Current perspectives on the immunosuppressive tumor microenvironment in hepatocellular carcinoma: challenges and opportunities. *Mol. Cancer* 18:130. doi: 10.1186/s12943-019-1047-6

Lu, J., Zhang, X. P., Zhong, B. Y., Lau, W. Y., Madoff, D. C., Davidson, J. C., et al. (2019). Management of patients with hepatocellular carcinoma and portal vein tumour thrombosis: comparing east and west. *Lancet Gastroenterol. Hepatol.* 4, 721–730. doi: 10.1016/s2468-1253(19)30178-5

Neill, T., Schaefer, L., and Iozzo, R. V. (2016). Decorin as a multivalent therapeutic agent against cancer. *Adv. Drug Deliv. Rev.* 97, 174–185. doi: 10.1016/j.addr.2015.10.016

Renne, S. L., Woo, H. Y., Allegra, S., Rudini, N., Yano, H., Donadon, M., et al. (2020). Vessels Encapsulating Tumor Clusters (VETC) is a powerful predictor of aggressive hepatocellular carcinoma. *Hepatology* 71, 183–195. doi: 10.1002/hep.30814

Reszegi, A., Horváth, Z., Fehér, H., Wichmann, B., Tátrai, P., Kovalszky, I., et al. (2020). Protective role of decorin in primary hepatocellular carcinoma. *Front. Oncol.* 10:645. doi: 10.3389/fonc.2020.00645

Roayaie, S., Blume, I. N., Thung, S. N., Guido, M., Fiel, M. I., Hiotis, S., et al. (2009). A system of classifying microvascular invasion to predict outcome after resection in patients with hepatocellular carcinoma. *Gastroenterology* 137, 850–855. doi: 10.1053/j.gastro.2009.06.003

Sulaiman, S. A., Abu, N., Ab-Mutalib, N. S., Low, T. Y., and Jamal, R. (2019). Signatures of gene expression, DNA methylation and microRNAs of hepatocellular carcinoma with vascular invasion. *Future Oncol.* 15, 2603–2617. doi: 10.2217/fon-2018-0909

Tabrizian, P., Jibara, G., Shrager, B., Schwartz, M., and Roayaie, S. (2015). Recurrence of hepatocellular cancer after resection: patterns, treatments, and prognosis. *Ann. Surg.* 261, 947–955. doi: 10.1097/sla.0000000000000710

Vilarinho, S., Erson-Omay, E. Z., Mitchell-Richards, K., Cha, C., Nelson-Williams, C., Harmancı, A. S., et al. (2017). Exome analysis of the evolutionary path of hepatocellular adenoma-carcinoma transition, vascular invasion and brain dissemination. *J. Hepatol.* 67, 186–191. doi: 10.1016/j.jhep.2017.03.009

Wei, X., Jiang, Y., Zhang, X., Feng, S., Zhou, B., Ye, X., et al. (2019). Neoadjuvant three-dimensional conformal radiotherapy for resectable hepatocellular carcinoma with portal vein tumor thrombus: a randomized, open-label, multicenter controlled study. *J. Clin. Oncol.* 37, 2141–2151. doi: 10.1200/jco.18.02184

Xu, X., Zhang, H. L., Liu, Q. P., Sun, S. W., Zhang, J., Zhu, F. P., et al. (2019). Radiomic analysis of contrast-enhanced CT predicts microvascular invasion and outcome in hepatocellular carcinoma. *J. Hepatol.* 70, 1133–1144. doi: 10.1016/j.jhep.2019.02.023

Yang, J., Antin, P., Berx, G., Blanpain, C., Brabletz, T., Bronner, M., et al. (2020). Guidelines and definitions for research on epithelial-mesenchymal transition. *Nat. Rev. Mol. Cell Biol.* 21, 341–352. doi: 10.1038/s41580-020-0237-9

Yang, Y., Chen, L., and Gu, J. (2017). Recurrently deregulated lncRNAs in hepatocellular carcinoma. *Nat. Commun.* 8:14421. doi: 10.1038/ncomms14421

Yu, C., Zhang, M., Song, J., Zheng, X., Xu, G., Bao, Y., et al. (2020). Integrin-Src-YAP1 signaling mediates the melanoma acquired resistance to MAPK and PI3K/mTOR dual targeted therapy. *Mol. Biomed.* 1:12. doi: 10.1186/s43556-020-00013-0

Zhang, H., Ye, J., Weng, X., Liu, F., He, L., Zhou, D., et al. (2015). Comparative transcriptome analysis reveals that the extracellular matrix receptor interaction contributes to the venous metastases of hepatocellular carcinoma. *Cancer Genet.* 208, 482–491. doi: 10.1016/j.cancergen.2015.06.002

Zhang, X. P., Gao, Y. Z., Chen, Z. H., Chen, M. S., Li, L. Q., Wen, T. F., et al. (2019). An eastern hepatobiliary surgery hospital/portal vein tumor thrombus scoring system as an aid to decision making on hepatectomy for hepatocellular carcinoma patients with portal vein tumor thrombus: a multicenter study. *Hepatology* 69, 2076–2090. doi: 10.1002/hep.30490

Conflict of Interest: The authors declare that the research was conducted in the absence of any commercial or financial relationships that could be construed as a potential conflict of interest.

Publisher's Note: All claims expressed in this article are solely those of the authors and do not necessarily represent those of their affiliated organizations, or those of the publisher, the editors and the reviewers. Any product that may be evaluated in this article, or claim that may be made by its manufacturer, is not guaranteed or endorsed by the publisher.

frontiers in Cell and Developmental Biology

ORIGINAL RESEARCH
published: 08 September 2021
doi: 10.3389/fcell.2021.710104

High Visceral Adipose Tissue Density Correlates With Unfavorable Outcomes in Patients With Intermediate-Stage Hepatocellular Carcinoma Undergoing Transarterial Chemoembolization

Qiang Li[1†], Lei Zhang[2†‡], Zhong-Heng Hou[2†], Dong-Xu Zhao[2†], Jian-Bin Li[1], Shuai Zhang[2], Yu Yin[2], Cai-Fang Ni[2‡] and Tao Chen[3‡]*

[1] Department of Radiology, The Affiliated People's Hospital of Ningbo University, Ningbo, China, [2] Department of Interventional Radiology, The First Affiliated Hospital of Soochow University, Suzhou, China, [3] Department of General Surgery, Jiangsu Province Hospital, The First Affiliated Hospital with Nanjing Medical University, Nanjing, China

Objectives: This study aimed to evaluate the association between different body composition features with prognostic outcomes of intermediate stage hepatocellular carcinoma (HCC) patients treated with transarterial chemoembolization (TACE).

Methods: The areas and density of skeletal muscle area (SM) and adipose tissue [subcutaneous (SAT); visceral (VAT)] were calculated on the pre-TACE CT scans. Overall survival (OS) and progression-free survival (PFS) curves were calculated using the Kaplan–Meier method and compared with log-rank test. The discrimination and performance of body composition features were measured by area under time-dependent receiver operating characteristic (ROC) curve. Univariate and multivariate Cox proportional hazard analyses were applied to identify the association between body composition parameters and outcomes.

Results: A significant prolonged OS and PFS was displayed by Kaplan–Meier curve analysis for HCC patients with VAT HU below −89.1 (25.1 months, 95% CI: 18.1–32.1 vs. 17.6 months, 95% CI: 16.3–18.8, $p < 0.0001$, 15.4 months, 95% CI: 10.6–20.2 vs. 6.6 months, 95% CI: 4.9–8.3, $p < 0.0001$, respectively). The 1-, 2-, 3-, and 5-year OS area under the curve (AUC) values of the VAT HU were higher than the other body composition parameters. Meanwhile, it is also found that 3-, 6-, 9-, and 12-month PFS AUC values of VAT HU were the highest among all the parameters. Univariate and multivariate Cox-regression analysis suggested a significant association between VAT density and outcomes (OS, HR: 1.015, 95% CI: 1.004–1.025, $p = 0.005$, PFS, HR: 1.026, 95% CI: 1.016–1.036, $p < 0.0001$, respectively).

Conclusion: The VAT density could provide prognostic prediction value and may be helpful to stratify the intermediate stage HCC patients.

Keywords: body composition, hepatocellular carcinoma, computed tomography, transarterial chemoembolization, adipose tissue

OPEN ACCESS

Edited by:
Daniel P. Bezerra, Oswaldo Cruz Foundation (Fiocruz), Brazil

Reviewed by:
Kangsheng Tu, The First Affiliated Hospital of Xi'an Jiaotong University, China
Heping Kan, Southern Medical University, China
Consolato M. Sergi, Children's Hospital of Eastern Ontario (CHEO), Canada

***Correspondence:**
Tao Chen
ct55979@163.com

[†] These authors have contributed equally to this work and share first authorship

[‡] These authors have contributed equally to this work

Specialty section:
This article was submitted to Molecular and Cellular Oncology, a section of the journal Frontiers in Cell and Developmental Biology

Received: *15 May 2021*
Accepted: *11 August 2021*
Published: *08 September 2021*

Citation:
Li Q, Zhang L, Hou Z-H, Zhao D-X, Li J-B, Zhang S, Yin Y, Ni C-F and Chen T (2021) High Visceral Adipose Tissue Density Correlates With Unfavorable Outcomes in Patients With Intermediate-Stage Hepatocellular Carcinoma Undergoing Transarterial Chemoembolization. Front. Cell Dev. Biol. 9:710104. doi: 10.3389/fcell.2021.710104

INTRODUCTION

Transarterial chemoembolization (TACE) is the standard treatment modality for patients with intermediate stage hepatocellular carcinoma (HCC) according to the widely applied Barcelona Clinic of Liver Cancer (BCLC) staging system (Marrero et al., 2018; Villanueva, 2019). However, the response rates and survival are heterogeneous, and the target patients who will benefit particularly well from TACE is still controversial (Forner et al., 2018). In brief, tumor burden, liver function, and etiology have great influence on the prognosis of BCLC B stage HCC patients. Additionally, simple predictive algorithms including 6 to 12, up to 7, HAP, BCLC sub-classifications, which are mainly based on the tumor number and size as well as Child–Pugh class, were suggested for making decisions for those patients with significant degree of disease heterogeneity (Kim et al., 2017; Lee et al., 2019; Wang et al., 2019). Nevertheless, considering that the predictive value of these parameters could not be validated in larger clinical trials, it is crucial that novel pre-treatment stratification strategies are corroborated in order to improve the overall survival (OS) for intermediate stage HCC patients.

In recent years, previous studies demonstrated that the sarcopenia, which is defined as the declination in muscle volume mass and strength was associated with poor outcomes of HCC patients (Fujiwara et al., 2015; Antonelli et al., 2018; Cruz-Jentoft and Sayer, 2019; Hamaguchi et al., 2019; Qayyum et al., 2021). However, the correlation between sarcopenia and outcomes such as tumor response and survival in intermediate stage HCC patients undergoing TACE treatment has not been largely evaluated (Marasco et al., 2020). In addition, the prognostic role of the pre-treatment skeletal muscle remains debated (Loosen et al., 2019). More recently, the increased visceral adiposity tissue (VAT) has been suggested as an independent risk factor for recurrence after resection in HCC patients (Imai et al., 2021). Nevertheless, its predictive value has not been well studied in these patients receiving TACE treatment. Except from the quantitative measurements of body composition, the mean tissue attenuation expressed in Housfield units (HU) can also offer a qualitative information as well as provide perception into the pathophysiology (Larsen et al., 2020). By contrast, although mean tissue attenuation is easily measured on the computed tomography (CT) images, limit data are shown regarding the prognostic impact of tissue density in BCLC B stage HCC patients.

This study aimed to evaluate the association of skeletal muscle and adipose tissue mass and density with prognostic outcomes of intermediate stage HCC patients treated with TACE.

Abbreviations: HCC, hepatocellular carcinoma; BCLC, Barcelona Clinic Liver Cancer; TACE, transarterial chemoembolization; OS, overall survival; PFS, progression-free survival; IRBs, Institutional Review Boards; CT, computed tomography; BMI, body mass index; HU, Hounsfield units; VEGF, vascular endothelial growth factor; MRI, magnetic resonance imaging; SM, skeletal muscle; VAT, visceral adipose tissue; SAT, subcutaneous adipose tissue; HR, hazard ratio; IQR, interquartile range; mRECIST, modified Response Evaluation Criteria in Solid Tumors; CI, confidence interval.

MATERIALS AND METHODS

Study Population

The current study was reviewed and approved by the Institutional Review Board of the Soochow University and was conducted in accordance with the ethical standards laid down in the Declaration of Helsinki. Consecutive treatment-naïve intermediate-stage HCC patients undergoing TACE treatment between 2008 and 2018 were screened in this retrospective cohort study. The diagnosis of HCC was based on the non-invasive criteria [computed tomography (CT) or magnetic resonance (MR) imaging] or histological assessments. The inclusion criteria were as follows: (i) age >18 years, (ii) no prior HCC-related treatment (resection, ablation, systemic, and radiation therapy), (iii) Eastern Cooperative Oncology Group (ECOG) score 0 or 1, (iv) available CT scans at baseline. Among 256 patients, 209 patients met the inclusion criteria. Patients with decompensated liver function (n = 12), severe renal dysfunction (n = 3), and malignancy other than HCC (n = 2) were excluded. Finally, 192 HCC patients were included in this study. Patient and imaging data were anonymized and extracted from the electronic patient record system.

Transarterial Chemoembolization Treatment

Briefly, TACE was performed as selectively as possible through the segmental or subsegmental hepatic arteries according to the extent of tumor burden and patient's hepatic reserve. To identify the location and all of the feeding vessels of tumor, a thorough angiography was performed. An emulsion of 5–20 ml of iodized oil (Lipiodol; Guerbet Laboratories, Roissy, France) and 20–40 mg epirubicin hydrochloride (Shenzhen Main Luck Pharmaceutical Inc, Shenzhen, China) was infused into the feeding arteries using a 2.7F microcatheter (Renegade; Boston Scientific, Marlborough, Massachusetts; or Progreat; Terumo, Japan). This was followed by particle embolization with Gelfoam (Ailikang Inc, Hangzhou, China) until stasis in a second- or third-order branch was achieved. Repeated TACE treatments were conducted when vital tumor tissue was observed on the contrast-enhanced CT or MRI at every 6–8 weeks. All TACE procedures were performed by one of five interventional radiologists with more than 8 years of experience.

Computed Tomography Scan Analysis

All CT scans including non-contrast scan and contrast-enhanced triple phases were performed with the Siemens SOMATOM Sensation 64 CT scanner (Erlangen, Germany) within 7 days before the initial TACE treatment. For standardized analysis of each patient, a cross-sectional enhanced CT images at the third lumbar vertebra (L3) was selected. The areas of skeletal muscle area (SM) and adipose tissue [subcutaneous, (SAT); visceral (VAT)] were measured by using the Slice-O-Matic software (version 5.0; Tomovision, Montreal, Canada), and the calculation was based on the Hounsfield units (HU) thresholds (−29 to 150 HU for SM, −190 to −30 for SAT and −150 to −50 for VAT) (von Hessen et al., 2021). All of the three

variables were normalized for the height in m^2 and expressed as indexes (cm^2/m^2). The skeletal muscles at L3 consisted of the psoas major, the erector spinae, the quadratus lumborum, the rectus abdominis, the transversus abdominis, the internal oblique, and the external oblique. Additionally, the density of each variable was calculated in HU. For the measurements of the variables, two observers with more than 5 years of experience in abdominal radiology independently measured the CT images from 30 randomly selected patients and compared the results, and the inter-observer agreement was 97.0%.

Outcomes, Assessments, and Follow-Up

All HCC patients received routine blood tests and biochemistry tests before the initial TACE treatment, at 1 month after each TACE and, thereafter, every 8–12 weeks. Tumor response was evaluated with contrast-enhanced CT or MRI after first TACE treatment, 4 weeks after each TACE treatment bias according to modified Response Evaluation Criteria in Solid Tumors (mRECIST) criteria. Through the PACS system (NEUSOFTPACS/RIS, Shengyang Neusoft Co., Ltd, China), assessment of tumor response was performed on the target lesion by two radiologists with more than 5 years of experience in diagnostic radiology and divided into two groups (responder, complete response, and partial response; non-responder, stable disease, and progressive disease). For the survival follow-up, each patient was contacted with regular interval (2 months) by telephone or outpatient review until September 30, 2019, or death, or lost to follow-up.

The primary outcome was overall survival (OS). OS was defined as the time from the date of initial TACE treatment to the date of death or last follow-up (September 30, 2019). The second outcome was progression-free survival (PFS). PFS was defined as the time from the date of initial TACE treatment to the date of radiological progression or death.

Statistical Analysis

All variables were presented as median [interquartile range (IQR)] for quantitative variables and as count (percentage) for qualitative variables. For continuous variables, the Mann–Whitney *U*-test or Student *t*-test was used. The Fischer's exact test was used for categorical variables. The body composition features of patients with different Child–Pugh classes and responses (responder and non-responder) were also documented and compared. One-way ANOVA test was used to compare the differences between Child–Pugh classes and tumor responses. Survival curves were calculated using the Kaplan–Meier method and compared with log-rank test. Receiver operating characteristic (ROC) curve and binary logistic regression were performed to evaluate the predictive performance of the body composition features with respect to responder to TACE treatment. The median values of the parameters were considered as cutoff values. The discrimination and performance of body composition features were measured by area under time-dependent ROC curve. Univariate and multivariate Cox proportional hazard analyses were applied to identify the association between body composition parameters and outcomes. Parameters with p-value < 0.05 in univariate analysis were included in the multivariate analysis. Variables with p-value < 0.05 were regarded statistically significant. All statistical analyses were performed using SPSS 18.0 for Windows (IBM Corporation, Somers, NY, United States) or R version 3.3.2.

RESULTS

Patient Characteristics

Among the 192 intermediate stage HCC patients included in the present study, 157 (79.7%) were men and 35 (20.3%) were women. Median body mass index (BMI) was 22.5 (IQR, 20.8–24.2) and median age was 60 (IQR, 52–67). HBV infection (63.5%) was the main etiology, with a median tumor size of 6.3 cm (IQR, 3.0–9.6). There were 179 patients with Child–Pugh A and 13 patients with Child–Pugh B, 98 and 93 patients with ALBI grades 1 and 2, respectively. One hundred five patients of the entire cohort had cirrhosis. The body composition parameters are presented in **Table 1**. The median value of muscle index, VAT, and SAT were 46.3 (IQR, 39.6–52.8), 38.0 (IQR, 24.6–55.2), and 37.0 (IQR, 27.5–51.1) cm^2/m^2, respectively. The median HU of muscle index, VAT, and SAT were 50.2 (IQR, 46.6–54.3), −89.1 (IQR, −96.7 to −77.2), and −103.6 (IQR, −110.7 to −97.2), respectively. For tumor response after the initial

TABLE 1 | Baseline demographic and clinical characteristics of patients.

Characteristics	Overall (*n* = 192)
Age	60 (52–67)
Gender (male/female)	157 (81.8%)/35 (18.2%)
BMI	22.5 (20.8-24.2)
Etiology (HBV/Others)	122 (63.5%)/70(36.5%)
Tumor Size (cm)	6.3 (3.0–9.6)
Tumor Number	2 (2–4)
Tumor Location (Unilobar/bilobar)	127 (66.1%)/65 (33.9%)
Cirrhosis (Yes/No)	105 (54.7%)/87 (45.3%)
Ascites (Yes/No)	24 (12.5%)/168 (87.5%)
Child-Pugh Class (A/B)	179 (93.2%)/13 (6.8%)
ALBI grade (1/2/3)	98 (51.0%)/93 (48.5%)/1 (0.5%)
AST (U/L)	44.0 (29.0–61.8)
ALT (U/L)	34.0 (23.4–50.4)
Bilirubin	16.3 (11.6–22.4)
ALB (g/L)	39.8 (36.0–43.9)
AFP (ng/dl)	106.0 (10.1–1000.0)
Muscle index	46.3 (39.6–52.8)
VAT index	38.0 (24.6–55.2)
SAT index	37.0 (27.5–51.1)
Muscle HU	50.2 (46.6–54.3)
VAT HU	−89.1(−96.7 to −77.2)
SAT HU	−103.6(−110.7 to −97.2)
Tumor Response (Responder/non-responder)	129 (67.2%)/63 (32.8%)

BMI, Body mass index; ALBI, albumin-bilirubin; ALT, alanine transaminase; AST, aspartate transaminase; ALB, albumin; VAT, visceral adipose tissue; SAT, subcutaneous adipose tissue; AFP, alpha-fetoprotein; HU, hounsfield units.

TABLE 2 | Body mass parameters variability across Tumor Response after initial TACE.

Body Mass Parameters	N	Overall	N	CR + PR	N	PD + SD	*P*-value
Muscle index	192	46.3 (39.6–52.8)	129	46.2 (39.5–52.5)	63	46.4 (39.5–53.0)	0.835
Muscle HU	192	50.2 (46.6–54.3)	129	50.6 (46.6–54.3)	63	49.8 (46.8–54.3)	0.548
SAT index	192	37.0 (27.5–51.1)	129	38.7 (27.7–52.4)	63	34.2 (24.8–47.9)	0.133
SAT HU	192	−103.6 (−110.7 to −97.2)	129	−103.9 (−111.1 to −98.5)	63	−102.9 (−109.7 to −95.0)	0.106
VAT index	192	38.0 (24.6–55.2)	129	38.3 (26.1–55.3)	63	34.2 (21.0–53.6)	0.344
VAT HU	192	−89.1 (−96.7 to −77.2)	129	−90.6 (−98.2 to −80.7)	63	−81.9 (−94.8 to −70.4)	0.001
BMI	192	22.5 (20.8–24.2)	129	22.6 (20.8–24.2)	63	22.0 (20.7–24.7)	0.703

BMI, Body mass index; VAT, visceral adipose tissue; SAT, subcutaneous adipose tissue; HU, hounsfield units.

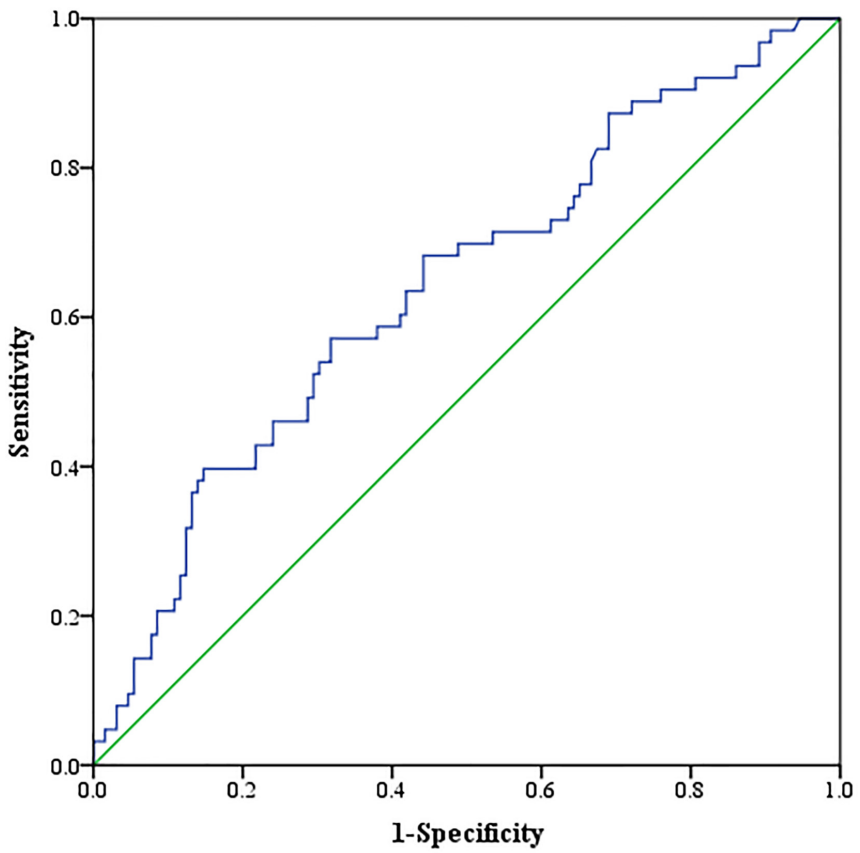

FIGURE 1 | Receiver operating characteristic (ROC) curve analysis concerning the discrimination of visceral adipose tissue (VAT) density between responder and non-responder patients.

TACE response, 129 and 63 patients are responders and non-responders, respectively. The median follow-up was 21.3 months (95% CI, 20.6–22.2). The median OS and PFS of all patients were 20.8 months (95% CI, 18.1–23.7) and 10.6 months (95% CI, 9.2–12.0), respectively.

Differences in Body Composition Features Among Child–Pugh Classes and Tumor Responses

Neither muscle mass nor adipose tissue index was identified to be associated with different Child–Pugh classes in the entire cohort ($p > 0.05$) (**Supplementary Table 1**). For tumor response, we found that a significant variation of VAT HU was detected in the entire group. VAT HU in the responder group tended to be lower than those in the non-responder group [−90.6 (95% CI, −98.2 to −80.7) vs. −81.9 (95% CI, −94.8 to −70.4), $p = 0.001$] (**Table 2**). In addition, the ROC curve analysis showed that VAT HU was suitable to distinguish between responder and non-responder patients, revealing an AUC value of 0.643 (**Figure 1**). The VAT density corresponds to the sensitivity values of 57.1% and specificity values of 68.2%, respectively. Moreover, univariate binary logistic regression analysis was applied to further evaluate the association of the VAT density with the tumor response to

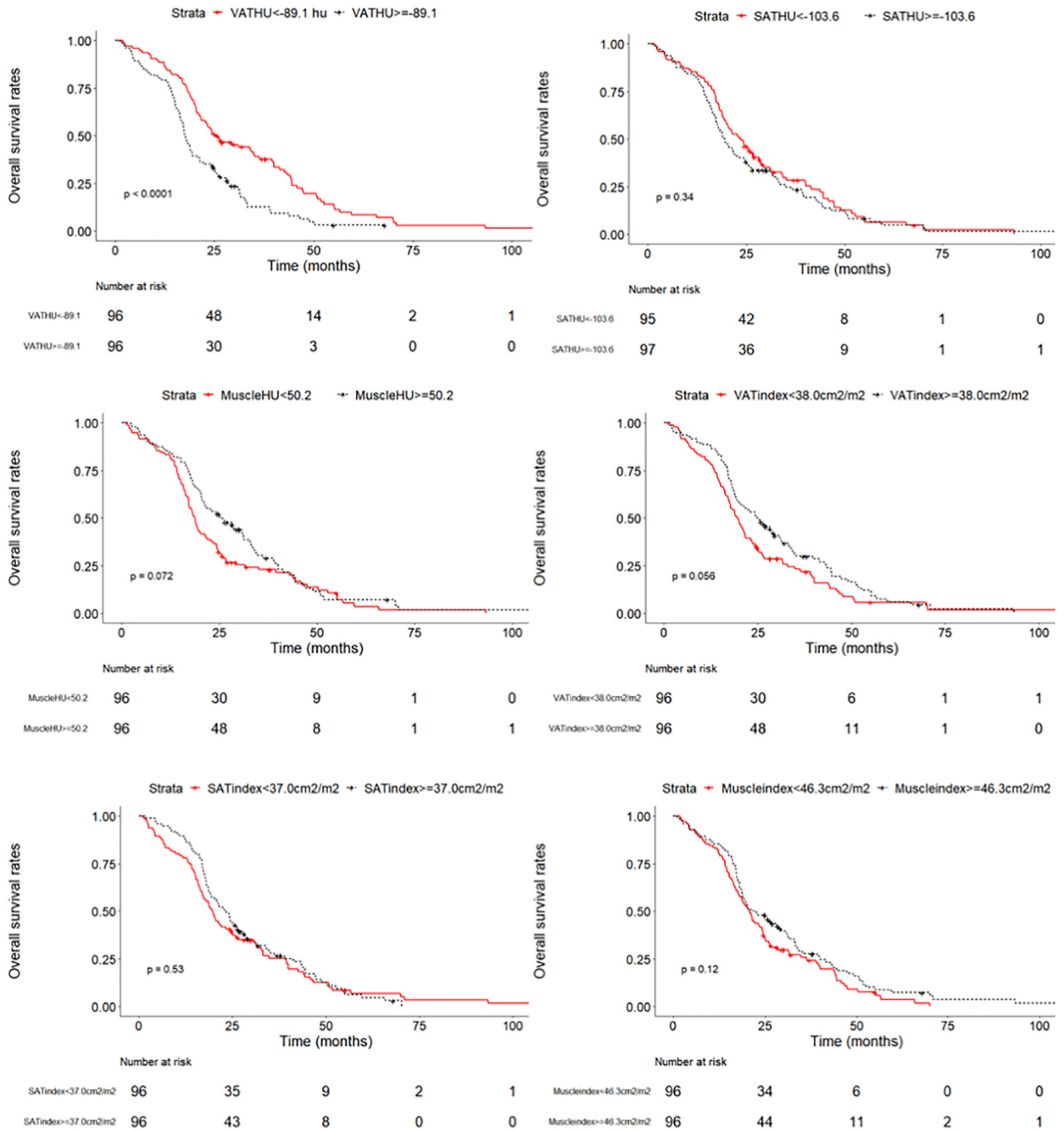

FIGURE 2 | Overall survival curves in patients with intermediate stage hepatocellular carcinoma according to the different body composition parameters.

TACE treatment, showing a statistical significance (odds ratio: 1.035, 95% CI: 1.014–1.058, $p = 0.001$).

Association of Body Composition Features With Outcomes After Transarterial Chemoembolization

We evaluated whether the body composition parameters might be associated with the OS and/or PFS. Hence, we divided the entire cohort into two subgroups with respect to their body composition features (either above or below the 50th percentile). By using this cutoff value, a significant prolonged OS and PFS was displayed by Kaplan–Meier curve analysis for HCC patients with VAT HU below −89.1 (25.1 months, 95% CI: 18.1–32.1 vs. 17.6 months, 95% CI: 16.3–18.8, $p < 0.0001$, 15.4 months, 95% CI: 10.6–20.2 vs. 6.6 months, 95% CI: 4.9–8.3, $p < 0.0001$, respectively) (**Figures 2**, **3**). The patients with muscle HU above 50.2 also had a PFS gain (11.3 months,

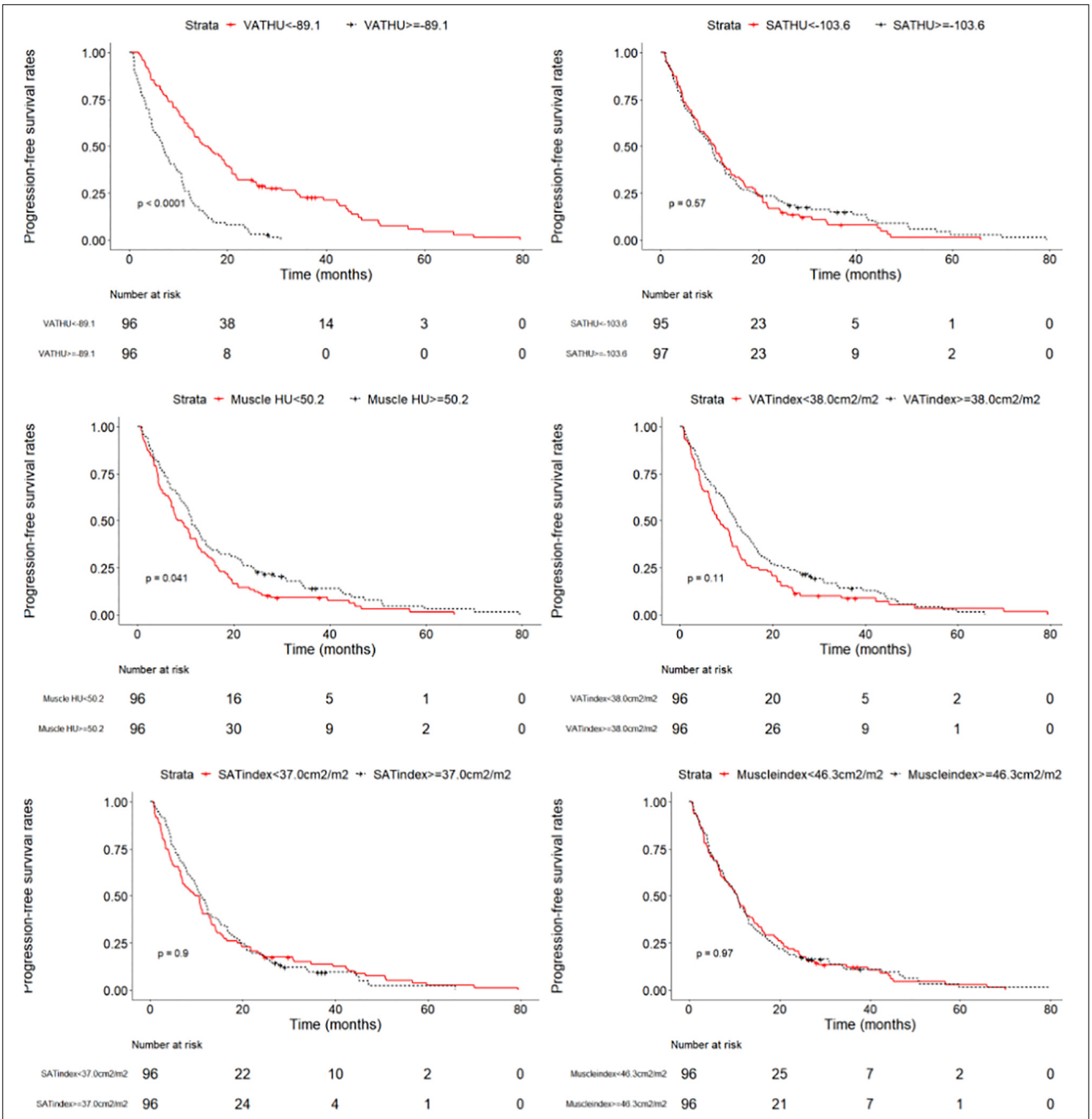

FIGURE 3 | Progression-free survival curves in patients with intermediate stage hepatocellular carcinoma according to the different body composition parameters.

95% CI: 9.6–13.0 vs. 8.3 months, 95% CI: 5.3–11.3, $p = 0.041$) (**Figure 3**). The performance and discrimination of the VAT HU and other body composition features were compared (**Supplementary Tables 2**, **3**). The 1-, 2-, 3-, and 5-year OS AUC values of the VAT HU were higher than the other body composition parameters, suggesting a favorable performance and discrimination (**Figure 4**). Meanwhile, it is also found that 3-, 6-, 9-, and 12-month PFS AUC values of VAT HU were the highest among all the parameters (**Figure 5**). In order to further investigate the predictive value of the body composition features in the context of TACE treatment, univariate and multivariate Cox-regression analyses were performed with respect to the outcomes, and we detected a significant association between VAT density and outcomes (OS, HR: 1.015, 95% CI: 1.004–1.025, $p = 0.005$, PFS, HR: 1.026, 95% CI: 1.016–1.036, $p < 0.0001$, respectively) (**Tables 3**, **4**).

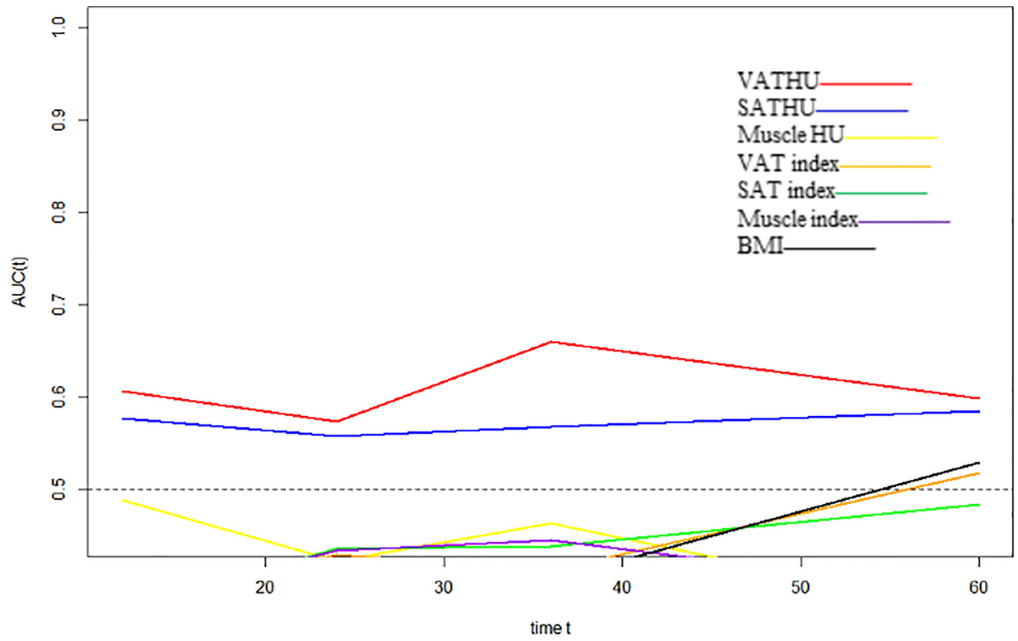

FIGURE 4 | Time-dependent area under the curve (AUC) values of the different body composition parameters in predicting overall survival.

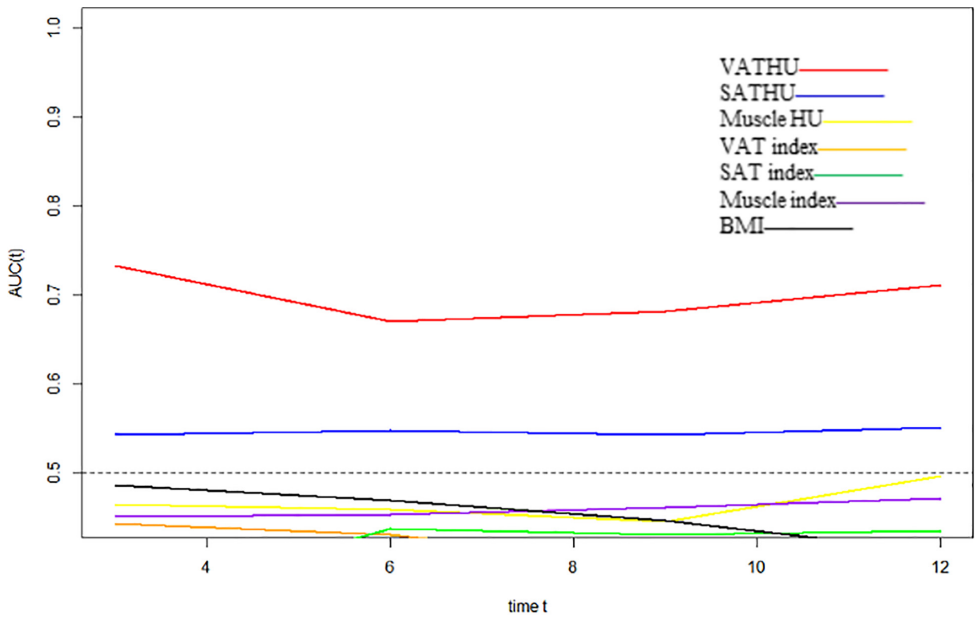

FIGURE 5 | Time-dependent AUC values of the different body composition parameters in predicting progression-free survival.

DISCUSSION

The current study showed the prognostic performance of VAT density for intermediate stage HCC patients treated with TACE. We demonstrated that the VAT density was not only associated with survival such as OS and PFS but also tumor response, suggesting that the influence of VAT HU on BCLC B stage HCC patients' outcomes could reflect tumor-specific factors.

Hepatocellular carcinoma patients with BCLC B stage are a group of highly heterogenous in terms of variable liver function, tumor burden, and disease etiology, leading to various individual responses (Arizumi et al., 2015). Furthermore, repeated TACE may induce impaired liver function and has an impact on the prognosis of the inter-mediated stage HCC patients (Kudo et al., 2014). To prolong OS of the intermediate-stage HCC patients, it is crucial to identify the target population who

TABLE 3 | Univariate and Multivariate analysis of prognostic factors for Overall Survival.

Characteristics	Univariate			Multivariate		
	HR	95% CI	*P*-value	HR	95% CI	*P*-value
Muscle index	0.984	0.969–0.998	0.028			0.065
VAT index	0.993	0.986–1.000	0.063			
SAT index	0.993	0.984–1.001	0.103			
Muscle HU	0.989	0.975–1.004	0.139			
VAT HU	1.015	1.004–1.025	0.005	1.015	1.004–1.025	0.005
SAT HU	1.012	1.000–1.024	0.050			0.393
BMI	0.943	0.894–0.995	0.032			0.127

BMI, Body mass index; VAT, visceral adipose tissue; SAT, subcutaneous adipose tissue; HU, hounsfield units.

TABLE 4 | Univariate and Multivariate analysis of prognostic factors for Progression-free Survival.

Characteristics	Univariate			Multivariate		
	HR	95% CI	*P*-value	HR	95% CI	*P*-value
Muscle index	0.993	0.980–1.007	0.340			
VAT index	0.992	0.986–0.999	0.020			0.695
SAT index	0.996	0.988–1.004	0.376			
Muscle HU	0.984	0.968–1.001	0.061			
VAT HU	1.026	1.017–1.035	<0.0001	1.026	1.016-1.036	<0.0001
SAT HU	1.007	0.995–1.019	0.233			
BMI	0.959	0.911–1.008	0.102			

BMI, Body mass index; VAT, visceral adipose tissue; SAT, subcutaneous adipose tissue; HU, hounsfield units.

may benefit from TACE and make risk stratification. There remains considerable uncertainty, which the existing guidelines do not adequately address criteria for prognostic factors, given the diversity of clinical responses (Vitale et al., 2018). Except the well-knowledged factors such as alpha-fetoprotein, bilirubin, performance status, the other non-invasive and simply applied factors are still on the prowl.

In recent years, previous evidence suggested that there is a correlation between obesity and prognosis of malignancies including HCC (Charette et al., 2019). In addition, non-alcoholic fatty liver disease (NAFLD), which is becoming the first cause of chronic liver disease, is the risk factor of HCC development and prognosis of HCC patients (Seror et al., 2021). Although the body mass index (BMI) is widely applied to characterize the body compositions, limitations persist in its use such as inability to differentiate fat and muscle mass (Strulov Shachar and Williams, 2017). In contrast, analytic morphomics, using semi-automated image-processing platform to evaluate body composition, was considered as offering an accurate approach to quantitate not only the aggressive nature of HCC itself but the underlying HCC patients' characteristics such as liver status (Singal et al., 2016). Moreover, with its available resolution of adipose tissue, CT scan is the gold standard quantitative assessment of tissue density (Doyle et al., 2013).

Previous studies showed that both SAT and VAT density were negatively correlated with survival, suggesting that an increased adipose tissue attenuation could be used as a novel non-invasive biomarker for predicting prognosis (Murphy et al., 2014; Rosenquist et al., 2015). More recently, Hessen et al. suggested that high SAT density correlates negatively with OS in patients with HCC (von Hessen et al., 2021). Our study showed that VAT density was significantly in correlation with tumor response (CR + PR) (odds ratio: 1.035, 95% CI: 1.014–1.058, $p = 0.001$). As such, a pre-TACE VAT HU below −89.1 was an independent predictor for favorable outcomes. HCC patients in this cohort below the cutoff value presented a median OS and PFS of 25.1 and 15.4 months compared with 17.6 and 6.6 months in patients with a VAT HU above the cutoff, highlighting the value of VAT in predicting outcomes of inter-mediated stage HCC patients undergoing TACE. Iwase et al. (2020) reported that a high VAT area was correlated with a reduced disease-free survival in breast cancer patients undergoing neoadjuvant chemotherapy. In general, SAT and VAT are two main compartments with different metabolic characteristics of body fat tissue (Shuster et al., 2012). Compared with SAT, previous studies showed the association between VAT and various pathologies such as insulin resistance, impaired glucose, and lipid metabolism could relate to the prognosis of patients with cancers, and VAT was regarded to be more pro-tumorigenic and pro-inflammatory (Neeland et al., 2019; Li et al., 2020). Moreover, hormones and bioactive molecules including interleutin 6 (IL-6), tumor necrosis factor, adiponectin, and resistin are released by the VAT (Shuster et al., 2012). Insulin can irritate the proliferation of HCC cells and accelerate the vascular invasion of HCC (Karagozian et al., 2014). In particular, considering that adiponectin has protective antiangiogenic activity, regulating

the vascular endothelial growth factor (VEGF) levels induced by TACE could have an impact on outcomes of HCC patients (Bagchi et al., 2013). The reasons for only high VAT density had a negative impact on outcomes are speculated as follows: First, adipose tissue density might be qualitative biomarker and a high adipose tissue density is in correlation with a depletion of adipose, which could reflect the poor nutritional condition (Charette et al., 2019). In addition, the underlying diseases in HCC patients and chronic inflammation could also lead to a higher VAT density (Batista et al., 2016). Finally, in patients with cancer cachexia, the high CT density of fat tissue, which is determined by fat and lipid could result from the activation of brown adipose tissue (Beijer et al., 2012). Interestingly, a cutoff value of −89.1 HU, which has been demonstrated in the present study, was close to the previous study in HCC patients, with a cutoff value of −88 HU (von Hessen et al., 2021).

Numerous studies showed that sarcopenia, which is defined as a progressive and generalized skeletal disorder, was considered associated with a higher incidence of adverse events and poor prognosis in HCC patients treated with various therapies (Choi et al., 2020; Uojima et al., 2020). Nevertheless, there is little data concerning the prognosis value of sarcopenia in HCC patients receiving TACE (Marasco et al., 2020). This study suggested that patients with a higher muscle density had a PFS gain, whereas the muscle mass and density had no correlation with the OS and tumor response. Kobayashi et al. (2018) and Fujita et al. (2019) showed there was no significance between pre-TACE muscle mass and clinical outcomes. In contrast, two other studies indicated pre-TACE sarcopenia was an independent factor of negative outcomes (Dodson et al., 2013; Loosen et al., 2019). These finding demonstrated that the role of the sarcopenia in predicting prognosis may mainly depend on the general clinical status of HCC patients and not directly on the local response of TACE treatment (Marasco et al., 2020).

Of note, there are some limitations in this study. First, it is a small sample retrospective study and subject to collection and selection bias. HCC patients with unavailable CT scans were excluded in this study. Additionally, the lack of a control group represents limit in the convincing evidence of the analysis. The results also need to be confirmed with external validation. Finally, changes in the body composition parameters after TACE treatment were not analyzed in the study. The impact of changes of these parameters on the outcomes of intermediate stage HCC patients treated with TACE should be further conducted with future large sample size studies.

In conclusion, the VAT density could provide prognostic prediction value and may be helpful to stratify the BCLC B stage patients in order to optimize the selection criteria for undergoing TACE treatment.

DATA AVAILABILITY STATEMENT

The raw data supporting the conclusions of this article will be made available by the authors, without undue reservation.

ETHICS STATEMENT

The current study was reviewed and approved by the Institutional Review Board of the Soochow University and was conducted in accordance with the ethical standards laid down in the Declaration of Helsinki. The requirement for informed consent was waived due to its retrospective nature.

AUTHOR CONTRIBUTIONS

All authors contributed to the review and critical revision of the manuscript and approved the final version of the manuscript. TC, C-FN, QL, and LZ contributed to the study concept and design. QL, LZ, Z-HH, D-XZ, and SZ contributed to the acquisition of data. LZ, Z-HH, D-XZ, and J-BL contributed to the analysis and interpretation of the data. LZ, Z-HH, D-XZ, and YY contributed to the statistical analysis. QL, LZ, Z-HH, and D-XZ contributed to the drafting of the manuscript. The corresponding author had full access to all the data and took full responsibility for the veracity of the data and the statistical analyses.

FUNDING

This study was supported by the Natural Science Foundation of Zhejiang Province (LGF20H180005), Zhejiang Province Medicine and Health Project (2019RC273), and the Jiangsu Medical Innovation Team (CXTDB2017006). The funding source had no involvement in the financial support for the conduct of the research and preparation of the manuscript.

SUPPLEMENTARY MATERIAL

The Supplementary Material for this article can be found online at: https://www.frontiersin.org/articles/10.3389/fcell.2021.710104/full#supplementary-material

REFERENCES

Antonelli, G., Gigante, E., Iavarone, M., Begini, P., Sangiovanni, A., Iannicelli, E., et al. (2018). Sarcopenia is associated with reduced survival in patients with advanced hepatocellular carcinoma undergoing sorafenib treatment. *United European Gastroenterol. J.* 6, 1039–1048. doi: 10.1177/2050640618781188

Arizumi, T., Ueshima, K., Minami, T., Kono, M., Chishina, H., Takita, M., et al. (2015). Effectiveness of sorafenib in patients with Transcatheter Arterial Chemoembolization (TACE) refractory and intermediate-stage hepatocellular carcinoma. *Liver Cancer* 4, 253–262. doi: 10.1159/000367743

Bagchi, M., Kim, L. A., Boucher, J., Walshe, T. E., Kahn, C. R., and D'Amore, P. A. (2013). Vascular endothelial growth factor is important for brown adipose tissue development and maintenance. *FASEB J.* 27, 3257–3271. doi: 10.1096/fj.12-221812

Batista, M. L. Jr., Henriques, F. S., Neves, R. X., Olivan, M. R., Matos-Neto, E. M., Alcantara, P. S. M., et al. (2016). Cachexia-associated adipose tissue

morphological rearrangement in gastrointestinal cancer patients. *J. Cachexia Sarcopenia Muscle* 7, 37–47. doi: 10.1002/jcsm.12037

Beijer, E., Schoenmakers, J., Vijgen, G., Kessels, F., Dingemans, A.-M., Schrauwen, P., et al. (2012). A role of active brown adipose tissue in cancer cachexia? *Oncol. Rev.* 6:e11. doi: 10.4081/oncol.2012.174

Charette, N., Vandeputte, C., Ameye, L., Bogaert, C. V., Krygier, J., Guiot, T., et al. (2019). Prognostic value of adipose tissue and muscle mass in advanced colorectal cancer: a post hoc analysis of two non-randomized phase II trials. *BMC Cancer* 19:134. doi: 10.1186/s12885-019-5319-8

Choi, K., Jang, H. Y., Ahn, J. M., Hwang, S. H., Chung, J. W., Choi, Y. S., et al. (2020). The association of the serum levels of myostatin, follistatin, and interleukin-6 with sarcopenia, and their impacts on survival in patients with hepatocellular carcinoma. *Clin. Mol. Hepatol.* 26, 492–505. doi: 10.3350/cmh.2020.0005

Cruz-Jentoft, A. J., and Sayer, A. A. (2019). Sarcopenia. *Lancet* 393, 2636–2646. doi: 10.1016/S0140-6736(19)31138-9

Dodson, R. M., Firoozmand, A., Hyder, O., Tacher, V., Cosgrove, D. P., Bhagat, N., et al. (2013). Impact of sarcopenia on outcomes following intra-arterial therapy of hepatic malignancies. *J. Gastrointest. Surg.* 17, 2123–2132. doi: 10.1007/s11605-013-2348-5

Doyle, S. L., Bennett, A. M., Donohoe, C. L., Mongan, A. M., Howard, J. M., Lithander, F. E., et al. (2013). Establishing computed tomography-defined visceral fat area thresholds for use in obesity-related cancer research. *Nutr. Res.* 33, 171–179. doi: 10.1016/j.nutres.2012.12.007

Forner, A., Reig, M., and Bruix, J. (2018). Hepatocellular carcinoma. *Lancet* 391, 1301–1314. doi: 10.1016/S0140-6736(18)30010-2

Fujita, M., Takahashi, A., Hayashi, M., Okai, K., Abe, K., and Ohira, H. (2019). Skeletal muscle volume loss during transarterial chemoembolization predicts poor prognosis in patients with hepatocellular carcinoma. *Hepatol. Res.* 49, 778–786.

Fujiwara, N., Nakagawa, H., Kudo, Y., Tateishi, R., Taguri, M., Watadani, T., et al. (2015). Sarcopenia, intramuscular fat deposition, and visceral adiposity independently predict the outcomes of hepatocellular carcinoma. *J. Hepatol.* 63, 131–140. doi: 10.1016/j.jhep.2015.02.031

Hamaguchi, Y., Kaido, T., Okumura, S., Kobayashi, A., Shirai, H., Yao, S., et al. (2019). Preoperative visceral adiposity and muscularity predict poor outcomes after hepatectomy for hepatocellular carcinoma. *Liver Cancer* 8, 92–109. doi: 10.1159/000488779

Imai, K., Takai, K., Miwa, T., Maeda, T., Hanai, T., Shiraki, M., et al. (2021). Increased visceral adipose tissue and hyperinsulinemia raise the risk for recurrence of Non-B Non-C hepatocellular carcinoma after curative treatment. *Cancers* 13:1542. doi: 10.3390/cancers13071542

Iwase, T., Sangai, T., Fujimoto, H., Sawabe, Y., Matsushita, K., Nagashima, K., et al. (2020). Quality and quantity of visceral fat tissue are associated with insulin resistance and survival outcomes after chemotherapy in patients with breast cancer. *Breast Cancer Res. Treat.* 179, 435–443. doi: 10.1007/s10549-019-05467-7

Karagozian, R., Derdak, Z., and Baffy, G. (2014). Obesity-associated mechanisms of hepatocarcinogenesis. *Metabolism* 63, 607–617.

Kim, J. H., Shim, J. H., Lee, H. C., Sung, K. B., Ko, H. K., Ko, G. Y., et al. (2017). New intermediate-stage subclassification for patients with hepatocellular carcinoma treated with transarterial chemoembolization. *Liver Int.* 37, 1861–1868.

Kobayashi, T., Kawai, H., Nakano, O., Abe, S., Kamimura, H., Sakamaki, A., et al. (2018). Rapidly declining skeletal muscle mass predicts poor prognosis of hepatocellular carcinoma treated with transcatheter intra-arterial therapies. *BMC Cancer* 18:756. doi: 10.1186/s12885-018-4673-2

Kudo, M., Arizumi, T., and Ueshima, K. (2014). Assessment for retreatment (ART) score for repeated transarterial chemoembolization in patients with hepatocellular carcinoma. *Hepatology* 59, 2424–2425.

Larsen, B., Bellettiere, J., Allison, M., McClelland, R. L., Miljkovic, I., Vella, C. A., et al. (2020). Muscle area and density and risk of all-cause mortality: the multi-ethnic study of atherosclerosis. *Metabolism* 111:154321.

Lee, I. C., Hung, Y. W., Liu, C. A., Lee, R. C., Su, C. W., Huo, T. I., et al. (2019). A new ALBI-based model to predict survival after transarterial chemoembolization for BCLC stage B hepatocellular carcinoma. *Liver Int.* 39, 1704–1712. doi: 10.1111/liv.14194

Li, C. R., Spallanzani, R. G., and Mathis, D. (2020). Visceral adipose tissue tregs and the cells that nurture them. *Immunol. Rev.* 295, 114–125. doi: 10.1111/imr.12850

Loosen, S. H., Schulze-Hagen, M., Bruners, P., Tacke, F., Trautwein, C., Kuhl, C., et al. (2019). Sarcopenia is a negative prognostic factor in patients undergoing Transarterial Chemoembolization (TACE) for hepatic malignancies. *Cancers* 11:1503.

Marasco, G., Serenari, M., Renzulli, M., Alemanni, L. V., Rossini, B., Pettinari, I., et al. (2020). Clinical impact of sarcopenia assessment in patients with hepatocellular carcinoma undergoing treatments. *J. Gastroenterol.* 55, 927–943.

Marrero, J. A., Kulik, L. M., Sirlin, C. B., Zhu, A. X., Finn, R. S., Abecassis, M. M., et al. (2018). Diagnosis, staging, and management of hepatocellular carcinoma: 2018 practice guidance by the american association for the study of liver diseases. *Hepatology* 68, 723–750. doi: 10.1002/hep.29913

Murphy, R. A., Register, T. C., Shively, C. A., Carr, J. J., Ge, Y., Heilbrun, M. E., et al. (2014). Adipose tissue density, a novel biomarker predicting mortality risk in older adults. *J. Gerontol. A Biol. Sci. Med. Sci.* 69, 109–117.

Neeland, I. J., Ross, R., Despres, J. P., Matsuzawa, Y., Yamashita, S., Shai, I., et al. (2019). Visceral and ectopic fat, atherosclerosis, and cardiometabolic disease: a position statement. *Lancet Diabetes Endocrinol.* 7, 715–725. doi: 10.1016/S2213-8587(19)30084-1

Qayyum, A., Bhosale, P., Aslam, R., Avritscher, R., Ma, J., Pagel, M. D., et al. (2021). Effect of sarcopenia on systemic targeted therapy response in patients with advanced hepatocellular carcinoma. *Abdom. Radiol. (NY)* 46, 1008–1015.

Rosenquist, K. J., Massaro, J. M., Pedley, A., Long, M. T., Kreger, B. E., Vasan, R. S., et al. (2015). Fat quality and incident cardiovascular disease, all-cause mortality, and cancer mortality. *J. Clin. Endocrinol. Metab.* 100, 227–234.

Seror, M., Sartoris, R., Hobeika, C., Bouattour, M., Paradis, V., Rautou, P.-E., et al. (2021). Computed tomography-derived liver surface nodularity and sarcopenia as prognostic factors in patients with resectable metabolic syndrome-related hepatocellular carcinoma. *Ann. Surg. Oncol.* 28, 405–416.

Shuster, A., Patlas, M., Pinthus, J. H., and Mourtzakis, M. (2012). The clinical importance of visceral adiposity: a critical review of methods for visceral adipose tissue analysis. *Br. J. Radiol.* 85, 1–10.

Singal, A. G., Zhang, P., Waljee, A. K., Ananthakrishnan, L., Parikh, N. D., Sharma, P., et al. (2016). Body composition features predict overall survival in patients with hepatocellular carcinoma. *Clin. Transl. Gastroenterol.* 7:e172.

Strulov Shachar, S., and Williams, G. R. (2017). The obesity paradox in cancer-moving beyond BMI. *Cancer Epidemiol. Biomarkers Prev.* 26, 13–16.

Uojima, H., Chuma, M., Tanaka, Y., Hidaka, H., Nakazawa, T., Iwabuchi, S., et al. (2020). Skeletal muscle mass influences tolerability and prognosis in hepatocellular carcinoma patients treated with lenvatinib. *Liver Cancer* 9, 193–206.

Villanueva, A. (2019). Hepatocellular carcinoma. *N. Engl. J. Med.* 380, 1450–1462. doi: 10.1056/NEJMra1713263

Vitale, A., Farinati, F., Noaro, G., Burra, P., Pawlik, T. M., Bucci, L., et al. (2018). Restaging patients with hepatocellular carcinoma before additional treatment decisions: a multicenter cohort study. *Hepatology* 68, 1232–1244.

von Hessen, L., Roumet, M., Maurer, M. H., Lange, N., Reeves, H., Dufour, J.-F., et al. (2021). High subcutaneous adipose tissue density correlates negatively with survival in patients with hepatocellular carcinoma. *Liver Int.* 41, 828–836.

Wang, Q., Xia, D., Bai, W., Wang, E., Sun, J., Huang, M., et al. (2019). Development of a prognostic score for recommended TACE candidates with hepatocellular carcinoma: a multicentre observational study. *J. Hepatol.* 70, 893–903. doi: 10.1016/j.jhep.2019.01.013

Conflict of Interest: The authors declare that the research was conducted in the absence of any commercial or financial relationships that could be construed as a potential conflict of interest.

Publisher's Note: All claims expressed in this article are solely those of the authors and do not necessarily represent those of their affiliated organizations, or those of the publisher, the editors and the reviewers. Any product that may be evaluated in this article, or claim that may be made by its manufacturer, is not guaranteed or endorsed by the publisher.

frontiers in Cell and Developmental Biology

ORIGINAL RESEARCH
published: 13 September 2021
doi: 10.3389/fcell.2021.727935

Uncovering the Association Between m^{5}C Regulator-Mediated Methylation Modification Patterns and Tumour Microenvironment Infiltration Characteristics in Hepatocellular Carcinoma

*Xinyu Gu†, Haibo Zhou†, Qingfei Chu†, Qiuxian Zheng, Jing Wang and Haihong Zhu**

State Key Laboratory for Diagnosis and Treatment of Infectious Diseases, National Clinical Research Center for Infectious Diseases, Collaborative Innovation Center for Diagnosis and Treatment of Infectious Diseases, The First Affiliated Hospital, College of Medicine, Zhejiang University, Hangzhou, China

OPEN ACCESS

Edited by:
Zhigang Ren, First Affiliated Hospital of Zhengzhou University, China

Reviewed by:
Yuting He, First Affiliated Hospital of Zhengzhou University, China
Guangxi Wang, Peking University Health Science Centre, China

***Correspondence:**
Haihong Zhu
zhuhh72@zju.edu.cn

† These authors have contributed equally to this work

Specialty section:
This article was submitted to Molecular and Cellular Oncology, a section of the journal Frontiers in Cell and Developmental Biology

Received: *20 June 2021*
Accepted: *24 August 2021*
Published: *13 September 2021*

Citation:
Gu X, Zhou H, Chu Q, Zheng Q, Wang J and Zhu H (2021) Uncovering the Association Between m^{5}C Regulator-Mediated Methylation Modification Patterns and Tumour Microenvironment Infiltration Characteristics in Hepatocellular Carcinoma. Front. Cell Dev. Biol. 9:727935. doi: 10.3389/fcell.2021.727935

Background: 5-Methylcytosine (m^{5}C) plays essential roles in hepatocellular carcinoma (HCC), but the association between m^{5}C regulation and immune cell infiltration in HCC has not yet been clarified.

Methods: In this study, we analysed 371 patients with HCC from The Cancer Genome Atlas (TCGA) database, and the expression of 13 m^{5}C regulators was investigated. Additionally, gene set variation analysis (GSVA), unsupervised clustering analysis, single-sample gene set enrichment analysis (ssGSEA), correlation analysis, and immunohistochemical (IHC) staining were performed.

Results: Among the 371 patients, 41 had mutations in m^{5}C regulators, the frequency of which was 11.26%. Compared with normal hepatic tissues, the expression of m^{5}C regulators with copy number variations (CNVs) expansion was significantly higher than that in HCC tissues. Then, we identified three m^{5}C modification patterns that had obvious tumour microenvironment (TME) cell infiltration characteristics. The prognostic analysis of the three major m^{5}C modification subtypes showed that Cluster-2 had a clear survival advantage over the others. In addition, we found that DNMT1 was highly expressed in tumour tissues compared with normal tissues in a tissue microarray (TMA) and that it was positively correlated with many TME-infiltrating immune cells. High expression of the m^{5}C regulator DNMT1 was related to a poor prognosis in patients with HCC. Furthermore, we developed three distinct Immu-clusters. Importantly, mRNAs related to the transcription of growth factor β (TGF-β)/EMT pathway were significantly up-regulated in Immu-cluster 2, indicating that this cluster is considered to be the immune rejection

phenotype. Immu-cluster 3 showed elevated expression of mRNAs related to immune checkpoint genes.

Conclusion: Our work revealed the association between m5C modification and immune regulators in the TME. These findings also suggest that DNMT1 has great potential as a prognostic biomarker and therapeutic target for HCC.

Keywords: HCC, DNMT1, m5C modification patterns, TME, prognosis

INTRODUCTION

Hepatocellular carcinoma (HCC) is the sixth most common cancer and the fourth leading cause of cancer-related death worldwide (Llovet et al., 2021). Risk factors for HCC include hepatitis B virus (HBV), hepatitis C virus (HCV), non-alcoholic fatty liver disease, obesity with diabetes, etc. Patients who are infected with HCV can be treated with antiviral therapies, while patients who are infected with HBV remain infected throughout life (European Association for the Study of the Liver, 2017). The survival of patients is driven by tumour stage, with a 5-year survival rate exceeding 70% for those with early-stage HCC compared to a median survival time of 1–1.5 years for those with advanced-stage HCC (Llovet et al., 2016). Most HCC patients are diagnosed at advanced stages, and limited effective therapeutic strategies are available (Hernandez-Gea et al., 2013).

Tumour cells are the driving cause of tumour development and progression. However, without the tumour microenvironment (TME), tumour cells cannot act alone in the progression of cancer. The TME includes the surrounding blood vessels, fibroblasts, immune cells, extracellular matrix, and signalling molecules. These elements contribute to the processes of carcinogenesis and progression, while it is still a major challenge to fully evaluate the complex TME (Hanahan and Coussens, 2012).

Epigenetic deregulation, such as aberrant DNA methylation and reversible chemical RNA modifications play a critical role in cancer (Davalos et al., 2018; García-Vílchez et al., 2019). Previous studies have mainly focused on m6A modification in regulating coding and non-coding RNA processing and function (Nombela et al., 2021). Emerging evidence has revealed the important role of 5-methylcytosine (m5C) in posttranscriptional regulation (Xue et al., 2020a). In addition, m5C modification was found to be abundant in mammalian cells, characterised by the addition of a methyl group at the carbon-5 position of the cytosine base (Bestor, 1988). m5C is mainly distributed in GC-rich areas. Over 10,000 potential sites of m5C modification have been detected in the whole human transcriptome (Bourgeois et al., 2015). The regulation of m5C is a dynamic process controlled by three major regulators, termed "writers" (add a special modification), "readers" (identify and bind modified nucleotides), and "erasers" (remove a special modification) (Yang et al., 2018).

Recently, targeting the TME has been an encouraging method for cancer treatment (Bejarano et al., 2021). Some studies showed a correlation between m6A and TME-infiltrating immune cells (Yi et al., 2020; Zhang et al., 2020a; Chong et al., 2021; Shen et al., 2021). However, due to technological limitations, the research above was restricted to one or two type of modification regulators or cell types, while anti-tumour effects involve multiple tumour suppressors interacting in a vitally cooperative way. Hence, a deep understanding of TME cell infiltration mediated by several regulators of gene modifications will help to enhance the perception of TME immune regulation, especially m5C modification.

In this study, we analysed 371 patients with HCC from The Cancer Genome Atlas (TCGA) database, and the samples were integrated to evaluate m5C modification patterns. Correlation analysis was performed between the m5C modification pattern and TME cell infiltration characteristics. Three different m5C modification patterns were discovered based on the expression of 13 m5C regulators. Besides, we found that distinct m5C modification patterns were closely associated with different enrichment pathways and immune cell infiltration characteristics, indicating that m5C modification might play an essential role in forming an individual TME.

MATERIALS AND METHODS

HCC Data Source and Preprocessing

Gene expression and clinical annotation data were downloaded from the TCGA database. Patients without complete survival data were excluded. The TCGA-Liver Hepatocellular Carcinoma (TCGA-LIHC) dataset was used for further analysis. Finally, a total of 371 patient in the TCGA-LIHC cohort were selected for this study.

For the TCGA dataset, the R package TCGA biolinks (Colaprico et al., 2016), which was developed to analyse Genomic Data Commons (GDC) data, was utilised to download the fragments per kilobase per million mapped reads (FPKM) values of gene expression from the GDC.[1] FPKM values were further converted to transcripts per kilobase million (TPM) values. Batch effects generated by factors unrelated to any biological variations

Abbreviations: m5C, 5-methylcytosine; HCC, hepatocellular carcinoma; TCGA, The Cancer Genome Atlas; GSVA, gene set variation analysis; ssGSEA, single-sample gene set enrichment analysis; IHC, immunohistochemical; TME, tumour microenvironment; TMA, tissue microarray; HBV, hepatitis B virus; HCV, hepatitis C virus; m6A, N^6-methyladenosine; GDC, Genomic Data Commons; FPKM, fragments per kilobase per million mapped reads; TPM, transcripts per kilobase million; MsigDB, Molecular Signatures Database; FDR, false discovery rate; DCs, dendritic cells; NK, natural killer; DEGs, differentially expressed genes; ANOVA, one-way analysis of variance; CNVs, copy number variations; OS, overall survival; MDSCs, myeloid-derived suppressor cells; TIME, tumour immune-microenvironment.

[1] https://portal.gdc.cancer.gov

were corrected for using the parametric and non-parametric empirical Bayes framework algorithm from the sva package. Data related to somatic mutations were downloaded from the TCGA database. R (3.6.1) together with Bioconductor packages were employed in the study.

Unsupervised Clustering Analysis of m^{5}C Regulators

A total of 13 m^{5}C regulators were extracted from 371 patients in the TCGA-LIHC cohort: 11 writers (NOP2, NSUN2, NSUN3, NSUN4, NSUN5, NSUN6, NSUN7, DNMT1, TRDMT1, DNMT3A, and DNMT3B), 1 eraser (TET2), and 1 reader (ALYREF). Unsupervised clustering analysis was employed to distinguish different m^{5}C modifications, after which the classification of patients was conducted for subsequent analysis.

A consensus clustering algorithm (Hartigan and Wong, 1979) was employed to assure the number of clusters and their stability. The ConsensusClusterPlus package was applied to execute the workflow mentioned above, and the stability of the classification was accomplished by conducting 1000 repetitions (Wilkerson and Hayes, 2010).

Gene Set Variation Analysis and Functional Annotation

To explore the disparity of biological processes in m^{5}C modification patterns, the gene set variation analysis ("GSVA") R package was used to perform GSVA. This package is based on a non-parametric and unsupervised algorithm and is widely used to estimate the variation in gene set enrichment in expression datasets (Hänzelmann et al., 2013). GSVA was implemented with "c2.cp.kegg.v6.2.symbols" gene sets obtained from the Molecular Signatures Database (MsigDB). An adjusted *P*-value of less than 0.05 was regarded as statistically significant. We applied the "ClusterProfiler" R package to functionally annotate m^{5}C-related genes under the false discovery rate (FDR) threshold of <0.05.

Single-Sample Gene Set Enrichment Analysis

The single-sample gene set enrichment analysis (ssGSEA) algorithm was used to determine the relative richness in cell infiltration in the TME. We obtained the gene set associated with each infiltrating immune cell type in the TME from Charoentong, who stores information on various human immune cells, including CD8 T cells, dendritic cells (DCs), natural killer (NK) T cells, macrophages, regulatory T cells, etc. (Barbie et al., 2009; Charoentong et al., 2017). ssGSEA was employed to determine the enrichment scores and define the relative abundance of each TME-infiltrating cell type in the corresponding sample.

Identification of Differentially Expressed Genes Among the m^{5}C Phenotypes

With the aim of distinguishing m^{5}C-related genes, all the patients were divided into three m^{5}C modification patterns according to the expression of m^{5}C regulators. The empirical Bayesian algorithm under the limma package in R was used to assure differentially expressed genes (DEGs) in heterogeneous modification patterns.

Correlation Between the m^{5}C Gene Signature and Biological Pathways

A set of genes was constructed by Mariathasan et al. (2018), Rosenberg et al. (2016) and Şenbabaoğlu et al. (2016), in which genes associated with certain biological processes are stored. Correlation analysis was employed to explore the association between the gene signature of m^{5}C and biological pathways.

Cell Culture

Human liver cell line Huh7 and paired normal human liver cell L02 were purchased from Chinese Academy of Sciences (Shanghai, China) and cultured in DMEM (Gibco, Carlsbad, CA, United States) supplemented with 10% fetal bovine serum (FBS; Gibco; Thermo Fisher Scientific) and 1% penicillin n (MP Biomedicals, Santa Ana, CA, United States). The cells were cultured at 37°C in atmosphere of 5% CO_2.

Quantitative Reverse-Transcription PCR

Total RNA from Huh7 cell line was extracted with Rneasy Mini Kit (Qiagen, Valencia, CA, United States) and then reverse-transcribed into cDNA preformed using the PrimeScript^{TM} RT reagent Kit. GAPDH was used as the internal control. The expression levels of 11 writers (NOP2, NSUN2, NSUN3, NSUN4, NSUN5, NSUN6, NSUN7, DNMT1, TRDMT1, DNMT3A, and DNMT3B), 1 eraser (TET2), and 1 reader (ALYREF) were quantified using $2^{-\Delta\Delta Ct}$ method by ABI7500fast PCR instrument. The primers are listed in **Supplementary Table 1**.

Immunohistochemical Staining

Human HCC tissue arrays and normal tissues (catalogue number: HlivH180Su15) were purchased from Shanghai Outdo Biotech Co., Ltd. (Shanghai, China). The method of immunohistochemical (IHC) staining has been reported previously. Briefly, antigen retrieval was performed by heating the tissue sections at 100°C for 30 min in target retrieval solution. Then, the tissue microarray (TMA) was incubated with a DNMT1 primary antibody [(EPR18453) (ab188453) Abcam, Cambridge, MA, United States], followed by incubation with an anti-rabbit secondary antibody. Two independent pathologists blindly assessed the IHC results according to the staining area and intensity (Zhang et al., 2020b).

Statistical Analysis

Spearman and distance correlation analyses were performed to obtain the correlation coefficients of the TME-infiltrating immune cells and the corresponding expression of m^{5}C regulators. Student's *T*-test was used for comparisons two groups. One-way analysis of variance (ANOVA) and Kruskal–Wallis tests were performed to compare differences between three or more groups (Hazra and Gogtay, 2016). The Kaplan–Meier method was utilised to generate survival curves for the prognostic analysis, and the log-rank test was applied to identify significant differences. Univariate Cox regression was adopted to determine

the hazard ratios of m^{5}C regulators and genes related to specific m^{5}C phenotypes. Multivariable Cox regression was utilised to identify independent prognostic risk factors. Patients with complete relevant data were subjected to further analysis with a multivariate model. The multivariate results were visualised with the forestplot package in R. Copy number variations (CNVs)

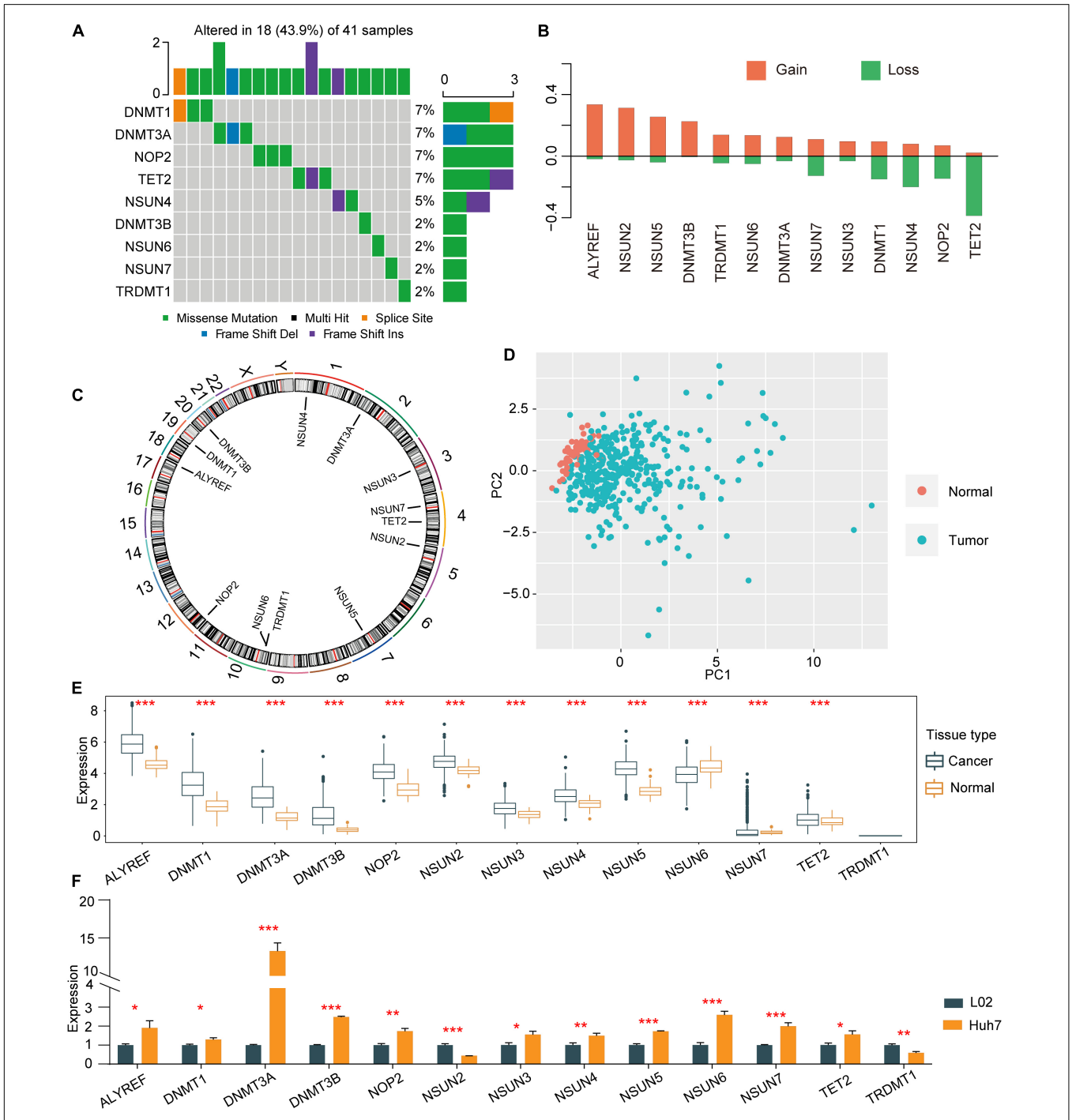

FIGURE 1 | Copy number variations and somatic mutations in 13 m^{5}C regulators in HCC. **(A)** Mutation frequencies of the top 9 m^{5}C regulators. **(B)** CNV alterations among the 13 regulators. **(C)** Locations of mutations in the m^{5}C regulators at the chromosome level. **(D)** Principal component analysis was used to distinguish tumour tissues and normal tissues based on the expression of m^{5}C regulators. **(E)** The expression profiles of m^{5}C regulator genes in tumour tissues and adjacent normal tissues. **(F)** qRT-PCR was used to determine the relative expression of NOP2, NSUN2, NSUN3, NSUN4, NSUN5, NSUN6, NSUN7, DNMT1, TRDMT1, DNMT3A, DNMT3B, TET2, and ALYREF in HCC cell line Huh7 and normal control cell line L02. *$p < 0.05$, **$p < 0.01$, ***$p < 0.001$.

in 13 m^{5}C regulators were plotted with the Rcircos package (Mayakonda et al., 2018). All *P*-values were two-sided, with $P < 0.05$ considered statistically significant. The analysis was accomplished in R 3.6.1 software.

RESULTS

Landscape of Genetic Variations in m^{5}C Regulators in HCC

A total of 13 regulators of m^{5}C were identified, including 11 writers, 1 eraser, and 1 reader. First, the incidence of CNVs and somatic mutations in regulators in HCC were summarised. In 364 samples, 41 showed mutations in m^{5}C regulators, the occurrence of which was 11.26%. DNMT1 was found to be exposed to a higher frequency of mutations, followed by DNMT3A, while ALYREF, NSUN2, NSUN3, and NSUN5 were not (**Figure 1A**). CNVs were also detected in 13 other regulators upon exploration of their modification frequencies. Most of the modifications involved a copy number expansion, but TET2, NOP2, and NSUN4 had a broad occurrence of deletions (**Figure 1B**). The chromosome sites of the m^{5}C regulators are shown in **Figure 1C**. Based on the expression of 13 m^{5}C regulators in HCC patients, HCC samples could be thoroughly differentiated from normal

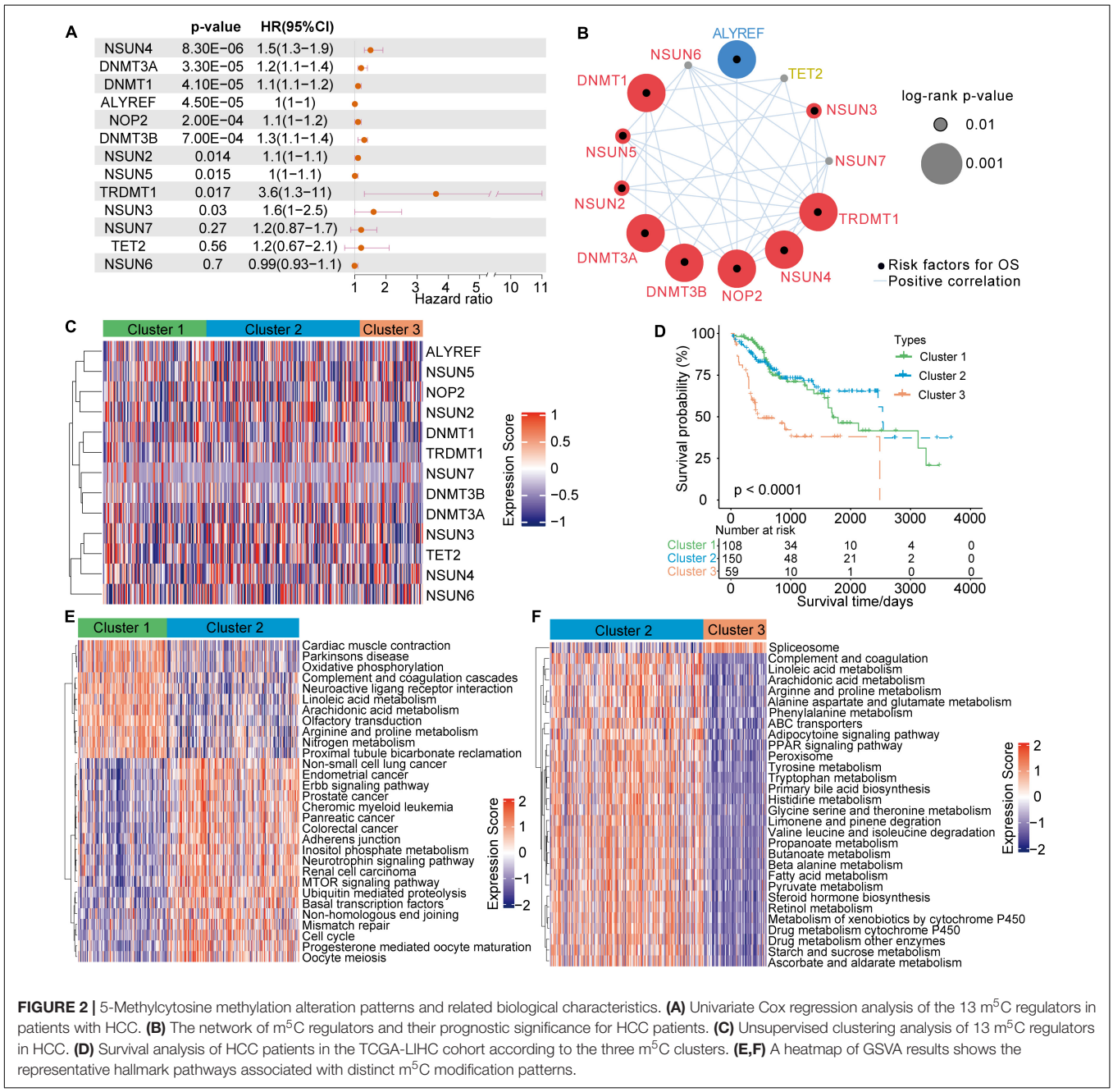

FIGURE 2 | 5-Methylcytosine methylation alteration patterns and related biological characteristics. **(A)** Univariate Cox regression analysis of the 13 m^{5}C regulators in patients with HCC. **(B)** The network of m^{5}C regulators and their prognostic significance for HCC patients. **(C)** Unsupervised clustering analysis of 13 m^{5}C regulators in HCC. **(D)** Survival analysis of HCC patients in the TCGA-LIHC cohort according to the three m^{5}C clusters. **(E,F)** A heatmap of GSVA results shows the representative hallmark pathways associated with distinct m^{5}C modification patterns.

samples (**Figure 1D**). To determine whether the expression of m^{5}C regulators was influenced by the genetic mutations mentioned above, the mRNA expression of regulators was explored. We found that a change in m^{5}C was an important factor leading to perturbations in the expression of m^{5}C regulators. Compared with normal hepatic tissues, the expression of m^{5}C regulators with a CNV expansion was significantly higher than that in HCC tissues (e.g., ALYREF and NSUN2) (**Figures 1B,E**). In addition, the expression of in HCC cell line Huh7 and normal control cell line L02 were detected by quantitative reverse-transcription PCR (qRT-PCR). Assistant with the expression in TCGA, the expression of ALYREF, DNMT1, DNMT3A, DNMT3B, NOP2, NSUN3, NSUN4, NSUN5, NSUN6, NSUN7, and TET2 were higher in HCC cell line Huh7 than in normal cell line L02. While the expression level of TRDMT1 and NSUN2 was lower in Huh7 than in L02 (**Figure 1F**). The analyses above showed that the genetic and expression alteration landscape of m^{5}C regulators in normal tissues and HCC tissues is highly heterogeneous, suggesting that the expression imbalance of m^{5}C regulators plays an important role in HCC occurrence and progression.

m^{5}C Methylation Alteration Patterns Mediated by 13 Regulators

Univariate Cox regression analysis showed that 13 m^{5}C modulators have prognostic significance in HCC patients (**Figure 2A**). The m^{5}C regulator network revealed m^{5}C modulator interactions, modulator connections and their prognostic significance for patients (**Figure 2B**). The R package Consensus Cluster Plus was applied to classify patients with qualitatively different m^{5}C alteration patterns according to the expression of 13 m^{5}C regulators, and unsupervised clustering analysis was performed to identify a total of 3 different modification patterns (120 cases in modification pattern 1, 178 cases in modification pattern 2, and 73 cases in modification pattern 3; referred to as m^{5}C Clusters 1–3, respectively) (**Figure 2C** and **Supplementary Table 2**). The prognostic analysis of the three major m^{5}C modification subtypes showed that Cluster-2 had a clear survival advantage over the others (**Figure 2D**). The above results indicate that the regulators of m^{5}C may play an important role in m^{5}C alteration patterns and TME cell infiltration characteristics between individual tumours.

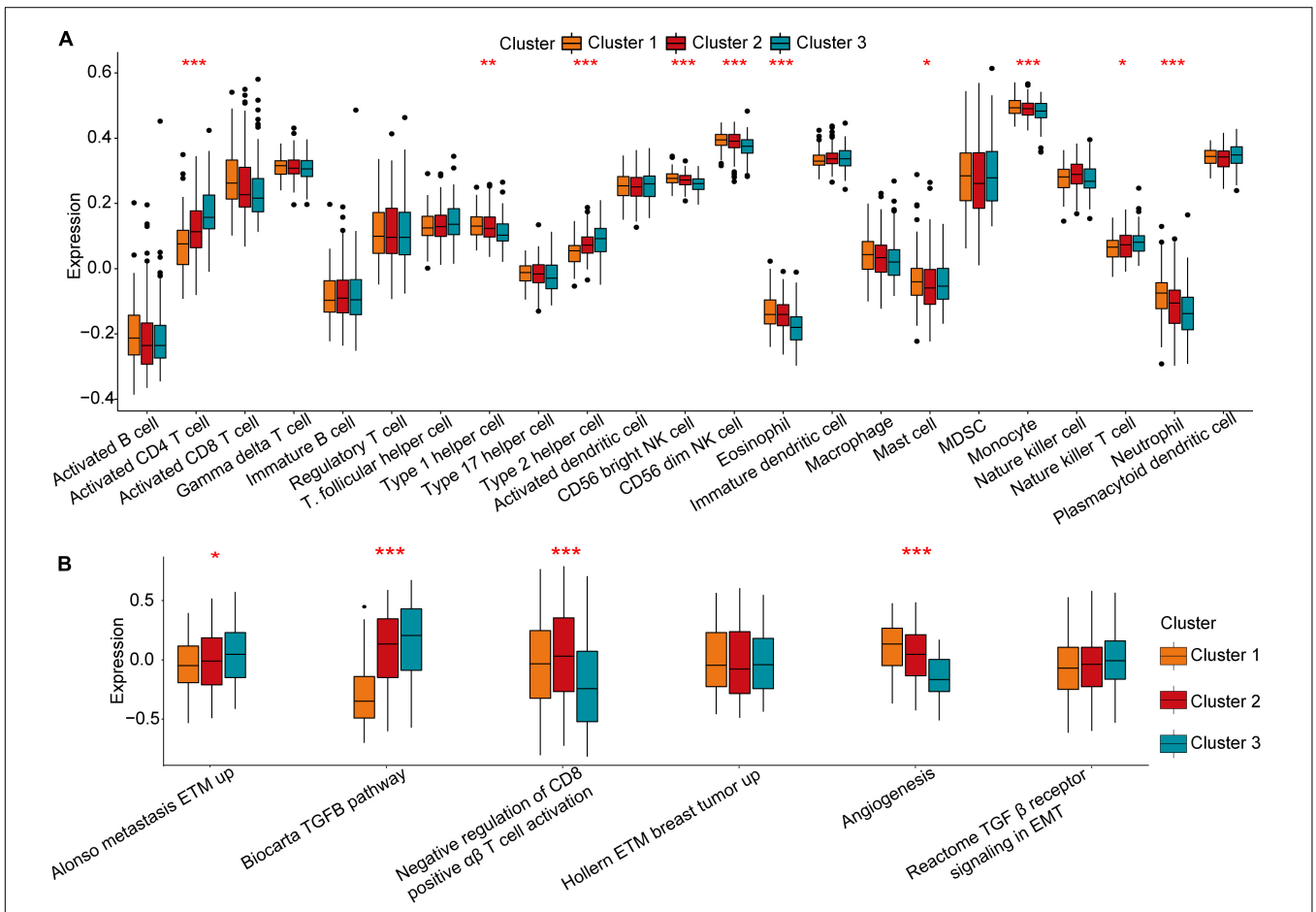

FIGURE 3 | Tumour microenvironment characteristics in different m^{5}C modification patterns. **(A)** Comparison of the abundance of immune infiltrating cells in three clusters. **(B)** Differences in cellular biological pathways among the three clusters. *$p < 0.05$, **$p < 0.01$, ***$p < 0.001$.

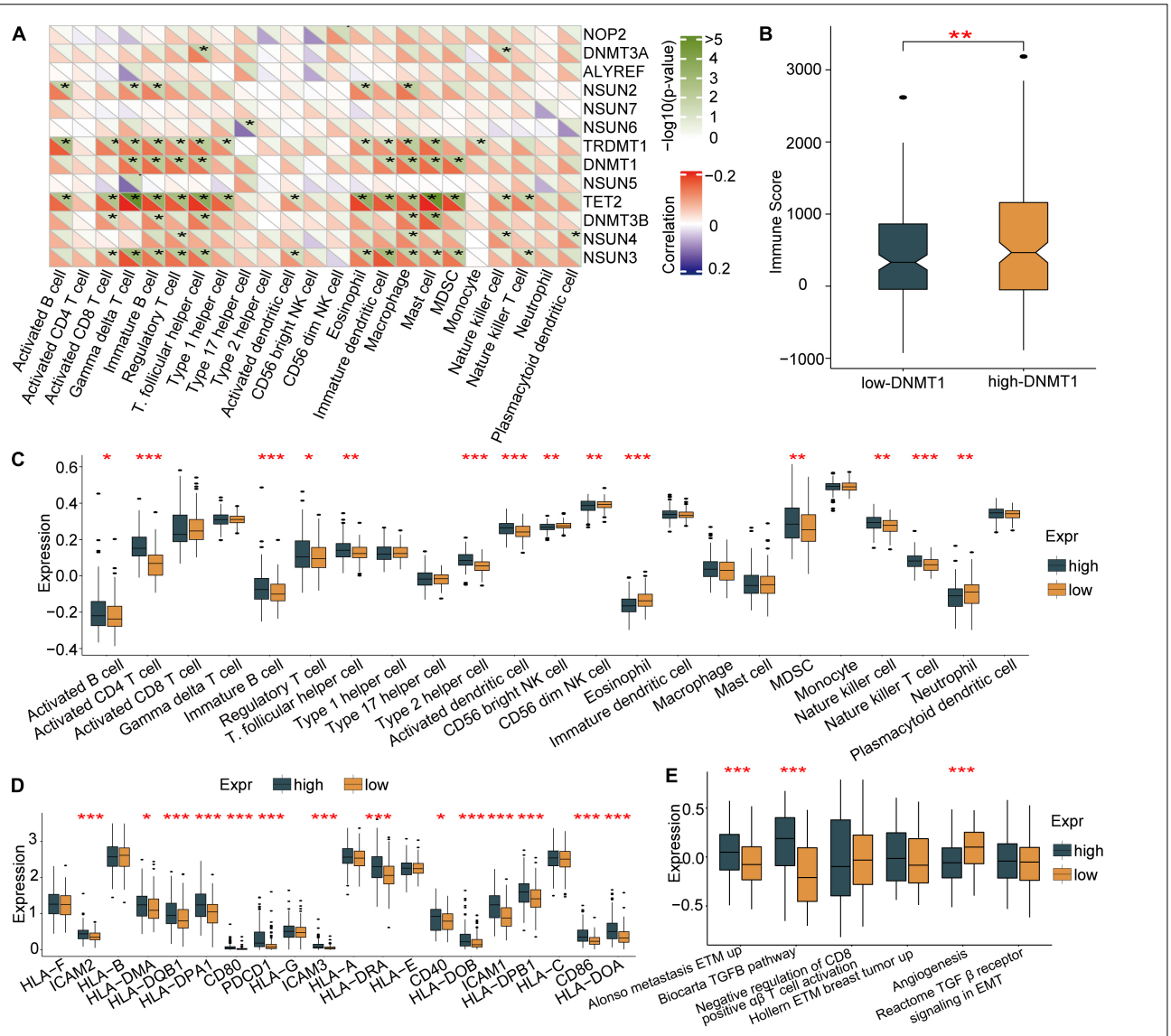

FIGURE 4 | Association of TME-infiltrating cells with the m^{5}C regulator of DNMT1. **(A)** Correlation between m^{5}C regulators and different immune cells using Spearman analysis. **(B)** Immune scores of the low DNMT1 group and the high DNMT1 group. **(C)** Comparison of the abundance of immune-infiltrating cells in the low DNMT1 group and high DNMT1 group. **(D)** Correlation between m^{5}C regulators and the activation of dendritic cells. **(E)** High DNMT1 expression shows significant enhancement of the immune-activated pathway. *$p < 0.05$, **$p < 0.01$, ***$p < 0.001$.

TME Cell Infiltration Characteristics in Different m^{5}C Modification Patterns

To investigate the biological actions associated with m^{5}C modification patterns, GSVA was conducted. As shown in **Figure 2E** and **Supplementary Table 2**, m^{5}C Cluster-2 was remarkably enriched in carcinogenesis pathways, such as the ERBB signalling pathway, cell cycle signalling pathway, and adherens junction pathway. Cluster-1 was associated with many metabolism pathways, such as, oxidative phosphorylation, linoleic acid metabolism, arachidonic acid metabolism, arginine and proline metabolism, and nitrogen metabolism (**Figure 2E**). Cluster-3 was highly associated with spliceosome (**Figure 2F**). Further analysis of TME cell infiltration showed that Cluster-1 was significantly enriched in the infiltration of innate immune cells, including eosinophils, NK cells, macrophages, CD8 T cells, and mast cells (**Figure 3A**). Prior research has shown that tumours with an immune rejection phenotype exhibit large amounts of immune cells, and these immune cells are in the matrix around the tumour cell nest instead of inside the tissue (Chen and Mellman, 2017). GSVA showed that the modification of Cluster-1 was significantly related to matrix activation. Therefore, it was speculated that the Cluster-1 matrix serves as an activation inhibitor of the anti-tumour effect of immune cells. Further analysis showed that matrix activity was greatly upgraded in Cluster 1, activating the angiogenesis pathway. These results supported our hypothesis (**Figure 3B**).

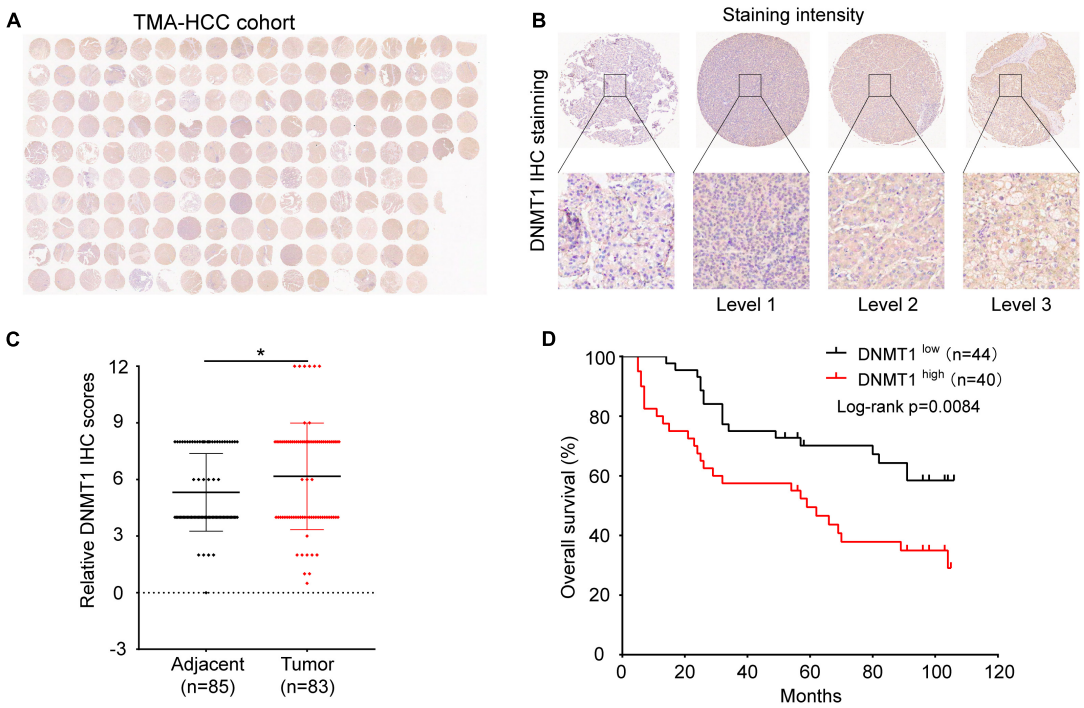

FIGURE 5 | Expression of DNMT1 in human HCC tumour tissues and control tissues. **(A)** Panoramic scanning of DNMT1 by IHC staining. **(B)** Representative IHC staining of DNMT1 in samples. **(C)** The expression of DNMT1 is higher in HCC tissues than in normal tissues. **(D)** Kaplan–Meier analysis showed that patients with higher levels of DNMT1 had shorter OS times than those with low levels of DNMT1. *$p < 0.05$.

The m^{5}C Regulator DNMT1 Has a Strong Relationship With Infiltrating Immune Cells

To further explore the role of each m^{5}C regulator in the TME, Spearman correlation analysis was applied to examine the correlation between each TME-infiltrating cell type and m^{5}C regulators (**Figure 4A**). An emphasis was placed on the regulator DNMT1, an m^{5}C methyltransferase, and we revealed its positive relationship with the infiltration of many TME immune cells. An estimation method was applied to determine the expression of DNMT1 and the infiltration of immune cells. The results showed that higher DNMT1 expression was related to a higher immune score, which means that a TME with high DNMT1 expression has significantly high immune cell infiltration (**Figure 4B**). Based on these results, the specific differences in 23 TME-infiltrating immune cells were explored between patients with high and low DNMT1 expression. We found that tumours exhibiting high DNMT1 expression had markedly more infiltration of 13 TME immune cells than those exhibiting low expression (**Figure 4C**). Recently, attention was drawn to the regulatory mechanisms of m^{5}C modification on the activation of DCs, which are the bridge connecting innate immunity with adaptive immunity, the activation of which depends on upregulating the expression of MHC molecules, adhesion molecules, and costimulatory molecules (**Figure 4D**). As expected, subsequent enrichment analysis showed that tumours with high DNMT1 expression showed remarkable enrichment in immune activation pathways (**Figure 4E**). Therefore, it was speculated that m^{5}C methylation modification mediated by DNMT1 may contribute to activated DCs in the TME, thus promoting the anti-tumour immune response in HCC.

High Expression of the m^{5}C Regulator DNMT1 in Tumour Tissues Is Related to a Poor Prognosis in Patients With HCC

Immunohistochemical staining was used to determine the expression pattern of DNMT1 on a TMA consisting of 90 pairs of HCC tissues and adjacent tissues. Representative micrographs illustrate the various degrees of DNMT1 expression (**Figures 5A,B**). The expression of DNMT1 was higher in tumour tissues than in control tissues (**Figure 5C**), which was consistent with the findings in the TCGA-LIHC cohort (**Figure 1E**). The correlation of DNMT1 expression with the clinicopathological characteristics of patients with HCC is shown in **Supplementary Table 3**. In addition, Kaplan–Meier curve analysis showed that patients with high DNMT1 expression had shorter overall survival (OS) than those with low DNMT1 expression (**Figure 5D**). Univariable and multivariable Cox regression analyses were used to determine whether the expression of DNMT1 was an independent risk factor. The univariable analysis revealed that DNMT1 expression was associated with tumour size and TB, AFP, and PD-L1 levels ($P < 0.05$, **Supplementary Table 4**). Further analysis demonstrated that DNMT1 might serve as a prognostic predictor for HCC.

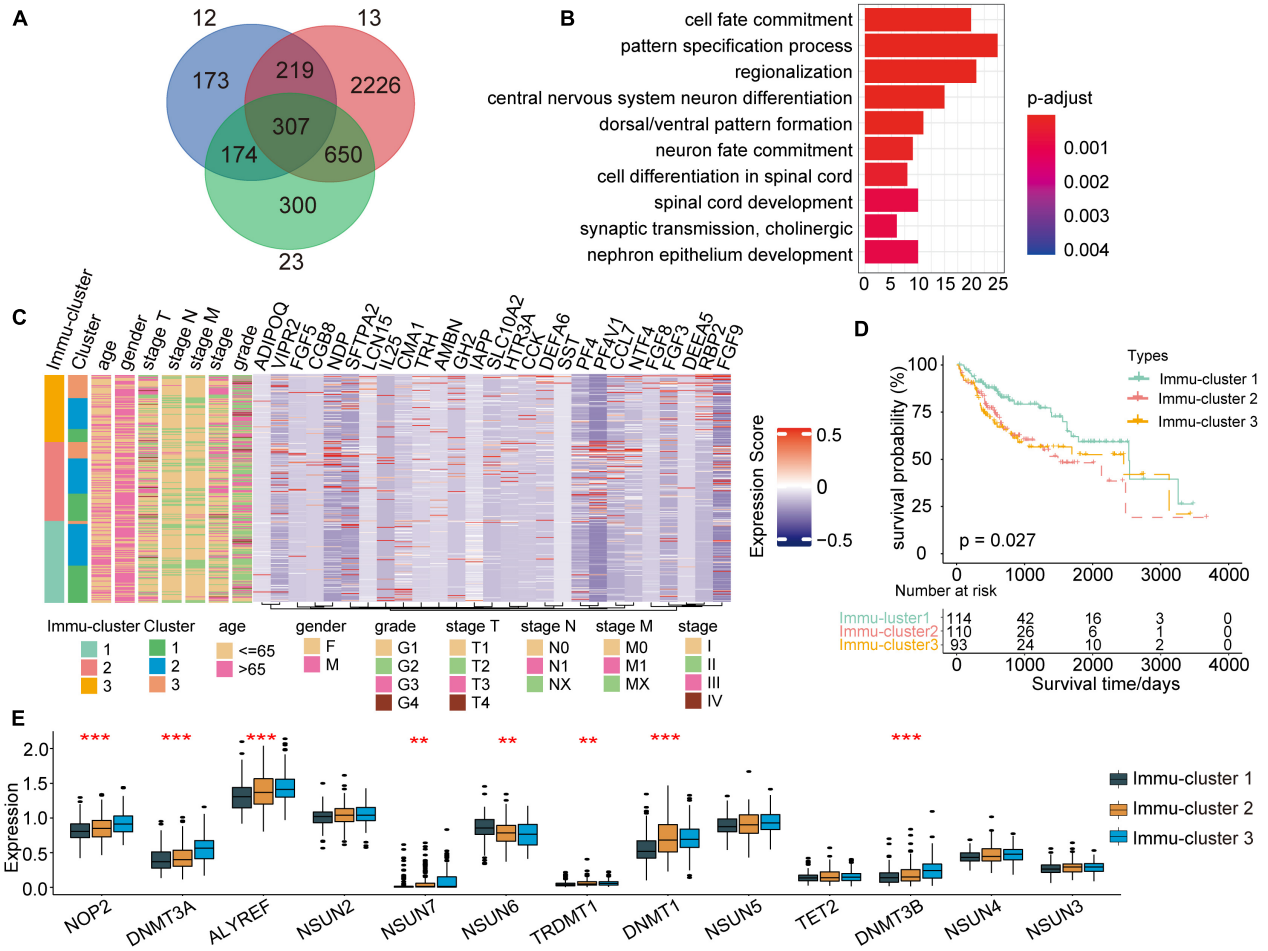

FIGURE 6 | Identification of distinct Immu-clusters based on immune-related DEGs in m^{5}C modification patterns. **(A)** A total of 307 m^{5}C-related DEGs between three m^{5}C clusters were identified, as shown in the Venn diagram. **(B)** Enrichment of biological processes significantly related to DEGs. **(C)** The selected genes were used to classify patients into different genomic subtypes by unsupervised clustering analysis. **(D)** Kaplan–Meier curves indicated that the genomic subtypes were correlated with the prognosis of patients with HCC. **(E)** Significant differences in the expression of m^{5}C regulators. $^{**}p < 0.01$, $^{***}p < 0.001$.

Generation of the m^{5}C Gene Signature and Functional Annotation

For subsequent exploration of the biological behaviour of each m^{5}C modification pattern, we ascertained 307 m^{5}C phenotype-related DEGs with the limma package (**Figure 6A**). Cluster profiler was employed to implement enrichment analysis on the DEGs. **Supplementary Table 5** summarises the significantly enriched pathways. As expected, we detected enrichment in biological processes that are notably related to m^{5}C modification and immunity, which verified the important role that m^{5}C modification plays in immune regulation in the TME (**Figure 6B**).

To further explain the association, we performed unsupervised clustering analysis to classify 307 m^{5}C phenotype-related genes and extracting 27 immune-related genes: VIPR2, CCL7, RBP2, SLC10A2, FGF5, DEFA5, HTR3A, TRH, LCN15, AMBN, ADIPOQ, FGF3, CCK, NTF4, NDP, FGF9, PF4, CMA1, SFTPA2, CGB8, DEFA6, PF4V1, IL25, GH2, FGF8, SST, and IAPP. Furthermore, we performed unsupervised clustering analysis based on these genes to categorise patients into different subtypes (**Supplementary Figures 1A–D**). In line with the clustering analysis of m^{5}C modification patterns, unsupervised clustering analysis revealed three different m^{5}C-modified phenotypes termed Immu-clusters 1–3, respectively. Thus, there are three different distinct immune-related m^{5}C methylation patterns. We observed that tumours in Immu-clusters 2 and 3 were associated with poor differentiation and enriched in diffuse histological subtypes. The opposite pattern was observed in Immu-cluster 1. Patients whose survival status was known were mainly concentrated in Immu-cluster 1, while patients in clinical stage IV or with a high TNM grade were mainly concentrated in Immu-cluster 2 (**Figure 6C**). The analysis also showed that three different gene clusters had different feature genes (**Figure 6C**). In total, 114 of the 317 HCC patients clustered in Immu-cluster 1, which was associated with a better prognosis. The prognosis of patients in

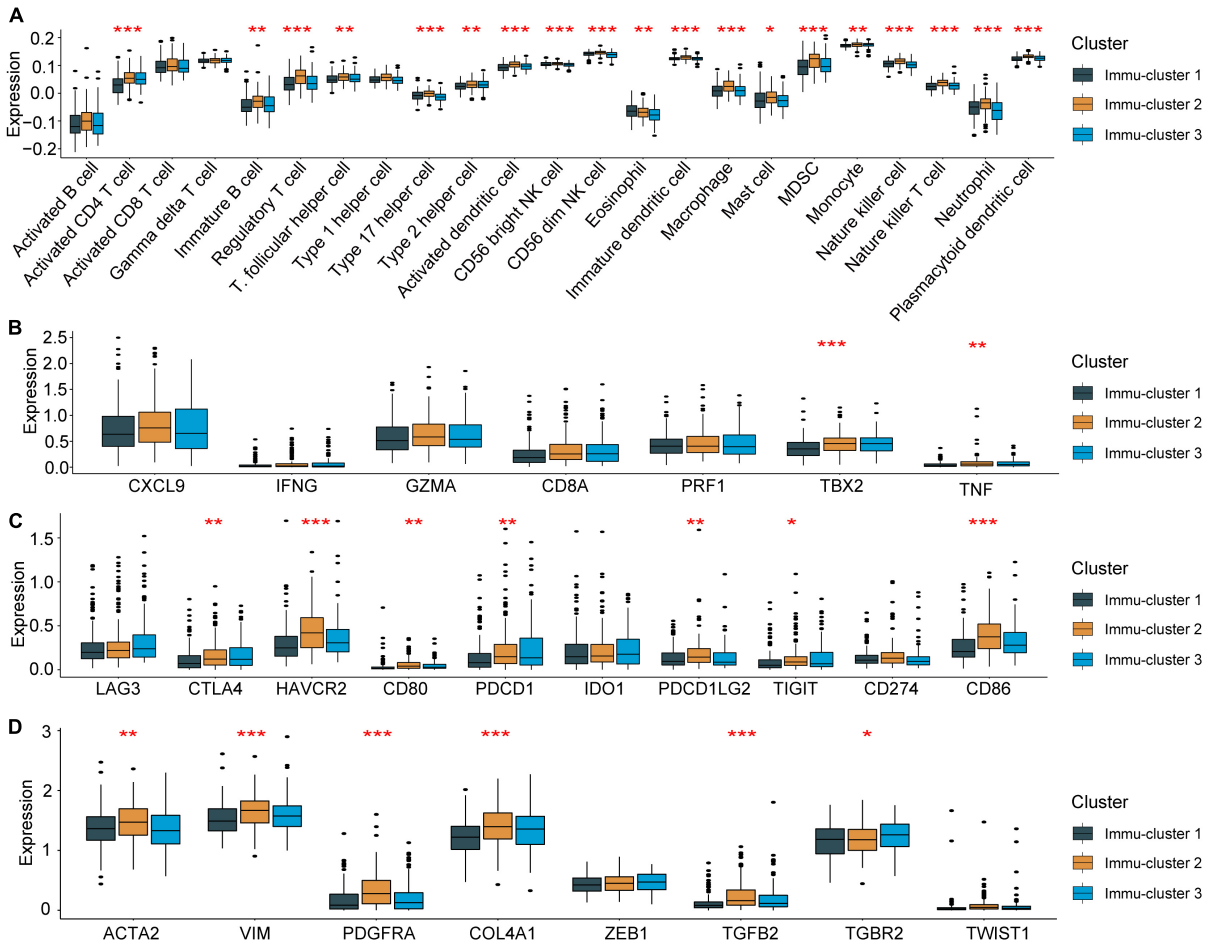

FIGURE 7 | Association between the expression of m^{5}C regulators and immunoregulation in the TME. **(A)** Differences in immune cell infiltration in the three Immu-clusters. **(B)** Comparison of immune-related cytokine expression in the three Immu-clusters. **(C)** Comparison of the transcription of immune checkpoint genes in the three Immu-clusters. **(D)** Immu-clusters involved in the transcription of the TGF-β/EMT pathway. $^*p < 0.05$, $^{**}p < 0.01$, $^{***}p < 0.001$.

Immu-cluster 2 (110 patients) and Immu-cluster 3 (93 patients) was poor (**Figure 6D**). In the three immune clusters, a significant distinction in the expression of m^{5}C regulatory factors emerged. This result was consistent with the m^{5}C methylation modification patterns (**Figure 6E**).

Clinical and Transcriptional Features of the m^{5}C-Related Phenotypes

To further explain the role that m^{5}C-related phenotypes play in TME immune regulation, the levels of immune cells and expression of chemokines and cytokines in the three Immu-clusters were examined. The chosen cytokines and chemokines were taken from previously existing studies (Turley et al., 2015). Our analysis showed that activated CT4 T cells, immature B cells, regulatory T cells, NK cells, macrophages, mast cells, myeloid-derived suppressor cells (MDSCs), monocytes, neutrophils, and plasmacytoid DCs were significantly different among the Immu-clusters. Besides, the immunosuppressive cells (including MDSCs and regulatory T cells) were significantly upregulated in Immu-cluster 2 (**Figure 7A**). Tumour necrosis factor, interferon, CD8A, CXCL9, CXCL10, GZMA, GZMB, PRF1, and TBX2 were associated with immune activation transcription (Barbie et al., 2009; Zeng et al., 2019). The expression of TNF and TBX2 were different in this three Immu-clusters (**Figure 7B**). PD-L1, CD80, CD86, CTLA-4, HAVCR2, etc., were thought to be related to the transcription of immune checkpoints. We compared the transcription of these immune checkpoint genes in the three Immu-clusters and found that the expression of most of the immune checkpoint genes were remarkedly different (**Figure 7C**). ACTA2, CLDN3, VIM, COL4A1, SMAD9, TWIST1, TGFBR2, TGRB1, and ZEB1 are related to the transcription of growth factor β (TGF-β)/EMT pathway transformation and exhibited significant differences between the three Immu-clusters (**Figure 7D**). We found that mRNAs related to the TGF-β/EMT pathway were significantly upregulated in Immu-cluster 2, indicating that this cluster is the matrix-activated group and associated with immunosuppression. Immu-cluster 3 showed elevated expression of mRNAs related to immune checkpoint

genes, suggesting that the patients in this group may respond better to immune checkpoint drugs, which requires further study.

DISCUSSION

According to previous reports, tumours, including HCC, are mainly driven by genetic mutations. In recent years, epigenetic modifications have been found to play a critical role in the carcinogenesis and molecular pathogenesis of HCC (Xue et al., 2020a; Nombela et al., 2021). m^5C is the most preventative and best understood DNA modification in eukaryotes (Piperi and Papavassiliou, 2011). In recent years, emerging evidence has revealed the important role of RNA m^5C in posttranscriptional regulation. Several studies have revealed that m^5C regulators and m^5C methylation play essential roles in different cancer types, including HCC. He et al. (2020b) found that ALYREF and NSUN4 could be promising targets for HCC therapies. In addition, studies showed the map of m^5C methylation based on HCC tissues and paired non-tumour tissues at the mRNA, lncRNA, and circRNA levels (He et al., 2020a,c; Zhang et al., 2020c). Recent studies showed that NSUN2 could promote tumour progression in HCC (Sun et al., 2020) and gastric cancer (Mei et al., 2020). Similar to our findings, Cui et al. (2021) and Xue et al. (2020b) found that DNMT1 played important roles in head and neck squamous cell carcinoma.

Recently, increasing evidence has shown interactions between the tumour immune-microenvironment (TIME) and m^6A modifications. Yi et al. (2020) reported that copy number alterations in m^6A methylation regulators affected immune cell infiltration in head and neck squamous cell carcinoma. Lin et al. (2020) also attempted to explore the relationship between m^6A regulators and tumour-infiltrating immune cells by ssGSEA in glioma. Shen et al. (2021) found that m^6A modification patterns were correlated with immune regulation in HCC and might provide novel immune therapeutic targets. However, as an important epigenetic modification, the role of m^5C methylation in the immune regulation of HCC is still unclear. Here, we described the TME cell infiltration characteristics in different m^5C modification patterns. Furthermore, we identified three distinct immune-related m^5C methylation subtypes and investigated the levels of immune cells and expression of chemokines and cytokines in the three Immu-clusters. All the results indicate that the generation of immune-related m^5C methylation subtypes contribute to understanding the molecular mechanisms of HCC and provide novel clues for predicting the prognosis of patients with HCC.

It has been demonstrated that DNMT1 is an essential methyltransferase for the maintenance of DNA methylation. Previous evidence has shown that DNMT1 is overexpressed in breast cancer (Wang et al., 2018), thyroid cancer cells (Zhang et al., 2018), and pancreatic cancer (Peng et al., 2005). Furthermore, high DNMT1 expression is significantly associated with a poor prognosis (Li et al., 2010; Hong et al., 2018). Consistent with our results, we found that DNMT1 expression was increased in tumour tissues compared with normal tissues in the TMA and TCGA cohort. In our study, Kaplan–Meier curve analysis and univariable and multivariable Cox regression analysis further demonstrated that the expression of DNMT1 is an independent risk factor for HCC. Therefore, DNMT1 might serve as a promising prognostic predictor and therapeutic target for HCC.

CONCLUSION

Taken together, our results showed the association between m^5C modification and TME. Moreover, we found a key m^5C modification regulator, DNMT1, which has great potential as a prognostic biomarker and therapeutic target for HCC.

DATA AVAILABILITY STATEMENT

The datasets presented in this study can be found in online repositories. The names of the repository/repositories and accession number(s) can be found in the article/**Supplementary Material**.

ETHICS STATEMENT

The studies involving human participants were reviewed and approved by The First Affiliated Hospital, College of Medicine, Zhejiang University. The patients/participants provided their written informed consent to participate in this study.

AUTHOR CONTRIBUTIONS

XG and HZo designed the whole study. QZ and JW conducted the statistical analysis. XG and QC draft the manuscript. QC made the relevant edits to the manuscript. XG and HZu revised the manuscript. All authors read and approved the final manuscript.

FUNDING

This study was supported by grants awarded by the National Science and Technology Major Project of China (No. 2018ZX10302206), Science and Technology Major Projects of Zhejiang Province (No. 2018C04016), and the Science and Technology Major Projects of Ningbo (No. 2016C51008).

SUPPLEMENTARY MATERIAL

The Supplementary Material for this article can be found online at: https://www.frontiersin.org/articles/10.3389/fcell.2021.727935/full#supplementary-material

Supplementary Figure 1 | Consensus map of unsupervised clustering results used for subtype analysis.

Supplementary Table 1 | The primers for the qRT-PCR assay.

Supplementary Table 2 | Estimating the relative abundance of tumour cells in the TME in the TCGA-LIHC cohort by single-sample gene set enrichment analysis (ssGSEA).

Supplementary Table 3 | Activation states of biological pathways in distinct m^{5}C modification patterns by GSVA.

Supplementary Table 4 | Correlation between DNMT1 expression and clinicopathological characteristics.

Supplementary Table 5 | Univariate and multivariate analyses of the factors correlated with the OS of HCC patients.

Supplementary Table 6 | Functional annotation of m^{5}C phenotype-related genes.

REFERENCES

Barbie, D. A., Tamayo, P., Boehm, J. S., Kim, S. Y., Moody, S. E., Dunn, I. F., et al. (2009). Systematic RNA interference reveals that oncogenic KRAS-driven cancers require TBK1. *Nature* 462, 108–112. doi: 10.1038/nature08460

Bejarano, L., Jordão, M. J. C., and Joyce, J. A. (2021). Therapeutic targeting of the tumor microenvironment. *Cancer Discov.* 11, 933–959. doi: 10.1158/2159-8290.Cd-20-1808

Bestor, T. H. (1988). Cloning of a mammalian DNA methyltransferase. *Gene* 74, 9–12. doi: 10.1016/0378-1119(88)90238-7

Bourgeois, G., Ney, M., Gaspar, I., Aigueperse, C., Schaefer, M., Kellner, S., et al. (2015). Eukaryotic rRNA modification by yeast 5-methylcytosine-methyltransferases and human proliferation-associated antigen p120. *PLoS One* 10:e0133321. doi: 10.1371/journal.pone.0133321

Charoentong, P., Finotello, F., Angelova, M., Mayer, C., Efremova, M., Rieder, D., et al. (2017). Pan-cancer immunogenomic analyses reveal genotype-immunophenotype relationships and predictors of response to checkpoint blockade. *Cell Rep.* 18, 248–262. doi: 10.1016/j.celrep.2016.12.019

Chen, D. S., and Mellman, I. (2017). Elements of cancer immunity and the cancer–immune set point. *Nature* 541, 321–330. doi: 10.1038/nature21349

Chong, W., Shang, L., Liu, J., Fang, Z., Du, F., Wu, H., et al. (2021). m(6)A regulator-based methylation modification patterns characterized by distinct tumor microenvironment immune profiles in colon cancer. *Theranostics* 11, 2201–2217. doi: 10.7150/thno.52717

Colaprico, A., Silva, T. C., Olsen, C., Garofano, L., Cava, C., Garolini, D., et al. (2016). TCGAbiolinks: an R/Bioconductor package for integrative analysis of TCGA data. *Nucleic Acids Res.* 44:e71. doi: 10.1093/nar/gkv1507

Cui, J., Zheng, L., Zhang, Y., and Xue, M. (2021). Bioinformatics analysis of DNMT1 expression and its role in head and neck squamous cell carcinoma prognosis. *Sci. Rep.* 11:2267. doi: 10.1038/s41598-021-81971-5

Davalos, V., Blanco, S., and Esteller, M. (2018). SnapShot: messenger RNA modifications. *Cell* 174:46. doi: 10.1016/j.cell.2018.06.046

European Association for the Study of the Liver. (2017). EASL 2017 clinical practice guidelines on the management of hepatitis B virus infection. *J. Hepatol.* 67, 370–398. doi: 10.1016/j.jhep.2017.03.021

García-Vílchez, R., Sevilla, A., and Blanco, S. (2019). Post-transcriptional regulation by cytosine-5 methylation of RNA. *Biochim. Biophys. Acta Gene Regul. Mech.* 1862, 240–252. doi: 10.1016/j.bbagrm.2018.12.003

Hanahan, D., and Coussens, L. M. (2012). Accessories to the crime: functions of cells recruited to the tumor microenvironment. *Cancer Cell* 21, 309–322. doi: 10.1016/j.ccr.2012.02.022

Hänzelmann, S., Castelo, R., and Guinney, J. (2013). GSVA: gene set variation analysis for microarray and RNA-seq data. *BMC Bioinform.* 14:7. doi: 10.1186/1471-2105-14-7

Hartigan, J. A., and Wong, M. A. (1979). Algorithm AS 136: A K-means clustering algorithm. *J. R. Stat. Soc. C* 28, 100–108. doi: 10.2307/2346830

Hazra, A., and Gogtay, N. (2016). Biostatistics series module 3: comparing groups: numerical variables. *Indian J. Dermatol.* 61, 251–260. doi: 10.4103/0019-5154.182416

He, Y., Shi, Q., Zhang, Y., Yuan, X., and Yu, Z. (2020a). Transcriptome-wide 5-methylcytosine functional profiling of long non-coding RNA in hepatocellular carcinoma. *Cancer Manag. Res.* 12, 6877–6885. doi: 10.2147/cmar.S262450

He, Y., Yu, X., Li, J., Zhang, Q., Zheng, Q., and Guo, W. (2020b). Role of m(5)C-related regulatory genes in the diagnosis and prognosis of hepatocellular carcinoma. *Am. J. Transl. Res.* 12, 912–922.

He, Y., Zhang, Q., Zheng, Q., Yu, X., and Guo, W. (2020c). Distinct 5-methylcytosine profiles of circular RNA in human hepatocellular carcinoma. *Am. J. Transl. Res.* 12, 5719–5729.

Hernandez-Gea, V., Toffanin, S., Friedman, S. L., and Llovet, J. M. (2013). Role of the microenvironment in the pathogenesis and treatment of hepatocellular carcinoma. *Gastroenterology* 144, 512–527. doi: 10.1053/j.gastro.2013.01.002

Hong, L., Sun, G., Peng, L., Tu, Y., Wan, Z., Xiong, H., et al. (2018). The interaction between miR-148a and DNMT1 suppresses cell migration and invasion by reactivating tumor suppressor genes in pancreatic cancer. *Oncol. Rep.* 40, 2916–2925. doi: 10.3892/or.2018.6700

Li, A., Omura, N., Hong, S. M., and Goggins, M. (2010). Pancreatic cancer DNMT1 expression and sensitivity to DNMT1 inhibitors. *Cancer Biol. Ther.* 9, 321–329. doi: 10.4161/cbt.9.4.10750

Lin, S., Xu, H., Zhang, A., Ni, Y., Xu, Y., Meng, T., et al. (2020). Prognosis analysis and validation of m(6)A signature and tumor immune microenvironment in glioma. *Front. Oncol.* 10:541401. doi: 10.3389/fonc.2020.541401

Llovet, J. M., Kelley, R. K., Villanueva, A., Singal, A. G., Pikarsky, E., Roayaie, S., et al. (2021). Hepatocellular carcinoma. *Nat. Rev. Dis. Primers* 7:6. doi: 10.1038/s41572-020-00240-3

Llovet, J. M., Zucman-Rossi, J., Pikarsky, E., Sangro, B., Schwartz, M., Sherman, M., et al. (2016). Hepatocellular carcinoma. *Nat. Rev. Dis. Primers* 2:16018. doi: 10.1038/nrdp.2016.18

Mariathasan, S., Turley, S. J., Nickles, D., Castiglioni, A., Yuen, K., Wang, Y., et al. (2018). TGFβ attenuates tumour response to PD-L1 blockade by contributing to exclusion of T cells. *Nature* 554, 544–548. doi: 10.1038/nature25501

Mayakonda, A., Lin, D. C., Assenov, Y., Plass, C., and Koeffler, H. P. (2018). Maftools: efficient and comprehensive analysis of somatic variants in cancer. *Genome Res.* 28, 1747–1756. doi: 10.1101/gr.239244.118

Mei, L., Shen, C., Miao, R., Wang, J. Z., Cao, M. D., Zhang, Y. S., et al. (2020). RNA methyltransferase NSUN2 promotes gastric cancer cell proliferation by repressing p57(Kip2) by an m(5)C-dependent manner. *Cell Death Dis.* 11:270. doi: 10.1038/s41419-020-2487-z

Nombela, P., Miguel-López, B., and Blanco, S. (2021). The role of m^{6}A, m^{5}C and Ψ RNA modifications in cancer: novel therapeutic opportunities. *Mol. Cancer* 20:18. doi: 10.1186/s12943-020-01263-w

Peng, D. F., Kanai, Y., Sawada, M., Ushijima, S., Hiraoka, N., Kosuge, T., et al. (2005). Increased DNA methyltransferase 1 (DNMT1) protein expression in precancerous conditions and ductal carcinomas of the pancreas. *Cancer Sci.* 96, 403–408. doi: 10.1111/j.1349-7006.2005.00071.x

Piperi, C., and Papavassiliou, A. G. (2011). Strategies for DNA methylation analysis in developmental studies. *Dev. Growth Differ.* 53, 287–299. doi: 10.1111/j.1440-169X.2011.01253.x

Rosenberg, J. E., Hoffman-Censits, J., Powles, T., van der Heijden, M. S., Balar, A. V., Necchi, A., et al. (2016). Atezolizumab in patients with locally advanced and metastatic urothelial carcinoma who have progressed following treatment with platinum-based chemotherapy: a single-arm, multicentre, phase 2 trial. *Lancet* 387, 1909–1920. doi: 10.1016/s0140-6736(16)00561-4

Şenbabaoğlu, Y., Gejman, R. S., Winer, A. G., Liu, M., Van Allen, E. M., de Velasco, G., et al. (2016). Tumor immune microenvironment characterization in clear cell renal cell carcinoma identifies prognostic and immunotherapeutically relevant messenger RNA signatures. *Genome Biol.* 17:231. doi: 10.1186/s13059-016-1092-z

Shen, S., Yan, J., Zhang, Y., Dong, Z., Xing, J., and He, Y. (2021). N6-methyladenosine (m6A)-mediated messenger RNA signatures and the tumor immune microenvironment can predict the prognosis of hepatocellular carcinoma. *Ann. Transl. Med.* 9:59. doi: 10.21037/atm-20-7396

Sun, Z., Xue, S., Zhang, M., Xu, H., Hu, X., Chen, S., et al. (2020). Aberrant NSUN2-mediated m(5)C modification of H19 lncRNA is associated with poor differentiation of hepatocellular carcinoma. *Oncogene* 39, 6906–6919. doi: 10.1038/s41388-020-01475-w

Turley, S. J., Cremasco, V., and Astarita, J. L. (2015). Immunological hallmarks of stromal cells in the tumour microenvironment. *Nat. Rev. Immunol.* 15, 669–682. doi: 10.1038/nri3902

Wang, P., Chu, W., Zhang, X., Li, B., Wu, J., Qi, L., et al. (2018). Kindlin-2 interacts with and stabilizes DNMT1 to promote breast cancer development. *Int. J. Biochem. Cell Biol.* 105, 41–51. doi: 10.1016/j.biocel.2018.09.022

Wilkerson, M. D., and Hayes, D. N. (2010). Consensusclusterplus: a class discovery tool with confidence assessments and item tracking. *Bioinformatics* 26, 1572–1573. doi: 10.1093/bioinformatics/btq170

Xue, C., Zhao, Y., and Li, L. (2020a). Advances in RNA cytosine-5 methylation: detection, regulatory mechanisms, biological functions and links to cancer. *Biomark Res.* 8:43. doi: 10.1186/s40364-020-00225-0

Xue, M., Shi, Q., Zheng, L., Li, Q., Yang, L., and Zhang, Y. (2020b). Gene signatures of m5C regulators may predict prognoses of patients with head and neck squamous cell carcinoma. *Am. J. Transl. Res.* 12, 6841–6852.

Yang, Y., Hsu, P. J., Chen, Y. S., and Yang, Y. G. (2018). Dynamic transcriptomic m(6)A decoration: writers, erasers, readers and functions in RNA metabolism. *Cell Res.* 28, 616–624. doi: 10.1038/s41422-018-0040-8

Yi, L., Wu, G., Guo, L., Zou, X., and Huang, P. (2020). Comprehensive analysis of the PD-L1 and immune infiltrates of m(6)A RNA methylation regulators in head and neck squamous cell carcinoma. *Mol. Ther. Nucleic Acids* 21, 299–314. doi: 10.1016/j.omtn.2020.06.001

Zeng, D., Li, M., Zhou, R., Zhang, J., Sun, H., Shi, M., et al. (2019). Tumor microenvironment characterization in gastric cancer identifies prognostic and immunotherapeutically relevant gene signatures. *Cancer Immunol. Res.* 7, 737–750. doi: 10.1158/2326-6066.Cir-18-0436

Zhang, B., Wu, Q., Li, B., Wang, D., Wang, L., and Zhou, Y. L. (2020a). m(6)A regulator-mediated methylation modification patterns and tumor microenvironment infiltration characterization in gastric cancer. *Mol. Cancer* 19:53. doi: 10.1186/s12943-020-01170-0

Zhang, J. G., Zhou, H. M., Zhang, X., Mu, W., Hu, J. N., Liu, G. L., et al. (2020b). Hypoxic induction of vasculogenic mimicry in hepatocellular carcinoma: role of HIF-1 α. RhoA/ROCK and Rac1/PAK signaling. *BMC Cancer* 20:32. doi: 10.1186/s12885-019-6501-8

Zhang, Q., Zheng, Q., Yu, X., He, Y., and Guo, W. (2020c). Overview of distinct 5-methylcytosine profiles of messenger RNA in human hepatocellular carcinoma and paired adjacent non-tumor tissues. *J. Transl. Med.* 18:245. doi: 10.1186/s12967-020-02417-6

Zhang, Y., Sun, B., Huang, Z., Zhao, D. W., and Zeng, Q. (2018). Shikonin Inhibites migration and invasion of thyroid cancer cells by downregulating DNMT1. *Med. Sci. Monit.* 24, 661–670. doi: 10.12659/msm.908381

Conflict of Interest: The authors declare that the research was conducted in the absence of any commercial or financial relationships that could be construed as a potential conflict of interest.

Publisher's Note: All claims expressed in this article are solely those of the authors and do not necessarily represent those of their affiliated organizations, or those of the publisher, the editors and the reviewers. Any product that may be evaluated in this article, or claim that may be made by its manufacturer, is not guaranteed or endorsed by the publisher.

frontiers in Cell and Developmental Biology

ORIGINAL RESEARCH
published: 10 November 2021
doi: 10.3389/fcell.2021.761391

Analysis of Multi-Layer RNA Modification Patterns for the Characterization of Tumor Immune Microenvironment in Hepatocellular Carcinoma

OPEN ACCESS

Edited by:
Jiang Chen,
Zhejiang University, China

Reviewed by:
Shaohua Xu,
Tongji University, China
Antonio Giovanni Solimando,
University of Bari Aldo Moro, Italy
Gongbo Fu,
Nanjing General Hospital of Nanjing Military Command, China
Jinhui Liu,
Nanjing Medical University, China
Mingdi Liu,
Jilin University, China

***Correspondence:**
Zujiang Yu
johnyuem@zzu.edu.cn

Specialty section:
This article was submitted to Molecular and Cellular Oncology, a section of the journal Frontiers in Cell and Developmental Biology

Received: *19 August 2021*
Accepted: *28 October 2021*
Published: *10 November 2021*

Citation:
Xing J, Shen S, Dong Z, Hu X, Xu L, Liu X, Li Q, Zhang Y, Cui G and Yu Z (2021) Analysis of Multi-Layer RNA Modification Patterns for the Characterization of Tumor Immune Microenvironment in Hepatocellular Carcinoma. Front. Cell Dev. Biol. 9:761391. doi: 10.3389/fcell.2021.761391

*Jiyuan Xing[1,2], Shen Shen[1,2], Zihui Dong[1], Xiaobo Hu[1,2], Lixia Xu[1,2], Xiaorui Liu[1,2], Qinggang Li[1,2], Yize Zhang[1], Gangying Cui[1,2] and Zujiang Yu[1,2]**

[1]Gene Hospital of Henan Province, Precision Medicine Center, The First Affiliated Hospital of Zhengzhou University, Zhengzhou, China, [2]Department of Infectious Diseases, The First Affiliated Hospital of Zhengzhou University, Zhengzhou, China

Background: RNA modifications have emerged as important posttranscriptional changes in multiple tumor cellular processes and tumorigenesis, including hepatocellular carcinoma (HCC). However, the potential roles and the interaction between regulators of RNA modifications and the tumor microenvironment (TME) are unclear in HCC.

Methods: The gene expression profiles of 26 RNA modification "writers" were investigated in the TCGA cohort. The unsupervised clustering approach was used to class these RNA modification regulators. The characteristics of immune cell infiltration from TME for each cluster was tested by the CIBERSORT method. Additionally, we established a scoring model to evaluate the RNA modification characteristics of individual tumors. The associations between the scoring model and genetic as well as clinical characteristics, drug sensitivity, and response to immunotherapy were also analyzed.

Results: We mapped the somatic mutations and somatic copy number variation of the RNA modification regulators. The expression of all selected regulators was detected, and two modification patterns were identified that featured distinct immune cell infiltration characteristics. Subsequently, we developed a score model (termed as WM-Score model). Furthermore, the survival analysis showed that the WM-Score value was associated with HCC patient prognosis. The results of the ROC curves analysis and multivariate analysis all confirmed that the WM-Score value was strongly associated with anti-cancer drug resistance and therapeutic efficacy of immunotherapy, thus could be used as an independent risk factor in HCC.

Conclusion: Our research identified two RNA modification patterns characterized by distinct TME, and the WM-Score model was developed that might serve as reliable prognostic and immunotherapeutic effect predictor of HCC.

Keywords: hepatocellular carcinoma, RNA methylation modification, TME, immunotherapy, prognosis

INTRODUCTION

In 2018, hepatocellular carcinoma (HCC) was predicted to be the sixth most prevalent cancer worldwide (Bray et al., 2018), with a 5 years survival rate as low as 9.1%, and an overall median survival of 9 months (Giannini et al., 2015). Infection by HBV or HCV, chronic alcohol consumption, and obesity-related NASH are the principal causes of HCC (Llovet et al., 2021). The condition is usually diagnosed at an advanced stage, therefore, effective treatments for advanced metastatic HCC are limited. Although there are surgical and chemotherapy options, the mortality rate of HCC remains high. Forms of immunotherapy, such as immune checkpoint inhibitors (ICIs) have been used to capture the disease progression and to enhance adaptive immunity in advanced HCC (Ou et al., 2020). Meanwhile, only a subset of patients show therapeutic response to ICIs, and this response it is difficult to predict. Therefore, a deeper understanding of the molecular mechanism of HCC is necessary to improve patient survival.

Recently, RNA modifications, coined the "epitranscriptome", have emerged as crucial posttranscriptional regulators of the gene expression process (Barbieri and Kouzarides, 2020). Increasing evidence has revealed that these modifications have huge implications for human pathophysiology, including cancer (Frye et al., 2016; Jonkhout et al., 2017; Nachtergaele and He, 2017; Ontiveros et al., 2019). Accordingly, over 170 different types of chemical modifications of cellular RNAs have been described, among which methylation modifications account for two-thirds and are widely present in various RNA types (Barbieri and Kouzarides, 2020). The most abundant and better characterized internal RNA modification is N^6-methyladenosine (m^6A) that regulates multiple aspects of RNA metabolism, such as RNA processing, RNA translation, and nuclear export (Roundtree et al., 2017; Sun et al., 2019). N1-methyladenosine (m1A) is an important post-transcriptional RNA modification that has been found in tRNA, rRNA, mitochondrial RNA and mRNA (RajBhandary et al., 1966; Peifer et al., 2013; Li et al., 2017; Safra et al., 2017). APA is an RNA-processing mechanism that generates distinct 3′ termini on mRNAs and other RNA polymerase II transcripts (Tian and Manley, 2017). RNA editing mediated by adenosine deaminase acting on RNA enzymes a well-documented post-transcriptional mechanism altering nucleotide in selected transcripts (Nishikura, 2010). RNA modification is catalyzed by RNA methyltransferases called "writers" (they add a specific modification), demethylases or "erasers" (they remove a specific modification), and m^6A-binding proteins or "readers" (they recognize and bind modified nucleotides). The RNA modification is a dynamic process, and the interaction between each type of methylation modification has not yet been fully elucidated (Davalos et al., 2018; Xue et al., 2020; Nombela et al., 2021).

Accumulating evidence supports the prominent role of the complex and diverse tumor immune microenvironment (TIME), including cancer cells, locally infiltrating immune cells, stromal cells, and active medium, in tumor cell proliferation, invasion, and metastasis (Azambuja et al., 2019; Fu et al., 2019). Non-malignant cells are not only one of the major players of cancer progression, but also determine the immunotherapeutic response (Lu et al., 2019). Therefore, a comprehensive analysis of the diversity of TME and different immune phenotypes can guide and improve immunotherapeutic responsiveness (Binnewies et al., 2018).

In this study, we focused on the most heavily modified RNA types, including m^6A, alternative polyadenylation (APA), m^1A, and A-to-I RNA editing. Furthermore, we comprehensively analyzed the correlation between various types of RNA modification regulators and cell-infiltrating characteristics of TIME by integrating the genomic and transcriptomic alterations of samples from The Cancer Genome Atlas - Liver Hepatocellular Carcinoma (TCGA-LIHC) databases. Two distinct modification patterns with different immune cell characteristics were identified. In addition, we developed the WM-Score model to quantify the efficacy of "writers" in modifying individual tumors and to predict the prognosis and immunotherapeutic response of HCC patients.

METHODS

Data Acquisition and Processing

The gene expression profiles and clinical annotations were downloaded from the Cancer Genome Atlas (TCGA) portal (http://cancergenome.nih.gov/). Data cohorts with missing information were removed. A total of 356 cases of TCGA-LIHC were used for further analysis. The R Bioconductor package and R (version 3.6.2) were employed for data analysis.

Drug sensitivity data were collected from The Genomics of Drug Sensitivity in Cancer (GDSC) database (www.cancerRxgene.org) (Yang et al., 2013). Spearman's correlation analysis was utilized to evaluate the association between the scoring model and drug reaction, where $|Rs| > 0.2$, and FDR <0.05 was considered significant correlation.

The immunotherapy dataset IMvigor210 cohort was used to explore the immunotherapy response and prognosis of HCC patients with different WM-Score values. The standardized RNA-sequencing data of 1111 HCC patients with detailed clinicopathological data were downloaded from http://research-pub.gene.com. The data were analyzed using the IMvigor210CoreBiologies R package.

Unsupervised Clustering Analysis

In order to explore the robust clustering of HCC cases, we employed the unsupervised clustering approach to analyze the gene profiles of RNA modification writers. A total of 26 RNA modification regulators, including seven m^6A modification enzymes (KIAA1429, METTL14, ZC3H13, METTL3, WTAP, RBM15B, and RBM15), 12 APA modification enzymes (CPSF1, CPSF2, CPSF3, CPSF4, CSTF1, CSTF2, CSTF3, CF1, PCF11, CLP1, NUDT21, and PABPN1), four m^1A modification enzymes (TRMT10C, TRMT6, TRMT61A, and TRMT61B), and three A-I modification enzymes (ADARB1, ADARB2 and ADAR) were analyzed. An NMF-based consistent clustering algorithm was used to determine RNA modification patterns based on the mRNA expression of analyzed regulators. Unsupervised cluster analysis was performed by The

Consensus Cluster Plus package as previously described (Wilkerson and Hayes, 2010).

Gene Set Variation Analysis (GSVA)

GSVA is a gene set enrichment method that provides increased power to estimate changes of subtle pathway activity over a sample population in an unsupervised manner (Hänzelmann et al., 2013). We conducted GSVA analysis to explore the association between RNA modifications and biological processes. The gene set "h.all.v7.2" and "c2.cp.kegg.v7.1"were derived from the MSigDB database (Zhu et al., 2020). The functional annotation of 26 "writer" genes was conducted by the clusterProfiler R package, with a cutoff value of FDR <0.05. An adjusted P with value < 0.05 was considered as indicative of statistical significance.

Cell-type Identification by Estimating Relative Subsets of RNA Transcripts (CIBERSORT)

CIBERSORT is a method that can accurately estimate the fraction of diverse cell subsets in gene expression profiles from complex tissues (http://cibersort.stanford.edu) (Newman et al., 2015). To predict the immune subset composition of HCC samples from gene expression profiles, CIBERSORT was used to estimate the relative abundance of 22 types of immune cells (model = absolute, permutation = 1,000, disable quantile normalization for RNA-Seq data as recommended).

Construction of the WM-Score Scoring System

Firstly, the RNA modification-related differentially expressed genes (DEGs) among distinct RNA modification clusters were collected using "limma" package of R software. Next, we performed univariate cox regression model to analyze the correlation of each gene with overall survival, and the significant prognosis DEGs were used for further analysis. Subsequently, distinct genomic subtypes were determined by unsupervised clustering analyses. In addition, the prognostic analysis was performed for each genomic subtype and extract principal component 1 and 2 as the signature scores. Finally, the RNA modification score was defined using a method similar to that used in analyzing gene-gene interactions (GGIs): WM-Score = Σ (PC1i + PC2i), which is defined as the expression of final RNA modification phenotype-related genes (Sotiriou et al., 2006; Zeng et al., 2019).

Statistical Analysis

A Wilcoxon rank-sum test was utilized to compare differences between two groups, and Kruskal-Wallis test was used for comparisons of multiple groups. The discrimination accuracy of the WM-Score model was described by receiver operating characteristic (ROC) analysis. Kaplan-Meier method estimate curves were generated for prognostic analysis, and the differences between groups were evaluated by a log-rank test. Univariate and multivariate analyses were further carried out to assess independent risk factors. All data were analyzed by the R 4.0.1 software. A two-tailed $p < 0.05$ was considered as statistically significant.

RESULTS

Landscape of Genetic Alterations of 26 RNA Modification "Writers"

A total of 26 RNA modification "writers" were selected in this study, which included seven m^6A modification "writers", three A-I modification "writers", 12 APA modification "writers", and four m^1A modification "writers" (**Supplementary Table S1**) (Li et al., 2016; Tang S. J. et al., 2020; Shen et al., 2021). To explore the genetic alterations in RNA modification writers, we examined the incidence of somatic mutations and somatic copy number variation (CNV) for all "writers" based on the TCGA database. Among 356 samples from TCGA-LIHC, 42 (11.8%) exhibited genetic changes of these writers, and the details was shown in the **Figure 1A**. The highest mutation frequency was presented in CPSF1, followed by ADARB2 and KIAA1429 (**Figure 1A**), while METTL3, METTL14, TRMT61A, TRMT61B, CSTF3, and NUDT2 did not show any mutations in tumor samples. Next, we used the hallmark gene set to perform gene set variation analysis (GAVA) to compare the mutation groups and those without mutation in "writers". The GSVA indicated significantly enriched carcinogenic activation pathways in the mutation group, such as those of E2F targets, G2M checkpoint, MYC, and MTORC1 signaling pathway (**Figure 1B**). Furthermore, the investigation of CNV alteration in 26 regulators showed that ADAR, CPSF1, CPSF4, TRMT10C and KIAA1429 had a widespread frequency of CNV gain, while ZC3H13, CF1, METTL14, NUDT21, and WTAP had a significant CNV loss (**Figure 1C**). To explore whether the above CNV alterations affected the expression of the 26 RNA modification regulators, we compared the expression level of these regulators between tumor samples and paired normal samples. The results showed increased mRNA levels of most "writers" in tumor samples in comparison to normal samples (**Figure 1D**), suggesting that CNV might be the major factor leading to the aberrant expression of medication regulators. Notably, the mRNA levels of some "writers" were increased, while the frequencies of CNV loss for those were high. Therefore, further investigations were performed. According to the CNV value, patients were divided into 3 groups, including CNV amplification group, CNV deletion group, and normal group, and the mRNA expression of "writers" were compared between these groups (**Figure 1E**). The results showed mostly elevated expression for the group of patients with CNV amplification compared with the other groups with CNV deletion or normal CNV in these "writers". Taken together, we mapped the genetic alterations of the 26 RNA modification "writers" between control tissues and tumor tissues, suggesting that these changes might play vital functions in HCC tumorigenesis and progression.

The RNA Modification Patterns Are Characterized by Distinct TIME Cell Infiltration Characteristics

In order to further understand the role of RNA modification "writers" in HCC, we performed univariate analysis of the 26 regulators based on the TCGA-LIHC cohort. We found that 16 of 26 "writers" were markedly correlated with the OS of HCC patients (**Figure 2A**). Next, we explored the relationship

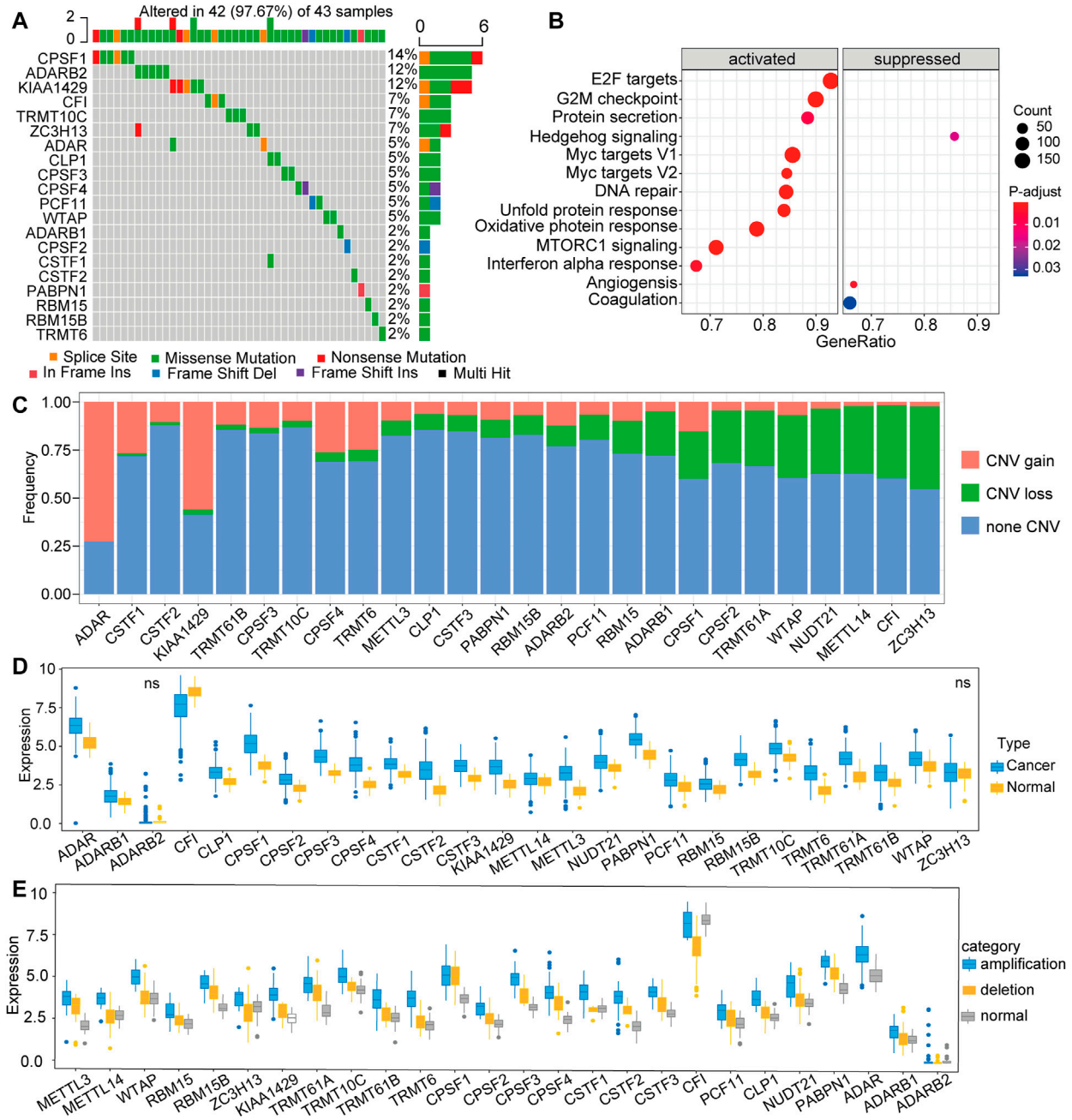

FIGURE 1 | Expression pattern of 26 RNA modification "writer" genes in TCGA-LIHC **(A)** Frequency of mutations of the 26 identified regulator genes **(B)** Gene set variation analysis (GAVA) was used to compare the regulator mutation group and the non-mutation group **(C)** The CNV mutation frequency of 26 regulator genes in TCGA-LIHC **(D)** The expression of 26 RNA modification regulator genes between tumor tissues and control tissues **(F)** The mRNA expression of "writer" among three groups, including amplification group, CNV deletion group, and normal group.

among "writers" and found that most were positively or negatively correlated with each other (**Figure 2B**). Thus, it is suspected that the crosstalk between different "writers" may have a vital function in the different modification patterns of HCC.

We performed consensus clustering to classify patients into distinct RNA modification patterns based on the mRNA expression of "writers" (**Supplementary Table S2**). Eventually, two RNA modification patterns with 204 cases were determined in pattern 1 (cluster 1), and 113 cases in pattern 2 (cluster 2) (**Figure 2C**). Subsequently, "GSVA" enrichment analysis was employed to further understand the biological behaviors between the distinct two clusters. Our results indicated that cluster 1 was significantly enriched in metabolism and drug metabolism pathways, such as sulfur metabolism, primary bile

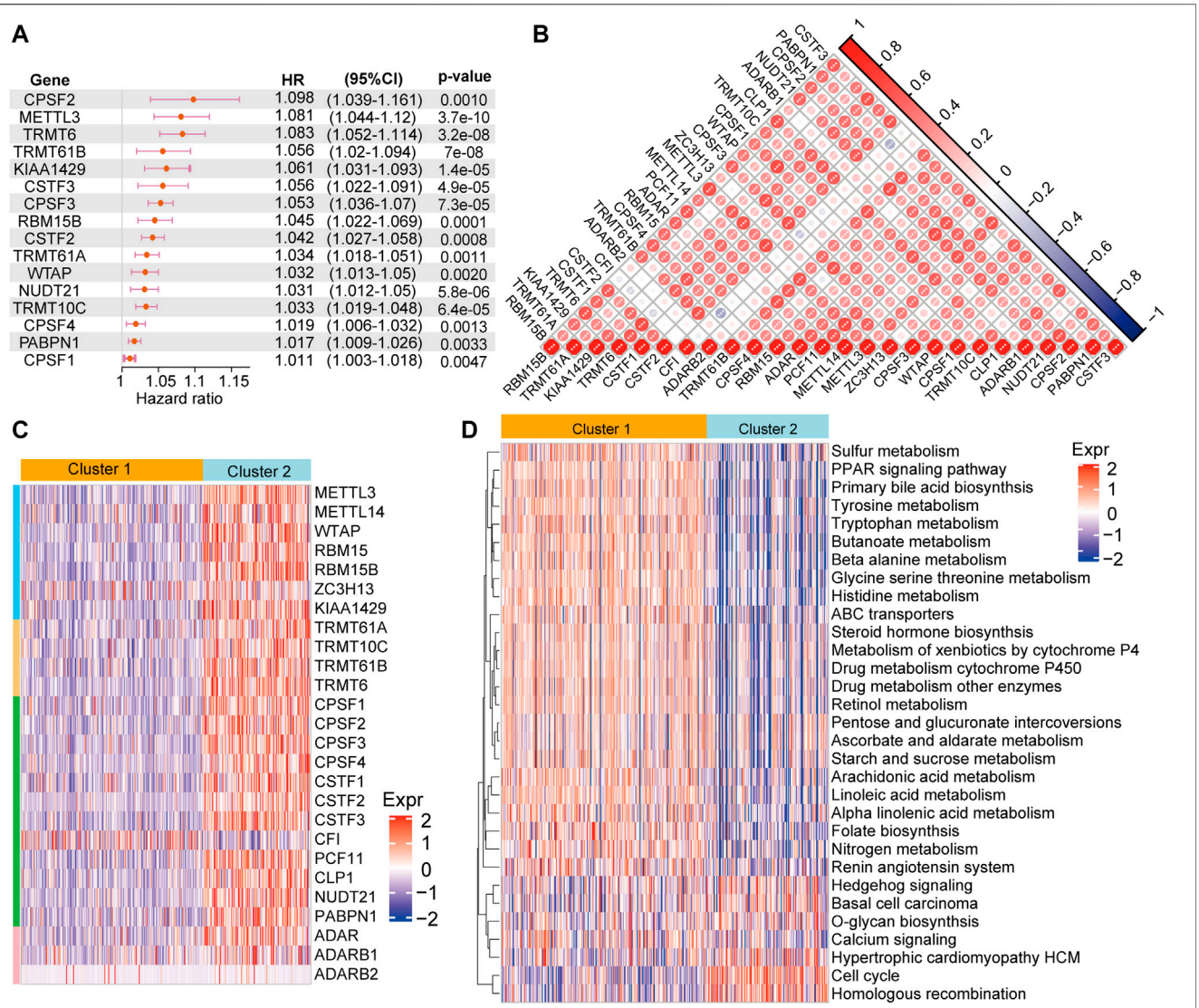

FIGURE 2 | RNA methylation modification pattern and related biological pathways **(A)** The univariate cox regression analysis shows that 16 of 26 regulators are associated with of patient prognosis in the TCGA-LIHC cohort **(B)** Heatmap of the Spearman's correlation analysis presenting negative (blue) and a positive (red) correlation among the "writers" in HCC **(C)** Unsupervised cluster analysis of 26 "writers" in HCC. Blue represents low expression of "writers" genes; red represents high expression of these genes **(D)** GSVA enrichment analysis of KEGG pathway chances between cluster 1 and 2. Blue indicate not activated pathways, and red indicates activated pathways.

acid biosynthesis, tyrosine metabolism, tryptophan metabolism, drug metabolism cytochrome P450, drug metabolism other enzymes, renin angiotensin system, while cluster 2 enrichment pathways were mainly linked to proliferation and signal transduction, including cell cycle, calcium conduction, etc. (**Figure 2D**).

Emerging evidence suggests that RNA modifications interact with the tumorigenic environment, thus affecting tumor occurrence, development, and prognosis (Jiang et al., 2020; Chen H. et al., 2021; Chong et al., 2021). Therefore, the function of the RNA methylations in the TME were further explored. The association analysis using the CIBERSORT method revealed that the identified RNA modification regulators might have close links with immune cell infiltration from the TME (**Figure 3A**). For instance, METTL14, ZC3H13, CSTF3, and ADAR were markedly negatively associated with Mo macrophage differentiation, while their positive association was observed with METTL3, RBM15B, KIAA1429, TRMT61A, TRMT6, CPSF1, and NUDT21. Moreover, we analyzed the difference in immune cell infiltration from TME between cluster 1 and cluster 2. The results revealed that the infiltration of M2, T cells, mast cells, and monocytes was higher in cluster 1. Notably, though, the infiltration of M1, regulatory T cells and follicular helper T cells was higher in cluster 2 (**Figures 3B,C**). Overall, cluster 2 was usually enriched in immunosuppressive cells, indicating a poor prognosis, whereas

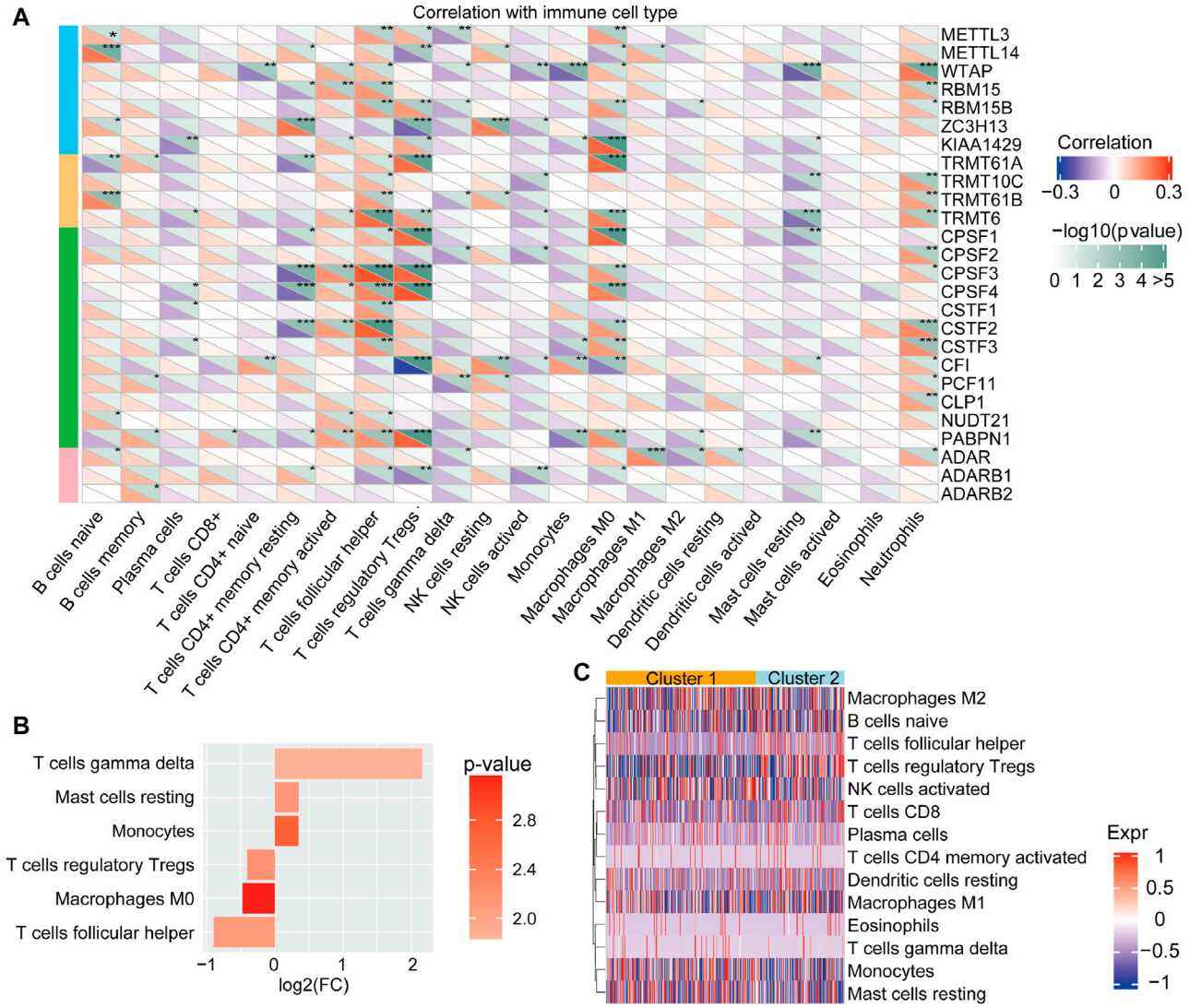

FIGURE 3 | Tumor immune microenvironment characterization of the RNA modification patterns **(A)** The correlation between the 26 "writers" and TME in HCC was analyzed by CIBERSORT **(B)** The different characters of immune cell infiltration between clusters. Log(FC) > 0 represents that the immune cells were enriched in cluster 1 **(C)** The types of immune cells between distinct RNA modification patterns.

cluster 1 was characterized by immune cell activity, indicating a beneficial prognosis. These findings suggested that RNA modification "writers" play crucial roles in immune cell infiltration and TME formation.

Generation of RNA Modification Signature Model

Our results above demonstrated the important role of RNA modification in TME formation and patient prognosis, while these findings were based on RNA modification patterns and could not accurately evaluate the capacity of the RNA modification as a prognostic predictor in individual HCC patients. The underlying genetic alterations in these two RNA modification patterns were still unclear. Based on these queries, we examined the transcriptional expression change between the two patterns. A total of 273 DEGs related to RNA modification patterns were identified, and the further enrichment analysis showed that these DEGs were enriched in many essential biological processes, including DNA-binding transcription activator activity, signaling receptor activator activity, and multicellular organismal response to stress (**Figures 4A–C**). Subsequently, according to unsupervised clustering analysis based on the 273 DEGs, patients were classified into two stable transcriptomic subtypes: cluster A and cluster B (**Figure 4D**), with 242 and 75 of the 317 HCC patients, respectively. The prognosis of patients in cluster B was poorer than those in gene cluster A (**Figure 4E**; $p < 0.0001$, log-rank test).

Furthermore, we developed a score model based on the DEGs between gene clusters. As described in the Methods section, a

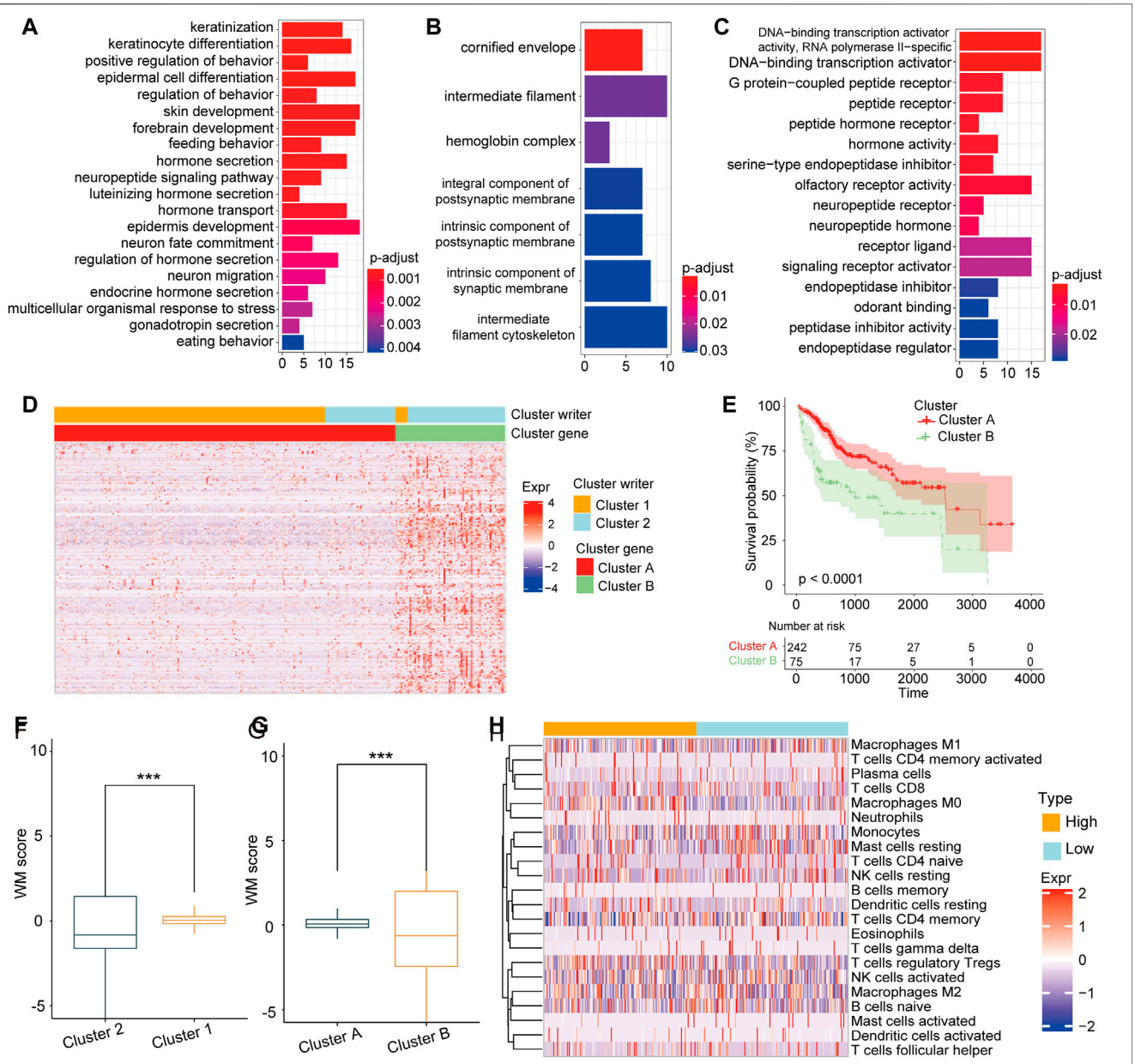

FIGURE 4 | Construction of RNA modification model **(A–C)**. GSVA enrichment analysis revealed the DNA transcription signaling pathways. Stress reception signaling pathways **(A)** and signal transduction activation signaling pathways **(B)** were correlated with **(C)** 273 DEGs between cluster 1 and cluster 2 **(D)**. Unsupervised clustering of the 273 DEGs to identify two genomic subtypes **(E)** Survival analysis showing the poor prognosis of patients in cluster A group compared with those in cluster B group ($p < 0.0001$, Log-rank test) **(F)**. The score of cluster 1 was higher than that of cluster 2. **G**. The score of cluster A was significantly higher than that of cluster B **(H)**. The difference of immune cell infiltration abundance between WM-Score groups calculated by the CIBERSORT algorithm.

scoring model named writers of RNA modification-score (WM-Score) was constructed. We discovered that cluster 1 had a higher WM-Score value than cluster 2 (**Figure 4F**). Consistently with this, cluster A also showed a higher score value than cluster B (**Figure 4G**). To evaluate the association of WM-Score value with TME, we further calculated the abundance of immune cell infiltration for the low and the high WM-Score value groups. We found that the infiltration rate of M0 macrophages, monocytes, and TfCD8 was higher in the high WM-Score value group, and that of activated NK-activated cells and M1 macrophages was higher in the low WM-Score value group (**Figure 4H**).

Association Between WM-Score and Clinical Characteristics

After confirming the efficacy of the WM-Score model in predicting patient prognosis, we investigated whether this

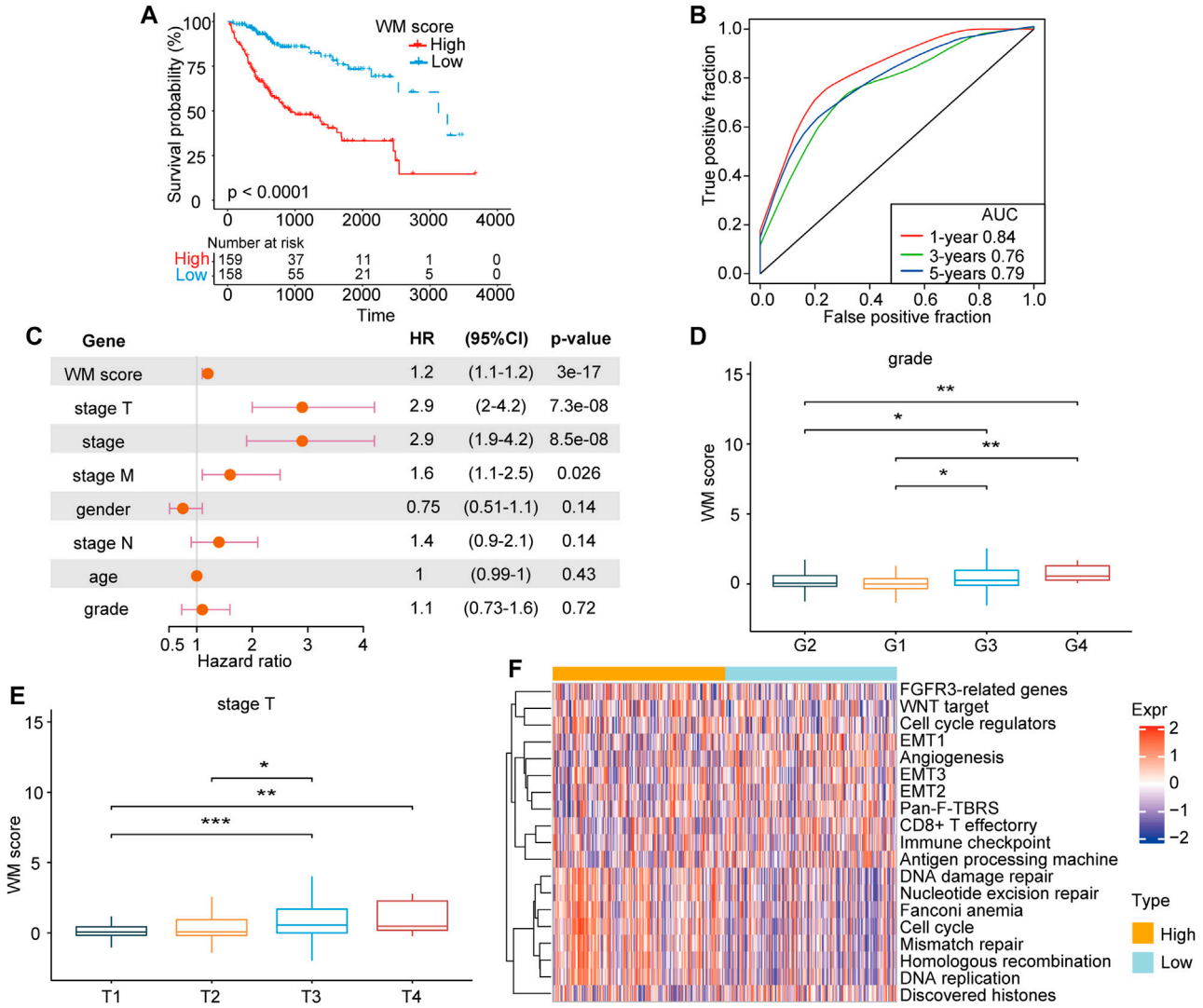

FIGURE 5 | The clinical characteristics and prognosis of HCC correlated with the WM-Score model. **(A)**. Kaplan-Meier overall survival for HCC patients in the high and low WM-Score groups. **(B)**. The predictive accuracy of the WM-Score model in the TCGA-LIHC cohort (AUC: 0.84, 076, and 0.79, corresponding to 365, 1,095, and 1825 days OS, respectively). **(C)**. Multivariate cox regression analysis of factors, which included WM-Score, stage-T, stage, stage-M, gender, stage-N, patient age, and grade in the TCGA-LIHC cohorts. **(E)**. WM-Score differences among grade and stage-T of HCC in TCGA-LIHC. **(F)**. Heatmap showing the GSVA score of EMT signaling pathways between different WM-Score groups in TCGA-LIHC.

model could be applied to determine the tumorigenesis, progression, invasion and metastasis of HCC. The prognostic efficiency of the scoring model was explored through classifying patients into low and high score groups the using "survminer" package. As expected, patients with high score demonstrated a poorer prognosis than those with low score in the TCGA-LIHC cohort (**Figure 5A**). We used ROC curve analysis to determine the discrimination accuracy of the scoring model in predicting patient prognosis. The area under the ROC curves (AUCs) of WM-Score values were 0.84, 0.76 and 0.79 at 1, 3 and 5 years overall survival, respectively (**Figure 5B**). Multivariate analysis for the TCGA-LIHC cohort also demonstrated that the WM-Score could serve as an independent prognostic predictor in HCC (**Figure 5C**). All of these results indicated that the WM-Score model has accurate prognostic value for HCC patients. The analysis of difference in WM-Scores between different TNM grades and clinical grades in the TCGA database indicated that samples with higher clinical grades and TNM stages usually have higher WM-Score values (**Figures 5D,E**). In addition, considering the EMT-related pathways, the samples with different WM-Score value had different pathway characteristics. For the TCGA database, samples with high WM-Score value were significantly related to cell cycle, DNA damage repair, and DNA replication, while samples with low WM-Score value were related to EMT, WNT target, and cell cycle regulators (**Figure 5F**).

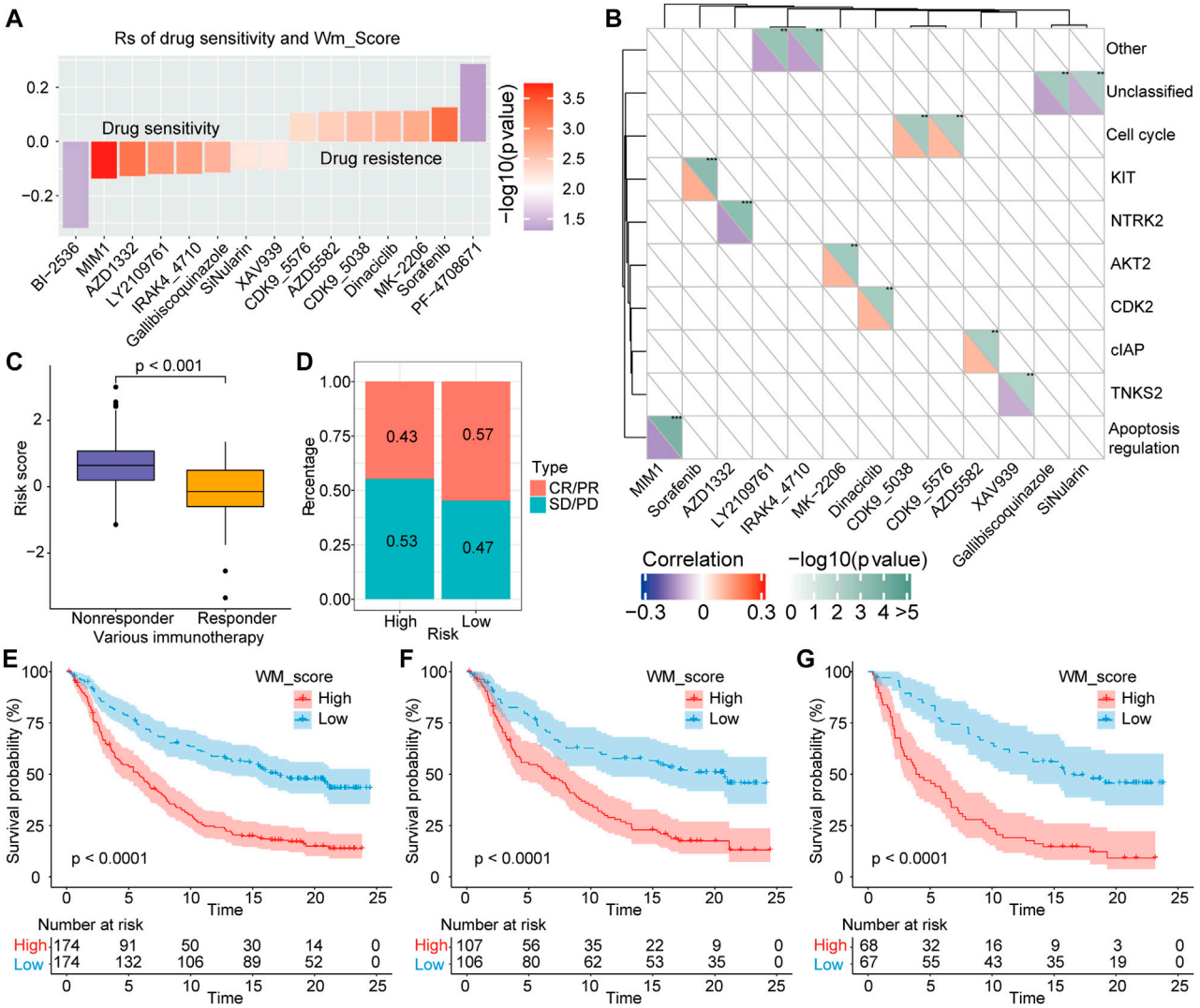

FIGURE 6 | Correlation of scoring model with drug reaction and immunotherapeutic response. **(A)**. Spearman's analysis was used to determine the correlation between score and drug response in GDSC. **(B)**. The association between drugs and targeted signaling pathways. **(C)**. The difference in the score between immunotherapeutic responder in the IMvigor210 cohort. **(D)**. The percentage of patients with different responses (including SD, PD, CR, and PR) to PD-L1 blockade immunotherapy. E-G. Total samples, or Stage I + II samples, or Stage III + IV samples in the IMvigor210 cohort all showed a significant difference in survival between samples with high and low WM-Scores based on survival analysis.

Value of WM-Score Model in Chemotherapy and Therapy Sensitivity

For several years, sorafenib has been approved a treatment option for advanced HCC patients, while efficacy of sorafenib is limited by drug resistance (Gnoni et al., 2019). Aiming to further investigate whether the WM-Score value affected drug sensitivity, we evaluated the correlation between the scoring model and the drug response of tumor cell lines. Using Spearman's correlation analysis, 15 significant correlation pairs were identified in the Cancer Drug Sensitivity Genomics (GDSC) database between scoring model and drug reaction (Yang et al., 2013). Among them, eight pairs of drug sensitivity were related to WM-Score value, and seven pairs showed resistance related to WM-Score value (**Figure 6A**). In addition, we also analyzed the signaling pathways of these drugs to determine target genes. We found that drugs associated with high WM-Score value mainly target KIT, CLAP, and cell cycle signaling pathways. In contrast, drugs related to low WM-Score value mostly target apoptosis regulation and cell cycle signaling pathways (**Figure 6B**). Taken together, these findings indicate that the WM-Score values are related to drug reaction, and thus might offer a framework to guide the treatment strategy of HCC.

Role of WM-Score Model in Predicting anti-PD-1/L1 Immunotherapy

In recent years, immune checkpoint inhibitors (ICIs) have made breakthroughs in the treatment of advanced HCC, while biomarkers

that could effectively predict the efficacy of immunotherapy are still lacking. Herein, we explored whether the WM-Score model could predict therapeutic response to ICI therapy in HCC patients. For the IMvigor210 cohort, the therapeutic efficacy was significantly better in patients with low WM-Score value compared to those with high WM-Score value (**Figure 6C**). The frequency of response to anti-PD-1/L1 treatment in the low WM-Score value group was higher than that in the high WM-Score value group (**Figure 6D**). We also analyzed the survival difference of all samples of IMvigor210 and those under different stages. The results showed that total samples (**Figure 6E**), or Stage I + II samples (**Figure 6F**), or Stage III + IV samples (**Figure 6G**) all exhibited a marked difference in survival between samples with high and low WM-Score value. Especially in the prediction of high-stage clinical samples, the WM-Score value demonstrated extremely high power. Collectively, our results proved that the WM-Score model might serve as a potential predictor of response to anti-PD-1/L1 immunotherapy.

DISCUSSION

A growing pool of evidence indicates that RNA modifications play a key role in gene expression, whose disruption impacts the pathogenesis of human disease, including cancer (Frye et al., 2016). Although RNA modifications as genetic or epigenetic alterations of genes are not traditionally considered as cancer drivers, cumulative evidence suggests that abnormal RNA modifications are functionally correlated with many hallmarks of cancer, such as proliferation, invasion, migration, differentiation, self-renewal, and response to therapy (Cui et al., 2017; Weng et al., 2018; Jin et al., 2019).

For instance, N6-methyladenosine (m^6A) is an RNA methylation that is the most abundant form of internal mRNA modification. Yang et al. reported the involvement of the m^6A modification in the 3′-UTR of oncogene CDCP1 mRNA in bladder cancer cell growth and progression (Yang et al., 2019). Lang et al. indicated that the m^6A modification showed an important function in regulating the stability of viral transcripts and EBV-mediated tumorigenesis (Lang et al., 2019). Furthermore, Lan et al. reported that m6A methyltransferase KIAA1429 was high expressed in HCC tissues and knockdown KIAA1429 inhibited cell proliferation and metastasis *in vitro* and *in vivo* (Lan et al., 2019). Chen et al. found the writer CPSF1 of APA was significantly increased in HCC tissues and associated with poor survival outcomes (Chen S.-l. et al., 2021). All these studies focused on one or two modification regulators to explore their dysregulation, function, and underlying mechanism in cancer, however, the deposition of RNA modifications is a dynamic process involving multiple modification regulators. In the present study, we comprehensively described the molecular and biological features of different regulators of RNA modifications and identified two distinct RNA modification subtypes based on multiple modification regulators. Importantly, the two subtypes (cluster 1 and cluster 2) are not only associated with clinical survival, but also with the abundance of immune cell infiltration.

Considering the diversity and complexity of TME, the thorough understanding of its implications in cancer is a significant challenge. In recent years, some research groups have documented that RNA modifications were closely associated with TME. Shen et al. attempted to explore the role of m^6A regulators in HCC immune cell infiltration and prognosis, and identified three m^6A subtypes based on TCGA and GEO database, which were related to three known immune phenotypes (including immune-inflamed phenotype, immune-excluded phenotype, and immune-desert phenotype) (Shen et al., 2021). Chong et al. also discovered three m^6A modification patterns among 1,370 colon cancer cases, which were correlated with different outcomes and TME characterization (Chong et al., 2021). Three m^6A modification patterns with distinct TME cell-infiltrating characteristics were also determined in gastric cancer (Zhang et al., 2020), lung adenocarcinoma (Li et al., 2020), pancreatic adenocarcinoma (Tang R. et al., 2020), and gliomas (Xu et al., 2020). Similar with our analysis, these studies were based on a large number of samples in the subject database, such as TCGA and GEO, in order to clarify the role of modification in tumor immune regulation and progression. In our study, we further identified two stable transcriptomic subtypes based on the DGEs of the two RNA modification clusters. Especially, the transcriptomic subtypes were significantly associated with the immune cell activation and prognosis of HCC patients. Thus, the systematical evaluation of RNA modification patterns provides novel clues for understanding TME characterization in HCC. Gu et al. found 3 m 5C regulator-mediated methylation modification patterns based on the expression of 13 m 5C regulators which were closely associated with different immune cell infiltration characteristics in HCC (Gu et al., 2021). Shen et al. demonstrated three m6A modification patterns which affect tumor immune infiltrates and prognosis of patients with HCC (Shen et al., 2021). Previous studies mainly centered upon one types of RNA modification to explore their effect on TME. Here, we performed a comprehensive analysis of multiple types of RNA modification and highlights the cross-talk and the roles of RNA modifications in the TME and response to immunotherapy.We developed the WM-Score model to accurately predict the prognostic value of the RNA modification in individual patients. We found that this model could be applied to assessing clinicopathological features, such as clinical grades and TNM grades, and patients with higher clinical grades and TNM grades usually had higher WM-Score value.

In addition, the RNA modification pattern with higher WM-Score value tended to correlate with immune cell suppression in the tumor microenvironment, while the pattern with lower WM-Score value was usually associated with immune activation. In the IMvigor210 cohort, WM-Scores model was found to be linked with immune cell infiltration in TME as well as response to anti-PD-1/L1 immunotherapy, suggesting the application potential of WM-Score model for predicting HCC anti-PD-1/L1 immunotherapy.

CONCLUSION

In the present work, the RNA modification regulators were comprehensively analyzed, and the correlation was demonstrated between RNA modification patterns and cell-

infiltrating characteristics in the TME. The systematic evaluation of individual tumor RNA modification pattern might serve as a useful predictor of prognosis for HCC patients and act as a valuable tool for developing more effective immunotherapy strategies.

DATA AVAILABILITY STATEMENT

The original contributions presented in the study are included in the article/**Supplementary Material** further inquiries can be directed to the corresponding author.

AUTHOR CONTRIBUTIONS

ZY and JX designed the study, JX, SS, and ZD wrote this manuscript XH, LX, XL, and QL searched the articles and made figures YZ and GC collected and analyzed the data All authors read and approved the final manuscript.

FUNDING

This work was supported by Henan Medical Science and Technology Joint Building Program (LHGJ20200320 and LHGJ20200387), the Science and Technology Research Project of Henan Province (202102310115), and National Natural Science Foundation of China (82070643 and U1904164).

ACKNOWLEDGMENTS

We thank the patients and investigators who participated in TCGA and other datasets for providing data.

SUPPLEMENTARY MATERIAL

The Supplementary Material for this article can be found online at: https://www.frontiersin.org/articles/10.3389/fcell.2021.761391/full#supplementary-material

REFERENCES

Azambuja, J. H., Ludwig, N., Braganhol, E., and Whiteside, T. L. (2019). Inhibition of the Adenosinergic Pathway in Cancer Rejuvenates Innate and Adaptive Immunity. *Ijms* 20, 5698. doi:10.3390/ijms20225698

Barbieri, I., and Kouzarides, T. (2020). Role of RNA Modifications in Cancer. *Nat. Rev. Cancer* 20, 303–322. doi:10.1038/s41568-020-0253-2

Binnewies, M., Roberts, E. W., Kersten, K., Chan, V., Fearon, D. F., Merad, M., et al. (2018). Understanding the Tumor Immune Microenvironment (TIME) for Effective Therapy. *Nat. Med.* 24, 541–550. doi:10.1038/s41591-018-0014-x

Bray, F., Ferlay, J., Soerjomataram, I., Siegel, R. L., Torre, L. A., and Jemal, A. (2018). Global Cancer Statistics 2018: GLOBOCAN Estimates of Incidence and Mortality Worldwide for 36 Cancers in 185 Countries. *CA: A Cancer J. Clinicians* 68, 394–424. doi:10.3322/caac.21492

Chen, H., Yao, J., Bao, R., Dong, Y., Zhang, T., Du, Y., et al. (2021a). Cross-talk of Four Types of RNA Modification Writers Defines Tumor Microenvironment and Pharmacogenomic Landscape in Colorectal Cancer. *Mol. Cancer* 20, 29. doi:10.1186/s12943-021-01322-w

Chen, S.-l., Zhu, Z.-x., Yang, X., Liu, L.-l., He, Y.-f., Yang, M.-m., et al. (2021b). Cleavage and Polyadenylation Specific Factor 1 Promotes Tumor Progression via Alternative Polyadenylation and Splicing in Hepatocellular Carcinoma. *Front. Cel Dev. Biol.* 9, 616835. doi:10.3389/fcell.2021.616835

Chong, W., Shang, L., Liu, J., Fang, Z., Du, F., Wu, H., et al. (2021). m6A Regulator-Based Methylation Modification Patterns Characterized by Distinct Tumor Microenvironment Immune Profiles in colon Cancer. *Theranostics* 11, 2201–2217. doi:10.7150/thno.52717

Cui, Q., Shi, H., Ye, P., Li, L., Qu, Q., Sun, G., et al. (2017). m 6 A RNA Methylation Regulates the Self-Renewal and Tumorigenesis of Glioblastoma Stem Cells. *Cel Rep.* 18, 2622–2634. doi:10.1016/j.celrep.2017.02.059

Davalos, V., Blanco, S., and Esteller, M. (2018). SnapShot: Messenger RNA Modifications. *Cell* 174, 498, 2018 . e491. doi:10.1016/j.cell.2018.06.046

Frye, M., Jaffrey, S. R., Pan, T., Rechavi, G., and Suzuki, T. (2016). RNA Modifications: what Have We Learned and where Are We Headed. *Nat. Rev. Genet.* 17, 365–372. doi:10.1038/nrg.2016.47

Fu, Y., Liu, S., Zeng, S., and Shen, H. (2019). From Bench to Bed: the Tumor Immune Microenvironment and Current Immunotherapeutic Strategies for Hepatocellular Carcinoma. *J. Exp. Clin. Cancer Res.* 38, 396. doi:10.1186/s13046-019-1396-4

Giannini, E. G., Farinati, F., Ciccarese, F., Pecorelli, A., Rapaccini, G. L., Di Marco, M., et al. (2015). Prognosis of Untreated Hepatocellular Carcinoma. *Hepatology* 61, 184–190. doi:10.1002/hep.27443

Gnoni, A., Licchetta, A., Memeo, R., Argentiero, A., Solimando, A. G., Longo, V., et al. (2019). Role of BRAF in Hepatocellular Carcinoma: A Rationale for Future Targeted Cancer Therapies. *Medicina* 55, 754. doi:10.3390/medicina55120754

Gu, X., Zhou, H., Chu, Q., Zheng, Q., Wang, J., and Zhu, H. (2021). Uncovering the Association between m5C Regulator-Mediated Methylation Modification Patterns and Tumour Microenvironment Infiltration Characteristics in Hepatocellular Carcinoma. *Front. Cel Dev. Biol.* 9, 727935. doi:10.3389/fcell.2021.727935

Hänzelmann, S., Castelo, R., and Guinney, J. (2013). GSVA: Gene Set Variation Analysis for Microarray and RNA-Seq Data. *BMC Bioinformatics* 14, 7. doi:10.1186/1471-2105-14-7

Jiang, Y., Wan, Y., Gong, M., Zhou, S., Qiu, J., and Cheng, W. (2020). RNA Demethylase ALKBH5 Promotes Ovarian Carcinogenesis in a Simulated Tumour Microenvironment through Stimulating NF- κ B Pathway. *J. Cel Mol Med* 24, 6137–6148. doi:10.1111/jcmm.15228

Jin, D., Guo, J., Wu, Y., Du, J., Yang, L., Wang, X., et al. (2019). m6A mRNA Methylation Initiated by METTL3 Directly Promotes YAP Translation and Increases YAP Activity by Regulating the MALAT1-miR-1914-3p-YAP axis to Induce NSCLC Drug Resistance and Metastasis. *J. Hematol. Oncol.* 12, 135. doi:10.1186/s13045-019-0830-6

Jonkhout, N., Tran, J., Smith, M. A., Schonrock, N., Mattick, J. S., and Novoa, E. M. (2017). The RNA Modification Landscape in Human Disease. *Rna* 23, 1754–1769. doi:10.1261/rna.063503.117

Lan, T., Li, H., Zhang, D., Xu, L., Liu, H., Hao, X., et al. (2019). KIAA1429 Contributes to Liver Cancer Progression through N6-methyladenosine-dependent post-transcriptional Modification of GATA3. *Mol. Cancer* 18, 186. doi:10.1186/s12943-019-1106-z

Lang, F., Singh, R. K., Pei, Y., Zhang, S., Sun, K., and Robertson, E. S. (2019). EBV Epitranscriptome Reprogramming by METTL14 Is Critical for Viral-Associated Tumorigenesis. *Plos Pathog.* 15, e1007796. doi:10.1371/journal.ppat.1007796

Li, X., Xiong, X., Wang, K., Wang, L., Shu, X., Ma, S., et al. (2016). Transcriptome-wide Mapping Reveals Reversible and Dynamic N1-Methyladenosine Methylome. *Nat. Chem. Biol.* 12, 311–316. doi:10.1038/nchembio.2040

Li, X., Xiong, X., Zhang, M., Wang, K., Chen, Y., Zhou, J., et al. (2017). Base-Resolution Mapping Reveals Distinct m1A Methylome in Nuclear- and Mitochondrial-Encoded Transcripts. *Mol. Cel* 68, 993–1005. e1009. doi:10.1016/j.molcel.2017.10.019

Li, Y., Gu, J., Xu, F., Zhu, Q., Chen, Y., Ge, D., et al. (2020). Molecular Characterization, Biological Function, Tumor Microenvironment

Association and Clinical Significance of m6A Regulators in Lung Adenocarcinoma. *Brief Bioinform* 22, bbaa225. doi:10.1093/bib/bbaa225

Llovet, J. M., Kelley, R. K., Villanueva, A., Singal, A. G., Pikarsky, E., Roayaie, S., et al. (2021). Hepatocellular Carcinoma. *Nat. Rev. Dis. Primers* 7, 6. doi:10.1038/s41572-020-00240-3

Lu, C., Rong, D., Zhang, B., Zheng, W., Wang, X., Chen, Z., et al. (2019). Current Perspectives on the Immunosuppressive Tumor Microenvironment in Hepatocellular Carcinoma: Challenges and Opportunities. *Mol. Cancer* 18, 130. doi:10.1186/s12943-019-1047-6

Nachtergaele, S., and He, C. (2017). The Emerging Biology of RNA post-transcriptional Modifications. *RNA Biol.* 14, 156–163. doi:10.1080/15476286.2016.1267096

Newman, A. M., Liu, C. L., Green, M. R., Gentles, A. J., Feng, W., Xu, Y., et al. (2015). Robust Enumeration of Cell Subsets from Tissue Expression Profiles. *Nat. Methods* 12, 453–457. doi:10.1038/nmeth.3337

Nishikura, K. (2010). Functions and Regulation of RNA Editing by ADAR Deaminases. *Annu. Rev. Biochem.* 79, 321–349. doi:10.1146/annurev-biochem-060208-105251

Nombela, P., Miguel-López, B., and Blanco, S. (2021). The Role of m6A, m5C and Ψ RNA Modifications in Cancer: Novel Therapeutic Opportunities. *Mol. Cancer* 20, 18. doi:10.1186/s12943-020-01263-w

Ontiveros, R. J., Stoute, J., and Liu, K. F. (2019). The Chemical Diversity of RNA Modifications. *Biochem. J.* 476, 1227–1245. doi:10.1042/bcj20180445

Ou, Q., Yu, Y., Li, A., Chen, J., Yu, T., Xu, X., et al. (2020). Association of Survival and Genomic Mutation Signature with Immunotherapy in Patients with Hepatocellular Carcinoma. *Ann. Transl Med.* 8, 230. doi:10.21037/atm.2020.01.32

Peifer, C., Sharma, S., Watzinger, P., Lamberth, S., Kötter, P., and Entian, K.-D. (2013). Yeast Rrp8p, a Novel Methyltransferase Responsible for m1A 645 Base Modification of 25S rRNA. *Nucleic Acids Res.* 41, 1151–1163. doi:10.1093/nar/gks1102

RajBhandary, U. L., Stuart, A., Faulkner, R. D., Chang, S. H., and Khorana, H. G. (1966). Nucleotide Sequence Studies on Yeast Phenylalanine sRNA. *Cold Spring Harbor Symposia Quantitative Biol.* 31, 425–434. doi:10.1101/sqb.1966.031.01.055

Roundtree, I. A., Evans, M. E., Pan, T., and He, C. (2017). Dynamic RNA Modifications in Gene Expression Regulation. *Cell* 169, 1187–1200. doi:10.1016/j.cell.2017.05.045

Safra, M., Sas-Chen, A., Nir, R., Winkler, R., Nachshon, A., Bar-Yaacov, D., et al. (2017). The m1A Landscape on Cytosolic and Mitochondrial mRNA at Single-Base Resolution. *Nature* 551, 251–255. doi:10.1038/nature24456

Shen, S., Yan, J., Zhang, Y., Dong, Z., Xing, J., and He, Y. (2021). N6-methyladenosine (m6A)-Mediated Messenger RNA Signatures and the Tumor Immune Microenvironment Can Predict the Prognosis of Hepatocellular Carcinoma. *Ann. Transl Med.* 9, 59. doi:10.21037/atm-20-7396

Sotiriou, C., Wirapati, P., Loi, S., Harris, A., Fox, S., Smeds, J., et al. (2006). Gene Expression Profiling in Breast Cancer: Understanding the Molecular Basis of Histologic Grade to Improve Prognosis. *J. Natl. Cancer Inst.* 98, 262–272. doi:10.1093/jnci/djj052

Sun, T., Wu, R., and Ming, L. (2019). The Role of m6A RNA Methylation in Cancer. *Biomed. Pharmacother.* 112, 108613. doi:10.1016/j.biopha.2019.108613

Tang, R., Zhang, Y., Liang, C., Xu, J., Meng, Q., Hua, J., et al. (2020a). The Role of m6A-Related Genes in the Prognosis and Immune Microenvironment of Pancreatic Adenocarcinoma. *PeerJ* 8, e9602. doi:10.7717/peerj.9602

Tang, S. J., Shen, H., An, O., Hong, H., Li, J., Song, Y., et al. (2020b). Cis- and Trans-regulations of Pre-mRNA Splicing by RNA Editing Enzymes Influence Cancer Development. *Nat. Commun.* 11, 799. doi:10.1038/s41467-020-14621-5

Tian, B., and Manley, J. L. (2017). Alternative Polyadenylation of mRNA Precursors. *Nat. Rev. Mol. Cel Biol* 18, 18–30. doi:10.1038/nrm.2016.116

Weng, H., Huang, H., Wu, H., Qin, X., Zhao, B. S., Dong, L., et al. (2018). METTL14 Inhibits Hematopoietic Stem/Progenitor Differentiation and Promotes Leukemogenesis via mRNA m6A Modification. *Cell Stem Cell* 22, 191–205. e199. doi:10.1016/j.stem.2017.11.016

Wilkerson, M. D., and Hayes, D. N. (2010). ConsensusClusterPlus: a Class Discovery Tool with Confidence Assessments and Item Tracking. *Bioinformatics* 26, 1572–1573. doi:10.1093/bioinformatics/btq170

Xu, S., Tang, L., Dai, G., Luo, C., and Liu, Z. (2020). Expression of m6A Regulators Correlated with Immune Microenvironment Predicts Therapeutic Efficacy and Prognosis in Gliomas. *Front. Cel Dev. Biol.* 8, 594112. doi:10.3389/fcell.2020.594112

Xue, C., Zhao, Y., and Li, L. (2020). Advances in RNA Cytosine-5 Methylation: Detection, Regulatory Mechanisms, Biological Functions and Links to Cancer. *Biomark Res.* 8, 43. doi:10.1186/s40364-020-00225-0

Yang, F., Jin, H., Que, B., Chao, Y., Zhang, H., Ying, X., et al. (2019). Dynamic m6A mRNA Methylation Reveals the Role of METTL3-m6A-CDCP1 Signaling axis in Chemical Carcinogenesis. *Oncogene* 38, 4755–4772. doi:10.1038/s41388-019-0755-0

Yang, W., Soares, J., Greninger, P., Edelman, E. J., Lightfoot, H., Forbes, S., et al. (2013). Genomics of Drug Sensitivity in Cancer (GDSC): a Resource for Therapeutic Biomarker Discovery in Cancer Cells. *Nucleic Acids Res.* 41, D955–D961. doi:10.1093/nar/gks1111

Zeng, D., Li, M., Zhou, R., Zhang, J., Sun, H., Shi, M., et al. (2019). Tumor Microenvironment Characterization in Gastric Cancer Identifies Prognostic and Immunotherapeutically Relevant Gene Signatures. *Cancer Immunol. Res.* 7, 737–750. doi:10.1158/2326-6066.Cir-18-0436

Zhang, B., Wu, Q., Li, B., Wang, D., Wang, L., and Zhou, Y. L. (2020). m6A Regulator-Mediated Methylation Modification Patterns and Tumor Microenvironment Infiltration Characterization in Gastric Cancer. *Mol. Cancer* 19, 53. doi:10.1186/s12943-020-01170-0

Zhu, S., Wu, Q., Zhang, B., Wei, H., Li, B., Shi, W., et al. (2020). Autophagy-related Gene Expression Classification Defines Three Molecular Subtypes with Distinct Clinical and Microenvironment Cell Infiltration Characteristics in colon Cancer. *Int. Immunopharmacology* 87, 106757. doi:10.1016/j.intimp.2020.106757

Conflict of Interest: The authors declare that the research was conducted in the absence of any commercial or financial relationships that could be construed as a potential conflict of interest.

Publisher's Note: All claims expressed in this article are solely those of the authors and do not necessarily represent those of their affiliated organizations, or those of the publisher, the editors and the reviewers. Any product that may be evaluated in this article, or claim that may be made by its manufacturer, is not guaranteed or endorsed by the publisher.

frontiers in Cell and Developmental Biology

ORIGINAL RESEARCH
published: 03 January 2022
doi: 10.3389/fcell.2021.801959

A Novel Lactate Metabolism-Related Gene Signature for Predicting Clinical Outcome and Tumor Microenvironment in Hepatocellular Carcinoma

Yue Li[1], *Huanye Mo*[1], *Shengli Wu*[1], *Xin Liu*[2]* *and Kangsheng Tu*[1]*

[1]*Department of Hepatobiliary Surgery, The First Affiliated Hospital of Xi'an Jiaotong University, Xi'an, China,* [2]*The Key Laboratory of Tumor Molecular Diagnosis and Individualized Medicine of Zhejiang Province, Zhejiang Provincial People's Hospital, Affiliated People's Hospital, Hangzhou Medical College, Hangzhou, China*

OPEN ACCESS

Edited by:
Jiang Chen,
Zhejiang University, China

Reviewed by:
Qiongzhu Dong,
Fudan University, China
Yanhong Zhang,
Brigham and Women's Hospital and Harvard Medical School, United States
Long Liu,
First Affiliated Hospital of Zhengzhou University, China

***Correspondence:**
Xin Liu
liuxindongdong@sina.com
Kangsheng Tu
tks0912@foxmail.com

Specialty section:
This article was submitted to Molecular and Cellular Oncology, a section of the journal Frontiers in Cell and Developmental Biology

Received: *26 October 2021*
Accepted: *02 December 2021*
Published: *03 January 2022*

Citation:
Li Y, Mo H, Wu S, Liu X and Tu K (2022) A Novel Lactate Metabolism-Related Gene Signature for Predicting Clinical Outcome and Tumor Microenvironment in Hepatocellular Carcinoma. Front. Cell Dev. Biol. 9:801959. doi: 10.3389/fcell.2021.801959

Hepatocellular carcinoma (HCC) is the main subtype of primary liver cancer with high malignancy and poor prognosis. Metabolic reprogramming is a hallmark of cancer and has great importance on the tumor microenvironment (TME). As an abundant metabolite, lactate plays a crucial role in cancer progression and the immunosuppressive TME. Nonetheless, the potential roles of lactate in HCC remain unclear. In this study, we downloaded transcriptomic data of HCC patients with corresponding clinical information from the TCGA and ICGC portals. The TCGA-HCC dataset used as the training cohort, while the ICGC-LIRI-JP dataset was served as an external validation cohort. Cox regression analysis and the LASSO regression model were combined to construct the lactate metabolism-related gene signature (LMRGS). Then, we assessed the clinical significance of LMRGS in HCC. Besides, enriched molecular functions, tumor mutation burden (TMB), infiltrating immune cells, and immune checkpoint were comprehensively analyzed in different LMRGS subgroups. In total, 66 differentially expressed lactate metabolism-related genes (LMRGs) were screened. The functions of LMRGs were mainly enriched in mitochondrial activity and metabolic processes. The LMRGS comprised of six key LMRGs (FKTN, PDSS1, PET117, PUS1, RARS1, and RNASEH1) had significant clinical value for independently predicting the prognosis of HCC patients. The overall survival and median survival of patients in the LMRGS-high group were significantly shorter than in the LMRGS-low group. In addition, there were differences in TMB between the two LMRGS subgroups. The probability of genetic mutations was higher in the LMRGS-high group. Most importantly, the LMRGS reflected the TME characteristics. In the LMRGS-high group, the immune microenvironment presented a suppressed state, accompanied by more inhibitory immune cell infiltration, including follicular helper T cells and regulatory T cells. Additionally, the expression of inhibitory checkpoint molecules was much higher in the LMRGS-high group. Our study suggested

Abbreviations: HCC, Hepatocellular carcinoma; LMRGs, Lactate metabolism-related genes; LMRGS, Lactate metabolism-related gene signature; TMB, Tumor mutation burden; TME, Tumor microenvironment.

that the LMRGS was a robust biomarker to predict the clinical outcomes and evaluate the TME of patients with HCC.

Keywords: hepatocellular carcinoma, metabolic reprogramming, lactate, prognosis, tumor microenvironment

INTRODUCTION

Hepatocellular carcinoma (HCC) is the most common histological type of primary liver cancer, the third leading cause of cancer death worldwide (Sung et al., 2021). As a highly malignant tumor, the 5-year survival rate of HCC is less than 18% (Villanueva, 2019). Treatment options for HCC include hepatic resection, liver transplantation, image-guided ablation, transarterial therapies, chemotherapy, and molecularly targeted therapy (Llovet et al., 2021). Clinically, patients with HCC are often treated by a combination of several modalities. However, the therapeutic outcomes of advanced HCC remain unsatisfactory. Even after successful tumor eradication, the recurrence rate of HCC is remarkably high. Recently, immunotherapy has been shown to improve the clinical efficacy of advanced HCC. Unlike the mechanism of action of conventional therapy, immunotherapy is based on activating the patient's own immune system to fight against tumors (Ringelhan et al., 2018). Cancer metabolism plays an essential role in affecting the anti-tumor immune response through modulating the interaction between tumor cells and the tumor microenvironment (TME) (Bader et al., 2020). Therefore, it is vital to identify a metabolism-related signature to assess the TME and improve the treatment efficacy of immunotherapy.

Metabolic alterations of tumor cells not only favor cell proliferation but also have profound influences on anti-tumor immunity through the release of metabolites, especially lactate (Xia et al., 2021). Unlike normal cells, tumor cells metabolize glucose to produce lactate even under adequate oxygen conditions. The accumulation of lactate provides an acidic microenvironment that benefits tumor growth and progression. Besides, lactate produced by aerobic glycolysis can be secreted into the extracellular environment as a signaling molecule to regulate intercellular interactions (Liao et al., 2021). In gastric cancer, lactate derived from tumor cells mediates the up-regulation of BDNF expression in cancer-associated fibroblasts by activating the NF-κB pathway, eventually resulting in acquired resistance (Jin et al., 2021). Alterations in lactate metabolism have been shown to be associated with cell invasion, migration, angiogenesis, drug resistance, and immune escape. High levels of lactate in the TME promote differentiation of tumor-associated macrophages to the M2 subtype, while activated macrophages facilitate tumor invasion through the CCL17/CCR4/mTORC1 signaling axis (Zhang et al., 2021). Lactate-induced PD-L1 up-regulation on neutrophils impairs T cell cytotoxicity in HCC (Deng et al., 2021). In addition, tumor cell-derived lactate induces the expression of GPR81 in dendritic cells via paracrine mode to inhibit the antigen presentation function of immune cells (Brown et al., 2020). Moreover, lactate has an important role in epigenetic regulation. Some studies have demonstrated that histone lysine lactylation takes part in modulating gene transcription (Izzo and Wellen, 2019; Yu et al., 2021). Given the vital role of lactate in oncogenesis and the immunosuppressive TME, targeting its metabolism promises to become an effective means for cancer treatment.

In this study, we screened the key lactate metabolism-related genes (LMRGs) and constructed a prognostic signature to predict the survival outcome. Next, we comprehensively analyze the tumor mutation burden (TMB) features in different subgroups. Then, the association between the TME and lactate metabolism-related gene signature (LMRGS) was explored using the R software package. We focused on the infiltrating immune cells in the TME and characterized the differential immune microenvironment in LMRGS subgroups. The results indicated that the LMRGS had a high value for evaluating the prognosis and reflecting the TME in HCC.

MATERIALS AND METHODS

Data Acquisition

RNA transcriptome sequencing data, somatic mutation profile, and corresponding clinical information of HCC were obtained from the TCGA data portal (https://portal.gdc.cancer.gov/). In this study, the TCGA-HCC cohort was served as the training set. To verify the training set results, we downloaded an independent dataset of HCC from the ICGC website (https://dcc.icgc.org/releases/current/Projects/LIRI-JP). Therefore, the ICGC-LIRI-JP cohort was used as a validation set. The detailed clinical information of HCC patients from two cohorts was summarized in **Table 1**.

Differentially Expressed LMRGs and Transcription Factors

The 289 LMRGs were retrieved from the Molecular Signatures database (Liberzon et al., 2015). Transcription factors associated with cancer were downloaded from the Cistrome (Zheng et al., 2019). To identify the LMRGs and transcription factors involved in the progression of HCC, we carried out differential expression analysis between 50 normal tissues and 374 tumor tissues in the TCGA-HCC cohort. Genes with $|\log2$ fold change (FC)$| > 1$ and false discovery rate (FDR) < 0.05 were defined as differentially expressed. For further understanding the biological function and pathway of differentially expressed LMRGs and transcription factors, we used the "clusterprofiler" package in R (version 4.1.0) to carry out the GO and KEGG enrichment analyses.

Construction and Assessment of LMRGS

The differentially expressed LMRGs were subjected to univariate Cox regression analysis to determine the LMRGs with prognostic

TABLE 1 | Clinical and pathological characters of HCC patients in TCGA and ICGC cohort.

Characteristics		Number
TCGA cohort (*N* = 376)		
Age	≤60	180
	>60	196
Gender	Female	122
	Male	254
Pathological grade	G1	55
	G2	180
	G3	123
	G4	13
	NA	5
T	T1	185
	T2	94
	T3	81
	T4	13
	NA	3
N	N0	257
	N1	4
	NA	115
M	M0	272
	M1	4
	NA	100
Clinical Stage	I	175
	II	86
	III	86
	IV	5
	NA	24
Fibrosis	No	76
	Yes	141
	NA	159
Virus infection	No	210
	Yes	166
Vascular invasion	No	210
	Yes	110
	NA	56
ICGC cohort (*N* = 231)		
Age	≤60	49
	>60	182
Gender	Female	61
	Male	170
Clinical Stage	I	36
	II	105
	III	71
	IV	19

value. To avoid overfitting, we further performed the LASSO Cox regression (iteration = 1000) using the "glmnet" package (Friedman et al., 2010; Liu et al., 2021a; Liu et al., 2021b). After screening by LASSO regression, the selected LMRGs were applied to establish the LMRGS through the multivariate Cox regression analysis. The LMRGS score was calculated as the following formula: LMRGS score = expression level of $gene_1$ × coefficient of $gene_1$ + expression level of $gene_2$ × coefficient of $gene_2$ + . . . + expression level of $gene_n$ × coefficient of $gene_n$. We classified HCC patients into two subgroups according to the median LMRGS score, including the LMRGS-high and the LMRGS-low groups. Principal component analysis (PCA) was used to evaluate the classification accuracy of the signature. For assessing the prognostic value of the LMRGS, we conducted the Kaplan–Meier (KM) survival analysis to compare the overall survival (OS) and median survival time between the two LMRGS groups. The time-dependent ROC curve was performed by the "timeROC" package in R. We also applied the Cox proportional hazards regression model to identify the LMRGS as an independent predictor for OS. To explore the influence of the LMRGS on HCC progression, we clarify the association between the LMRGS and clinicopathologic factors, such as TNM stage, pathological grade, fibrosis, vascular invasion, and virus infection.

Establishing a Nomogram

To predict the one-, three-, 5-year survival rate of HCC patients, we constructed a nomogram based on the LMRGS and significant clinicopathologic parameters (Iasonos et al., 2008). The calibration curve was used to estimate the consistency between predicted survival and actual survival. The time-dependent ROC curve was applied to evaluate the specificity and sensitivity of the model.

Calculation of TMB

For calculating the TMB of each HCC tumor sample, we selected the somatic mutation data processed by the VarScan platform in the TCGA-HCC cohort. Then, we compared the difference of TMB between the LMRGS-high and the LMRGS-low groups. Visualization of somatic mutations in the two LMRGS groups was performed by the R package "maftools". Moreover, we explored the impact of the LMRGS score combined with the TMB on the survival of HCC.

Comprehensive Analysis of TME in Different LMRGS Subgroups

The TME is mainly composed of stromal cells and immune cells (Gysler and Drapkin, 2021). Firstly, we used the ESTIMATE algorithm to calculate the stromal score of all samples (Yoshihara et al., 2013). ESTIMATE is a prevalent R package, which is widely utilized in the cancer-related studies (Liu et al., 2021c; 2021d; 2021e). Then, the single sample gene set enrichment analysis (ssGSEA) was performed to derive the immune enrichment score based on the 29 immune gene sets (Bindea et al., 2013). To identify the immune infiltration features of HCC samples, we imported their gene expression profiles to the CIBERSORTx website with 1000 permutations (https://cibersortx.stanford.edu/). According to the obtained results, we compared the relative fractions of 22 tumor-infiltrating immune cells in the two LMRGS subgroups. Moreover, correlation analysis was carried out to clarify the relationship between the immune cell and the LMRGS score. Immune checkpoints expression and immune function have crucial influences on the treatment responses of immunotherapy. For further investigating the effect of the LMRGS score on immunotherapy, comparisons between the two LMRGS subgroups were analyzed to evaluate the differences of immune checkpoints and immune function.

Gene Set Enrichment Analysis

The HCC samples were stratified into high- and low-LMRGS score groups as described above. To determine the primary signaling pathways and hallmark gene sets involved in the

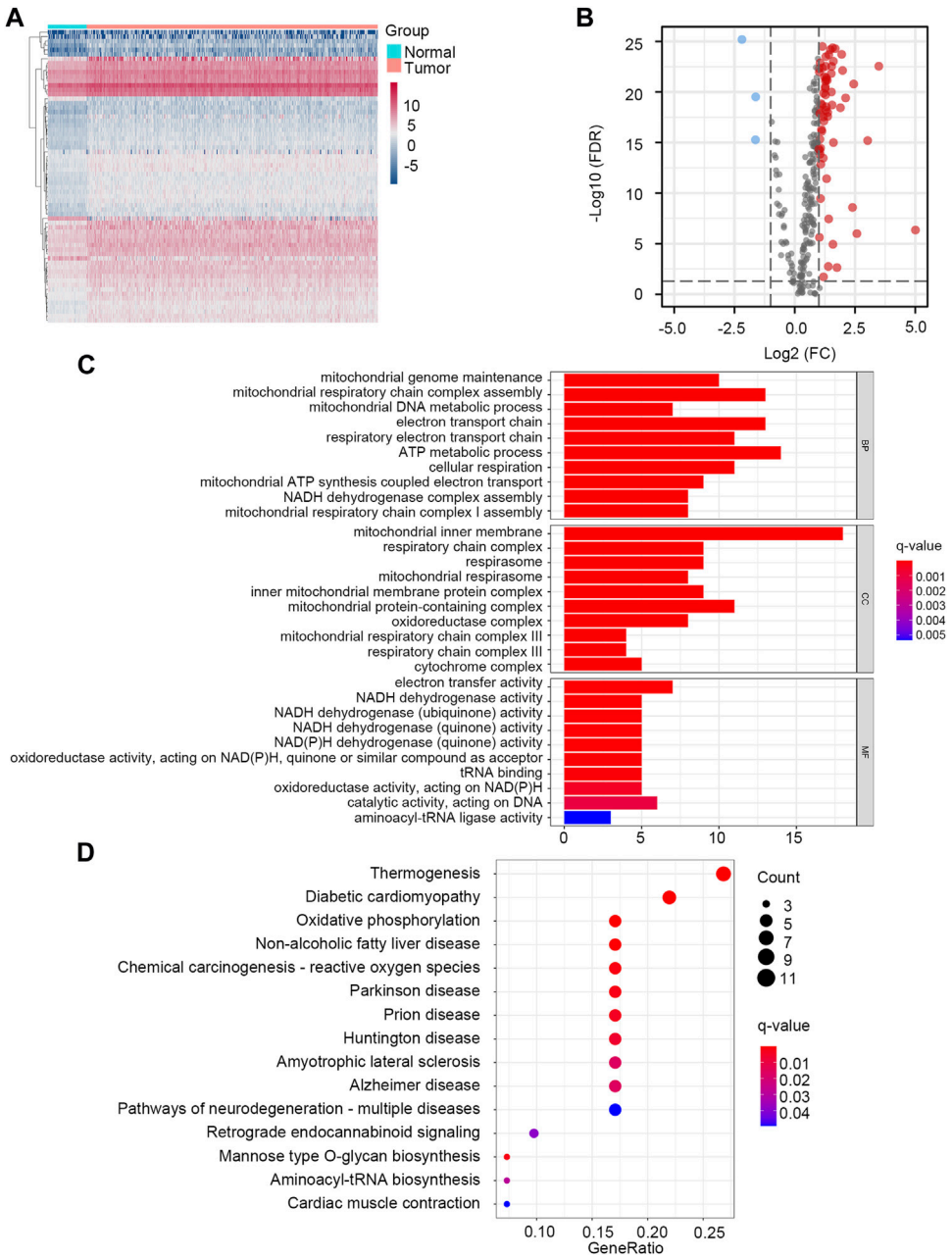

FIGURE 1 | Identification and enrichment analysis of LMRGs in HCC. **(A)** The heatmap showed the expression level of LMRGs in each sample. **(B)** The volcano plot displayed down-regulated and up-regulated LMRGs. **(C)** GO enrichment analysis. **(D)** KEGG pathway enrichment analysis.

signature, we uploaded sample grouping and gene expression files into the GSEA software (version 4.1.0) to conduct enrichment analysis.

Statistical Analysis

All data analysis and visualization were completed by R software. If the data did not follow a normal distribution and the variance was uninformed, the differences between groups were compared by the Wilcoxon rank-sum test or Kruskal–Wallis test. The Cox regression model was used to perform univariate and multivariate analyses. The log-rank test was performed to evaluate the survival difference. Correlation analyses of LMRGS score and immune infiltration cells were conducted by Spearman's rank correlation test. In this study, p-value < 0.05 was considered statistically significant as indicated.

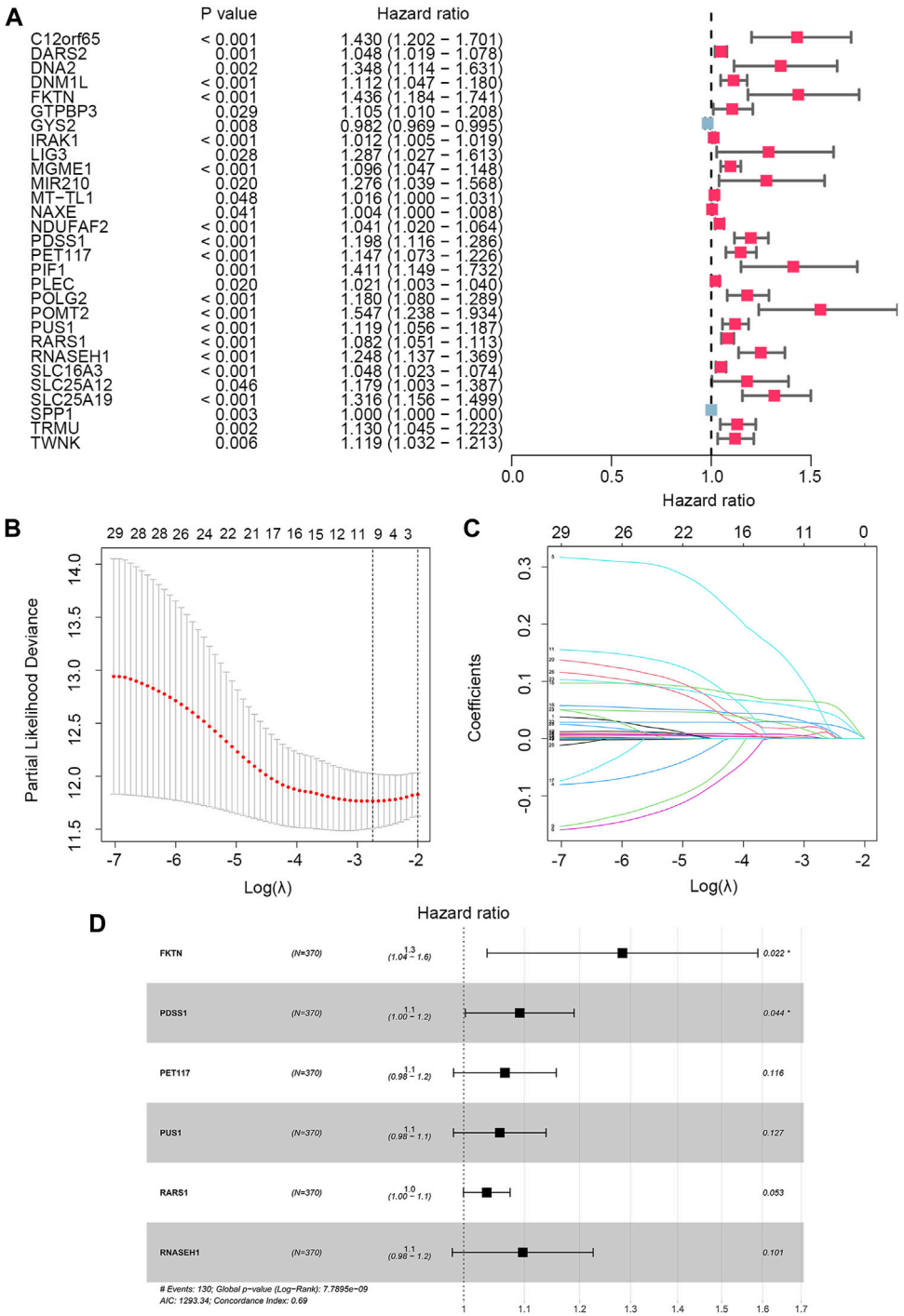

FIGURE 2 | Cox regression analysis and LASSO analysis of LMRGs. **(A)** Univariate Cox regression analysis screened 29 prognostic LMRGs. **(B)** Tuning parameter (λ) selection in LASSO model using cross-validation. **(C)** The LASSO coefficient profile of 29 prognostic LMRGs. **(D)** Multivariate Cox regression analysis of LMRGs was shown by forest plot.

RESULTS

Identification of LMRGs

Through the differential gene screening analysis, we obtained 66 differentially expressed LMRGs, including three down-regulated and 63 up-regulated genes. The heat map displayed the expression of LMRGs in HCC samples and normal samples (**Figure 1A**). The differential expression of down-regulated and up-regulated LMRGs was represented in the volcano plot (**Figure 1B**). The 66 differentially expressed LMRGs were further

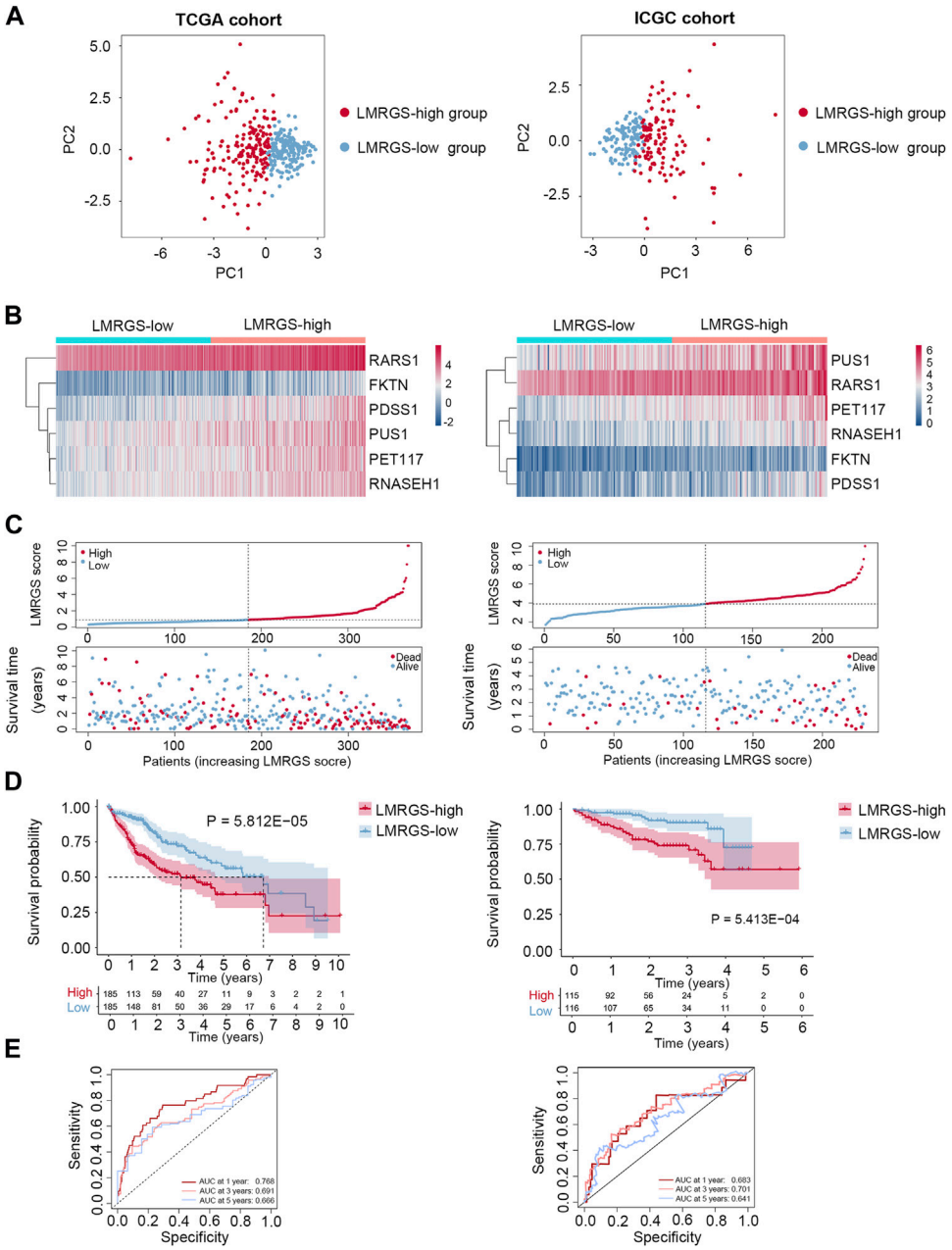

FIGURE 3 | Prognostic value of LMRGS in HCC. **(A)** PCA was used to determine whether the samples could be grouped correctly based on the LMRGS score. **(B)** Heatmap for the expression of six crucial genes in LMRGS-low and LMRGS-high groups. **(C)** The distribution of LMRGS scores and survival status of HCC patients with increasing LMRGS score. **(D)** KM survival analysis between LMRGS-low and LMRGS-high groups. **(E)** ROC curves analysis of LMRGS on OS at 1 year, 3 years, and 5 years.

analyzed by functional enrichment analysis. The primary biological processes (BP) of LMRGs were involved in mitochondrial genome maintenance, mitochondrial respiratory chain complex assembly, electron transport chain, and metabolic process. For cellular components (CC), the LMRGs primarily existed in the mitochondrial inner membrane, respiratory chain complex, and mitochondrial respirasome. The molecular functions (MF) of LMRGs were mainly enriched in electron transfer activity, NADH dehydrogenase activity, and oxidoreductase activity (**Figure 1C**). Signaling pathway analysis indicated that the differentially expressed LMRGs were related to thermogenesis, diabetic cardiomyopathy, oxidative phosphorylation, non-alcoholic fatty liver disease, and reactive oxygen species (**Figure 1D**). The above results showed that the LMRGs were mainly associated with metabolic processes and oxidation responses.

TABLE 2 | Univariate and multivariate Cox regression analyses of the LMRGS score in the TCGA.

Variable	Univariate analysis			Multivariate analysis		
	HR	95% CI	*p*-value	HR	95% CI	*p*-value
LMRGS score	3.461	2.179–5.499	1.469E-7	3.576	2.105–6.074	2.44E-6
Age	1.015	0.993–1.037	0.177	1.015	0.993–1.039	0.189
Gender	0.574	0.335–0.982	0.043	0.851	0.446–1.624	0.625
Grade	1.235	0.847–1.799	0.273	1.247	0.808–1.925	0.318
Clinical Stage	1.692	1.273–2.249	0.000	1.374	0.300–6.283	0.682
T	1.616	1.229–2.125	0.001	0.950	0.235–3.847	0.943
N	2.983	0.410–21.704	0.280	0.663	0.017–25.662	0.826
M	4.895	1.515–15.819	0.008	3.349	0.711–15.767	0.126
Fibrosis	0.589	0.335–1.035	0.066	0.875	0.468–1.636	0.675
Virus infection	2.252	1.310–3.872	0.003	1.923	1.050–3.552	0.034
Vascular invasion	1.330	0.760–2.329	0.317	0.828	0.451–1.517	0.540

HR, hazard ratio; 95%CI, 95% confidence interval.

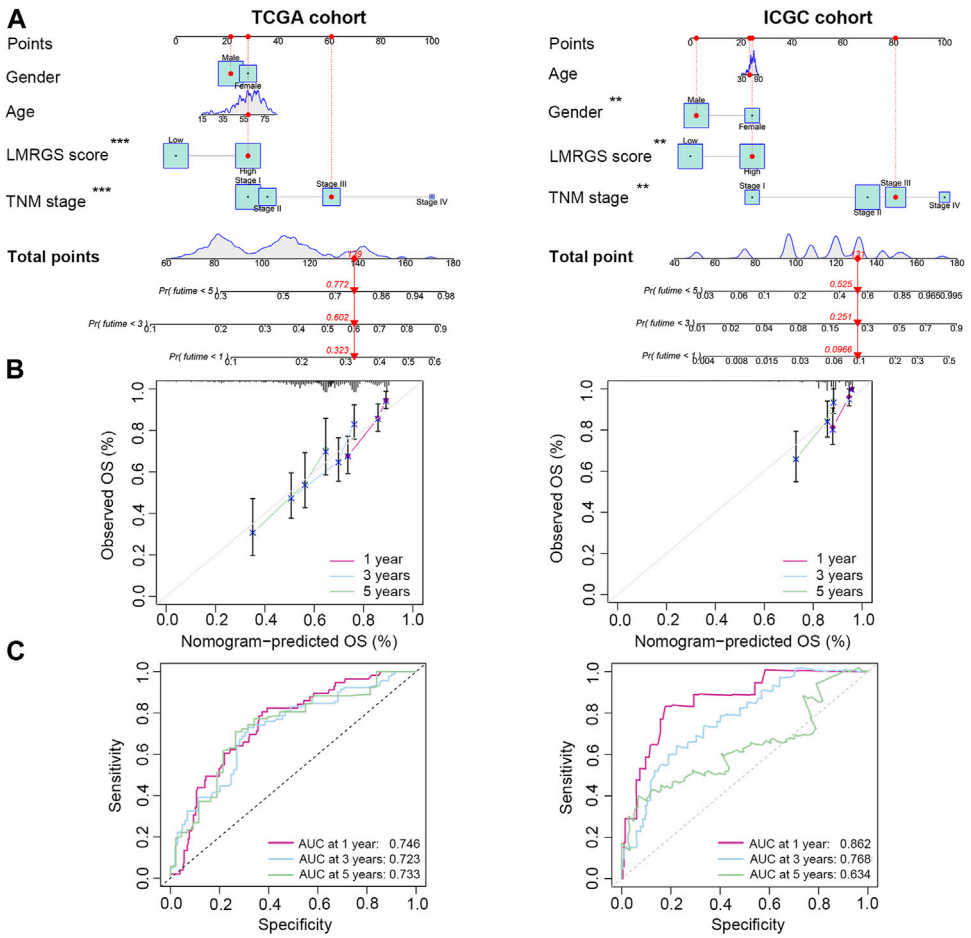

FIGURE 4 | A nomogram was generated to estimate the survival rate of HCC patients. **(A)** Development of a nomogram by combining LMRGS score with age, gender, and TNM stage to predict the survival probability. **(B)** Calibration plots of the nomogram. **(C)** ROC curves of the nomogram. **p* < 0.05, ***p* < 0.01, ****p* < 0.001.

Development of the LMRGS

To identify the LMRGs correlated with OS, we performed the univariate Cox regression analysis. A total of 29 LMRGs were related to prognosis (**Figure 2A**). After selection by LASSO regression, only 10 LMRGs were subjected to multivariate Cox regression analysis to construct the LMRGS (**Figures 2B,C**). Based on the coefficient and the expression of six crucial genes involved in the LMRGS, we calculated the LMRGS score

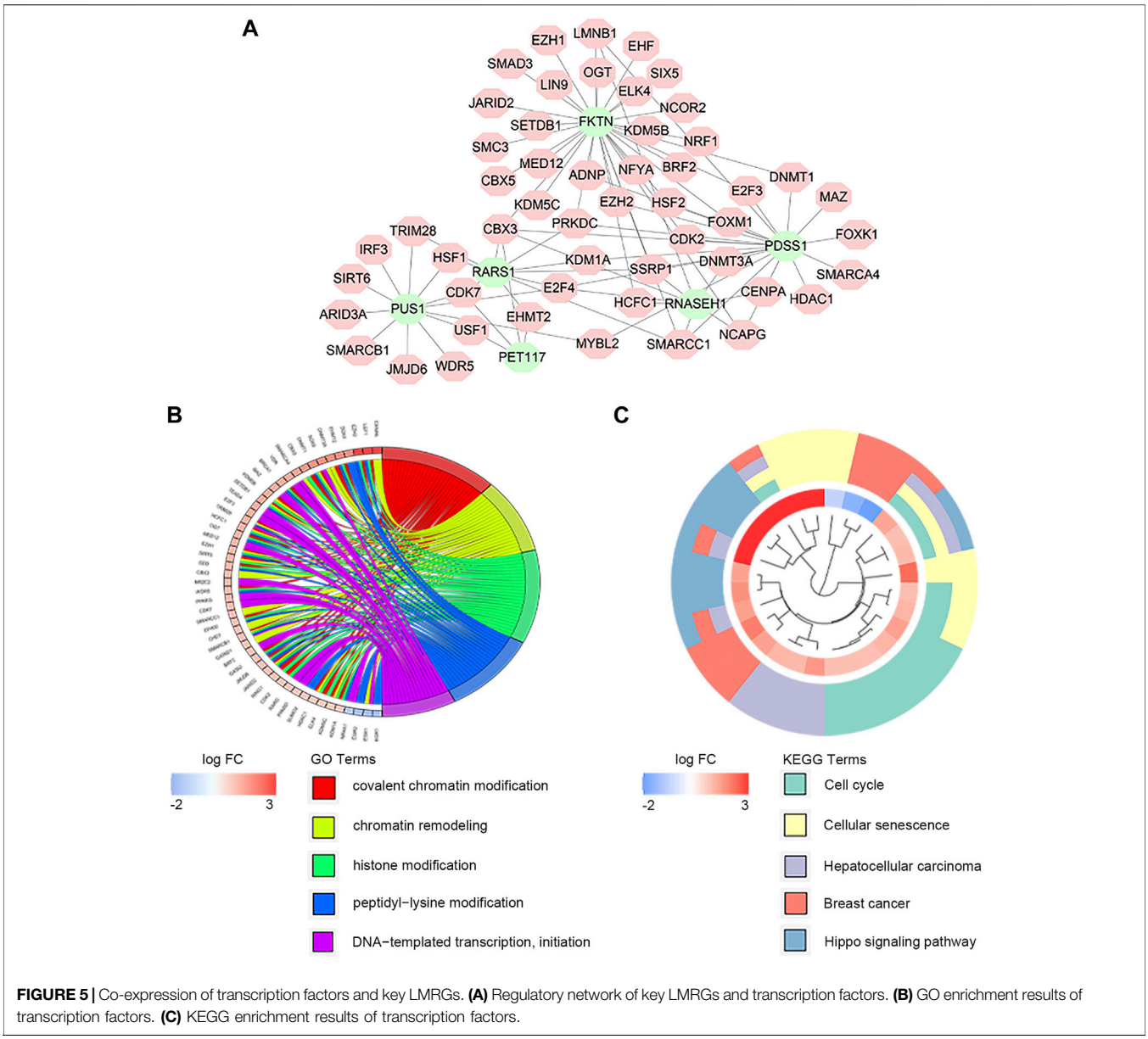

FIGURE 5 | Co-expression of transcription factors and key LMRGs. **(A)** Regulatory network of key LMRGs and transcription factors. **(B)** GO enrichment results of transcription factors. **(C)** KEGG enrichment results of transcription factors.

(**Figure 2D**). The LMRGS score of every HCC patient was obtained as follows: LMRGS score = FKTN expression × 0.2496 + PDSS1 expression × 0.0881 + PET117 expression × 0.0648 + PUS1 expression × 0.0567 + RARS1 expression × 0.0362 + RNASEH1 expression × 0.0928.

Prognostic Significance of the LMRGS

Taking the median LMRGS score as cut-off, we divided the HCC patients into two subgroups: LMRGS-high and LMRGS-low groups (**Figure 3A**). The heat map showed the differential expression of six crucial genes in the two LMRGS subgroups (**Figure 3B**). The LMRGS score and survival status of every HCC patient were displayed in **Figure 3C**. KM analysis indicated that patients with the high LMRGS score had shorter OS and median survival than patients with the low LMRGS score (**Figure 3D**). According to the different clinical characteristics, subgroup survival analysis also confirmed this result (**Supplementary Figure S1**). As shown in **Figure 3E**, the area under curve (AUC) value of 1 year, 3 years, and 5 years for ROC analysis was 0.768, 0.691, and 0.666, respectively, in the TCGA cohort. Moreover, the univariate and multivariate regression analyses demonstrated that the LMRGS score was an independent risk factor for OS (HR = 3.576, 95%CI = 2.105–6.074, p = 2.44E-06) (**Table 2**). The correlation of the LMRGS score and clinicopathological factors was clarified in the TCGA cohort. The results suggested that the LMRGS score was closely associated with pathological grade, clinical stage, vascular invasion, and virus infection (**Supplementary Figure S2**). The above results indicated that the LMRGS score played a vital role in HCC progression.

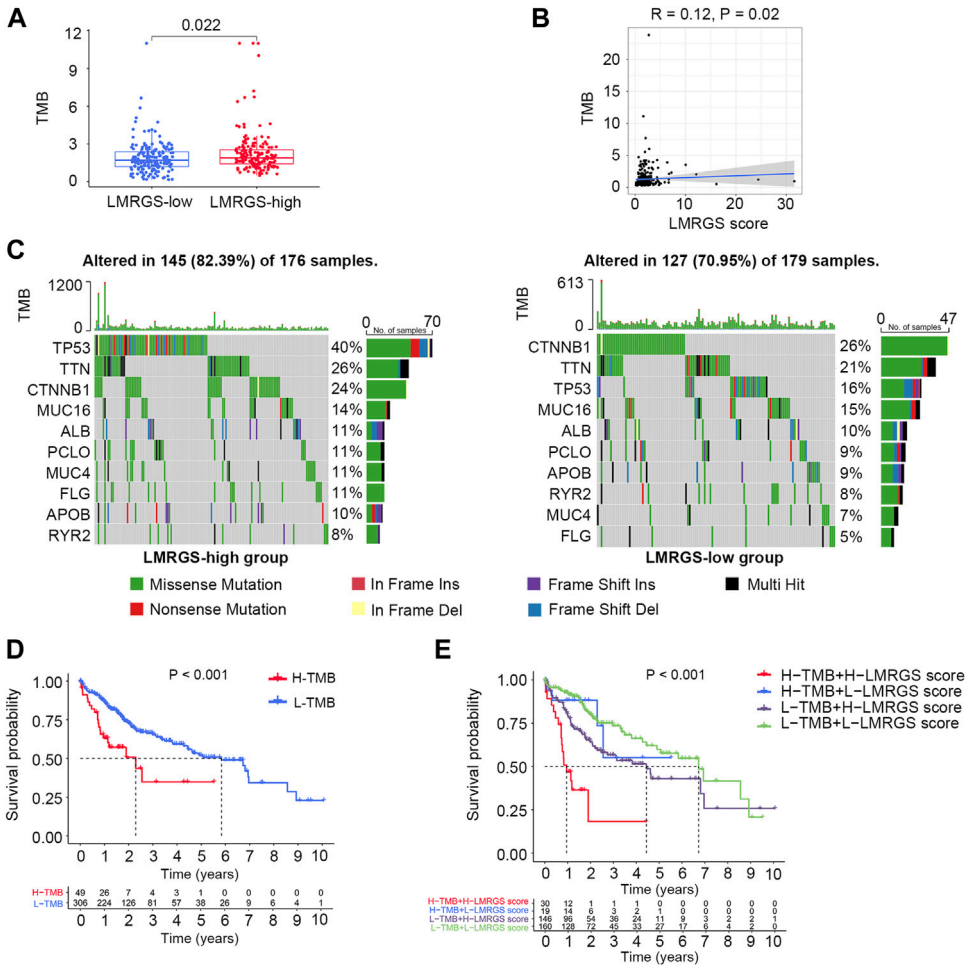

FIGURE 6 | Tumor mutation characteristics in different LMRGS subgroups. **(A)** The differences of TMB in LMRGS-low and LMRGS-high groups. **(B)** The association of TMB with LMRGS score. **(C)** Top 10 mutated genes in different LMRGS subgroups. **(D)** KM survival analysis of TMB. **(E)** Effects of the LMRGS score combined with TMB on the overall survival.

A Nomogram for Predicting Survival

To accurately predict the probability of OS, we established a nomogram that integrated the LMRGS score and other clinicopathological features, including age, gender, and TNM stage (**Figure 4A**). We could estimate the survival rate of 1 year, 3 years, and 5 years based on the total points. The calibration curve demonstrated that the prediction value was highly consistent with the actual value (**Figure 4B**). The time-dependent ROC curve also indicated that this nomogram had high accuracy for predicting survival (**Figure 4C**).

Regulation Network of Transcription Factors

There exist close interactions between the LMRGs and transcription factors. For exploring the relationship, we carried out the co-expression analysis. As displayed in **Figure 5A**, we identified 52 differential expressed transcription factors co-expressed with six significant LMRGs. The main functions of co-expressed transcription factors were chromatin remodeling and histone modification (**Figure 5B**). KEGG analysis revelated that these transcription factors mainly participated in the cell cycle, cellular senescence, and Hippo signaling pathway (**Figure 5C**).

Association With TMB

In the TCGA training cohort, we calculated the TMB of each HCC patient. We found that the TMB was higher in the LMRGS-high group (**Figures 6A,B**). Then, mutant situations of different LMRGS subgroups were visualized by the waterfall plots (**Figure 6C**). For the entire dataset, the top 10 mutated genes in HCC were TP53, CTNNB1, TTN, MUC16, ALB, PCLO, APOB, RYR2, MUC4, and FLG. Missense mutations were the most common somatic mutational types. The mutation frequency of samples was higher in the LMRGS-high group. Moreover, patients with high LMRGS scores had a higher mutation probability of crucial genes, especially TP53. Subsequently, we performed KM analysis to evaluate the influence of the LMRGS score combined with the

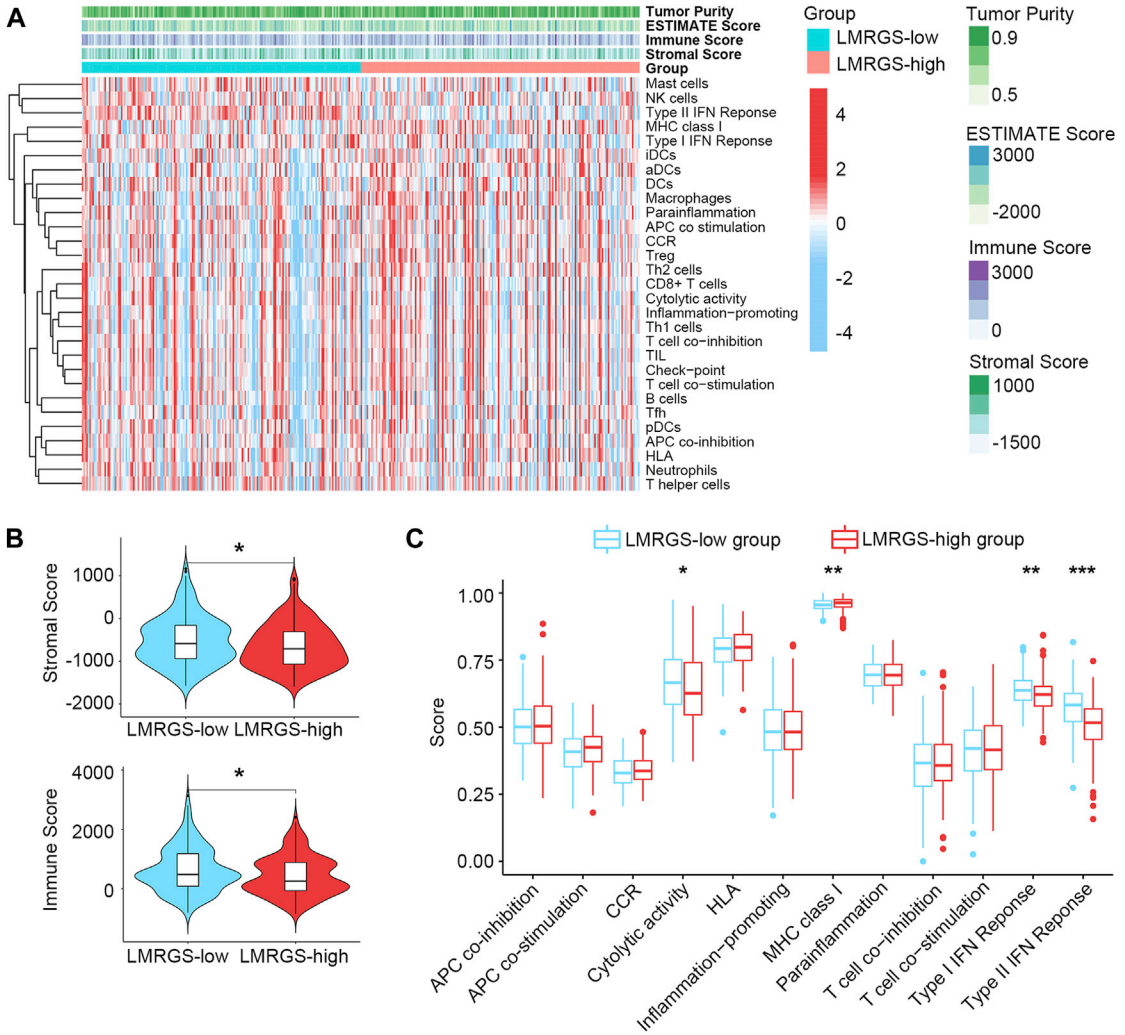

FIGURE 7 | The landscape of TME in HCC. **(A)** Stromal score and immune activity of all HCC samples. **(B)** The violin plot showed the difference in stromal scores and immune scores between LMRGS-low and LMRGS-high groups. **(C)** Differences in immune function between the two subgroups. *$p < 0.05$, **$p < 0.01$, ***$p < 0.001$.

TMB on survival. The result showed that the survival time of the high-TMB group was shorter than the low-TMB group (**Figure 6D**). More importantly, patients with a low LMRGS score and low TMB had a significantly longer OS than patients with a high LMRGS score and high TMB (**Figure 6E**). In the ICGC validation cohort, we also analyzed the mutation profiles of all samples. There existed no TMB difference among the two LMRGS subgroups (**Supplementary Figures S3A,B**). However, the mutation frequencies of prevalently mutated genes in HCC were higher in the LMRGS-high group (**Supplementary Figure S3C**). Survival analysis results of the LMRGS score combined with the TMB were consistent with the training cohort (**Supplementary Figures 3D,E**).

TME Characteristics in Different LMRGS Subgroups

Stromal cells and immune cells in the TME have profound impacts on tumor progression, treatment efficacy, and clinical outcomes. The heatmap shown in **Figure 7A** and **Supplementary Figure S4A** displayed the stromal score and immune activity of all samples. We found that the abundance of stromal cells was relatively higher in the LMRGS-low group. In addition, the LMRGS-low group had higher immune scores than the LMRGS-high group (**Figure 7B** and **Supplementary Figure S4B**). As shown in **Figure 7C** and **Supplementary Figure S4C**, there were differences in immune function between the LMRGS-high and LMRGS-low groups. The activity of cytolysis and IFN response was higher in the LMRGS-low group. In the LMRGS-high group, there was a higher expression of MHC class I.

To comprehensively analyze the immune microenvironment, we used the CIBERSORTx to calculate the infiltration degree of 22 immune cells. The immune landscape of TCGA-HCC samples was shown in **Figure 8A**. By comparing the immune cell profiles, we found that follicular helper T (Tfh) cells, regulatory T cells (Tregs), and M0 macrophages were significantly increased in the

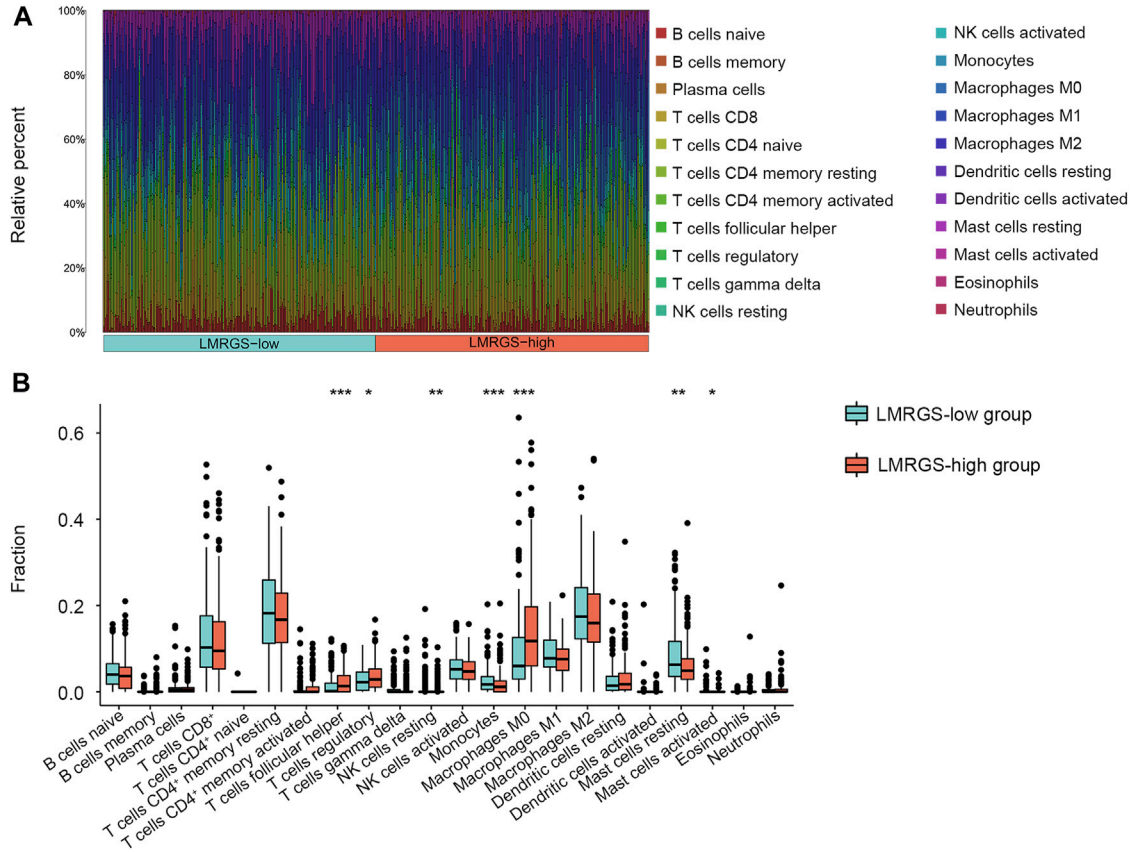

FIGURE 8 | Features of immune cell infiltrate in different LMRGS subgroups. **(A)** The heatmap displayed the proportion of immune cell infiltration in each HCC sample. **(B)** Differences in immune cell infiltration between LMRGS-low and LMRGS-high groups. *$p < 0.05$, **$p < 0.01$, ***$p < 0.001$.

LMRGS-high group. On the contrary, resting NK cells, monocytes, resting mast cells, and activated mast cells infiltrated more in the LMRGS-low group (**Figure 8B**). Apart from immune cells, we further explored the correlation of immune molecular and the LMRGS score. In our results, the LMRGS score was positively associated with the expression of immune checkpoints, including PD-1, CTLA4, LAG3, TIM3, and TIGIT (**Figure 9**).

GSEA of the LMRGS

To explore the molecular mechanisms involved in the LMRGS, GSEA was used to analyze the TCGA cohort. Enrichment results of hallmark revealed that DNA repair, E2F targets, G2M checkpoint, glycolysis, mitotic spindle, mTOR signaling, MYC targets, and unfolded protein response were activated by the LMRGS-high group (**Figure 10A**). Besides, the LMRGS also participated in regulating the transcription factors, DNA repair, cell cycle, and metabolism-related signaling pathways (**Figure 10B**).

DISCUSSION

Despite some advances in diagnosis and treatment, HCC is still cancer with high morbidity and mortality (Forner et al., 2018). As inflammation-driven cancer, there is an intricate interplay between the TME and HCC development (Ringelhan et al., 2018). Increasing evidence indicates that metabolic changes of tumors can sculpt their microenvironment, and then the remodeled TME confer a growth advantage to tumor cells (Dimri et al., 2020; Li et al., 2021). Aerobic glycolysis is a vital hallmark of tumor metabolic reprogramming. Glucose is not completely oxidized but metabolized to produce lactate, even in the presence of oxygen (Palsson-McDermott and O'Neill, 2013). Recently, some studies have reported that there is lactate accumulation in tumors (Yu et al., 2021). Lactate is now considered an essential energy substance for tumor metabolism and plays an indispensable role in restructuring the TME (Certo et al., 2021). Hence, we constructed a novel LMRGS based on LMRGs in this study. The results suggested that the LMRGS was an independent prognostic factor for OS. In addition, the LMRGS proved to have substantial value for predicting the TME in HCC.

The LMRGS was composed of six crucial genes, including FKTN, PDSS1, PET117, PUS1, RARS1, and RNASEH1. FKTN participates in protein glycosylation modification (Kanagawa et al., 2016). A study of gastric cancer indicated that higher FKTN expression is associated with tumor progression, which may be due to the protein encoded by FKTN promoting the

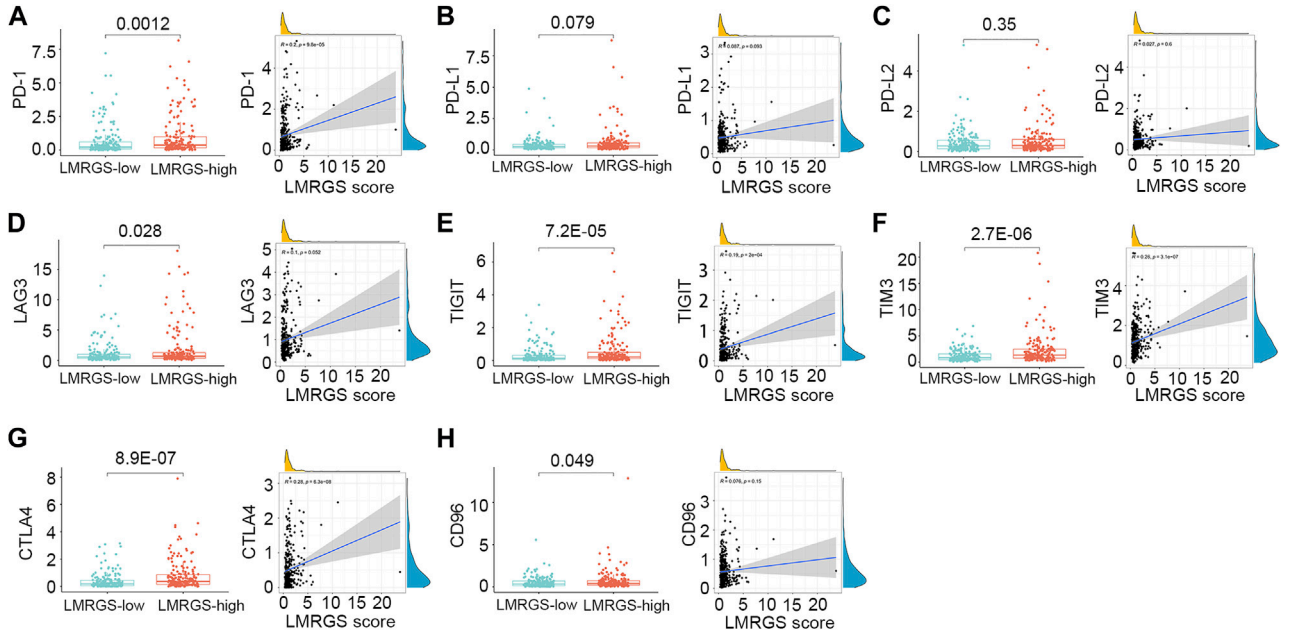

FIGURE 9 | Correlation of LMRGS score with immune checkpoints. **(A)** PD-1. **(B)** PD-L1. **(C)** PD-L2. **(D)** LAG3. **(E)** TIGIT. **(F)** TIM3. **(G)** CTLA4. **(H)** CD96.

interaction between tumor cells and the extracellular matrix (Oo et al., 2016). PDSS1 is the critical enzyme in CoQ10 biosynthesis, mediating metabolism and mitochondrial function. The mutation of PDSS1 has an impact on ATP production and oxidative stress (Mollet et al., 2007). As for PET117, mainly distributed in the mitochondrial matrix, it is related to oxidative phosphorylation *via* influencing the biogenesis of cytochrome c oxidase (Vidoni et al., 2017). PUS1 involves in the structural modification of mRNA and is correlated with mitochondrial disorders (Carlile et al., 2019). RARS1 fusion with MAD1L1 has been reported to stimulate the FUBP1/c-Myc signaling pathway, inducing tumorigenesis in nasopharyngeal carcinoma (Zhong et al., 2018). RNASEH1 plays a vital role in maintaining the stability of mitochondrial DNA under oxidative stress (Renaudin et al., 2021). However, the role of six essential genes remains unclear in HCC. To clarify the regulation mechanism of these crucial genes, we performed co-expression analysis between transcription factors and six genes. A total of 52 co-expressed transcription factors were identified, and their functions were mainly reflected in chromatin remodeling and histone modification.

Genomic alterations are the main intrinsic drivers of tumor heterogeneity (Müller et al., 2020). To further understand the molecular features, we compared the gene mutations in different LMRGS groups. As suggested by the results, missense mutation was the most common type of mutations. In the LMRGS-high group, the TP53 gene had the highest mutation rate, while CTNNB1 and TTN were the most frequently mutated genes in the LMRGS-low group. TP53 is not only playing a central role in response to genotoxic stress but also in regulating metabolic homeostasis (Levine, 2020). Increasing evidence reveals the critical functions of TP53 in cellular metabolism (Wang et al., 2018; Kim et al., 2019). The dysfunction of p53 protein encoded by TP53 affects the tumor initiation and progression by mediating the metabolism of tumor cells (Lonetto et al., 2019). The poor prognosis of the LMRGS-high group could be due to TP53 hypermutation. A study reported that increased lactate better meets the metabolic needs of tumor cells and thus favors cell proliferation in p53 mutated tumor cells (Boidot et al., 2012). CTNNB1 and TTN also have links with the malignant transformation of liver cells (Jhunjhunwala et al., 2014). However, patients in the LMRGS-low group had lower probabilities of genetic mutations than those in the LMRGS-high group. Based on the gene mutations of the whole genome, the TMB of every patient was calculated. We found that patients with high TMB and high LMRGS scores had the worst clinical outcomes, which might be because of the genome instability caused by the high TMB (Ferguson et al., 2015).

Complex TME influences tumor progression and response to treatment. There were great differences in the TME between the two LMRGS subgroups, especially in the tumor immune microenvironment. The two groups showed different immune function statuses, including cytolytic activity, MHC class I expression, and IFN response. Cytolytic activity of immune cells reflects the ability to kill tumor cells. Transcriptome hypomethylation of $CD8^+$ T cells activates cytolytic activity and effector function, which in turn enhances anti-tumor responses (Loo Yau et al., 2021). In HCC, patients with a high cytolytic activity score have favorable TME and more robust immunogenicity, resulting in better prognoses (Takahashi et al., 2020). Increased expression of MHC class I with high T cell infiltration benefits the prognosis of patients with liver metastases from colon cancer (Turcotte et al., 2014). In our analysis, MHC class I expression was higher in patients with high LMRGS scores.

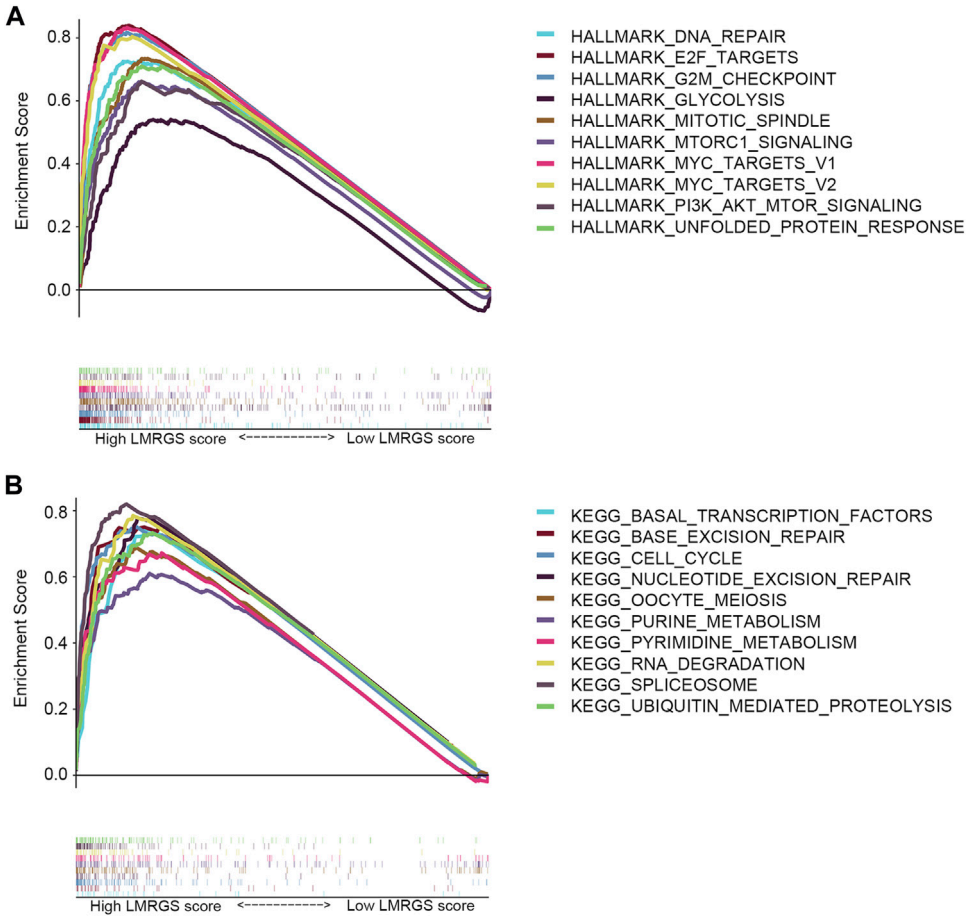

FIGURE 10 | GSEA of LMRGS-low and LMRGS-high groups. **(A)** Enrichment results of hallmark. **(B)** Enrichment results of signaling pathways.

Consequently, the impact of MHC class I expression on the prognosis of HCC patients needs to be further clarified. Besides, the activation of IFN response is an essential link to anti-tumor immunity (Takahashi et al., 2021). As it could be seen, patients in the LMRGS-low group had better anti-tumor immune activity.

Tumor-infiltrating immune cells are one of the most important components in the TME, which can be affected by the lactate level (Certo et al., 2021). Low glucose and high lactate accumulation in the TME have immunosuppressive effects. Under lactate-rich conditions, reducing NAD^+ to NADH by lactate dehydrogenase (LDH) leads to blocked production of GAPDH and PDGH, which in turn impairs effector T cell proliferation dependent on post-GAPDH glycolytic intermediates (Quinn et al., 2020). Tregs have inhibitory effects on immune response and antigen activation, facilitating cancer progression. Increased aerobic glycolytic activity creates a lactate-enrich microenvironment that favors Tregs survival and contributes immunosuppressive functions (Wang et al., 2017). Moreover, elevated lactate levels in the TME can supply potential nutrition to Tregs, which is due to lactate reversal to pyruvate and NADH in the presence of LDH (Lochner et al., 2015). A study suggested that inhibiting glycolysis and promoting oxidative phosphorylation recover the differentiation of Tfh cells and reduce inflammatory damage (Dong et al., 2019). Another interesting study found that high lactate accumulation decreases the PH of the microenvironment, then promotes NK cell apoptosis and inhibits its natural killer function (Harmon et al., 2019). B cells are of great significance in humoral immune responses through antibody production. Altered intra- and extracellular metabolic signaling can affect the immune regulatory function of B cells (Rosser and Mauri, 2021). Monocytes and mast cells play a vital role in regulating immune responses, and they can alter the TME toward anti-tumor immunity when fully triggered (Guilliams et al., 2018; Dudeck et al., 2019). In addition, macrophages have two central polarization states, including M1 and M2. Different TME leads M0 macrophages polarization to different states, resulting in very opposed effects. M1 macrophages polarization contributes to the immunity against the tumor, while M2 macrophages promote cancer progression and treatment resistance (Chen et al., 2021). Lactate derived from tumors leads to M2 macrophages polarization *via* activating the mTORC2 and ERK signaling pathways (Zhang et al., 2021). The results of our study were consistent with these conclusions. The infiltration levels of B cells,

NK cells, monocytes, and mast cells were higher in the LMRGS-low group. Conversely, Tfh cells, Tregs, and M0 macrophages were more abundant in the LMRGS-high group. The results indicated that the immune cells of patients in the LMRGS-high group were affected by lactate metabolism, so the TME was more inclined to an immunosuppressive state.

Apart from the accumulation of immune cells that negatively regulate immune activity, the immunosuppressive TME is also associated with the up-regulated expression of inhibitory immune checkpoints (Sangro et al., 2021). We further explored the differences in the expression of inhibitory molecules between the LMRGS subgroups. In the LMRGS-high group, inhibitory immune checkpoint expressions were significantly higher, including PD-1, CTLA4, LAG3, TIM3, TIGIT, and CD96. In addition, the LMRGS score was positively correlated with PD-1, CTLA4, TIM3, and TIGIT. Recently, immunotherapy targeting inhibitory immune checkpoints has shown promising efficacy in treating advanced HCC (Yau et al., 2020). The expression level of the immune checkpoint is the predictive biomarker of immunotherapy response. From our results, we speculated that patients with high LMRGS scores might gain more benefit from immunotherapy. Besides, TMB associated with neoantigen production is an essential factor in driving anti-tumor immunity. High TMB increases the efficiency of stimulating host immune response (Shum et al., 2021). In our study, HCC patients with high LMRGS scores had high expression of inhibitory immune checkpoints and high TMB. Thus, the LMRGS might have a good value for precisely predicting which patients could respond to immunotherapy.

This study developed a novel LMRGS to predict the prognosis and TME in HCC. Notably, there are certain limitations in the present study. Firstly, the specific molecular functions of six genes involved in the LMRGS remain unclear. There need further experiments to elucidate the role of genes in HCC. Secondly, the LMRGS was constructed and validated using the retrospective data. In the future, we need to carry out multicenter prospective studies to validate the clinical value.

In summary, our study constructed a novel LMRGS with a high value for predicting prognosis and reflecting the TME in HCC. The LMRGS was closely associated with clinical outcomes and was an independent prognostic indicator. In addition, patients with different LMRGS scores had different TME statuses, including infiltration degree of stromal cells and immune cells, immune activity, and expression of immune checkpoints. Thus, the LMRGS was a promising biomarker to speculate molecular and immune features in HCC, which might provide new therapeutic strategies for HCC treatment.

DATA AVAILABILITY STATEMENT

Publicly available datasets were analyzed in this study. This data can be found here: https://portal.gdc.cancer.gov/, https://dcc.icgc.org/releases/current/Projects/LIRI-JP.

AUTHOR CONTRIBUTIONS

KT and XL conceived and designed the experiments; YL, HM and SW analyzed the data; YL and KT wrote the paper. All authors read and approved the final manuscript.

FUNDING

This study was supported by grants from the Natural Science Basic Research Program of Shaanxi (2020JC-36), the Key Research and Development Program of Shaanxi (2020SF-060), the Zhejiang Medical and Health Science and Technology Plan Project (2022RC101), the Zhejiang Provincial Department of Education Project (Y202146077), China Postdoctoral Science Foundation (2020T130517, 2020M683512), and Fundamental Research Funds for the Central Universities (xtr042019011).

SUPPLEMENTARY MATERIAL

The Supplementary Material for this article can be found online at: https://www.frontiersin.org/articles/10.3389/fcell.2021.801959/full#supplementary-material

REFERENCES

Bader, J. E., Voss, K., and Rathmell, J. C. (2020). Targeting Metabolism to Improve the Tumor Microenvironment for Cancer Immunotherapy. *Mol. Cel* 78, 1019–1033. doi:10.1016/j.molcel.2020.05.034

Bindea, G., Mlecnik, B., Tosolini, M., Kirilovsky, A., Waldner, M., Obenauf, A. C., et al. (2013). Spatiotemporal Dynamics of Intratumoral Immune Cells Reveal the Immune Landscape in Human Cancer. *Immunity* 39, 782–795. doi:10.1016/j.immuni.2013.10.003

Boidot, R., Végran, F., Meulle, A., Le Breton, A., Dessy, C., Sonveaux, P., et al. (2012). Regulation of Monocarboxylate Transporter MCT1 Expression by P53 Mediates Inward and Outward Lactate Fluxes in Tumors. *Cancer Res.* 72, 939–948. doi:10.1158/0008-5472.CAN-11-2474

Brown, T. P., Bhattacharjee, P., Ramachandran, S., Sivaprakasam, S., Ristic, B., Sikder, M. O. F., et al. (2020). The Lactate Receptor GPR81 Promotes Breast Cancer Growth *via* a Paracrine Mechanism Involving Antigen-Presenting Cells in the Tumor Microenvironment. *Oncogene* 39, 3292–3304. doi:10.1038/s41388-020-1216-5

Carlile, T. M., Martinez, N. M., Schaening, C., Su, A., Bell, T. A., Zinshteyn, B., et al. (2019). mRNA Structure Determines Modification by Pseudouridine Synthase 1. *Nat. Chem. Biol.* 15, 966–974. doi:10.1038/s41589-019-0353-z

Certo, M., Tsai, C.-H., Pucino, V., Ho, P.-C., and Mauro, C. (2021). Lactate Modulation of Immune Responses in Inflammatory versus Tumour Microenvironments. *Nat. Rev. Immunol.* 21, 151–161. doi:10.1038/s41577-020-0406-2

Chen, H., Jiang, S., Zhang, P., Ren, Z., and Wen, J. (2021). Exosomes Synergized with PIONs@E6 Enhance Their Immunity against Hepatocellular Carcinoma via Promoting M1 Macrophages Polarization. *Int. Immunopharmacology* 99, 107960. doi:10.1016/j.intimp.2021.107960

Deng, H., Kan, A., Lyu, N., He, M., Huang, X., Qiao, S., et al. (2021). Tumor-derived Lactate Inhibit the Efficacy of Lenvatinib through Regulating PD-L1 Expression on Neutrophil in Hepatocellular Carcinoma. *J. Immunother. Cancer* 9, e002305. doi:10.1136/jitc-2020-002305

Dimri, M., Humphries, A., Laknaur, A., Elattar, S., Lee, T. J., Sharma, A., et al. (2020). NAD(P)H Quinone Dehydrogenase 1 Ablation Inhibits Activation of the Phosphoinositide 3-Kinase/Akt Serine/Threonine Kinase and Mitogen-Activated Protein Kinase/Extracellular Signal-Regulated Kinase Pathways and Blocks Metabolic Adaptation in Hepatocellular Carcinoma. *Hepatology* 71, 549–568. doi:10.1002/hep.30818

Dong, L., He, Y., Zhou, S., Cao, Y., Li, Y., Bi, Y., et al. (2019). HIF1α-Dependent Metabolic Signals Control the Differentiation of Follicular Helper T Cells. *Cells* 8, 1450. doi:10.3390/cells8111450

Dudeck, A., Köberle, M., Goldmann, O., Meyer, N., Dudeck, J., Lemmens, S., et al. (2019). Mast Cells as Protectors of Health. *J. Allergy Clin. Immunol.* 144, S4–S18. doi:10.1016/j.jaci.2018.10.054

Ferguson, L. R., Chen, H., Collins, A. R., Connell, M., Damia, G., Dasgupta, S., et al. (2015). Genomic Instability in Human Cancer: Molecular Insights and Opportunities for Therapeutic Attack and Prevention through Diet and Nutrition. *Semin. Cancer Biol.* 35, S5–S24. doi:10.1016/j.semcancer.2015.03.005

Forner, A., Reig, M., and Bruix, J. (2018). Hepatocellular Carcinoma. *The Lancet* 391, 1301–1314. doi:10.1016/S0140-6736(18)30010-2

Friedman, J., Hastie, T., and Tibshirani, R. (2010). Regularization Paths for Generalized Linear Models via Coordinate Descent. *J. Stat. Softw.* 33, 1–22. doi:10.18637/jss.v033.i01

Guilliams, M., Mildner, A., and Yona, S. (2018). Developmental and Functional Heterogeneity of Monocytes. *Immunity* 49, 595–613. doi:10.1016/j.immuni.2018.10.005

Gysler, S. M., and Drapkin, R. (2021). Tumor Innervation: Peripheral Nerves Take Control of the Tumor Microenvironment. *J. Clin. Invest.* 131, e147276. doi:10.1172/JCI147276

Harmon, C., Robinson, M. W., Hand, F., Almuaili, D., Mentor, K., Houlihan, D. D., et al. (2019). Lactate-mediated Acidification of Tumor Microenvironment Induces Apoptosis of Liver-Resident NK Cells in Colorectal Liver Metastasis. *Cancer Immunol. Res.* 7, 335–346. doi:10.1158/2326-6066.CIR-18-0481

Iasonos, A., Schrag, D., Raj, G. V., and Panageas, K. S. (2008). How to Build and Interpret a Nomogram for Cancer Prognosis. *Jco* 26, 1364–1370. doi:10.1200/JCO.2007.12.9791

Izzo, L. T., and Wellen, K. E. (2019). Histone Lactylation Links Metabolism and Gene Regulation. *Nature* 574, 492–493. doi:10.1038/d41586-019-03122-1

Jhunjhunwala, S., Jiang, Z., Stawiski, E. W., Gnad, F., Liu, J., Mayba, O., et al. (2014). Diverse Modes of Genomic Alteration in Hepatocellular Carcinoma. *Genome Biol.* 15, 436. doi:10.1186/s13059-014-0436-9

Jin, Z., Lu, Y., Wu, X., Pan, T., Yu, Z., Hou, J., et al. (2021). The Cross-Talk between Tumor Cells and Activated Fibroblasts Mediated by lactate/BDNF/TrkB Signaling Promotes Acquired Resistance to Anlotinib in Human Gastric Cancer. *Redox Biol.* 46, 102076. doi:10.1016/j.redox.2021.102076

Kanagawa, M., Kobayashi, K., Tajiri, M., Manya, H., Kuga, A., Yamaguchi, Y., et al. (2016). Identification of a post-translational Modification with Ribitol-Phosphate and its Defect in Muscular Dystrophy. *Cel Rep.* 14, 2209–2223. doi:10.1016/j.celrep.2016.02.017

Kim, J., Yu, L., Chen, W., Xu, Y., Wu, M., Todorova, D., et al. (2019). Wild-type P53 Promotes Cancer Metabolic Switch by Inducing PUMA-dependent Suppression of Oxidative Phosphorylation. *Cancer Cell* 35, 191e8–203. doi:10.1016/j.ccell.2018.12.012

Levine, A. J. (2020). p53: 800 Million Years of Evolution and 40 Years of Discovery. *Nat. Rev. Cancer* 20, 471–480. doi:10.1038/s41568-020-0262-1

Li, S., Liu, Y., Bai, Y., Chen, M., Cheng, D., Wu, M., et al. (2021). Ras Homolog Family Member F, Filopodia Associated Promotes Hepatocellular Carcinoma Metastasis by Altering the Metabolic Status of Cancer Cells through RAB3D. *Hepatology* 73, 2361–2379. doi:10.1002/hep.31641

Liao, Z.-X., Kempson, I. M., Hsieh, C.-C., Tseng, S.-J., and Yang, P.-C. (2021). Potential Therapeutics Using Tumor-Secreted Lactate in Nonsmall Cell Lung Cancer. *Drug Discov. Today* 26, 2508–2514. doi:10.1016/j.drudis.2021.07.014

Liberzon, A., Birger, C., Thorvaldsdóttir, H., Ghandi, M., Mesirov, J. P., and Tamayo, P. (2015). The Molecular Signatures Database Hallmark Gene Set Collection. *Cel Syst.* 1, 417–425. doi:10.1016/j.cels.2015.12.004

Liu, Z., Liu, L., Jiao, D., Guo, C., Wang, L., Li, Z., et al. (2021c). Association of RYR2 Mutation with Tumor Mutation burden, Prognosis, and Antitumor Immunity in Patients with Esophageal Adenocarcinoma. *Front. Genet.* 12, 669694. doi:10.3389/fgene.2021.669694

Liu, Z., Lu, T., Li, J., Wang, L., Xu, K., Dang, Q., et al. (2021b). Development and Clinical Validation of a Novel Six-Gene Signature for Accurately Predicting the Recurrence Risk of Patients with Stage II/III Colorectal Cancer. *Cancer Cel Int* 21, 359. doi:10.1186/s12935-021-02070-z

Liu, Z., Lu, T., Li, J., Wang, L., Xu, K., Dang, Q., et al. (2021a). Clinical Significance and Inflammatory Landscape of aNovel Recurrence-Associated Immune Signature in Stage II/III Colorectal Cancer. *Front. Immunol.* 12, 702594. doi:10.3389/fimmu.2021.702594

Liu, Z., Lu, T., Wang, L., Liu, L., Li, L., and Han, X. (2021d). Comprehensive Molecular Analyses of a Novel Mutational Signature Classification System with Regard to Prognosis, Genomic Alterations, and Immune Landscape in Glioma. *Front. Mol. Biosci.* 8, 682084. doi:10.3389/fmolb.2021.682084

Liu, Z., Wang, L., Liu, L., Lu, T., Jiao, D., Sun, Y., et al. (2021e). The Identification and Validation of Two Heterogenous Subtypes and a Risk Signature Based on Ferroptosis in Hepatocellular Carcinoma. *Front. Oncol.* 11, 619242. doi:10.3389/fonc.2021.619242

Llovet, J. M., Kelley, R. K., Villanueva, A., Singal, A. G., Pikarsky, E., Roayaie, S., et al. (2021). Hepatocellular Carcinoma. *Nat. Rev. Dis. Primers* 7, 6. doi:10.1038/s41572-020-00240-3

Lochner, M., Berod, L., and Sparwasser, T. (2015). Fatty Acid Metabolism in the Regulation of T Cell Function. *Trends Immunol.* 36, 81–91. doi:10.1016/j.it.2014.12.005

Lonetto, G., Koifman, G., Silberman, A., Attery, A., Solomon, H., Levin-Zaidman, S., et al. (2019). Mutant P53-dependent Mitochondrial Metabolic Alterations in a Mesenchymal Stem Cell-Based Model of Progressive Malignancy. *Cell Death Differ* 26, 1566–1581. doi:10.1038/s41418-018-0227-z

Loo Yau, H., Bell, E., Ettayebi, I., de Almeida, F. C., Boukhaled, G. M., Shen, S. Y., et al. (2021). DNA Hypomethylating Agents Increase Activation and Cytolytic Activity of CD8+ T Cells. *Mol. Cel* 81, 1469e1468–1483. doi:10.1016/j.molcel.2021.01.038

Mollet, J., Giurgea, I., Schlemmer, D., Dallner, G., Chretien, D., Delahodde, A., et al. (2007). Prenyldiphosphate Synthase, Subunit 1 (PDSS1) and OH-benzoate Polyprenyltransferase (COQ2) Mutations in Ubiquinone Deficiency and Oxidative Phosphorylation Disorders. *J. Clin. Invest.* 117, 765–772. doi:10.1172/JCI29089

Müller, M., Bird, T. G., and Nault, J.-C. (2020). The Landscape of Gene Mutations in Cirrhosis and Hepatocellular Carcinoma. *J. Hepatol.* 72, 990–1002. doi:10.1016/j.jhep.2020.01.019

Oo, H. Z., Sentani, K., Mukai, S., Hattori, T., Shinmei, S., Goto, K., et al. (2016). Fukutin, Identified by the Escherichia coli Ampicillin Secretion Trap (CAST) Method, Participates in Tumor Progression in Gastric Cancer. *Gastric Cancer* 19, 443–452. doi:10.1007/s10120-015-0511-2

Palsson-McDermott, E. M., and O'Neill, L. A. J. (2013). The Warburg Effect Then and Now: from Cancer to Inflammatory Diseases. *Bioessays* 35, 965–973. doi:10.1002/bies.201300084

Quinn, W. J., Jiao, J., TeSlaa, T., Stadanlick, J., Wang, Z., Wang, L., et al. (2020). Lactate Limits T Cell Proliferation via the NAD(H) Redox State. *Cel Rep.* 33, 108500. doi:10.1016/j.celrep.2020.108500

Renaudin, X., Lee, M., Shehata, M., Surmann, E.-M., and Venkitaraman, A. R. (2021). BRCA2 Deficiency Reveals that Oxidative Stress Impairs RNaseH1 Function to Cripple Mitochondrial DNA Maintenance. *Cel Rep.* 36, 109478. doi:10.1016/j.celrep.2021.109478

Ringelhan, M., Pfister, D., O'Connor, T., Pikarsky, E., and Heikenwalder, M. (2018). The Immunology of Hepatocellular Carcinoma. *Nat. Immunol.* 19, 222–232. doi:10.1038/s41590-018-0044-z

Rosser, E. C., and Mauri, C. (2021). The Emerging Field of Regulatory B Cell Immunometabolism. *Cel Metab.* 33, 1088–1097. doi:10.1016/j.cmet.2021.05.008

Sangro, B., Sarobe, P., Hervás-Stubbs, S., and Melero, I. (2021). Advances in Immunotherapy for Hepatocellular Carcinoma. *Nat. Rev. Gastroenterol. Hepatol.* 18, 525–543. doi:10.1038/s41575-021-00438-0

Shum, B., Larkin, J., and Turajlic, S. (2021). Predictive Biomarkers for Response to Immune Checkpoint Inhibition. *Semin. Cancer Biol.* S1044-579X (21), 00097-3. doi:10.1016/j.semcancer.2021.03.036

Sung, H., Ferlay, J., Siegel, R. L., Laversanne, M., Soerjomataram, I., Jemal, A., et al. (2021). Global Cancer Statistics 2020: GLOBOCAN Estimates of Incidence and Mortality Worldwide for 36 Cancers in 185 Countries. *CA A. Cancer J. Clin.* 71, 209–249. doi:10.3322/caac.21660

Takahashi, H., Kawaguchi, T., Yan, L., Peng, X., Qi, Q., Morris, L. G. T., et al. (2020). Immune Cytolytic Activity for Comprehensive Understanding of Immune Landscape in Hepatocellular Carcinoma. *Cancers* 12, 1221. doi:10.3390/cancers12051221

Takahashi, M., Lio, C.-W. J., Campeau, A., Steger, M., Ay, F., Mann, M., et al. (2021). The Tumor Suppressor Kinase DAPK3 Drives Tumor-Intrinsic Immunity through the STING-IFN-β Pathway. *Nat. Immunol.* 22, 485–496. doi:10.1038/s41590-021-00896-3

Turcotte, S., Katz, S. C., Shia, J., Jarnagin, W. R., Kingham, T. P., Allen, P. J., et al. (2014). Tumor MHC Class I Expression Improves the Prognostic Value of T-Cell Density in Resected Colorectal Liver Metastases. *Cancer Immunol. Res.* 2, 530–537. doi:10.1158/2326-6066.CIR-13-0180

Vidoni, S., Harbour, M. E., Guerrero-Castillo, S., Signes, A., Ding, S., Fearnley, I. M., et al. (2017). MR-1S Interacts with PET100 and PET117 in Module-Based Assembly of Human Cytochrome C Oxidase. *Cel Rep.* 18, 1727–1738. doi:10.1016/j.celrep.2017.01.044

Villanueva, A. (2019). Hepatocellular Carcinoma. *N. Engl. J. Med.* 380, 1450–1462. doi:10.1056/NEJMra1713263

Wang, H., Franco, F., and Ho, P.-C. (2017). Metabolic Regulation of Tregs in Cancer: Opportunities for Immunotherapy. *Trends Cancer* 3, 583–592. doi:10.1016/j.trecan.2017.06.005

Wang, S., Peng, Z., Wang, S., Yang, L., Chen, Y., Kong, X., et al. (2018). KRAB-type Zinc-finger Proteins PITA and PISA Specifically Regulate P53-dependent Glycolysis and Mitochondrial Respiration. *Cell Res* 28, 572–592. doi:10.1038/s41422-018-0008-8

Xia, L., Oyang, L., Lin, J., Tan, S., Han, Y., Wu, N., et al. (2021). The Cancer Metabolic Reprogramming and Immune Response. *Mol. Cancer* 20, 28. doi:10.1186/s12943-021-01316-8

Yau, T., Kang, Y.-K., Kim, T.-Y., El-Khoueiry, A. B., Santoro, A., Sangro, B., et al. (2020). Efficacy and Safety of Nivolumab Plus Ipilimumab in Patients with Advanced Hepatocellular Carcinoma Previously Treated with Sorafenib. *JAMA Oncol.* 6, e204564. doi:10.1001/jamaoncol.2020.4564

Yoshihara, K., Shahmoradgoli, M., Martínez, E., Vegesna, R., Kim, H., Torres-Garcia, W., et al. (2013). Inferring Tumour Purity and Stromal and Immune Cell Admixture from Expression Data. *Nat. Commun.* 4, 2612. doi:10.1038/ncomms3612

Yu, J., Chai, P., Xie, M., Ge, S., Ruan, J., Fan, X., et al. (2021). Histone Lactylation Drives Oncogenesis by Facilitating m6A Reader Protein YTHDF2 Expression in Ocular Melanoma. *Genome Biol.* 22, 85. doi:10.1186/s13059-021-02308-z

Zhang, A., Xu, Y., Xu, H., Ren, J., Meng, T., Ni, Y., et al. (2021). Lactate-induced M2 Polarization of Tumor-Associated Macrophages Promotes the Invasion of Pituitary Adenoma by Secreting CCL17. *Theranostics* 11, 3839–3852. doi:10.7150/thno.53749

Zheng, R., Wan, C., Mei, S., Qin, Q., Wu, Q., Sun, H., et al. (2019). Cistrome Data Browser: Expanded Datasets and New Tools for Gene Regulatory Analysis. *Nucleic Acids Res.* 47, D729–D735. doi:10.1093/nar/gky1094

Zhong, Q., Liu, Z.-H., Lin, Z.-R., Hu, Z.-D., Yuan, L., Liu, Y.-m., et al. (2018). The RARS-Mad1l1 Fusion Gene Induces Cancer Stem Cell-like Properties and Therapeutic Resistance in Nasopharyngeal Carcinoma. *Clin. Cancer Res.* 24, 659–673. doi:10.1158/1078-0432.CCR-17-0352

Conflict of Interest: The authors declare that the research was conducted in the absence of any commercial or financial relationships that could be construed as a potential conflict of interest.

Publisher's Note: All claims expressed in this article are solely those of the authors and do not necessarily represent those of their affiliated organizations, or those of the publisher, the editors and the reviewers. Any product that may be evaluated in this article, or claim that may be made by its manufacturer, is not guaranteed or endorsed by the publisher.

frontiers in Cell and Developmental Biology

ORIGINAL RESEARCH
published: 09 March 2022
doi: 10.3389/fcell.2022.806989

Construction and Validation of Two Hepatocellular Carcinoma-Progression Prognostic Scores Based on Gene Set Variation Analysis

*Qifan He, Baorui Fan, Peng Du and Yonghai Jin**

Department of Interventional Radiology, The First Affiliated Hospital of Soochow University, Suzhou, China

Background: Liver hepatocellular carcinoma (LIHC) remains a global health challenge with a low early diagnosis rate and high mortality. Therefore, finding new biomarkers for diagnosis and prognosis is still one of the current research priorities.

Methods: Based on the variation of gene expression patterns in different stages, the LIHC-development genes (LDGs) were identified by differential expression analysis. Then, prognosis-related LDGs were screened out to construct the LIHC-unfavorable gene set (LUGs) and LIHC-favorable gene set (LFGs). Gene set variation analysis (GSVA) was conducted to build prognostic scoring models based on the LUGs and LFGs. ROC curve analysis and univariate and multivariate Cox regression analysis were carried out to verify the diagnostic and prognostic utility of the two GSVA scores in two independent datasets. Additionally, the key LCGs were identified by the intersection analysis of the PPI network and univariate Cox regression and further evaluated their performance in expression level and prognosis prediction. Single-sample GSEA (ssGSEA) was performed to understand the correlation between the two GSVA enrichment scores and immune activity.

Result: With the development of LIHC, 83 LDGs were gradually upregulated and 247 LDGs were gradually downregulated. Combining with LIHC survival analysis, 31 LUGs and 32 LFGs were identified and used to establish the LIHC-unfavorable GSVA score (LUG score) and LIHC-favorable GSVA score (LFG score). ROC curve analysis and univariate/multivariate Cox regression analysis suggested the LUG score and LFG score could be great indicators for the early diagnosis and prognosis prediction. Four genes (ESR1, EHHADH, CYP3A4, and ACADL) were considered as the key LCGs and closely related to good prognosis. The frequency of TP53 mutation and copy number variation (CNV) were high in some LCGs. Low-LFG score patients have active metabolic activity and a more robust immune response. The high-LFG score patients characterized immune activation with the higher infiltration abundance of type I T helper cells, DC, eosinophils, and neutrophils, while the high-LUG score patients characterized immunosuppression with the higher infiltration abundance of type II T helper cells, TRegs, and iDC. The high- and

OPEN ACCESS

Edited by:
Jiang Chen,
Zhejiang University, China

Reviewed by:
Xinwei Han,
Zhengzhou University, China
Yilin Pang,
Wenzhou Medical University, China

****Correspondence:***
Yonghai Jin
jinyonghai_dc@163.com

Specialty section:
This article was submitted to Molecular and Cellular Oncology, a section of the journal Frontiers in Cell and Developmental Biology

Received: *01 November 2021*
Accepted: *01 February 2022*
Published: *09 March 2022*

Citation:
He Q, Fan B, Du P and Jin Y (2022) Construction and Validation of Two Hepatocellular Carcinoma-Progression Prognostic Scores Based on Gene Set Variation Analysis. Front. Cell Dev. Biol. 10:806989. doi: 10.3389/fcell.2022.806989

low-LFG score groups differed significantly in immunotherapy response scores, immune checkpoints expression, and IC50 values of common drugs.

Conclusion: Overall, the LIHC-progression characteristic genes can be great diagnostic and prognostic signatures and the two GSVA score systems may become promising indices for guiding the tumor treatment of LIHC patients.

Keywords: hepatocellular carcinoma, prognostic stratification system, gene set variation analysis, PPI, tumor infiltrating immune cell

INTRODUCTION

Liver cancer is the sixth most common malignant tumor and the fourth most common cause of cancer-related death (Villanueva 2019). Cirrhosis, mostly as a result of hepatitis virus infection or alcohol abuse, is currently considered to be the main cause of liver cancer (Marengo et al., 2016). Liver hepatocellular carcinoma (LIHC) is the most common type of liver cancer. The main treatment strategies for LIHC are surgery, radiotherapy, chemotherapy, and palliative therapies (Llovet et al., 2015). Regrettably, these treatments are less effective in patients with advanced LIHC (Tian et al., 2018). Therefore, it is urgent to explore significant diagnosis and prognosis indicators of LIHC. The wide use of high-throughput sequencing technology in Liver cancer research has revealed many promising targets for the early diagnosis and evaluation of prognosis (Zhang et al., 2017; Calderaro et al., 2019). AFP is the most common biomarker in LIHC for early diagnosis and tumor recurrence surveillance (Pinero et al., 2020). DKK1 has been found highly expressed in HCC tissue and proposed to be a novel HCC biomarker with a very good diagnostic performance (Shen et al., 2012). Higher expression of Glypican-3 was significantly associated with a worse prognosis in LIHC (Xiao et al., 2014). The upregulated expression of TBK1 can enhance tumor immune infiltration and predict the poor prognosis of patients with LIHC (Jiang et al., 2021). Other studies develop prognostic models based on gene sets and carry out validation analyses (Huo et al., 2020; Zhou et al., 2020). Nevertheless, most studies do not take the changes of gene expression patterns in different stages of tumors into account.

In our study, we identified LIHC-unfavorable gene set and LIHC-favorable gene set by integrating gene expression data and corresponding clinical data from TCGA. Gene set variation analysis (GSVA) was used to calculate the enrichment score of LIHC patients and construct two scoring systems. The diagnostic and prognostic capability of two scoring systems were verified in multiple datasets. By integrating the PPI network and univariate Cox regression analysis of all LCGs, ESR1, EHHADH, CYP3A4, and ACADL were determined as the key LCGs. Subsequently, we investigate the expression level and prognostic correlation of the key LDGs in different HCC datasets. Additionally, ssGSEA analysis was used to explore the correlation of the two gene sets with gene alteration and immune infiltration. These findings indicate that the two GSVA scoring systems may become reliable molecular markers and provide targets for the diagnosis and prognosis of LIHC.

MATERIALS AND METHODS

Data Collection

The gene expression data and corresponding clinical features of LIHC patients were downloaded from International Cancer Genome Consortium (ICGC) (Zhang et al., 2019), The Cancer Genome Atlas (TCGA) (Tomczak et al., 2015), and Gene Expression Omnibus (GEO) (Barrett et al., 2013). TCGA LIHC cohorts containing 50 control samples and 374 HCC samples (175 stage I samples, 87 stage II samples, 86 stage III samples, and 26 stage IV samples) were collected for subsequent analyses. In addition, we obtained gene expression array and prognostic information of GSE14520 cohorts (374 HCC samples and 50 control samples) and ICGC LIHC cohorts (212 HCC samples and 177 control samples) as validation sets. The genes with lower expression and samples with no prognostic information were excluded.

Identification of LIHC-Development Genes

The "normalizeBetweenArrays" function in "limma" R package was performed to background adjustment and quantile normalization. In TCGA datasets, DEGs between normal group and I-IV HCC stage groups were respectively identified utilizing the "limma" package with a fold-change of 1.5 and an adjusted p-value of <0.05 (Ritchie et al., 2015). We defined LDG as gradually upregulated DEGs (logFCstage I vs. control < logFCstage II vs. control < logFCstage III vs. control < logFCstage IV vs. control) and downregulated DEGs (logFCstage I vs. control > logFCstage II vs. control > logFCstage III vs. control > logFCstage IV vs. control). Potential functions and enriched pathways of LDGs were further explored by the "clusterProfiler" package (Yu et al., 2012), and $p < 0.05$ was considered as significant.

Establishment of the LIHC-Progression Gene Set Variation Analysis Score

According to the median expression level of LDGs, all samples were divided into high/low groups and subjected to Kaplan–Meier survival curves analyses, and $p < 0.05$ was considered to be statistically significant. Those LDGs that drastically influenced survival were considered as LIHC-progression characteristic genes (LCGs) and established two prognostic gene sets, including the LIHC-unfavorable gene set (LUGs, related to poor prognosis) and the LIHC-favorable gene set (LFGs, related to good prognosis). Several external microarray

datasets (GSE10143, GSE14520, GSE22058, GSE25097, GSE36376, GSE46444, GSE54236, GSE63898, GSE64041, and GSE76427) were performed to validate the differential expression of LCGs between HCC samples and adjacent normal samples.

Gene Set Variation Analysis (GSVA) is a non-parametric, unsupervised algorithm for calculating Normalized Enrichment score (NES) of pathways and functional annotation based on gene expression array, which was extensively utilized in cancer-related studies (Liu et al., 2021a; Liu et al., 2021b; Liu et al., 2021c). Next, we further performed GSVA approach based on the two prognostic gene sets to calculate the NES of each patient as LIHC-unfavorable GSVA score (LUG score) and LIHC-favorable GSVA score (LFG score) using the "GSVA" R package (Hanzelmann et al., 2013). Receiver operating characteristic curve (ROC) analysis was employed to illustrate the diagnostic veracity of two GSVA scores in different HCC cohorts (TCGA, ICGC, and GSE14520). Patients in TCGA, ICGC, and GSE14520 cohorts were divided into high/low-risk groups according to the median scores and subsequently carried out to Kaplan–Meier survival analysis.

Clinical Correlation Analyses of the LUG Score and LFG Score

To investigate the impact of the two GSVA scores on clinical characteristics, we further explore the relationship of the LUG score and LFG score with other clinical characteristics (age, gender, Child grade, T stage, M stage, N stage, and race). In addition, the univariate Cox regression analysis was employed to evaluate the correlation between prognosis and clinical characteristics, and multivariate Cox regression analysis was applied to analyze the independent prognostic ability of the risk factors.

Mutation and Immunohistochemistry Analyses of LCGs

To determine the somatic mutations of HCC patients between high- and low-GSVA score groups, the mutation annotation format (MAF) from the TCGA database was generated using the "maftools" R package (Mayakonda et al., 2018). The Human Protein Atlas is a human protein online database including normal and neoplastic tissues (Uhlen et al., 2010). We utilized the Human Protein Atlas web tool to validate the abnormal expression of LCGs between HCC and liver tissues at the protein level.

Exploration of the Molecular Mechanism

The GSVA method was used to quantify the activity of molecular pathways and find significantly correlated pathways with two GSVA scores. The differences in NES between the high- and low-GSVA scores groups were compared by independent-samples *t*-tests, and $p < 0.05$ was regarded as statistically significant. Gene Ontology (GO) enrichment analysis was performed on the DEGs identified by the "limma" R package between the high- and low-LUG score groups. Gene set enrichment analysis (GSEA) was applied to evaluate the immune response between the high- and low-LUG score groups, and adjusted *p*-value < 0.05 was considered to be different (Subramanian et al., 2005). The gene set "c2.cp.kegg.v6.2.symbols.gmt" and "h.all.v7.2.symbols.gmt" were chosen as the reference gene set.

Construction of PPI Network and Identification of the Hub LCGs

A PPI network between LDGs was constructed through the Search Tool for the Retrieval of Interacting Genes (STRING) online tool (Szklarczyk et al., 2021). Nodes with interaction scores >0.9 and containing LCGs were imported to the Cytoscape, a software for visualizing complex networks. Additionally, univariate regression analysis was utilized to evaluate the prognostic relevance of the LCGs. The key LCGs were screened out and the selection criteria was the number of adjacent nodes >4 in the network and *p*-value <0.05 in prognostic analysis. The Gene Set Cancer Analysis (GSCA) database integrates comprehensive cancer information from TCGA (Liu et al., 2018). We explored aberrant LCG expression in several types of cancer utilizing the GSCA online tool.

Comprehensive Analysis of the Key LCGs

The difference in expression level of key LCGs between tumor and normal samples were validated in various datasets using independent-samples *t*-test procedure. And the variation of the key LCGs' expression pattern as tumor stage increased was verified by the Gene Expression Profiling Interactive Analysis (GEPIA) database (Tang et al., 2017). Simultaneously, the external validation sets (ICGC and GSE14520) were carried out to Kaplan–Meier survival analysis between high- and low-expression groups, which were divided by the median expression value of the key LCGs. In order to further confirm the independent prognostic ability of each key LCGs, we combined the clinical features with the key LCGs to perform multivariate analyses based on TCGA and ICGC data. Furthermore, the GSCA database was employed to investigate the potential mechanism of abnormal expression of key LCGs in multiple aspects, including pathway activity and methylation. Respective co-expression networks of the key LCGs in HCC were achieved through the HCCDB online database (Lian et al., 2018), and then input into Metascape for gene annotation (Zhou et al., 2019).

Immune Infiltration Analysis and Drug Susceptibility Analysis

Single-sample gene set enrichment analysis (ssGSEA) (Barbie et al., 2009) was conducted to quantify infiltration levels for 24 different immune cell types in TCGA HCC samples (Bindea et al., 2013). The correlation between prognostic signatures and immunocyte infiltration levels was evaluated using the "Pearson" approach. The difference in the distribution of immunocyte infiltrating levels between high- and low-GSVA groups was analyzed by Wilcoxon test. The ESTIMATE score

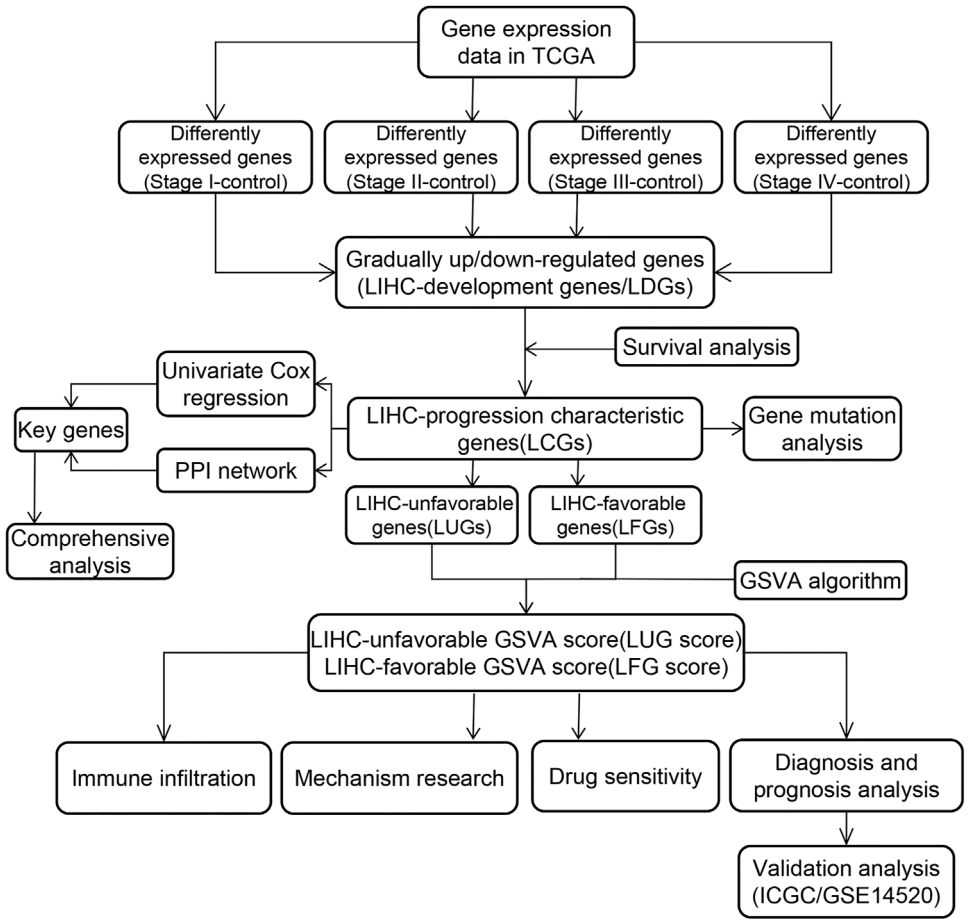

FIGURE 1 | Flow chart of our study.

of each sample, comprising StromalScore and ImmuneScore, was calculated using the R package "ESTIMATE" (Yoshihara et al., 2013). The distinction in immune infiltrating level and the ESTIMATE score between high- and low-score groups were analyzed by Wilcoxon test. Immune checkpoint inhibitor (ICI) was an advanced method for activating antitumor immunity (Topalian et al., 2015). Hence, the relationship between the GSVA scores and six common inhibitory checkpoint molecules (CD274, CTLA4, HAVCR2, LAG3, PDCD1, and TIGIT) was assessed to speculate the immunotherapy response targeting ICIs. The Tumor Immune Dysfunction and Exclusion (TIDE) score and Tumor microenvironment evaluation (TME) score are two different computational models for predicting response to immune checkpoint blockade (ICB) (Jiang et al., 2018; Zeng et al., 2021). We uploaded the TCGA transcriptome profiles to the TIDE web and then obtained every patient's TIDE score, and TME score was computed by "TMEscore" R packages. Moreover, to compare the therapeutic effects of chemotherapeutic drugs in the different score groups, we measure the semi-inhibitory concentration (IC50) values of commonly used chemotherapeutic drugs for LIHC by the "pRRophetic" package (Geeleher et al., 2014).

Statistical Analyses

All statistical analyses were conducted *via* R software (Version 3.6.7). The Student's *t*-test was used for statistical comparisons. Spearman's correlation was applied for the analysis of the correlation. The Benjamini–Hochberg false discovery rate (FDR) method was used for p-value adjustment. Fisher's test was used to identify the significant GO terms. A p-value <0.05 was regarded as statistically significant. The cut-off value of continuous variables, such as gene expression and immune infiltration level, was median.

RESULTS

Identification of the LIHC-Development Gene

The general analysis flow of our study is shown in **Figure 1**. We screened out a total of 487 common upregulated DEGs, and 892 common downregulated DEGs were identified by the intersection of DEGs between different subgroups (**Figure 2B**). Among them, 83 DEGs were gradually upregulated and 247 DEGs were gradually downregulated as the stage evolved. These DEGs

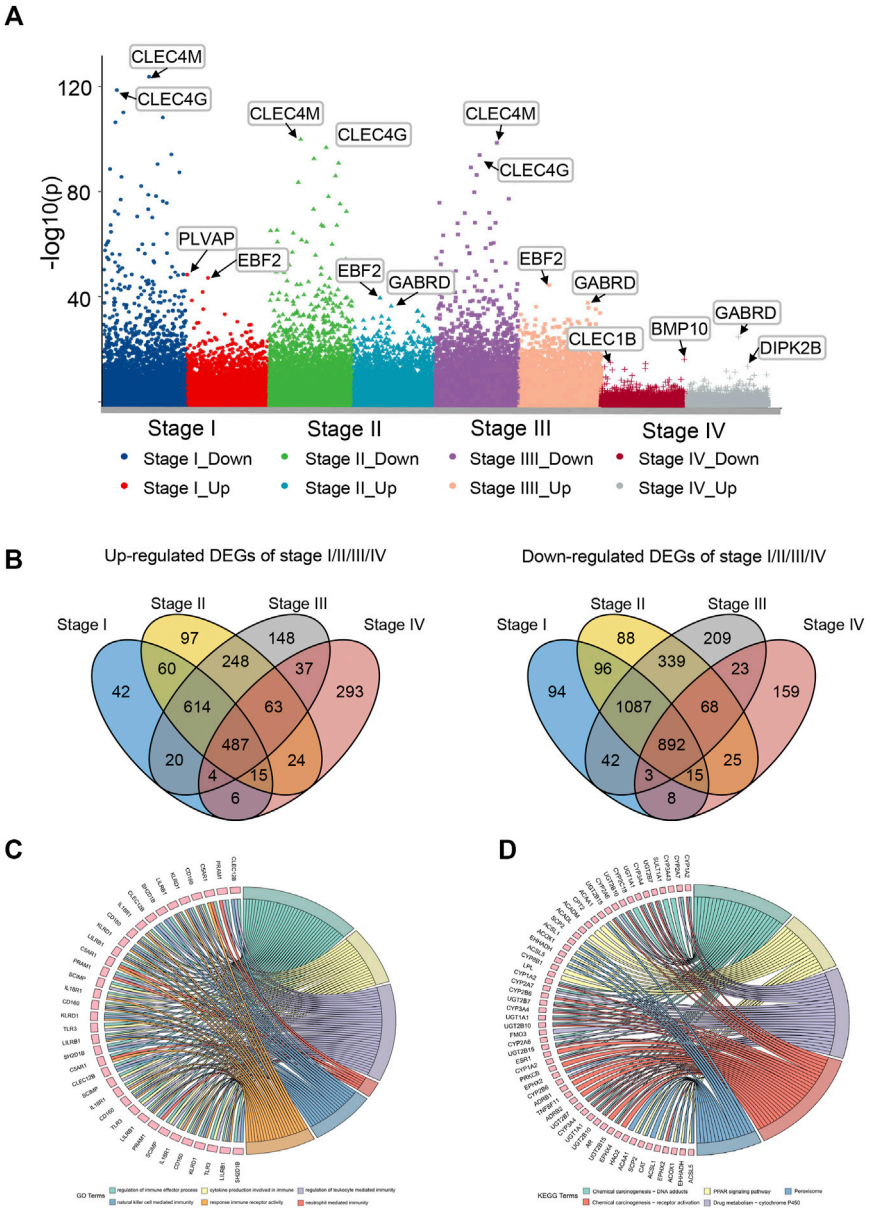

FIGURE 2 | Differential expression gene analysis and functional enrichment analysis. **(A)** Manhattan plot showed differentially expressed genes (DEGs) in different stages of LIHC. **(B)** Venn plot of up/downregulated common DEGs in LIHC stage I–IV. **(C)** GO enrichment analysis of LIHC-development genes. **(D)** KEGG pathway analysis of LIHC-development genes.

may have a sustained effect on HCC progression so they are considered as the LIHC-development genes (LDGs). In the result of the GO analysis, the TRGs were mainly associated with the regulation of cell cycle, chromosome segregation, mitotic nuclear division, regulation of inflammatory response and immune effector process, response to drug, and organelle fission (**Figure 2F**). The result of GO analysis showed that the LDGs were enriched in several immunoregulation ways, such as regulation of the immune effector process, cytokine production involved in immune response, regulation of leukocyte-mediated immunity, and neutrophil-mediated immunity (**Figure 2C**). As for the KEGG pathway enrichment, the LDGs were mainly associated with the chemical carcinogenesis, PPAR signaling pathway, peroxisome, and drug metabolism of cytochrome P450 (**Figure 2D**).

Two Groups of LDGs With Opposite Prognostic Characteristics Were Picked out

Kaplan–Meier (KM) curve analysis discovered that 63 LDGs were prominently associated with clinical outcome and named LIHC-progression characteristic genes (LCGs). Among them, the

TABLE 1 | LIHC-unfavorable gene set and LIHC-favorable gene set.

Gene set	Gene symbol
LIHC unfavorable genes	PYGO2, FAM189B, EHMT2, TARBP1, FLVCR1, ADAM15, TIGD1, LAMC1, LPL, EPHX4, EGFL6, CREG2, NXPH4, CEP72, HEY1, PSPH, H4C8, HPDL, GNAZ, NT5DC2, ATP6V0D2, NANOS1, MEX3A, HES2, CHML, GNG4, CYP19A1, ATP8A2, STK39, PNCK, ETV4
LIHC-favorable genes	VIPR1, CPEB3, ESR1, ADRA1A, CD5L, RANBP3L, GHR, HAO2, CYP3A43, ACADL, EPHX2, TERB2, IYD, CCT6B, DMGDH, GBP7, RDH16, SEC14L3, ABCA9, EHHADH, DHRS1, CYP3A4, MOGAT1, BHMT, SLC38A4, PACRG, ACOT12, TTPA, HDC, CYP8B1, HLF, DRD1

HCC, hepatocellular carcinoma; TCGA, the cancer genome atlas; ICGC, international cancer genome consortium; GEO, gene expression omnibus; LDGs, LIHC-development gene; LCGs, LIHC-progression characteristic gene; LUGs, LIHC-unfavorable gene set; LFGs, LIHC-favorable gene set; LUG score, LIHC-unfavorable GSVA score; LFG score, LIHC-favorable GSVA score; DEGs, differential expressed genes; GO, gene ontology; KEGG, Kyoto encyclopedia of genes and genomes; KM, Kaplan–Meier; ROC, receiver operating characteristic; AUC, area under curve; OS, overall survival; GSVA, gene set variation analysis; NES, normalized enrichment score; GSEA, gene set enrichment analysis; ssGSEA, single sample gene set enrichment analysis.

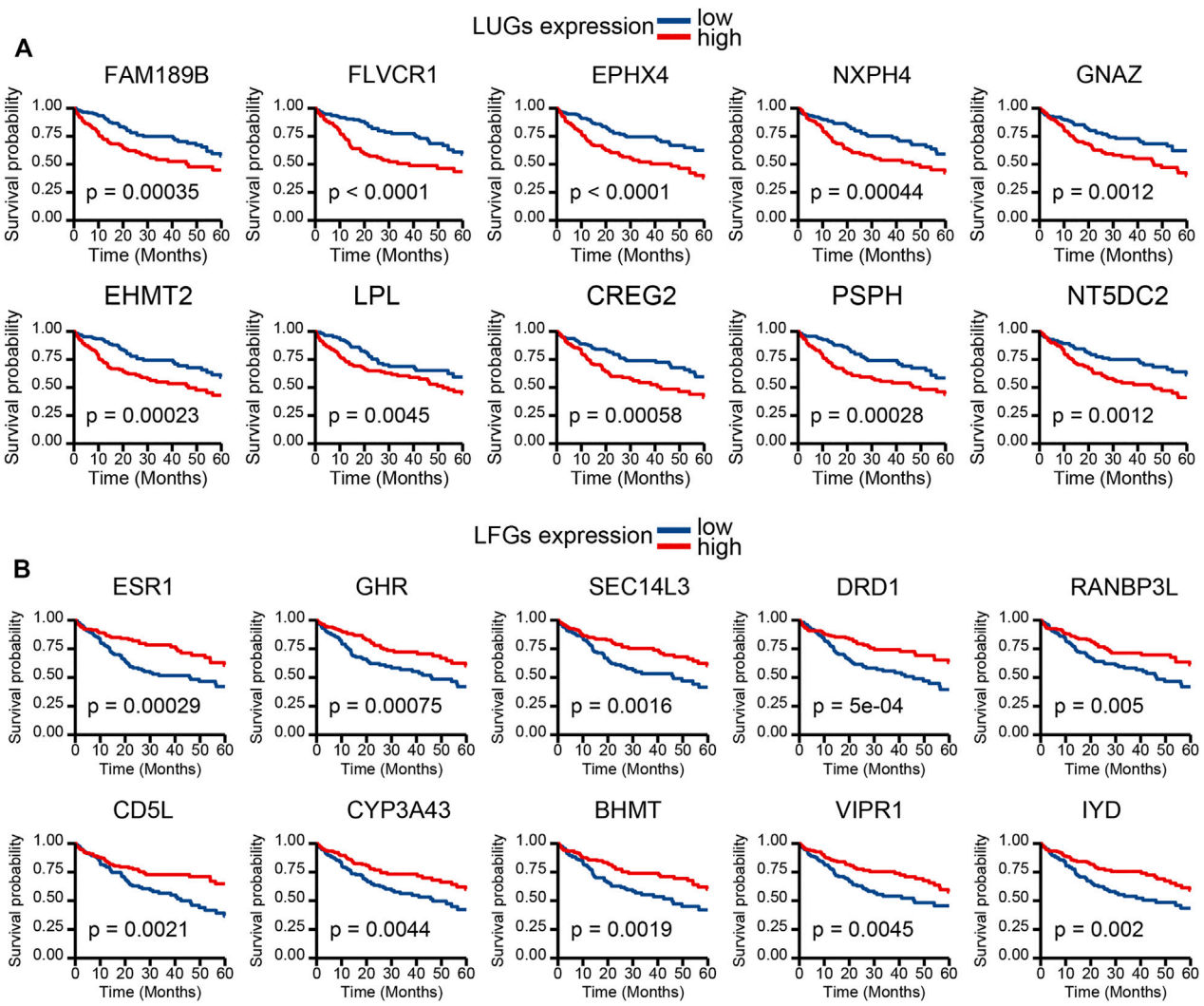

FIGURE 3 | Survival analysis. **(A)** KM survival curve of 10 most significant LIHC-unfavorable genes. **(B)** KM survival curve of 10 most significant LIHC-favorable genes.

LIHC-unfavorable gene set (LUGs) contained 31 LCGs related to poor prognosis, while the LIHC-favorable gene set (LFGs) incorporated 32 LCGs linked to good prognosis (**Table 1**). Kaplan–Meier (KM) curves based on TCGA cohorts of LUGs and LFGs are shown in **Figures 3A,B**. Additionally, all LCGs were differentially expressed between HCC and adjacent noncancerous

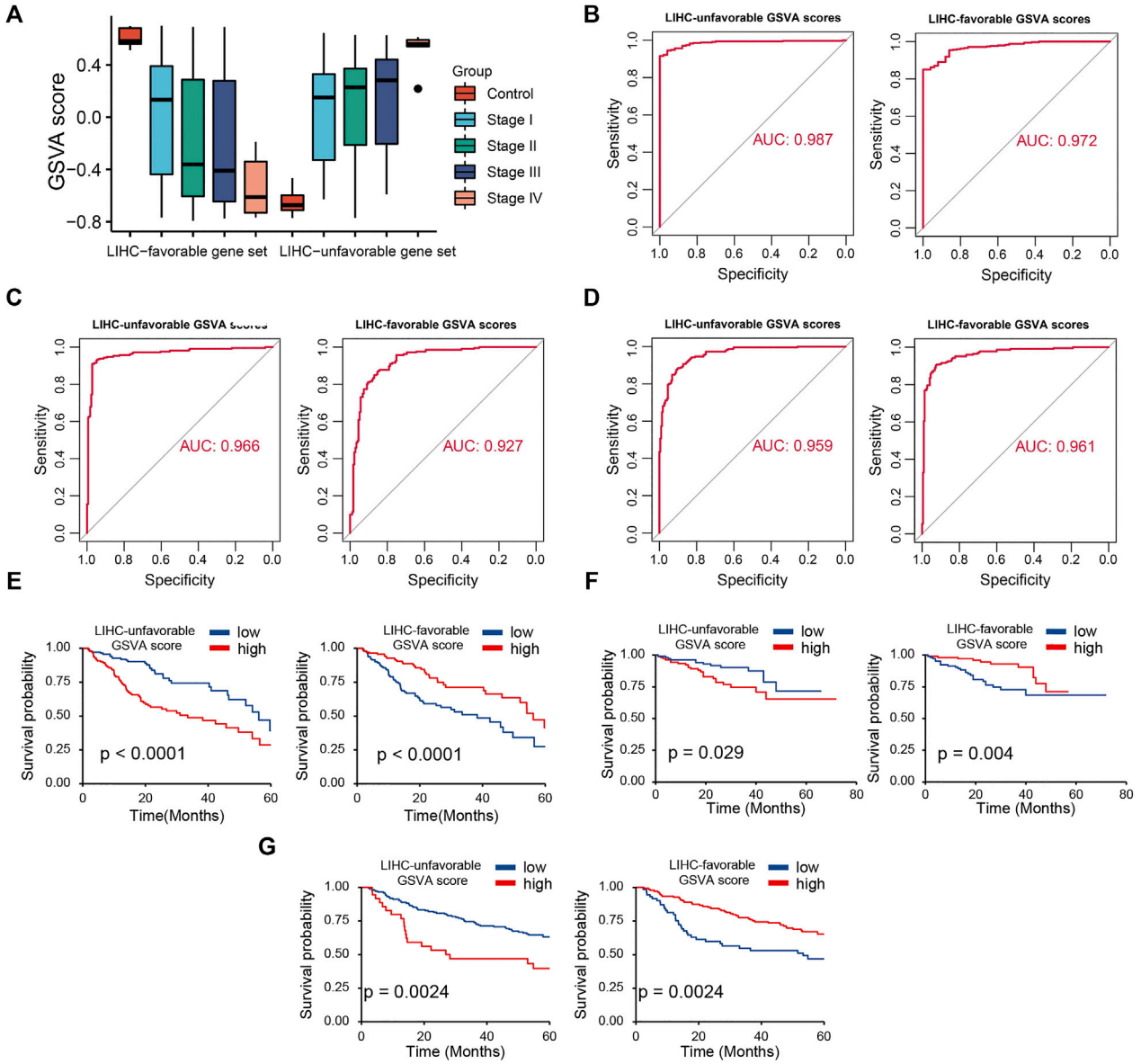

FIGURE 4 | Diagnostic and prognostic abilities of LIHC-unfavorable GSVA score (LUG score) and LIHC-favorable GSVA score (LFG score). **(A)** Box plot of LUG score and LFG score in different LIHC stages. **(B–D)** ROC curves analysis of LUG score and LFG score in TCGA, ICGC and GSE14520. **(E–G)** Survival analysis of LUG score and LFG score in TCGA, ICGC and GSE14520.

tissue in multiple validation datasets from different platforms (**Supplementary Figure S1**). IHC analyses from HPA database also confirmed aberrant expression of LCGs in tumor tissue (**Supplementary Figure S2**).

LIHC-Progression GSVA Score Could Effectively Predict Prognosis for LIHC Patients

Based on two prognosis-related gene sets (LUGs and LFGs), we used GSVA algorithm to construct two LIHC-progression GSVA scores, named LIHC-unfavorable GSVA score (LUG score) and LIHC-favorable GSVA score (LFG score) respectively. Obviously, the LUG score gradually increased as the tumor progresses in HCC patients, while the LFG score was complete opposite (**Figure 4A**). ROC analysis proved that both LUGs and LFGs had great diagnostic accuracy in diverse independent verification datasets, among which AUC = 0.987 and 0.972 in TCGA, AUC = 0.966 and 0.927 in GSE14520, and AUC = 0.959 and 0.961 in ICGC (**Figures 4B–D**). As shown in **Figures 4E–G**, survival analyses indicated patients from the low-LFG score group or high-LFG score group had a longer OS than those from the high-LFG score group or high-LFG score group. According to the univariate/multivariate Cox regression analysis, TNM stage, LUG score, and LFG score can serve as independent

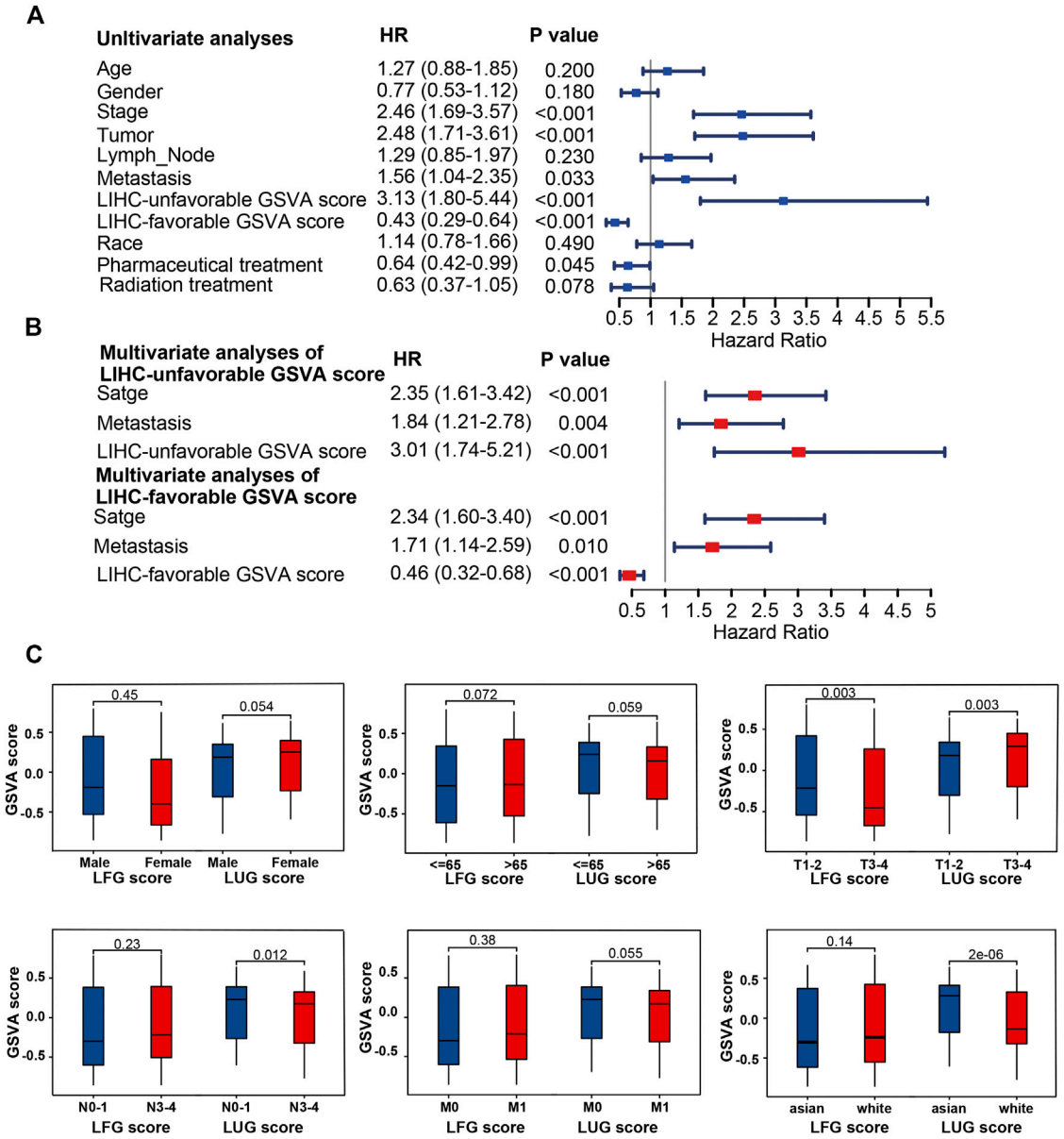

FIGURE 5 | Clinical correlation analyses and of LUG score and LFG score. **(A,B)** Univariate and multivariate Cox regression analysis. **(C)** Correlation of LUG score and LFG score with clinical features.

predictors to evaluate the prognosis of HCC patients (**Figures 5A,B**). Subsequently, we explored the relevance between the GSVA scores and other clinicopathological parameters. The result indicated the LFG score was significantly related to T stage, and the LUG score has a marked correlation with T stage, N stage, and race (**Figure 5C**).

Genetic and Transcriptional Alterations of GSVA Scores and LCGs in LIHC

Both the high-LUG score group and low-LFG score group had a higher TP53 mutation rate than the low-score groups (**Figures 6A–D**). The prognosis of patients with TP53 mutations was significantly worse than those with wild TP53 (**Figure 6E**). Because of the high mutation frequency and poor prognostic feature of TP53, we evaluated the relationship between TP53 mutation and LCGs expression. The results showed that the expression levels of 21 of the 63 LCGs were significantly associated with TP53 mutation status (**Supplementary Figure S3**).

We found high CNA frequency in patients who seemed to presage poor prognosis (**Figure 6F**) and prevalent copy number alterations in all LCGs (**Figure 6G**). LCGs with CNV gain, such as NT5DC2, GNAZ, and HPDL, were significantly elevated in LIHC samples, while LCGs with CNV loss, such as CYP3A4, GHR, and

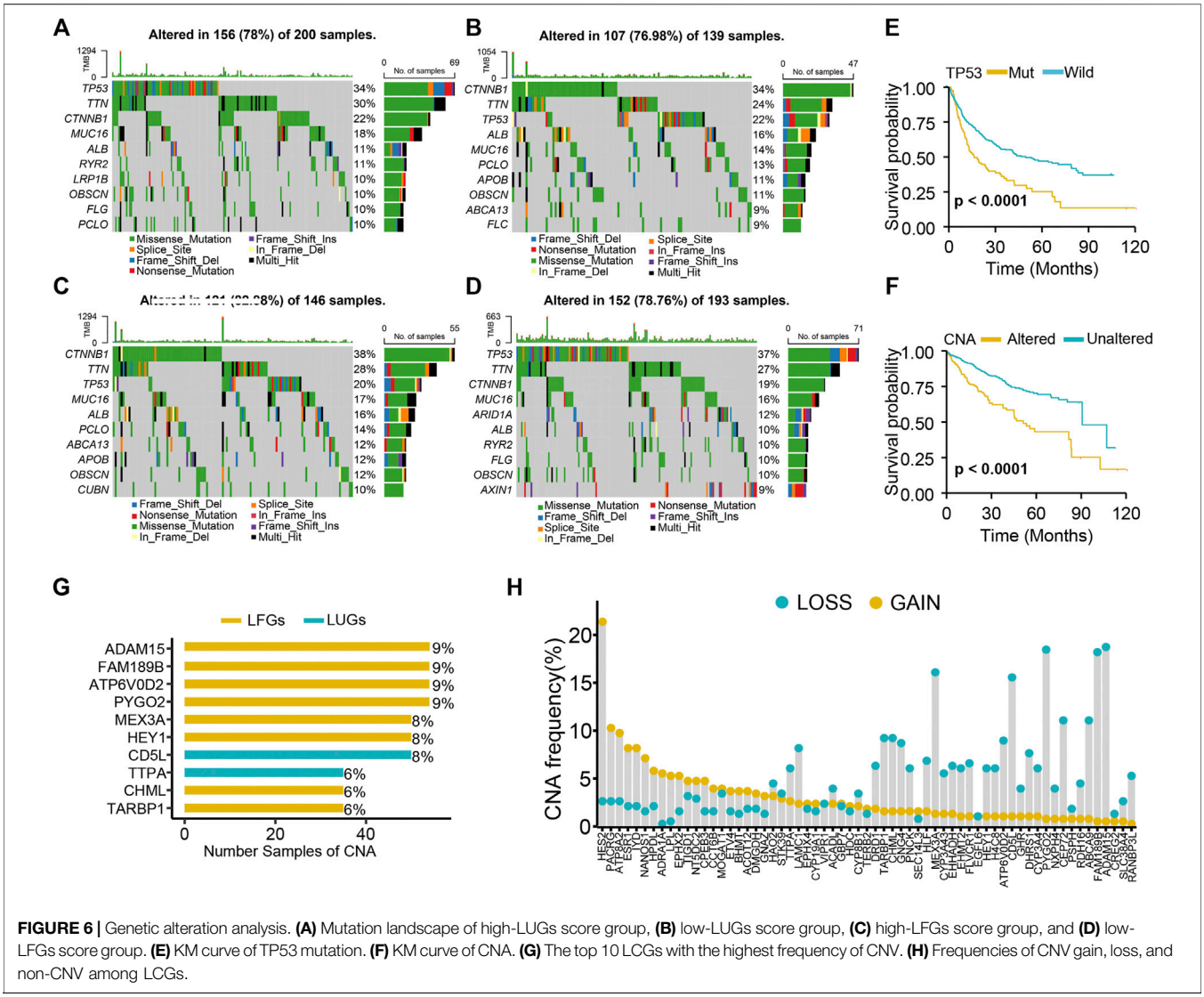

FIGURE 6 | Genetic alteration analysis. **(A)** Mutation landscape of high-LUGs score group, **(B)** low-LUGs score group, **(C)** high-LFGs score group, and **(D)** low-LFGs score group. **(E)** KM curve of TP53 mutation. **(F)** KM curve of CNA. **(G)** The top 10 LCGs with the highest frequency of CNV. **(H)** Frequencies of CNV gain, loss, and non-CNV among LCGs.

HLF, were decreased in LIHC samples, suggesting that CNV might regulate the mRNA expression of LCGs (**Figure 6H**). However, some LCGs with CNV loss, such as EHMT2 and HEY1, showed upregulated expression, while other LCGs with abnormal expression showed no differences of frequency between CNV gain and loss. Hence, although CNV can explain expression variation in many LCGs, CNV is not the only factor involved in the regulation of mRNA expression (Sebestyen et al., 2016).

Potential Molecular Mechanism of Two GSVA Scores

Both the high-LFG score group and low-LUG score group were significantly enriched for metabolisms, such as fatty acid metabolism, bile acid metabolism, and xenobiotic metabolism, while the activity of pathways related to cell cycle, such as G2M checkpoint, mitotic spindle, and DNA repair mitotic spindle enriched significantly in the low-LFG score group and high-LUG score group (**Figures 7A,B**). GO enriched the annotation of upregulated DEGs in the high-LUG score group showed the significant activated functional pathways related to cell differentiation, including differentiation regulation of the epidermal cell and epithelial cell (**Figures 7C,D**). It is worth noting that the immune responses were mainly active in the high-LUG score group, as revealed by GSEA (**Figure 7E**).

Four Key LCGs Were Screened out by PPI Network Analysis and Univariate Cox Regression Method

A PPI network, composed of 77 nodes and 152 edges, was built using the STRING database (**Figure 8A**). As shown in **Figure 8B**, the importance of LCGs was ordered by their number of adjacent nodes in the network. On the other hand, a total of 40 LCGs could affect the outcome of HCC patients according to univariate Cox regression analysis (**Figure 8C**). Eventually, four LFGs (ESR1,

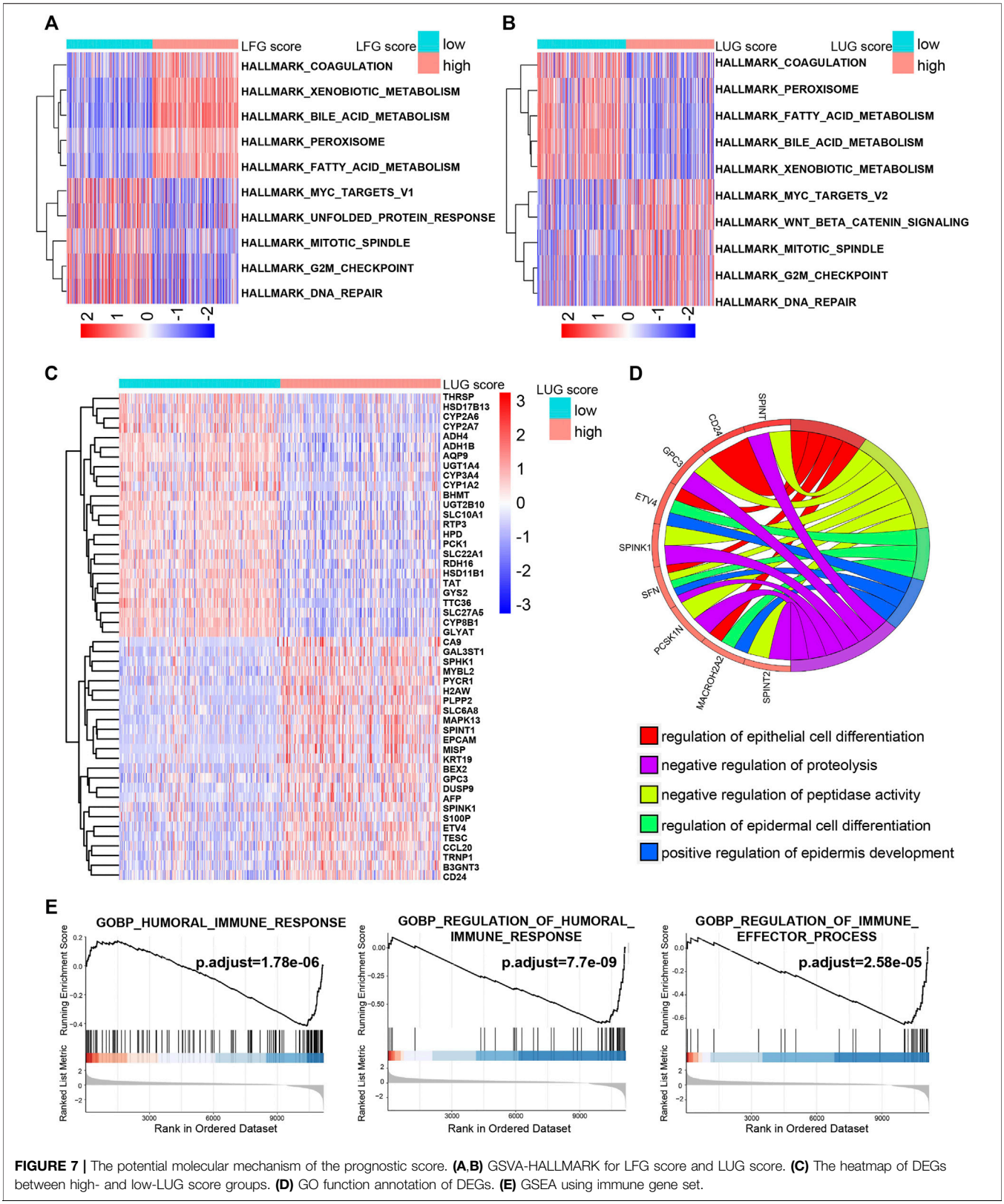

FIGURE 7 | The potential molecular mechanism of the prognostic score. **(A,B)** GSVA-HALLMARK for LFG score and LUG score. **(C)** The heatmap of DEGs between high- and low-LUG score groups. **(D)** GO function annotation of DEGs. **(E)** GSEA using immune gene set.

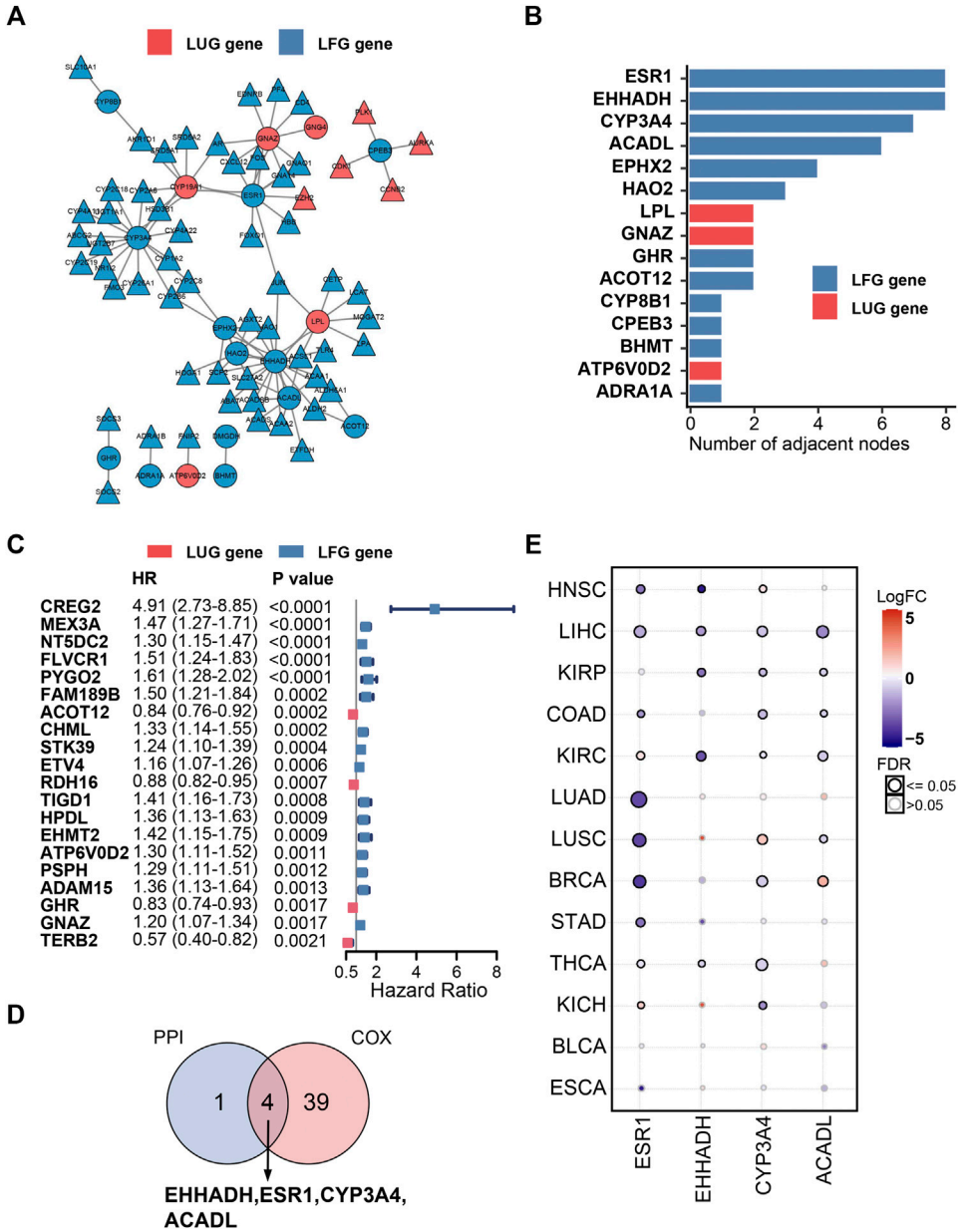

FIGURE 8 | PPI network and univariate Cox regression analysis. **(A)** PPI network of the LDGs. **(B)** The top 15 genes ordered by the number of nodes. **(C)** Univariate Cox regression analysis of LCGs. **(D)** Venn diagram displaying the key LCGs. **(E)** Pan-cancer analysis of key LCGs from GSCA database.

EHHADH, CYP3A4, and ACADL) were selected as the key LCGs by integrated analysis of survival evaluation and PPI network (**Figure 9D**). Pan-cancer research indicated these four key LCGs also apparently decreased in a variety of cancers (**Figure 8E**).

Validation of Key LCGs Expression and Prognosis in External Data

In the two external datasets (ICGC and GSE14520), gene expression levels of four key LCGs were also lower in the liver cancer tissue than adjacent tissue, which is in line with previous researches (**Figure 9A**). Moreover, the box plot of gene expression at different stages obtained from GEPIA proved that four key LCGs possessed similar expression patterns in the HCC progression (**Figure 9B**). KM survival curves based on ICGC and GSE14520 cohorts demonstrated key LCGs performed great efficiency for distinguishing prognostic different HCC patients (**Figure 9C**). Combining the clinical features with the key LCGs expression, multivariate Cox regression validated that the key LCGs were independent prognostic factors and protective factors (**Figure 9D**; **Supplementary Figure S4**). Pathway analyses of

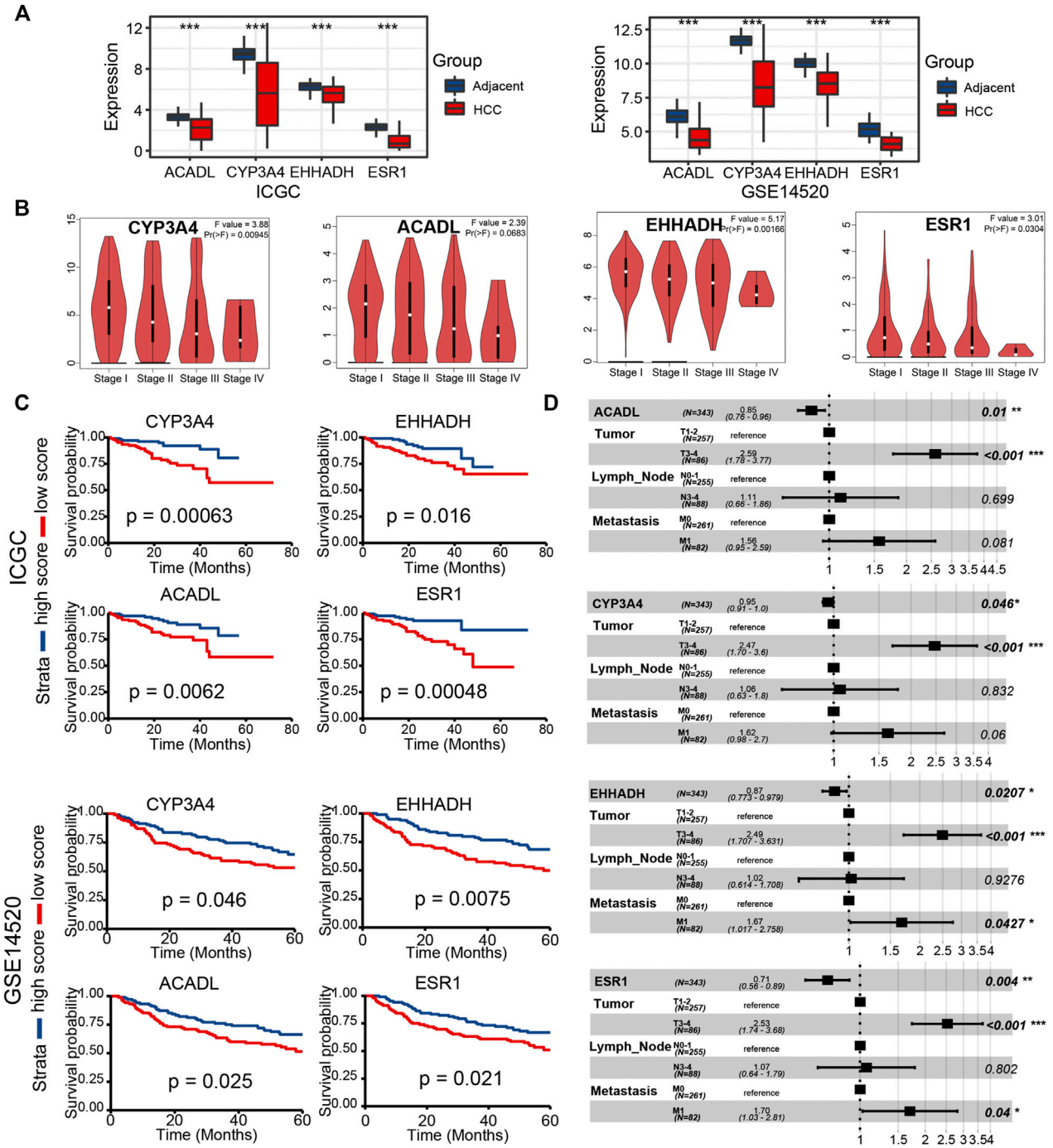

FIGURE 9 | Validation of key LCGs in expression level and prognostic signification **(A)** The expression level of key genes in LIHC tissues and normal tissues based on ICGC and GSE14520. **(B)** Differentiated expression of key genes in different LIHC stages based on the GEPIA database. **(C)** KM plots of key LCGs based on ICGC and GSE14520. **(D)** Multivariate Cox regression of key LCGs. *$p < 0.05$, **$p < 0.01$, ***$p < 0.001$, ****$p < 0.0001$.

GSCA showed that all key LCGs might participate in Hormone pathways, and EHHADH is probably connected with the RTK pathway (**Supplementary Figure S5A**). Meanwhile, the methylation level of ESR1 and CYP3A4 in tumor samples was significantly higher than that in normal samples, implying that methylation could be one of the factors leading to abnormal gene expression (**Supplementary Figure S5B**). Single gene enrichment analysis based on HCCDB and Metascape revealed that the key LCGs had remarkable correlation with metabolism pathways, which was in

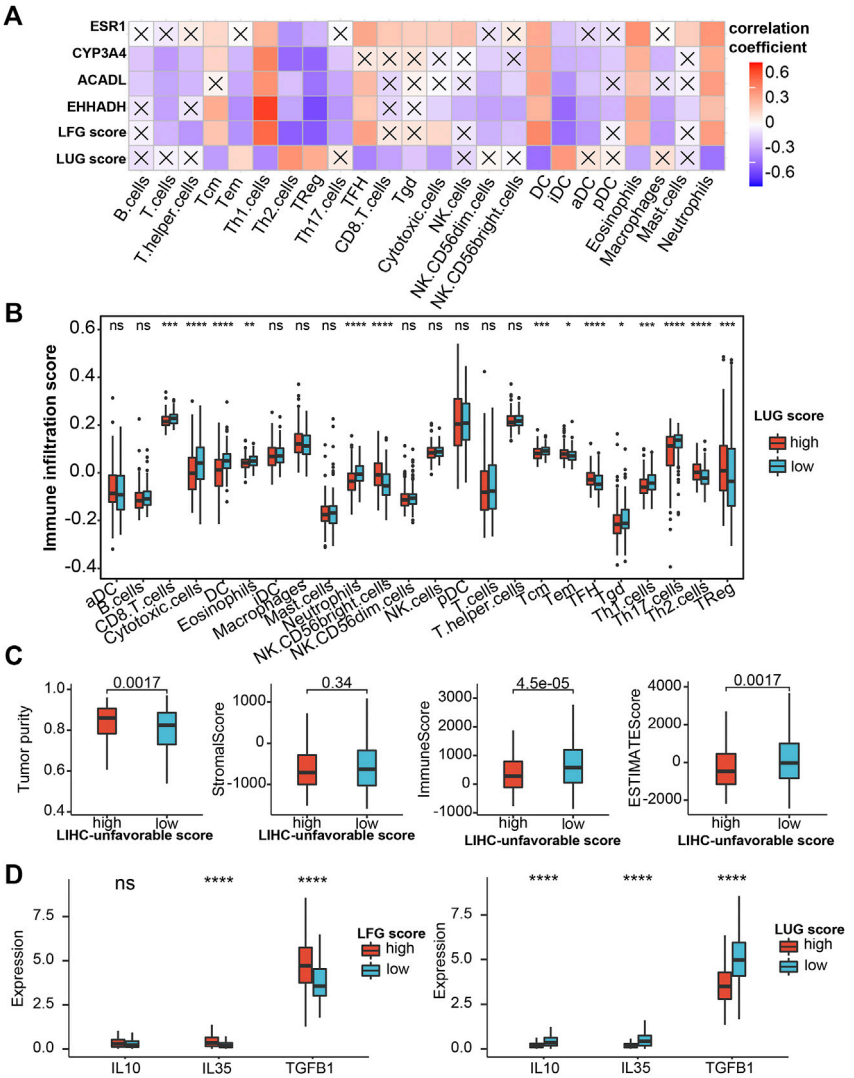

FIGURE 10 | Evaluation of immune infiltration **(A)** Correlation heatmap of LFG score, LUG score and key LCGs with 24 immune cells. The cross indicates no significance. **(B)** Immune infiltration score in the high- and low-LUG score group. **(C)** Correlations of LUG score with immune score, stromal score, ESTIMATEScore and tumor purity. **(D)** Expression of the immune suppressive cytokines between high- and low-LUG/LFG score group. *$p < 0.05$, **$p < 0.01$, ***$p < 0.001$, ****$p < 0.0001$.

keeping with previous results on GSVA scores (**Supplementary Figure S6**).

Immune Infiltration and Drug Susceptibility Analysis

We performed the ssGSEA algorithm to assess the association of the abundance of immune cells with two GSVA scores and the key LCGs. As shown in **Figures 10A,B**, the LFGs score similar to the key LCGs, were positively correlated with Th1 cells, DC, Eosinophils and Neutrophils, while negatively correlated withTh2 cells, TReg and iDC. Interestingly, the LFGs score performed oppositely in these immune cells compared with the LFGs score (**Figures 10A,B**). Tumor purity in the high-LFG score group was significantly higher than those in the low-LFG score group, and StromalScore, ImmuneScore, and ESTIMATEScore in the low-LFG score group were significantly higher than those in the high-LFG score group (**Figure 10C**). Chemokines involved in the immunosuppressive process induced by Tregs (IL-4, IL-35, and TGF-β) were also significantly upregulated in the high-LUG score group and low-LFG score group.

Immunotherapy Response and Drug Susceptibility Analysis

Subsequently, we analyzed the correlation between GSVA scores and multiple immunotherapy response-related indices to assess their impacts on immunotherapy. Patients with low-LUG scores get a higher TIDE score and lower TME score than those with

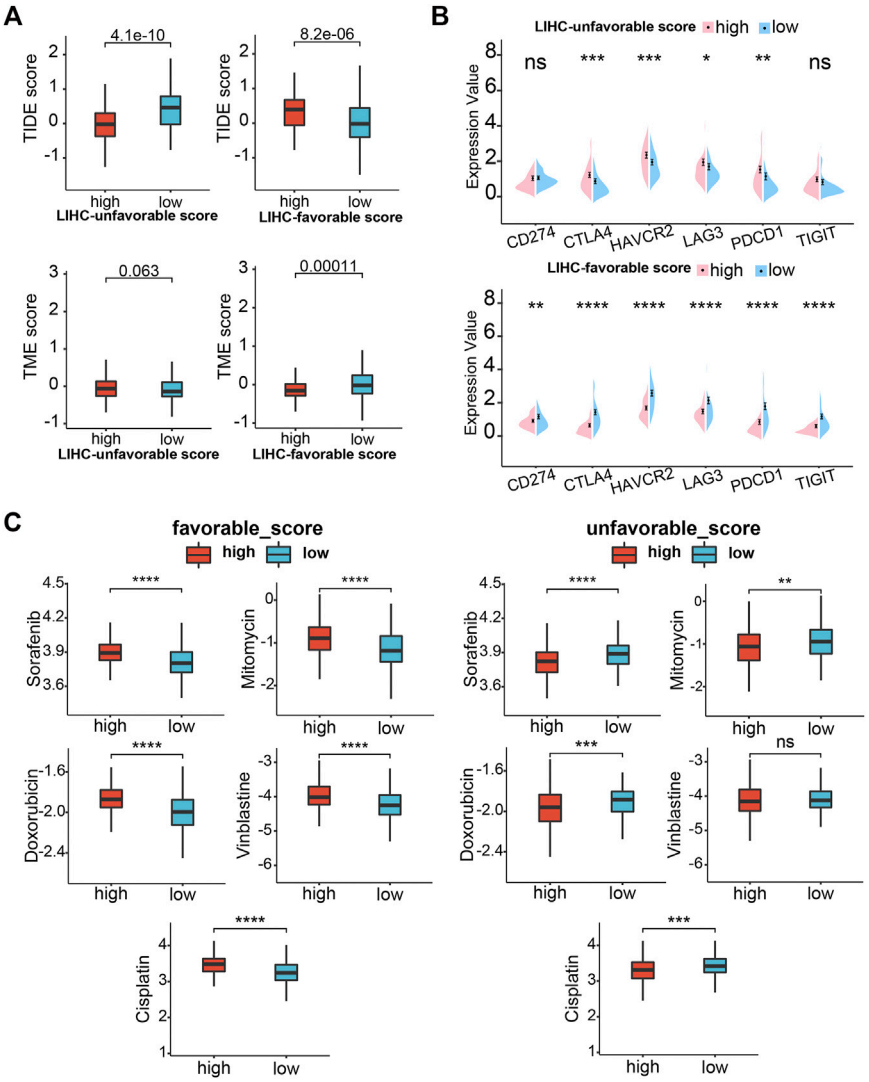

FIGURE 11 | Drug sensitivity analysis. **(A)** TIDE scores and TME score between high- and low-LUG/LFG score group. **(B)** Correlation analysis of two GSVA scores and six immune checkpoint genes. **(C)** Relationships between chemotherapeutic sensitivity and both LFG score and LUG score. *$p < 0.05$, **$p < 0.01$, ***$p < 0.001$, ****$p < 0.0001$.

high-LUG score (**Figure 11A**). In addition, we investigated the associations between immune checkpoints and our GSVA scores. **Figure 10E** shows that several immune checkpoints were differentially expressed in the two groups, including PD-1, PD-L1, and CTLA-4 (**Figure 11B**). These results demonstrated that patients with low LFG scores tended to have a better immunotherapy response. We next selected chemotherapy drugs recommended for liver cancer treatment by AJCC guidelines to evaluate the sensitivities of patients in the low- and high-GSVA score groups to these drugs. Interestingly, we found that the patients in the high-LUG score group or low-LFG score group had lower IC50 values for Sorafenib, Doxorubicin, Doxorubicin, and Cisplatin. Together, these results showed that LUG score and LFG score were related to drug sensitivity (**Figure 11C**).

DISCUSSION

LIHC is a common digestive system tumor with high aggressiveness and poor prognosis. LIHC is insensitive to conventional radiotherapy and chemotherapies; consequently, surgery becomes the main treatment (Novikova et al., 2017). Unfortunately, only 30%–40% of LIHC patients are eligible for surgical resection, and the recurrence rate after surgery is very high (Cao et al., 2012). Therefore, it is urgently needed to explore reliable biomarkers that can be regarded as potential diagnostic and therapeutic targets.

With the rapid progress and widespread application of high-throughput sequencing technology, integrated bioinformatics analysis has emerged as a promising approach to explore various diagnostic and prognostic biomarkers for different tumors. In our research, LIHC data from TCGA were used for

bioinformatics analysis to identify genes that were differentially expressed in different stages. Interestingly, we found gene expression patterns of some DEGs incrementally or digressively changed with LIHC development. For example, a gene may be obviously differentially expressed in the advanced stage but not in the early stage. Thus, we considered these LIHC-development genes may have an impact on cell malignant transformation and tumor evolution. With tumor deterioration, there were 330 LDGs screened out, including 83 LUGs gradually upregulated and 247 LFGs gradually downregulated. Additionally, GO functional enrichment analysis indicated that LDGs were significantly involved in the regulation of immunity. Results from KEGG pathway enrichment analysis manifested LDGs were enriched for the chemical carcinogenesis and PPAR signaling pathway.

After considering the prognostic factors, the number of LDGs was further reduced to 31 LUGs and 32 LFGs. It has been reported that certain LUGs and LFGs are related to the formation and regulation of tumor progression. EMHT2 encodes a methyltransferase that is significantly associated with HCC progression and aggression (Wei et al., 2017). CHML promotes HCC metastasis and leads to poor survival, early recurrence, and more satellite nodules (Chen et al., 2019). STK39 contributes to the progression of HCC by the PLK1/ERK signaling pathway (Zhang et al., 2021). ARID2 expression significantly decreased in metastatic HCC tissues, showing a negative correlation with pathological grade and organ metastasis, and a positive association with survival of HCC patients (Jiang et al., 2020). These results confirmed the possibility that LUGs and LFGs can be used as a prognostic model for LIHC.

In the previous studies, it is the common way that a gene set is analyzed by Cox regression and every gene can get a coefficient that can construct the prognostic model. Nevertheless, because of the heterogeneity of the tumor and the limitations of the sample size, the coefficient of a gene is almost impossible to determine. Thus, we took advantage of GSVA methods to calculate individual samples' NES as prognostic features based on LUGs and LFGs. ROC curve analysis and KM analysis suggested the two GSVA scores had precise diagnosis and prognosis capacity, which were verified in the other two independent LIHC datasets. Univariate and multivariate Cox regression analysis also substantiated that LUG score and LFG score were independent prognostic factors for LIHC.

Four LCGs (ESR1, EHHADH, CYP3A4, and ACADL) were identified as key prognosis-related LCGs based on a combination of the PPI network and univariate Cox regression analysis. CYP3A4 encodes a member of the cytochrome P450 superfamily of enzymes and can influent the chemoresistance of LIHC thus leading to a poor prognosis (Ashida et al., 2017). ESR1 has been a focus in breast cancer, and its mutation is a common cause of acquired resistance (Dustin et al., 2019). ACADL restrains hepatocellular carcinoma by targeting Hippo/YAP signaling (Zhao et al., 2020). We have reason to believe the potential effects of these genes to LIHC, although exploration is still insufficient now.

Through the research on the molecular mechanism of prognostic signatures and score models, we found that the high-LFG score group with a poor prognosis was remarkably enriched in the active metabolism, while the high-LUG score group with a poor prognosis not only exhibited low immune response and metabolic activity but also involved cell cycle regulation. The key LCGs belonged to protective factors and were involved in the metabolic process in HCC. Active metabolism was considered as one of the important signatures of a good prognosis of HCC (Yang et al., 2020; Liu et al., 2021c).

As a continuous breakthrough in the field of immunotherapy, emerging research shows that the tumor microenvironment can regulate cancer progression (Hinshaw and Shevde 2019). Increasing evidence shows that LIHC tissue is often infiltrated by many types of Immune cells (Ringelhan et al., 2018). Th1 cells participate in effective anti-cancer response but Th2 cells show a low cytolytic and antigen-presenting activity. Increase of T2 cells and decrease of T1 cells in intra-tumor are inversely associated with HCC patient survival (Foerster et al., 2018). Our research showed Th2 cells were significantly reduced in the high-LUG score group with a poor prognosis.

DCs play a key role in the initiation and regulation of the immune response. Mature DCs can guide the body to produce a specific immune response and play an anti-tumor role. On the other hand, immature DCs can lead to immune tolerance by activating the body to produce regulatory T cells, anergic T cells, or tolerant T cells (Dhodapkar et al., 2001). In this study, we found that high infiltration of immature DCs mainly happened in the high-LUG score group, while LUG score was negative with infiltration of Mature DCs.

Tregs can promote immunosuppression via secreting immune suppressive cytokines (IL-10, IL-35, TGF-β) or expressing co-inhibitory molecules such as CTLA-4, PD-1, LAG-3, and TIGIT (Josefowicz et al., 2012; Kumar et al., 2018). In the present study, Tregs are upregulated in the high-LUG score group and low-LFG score group. Additionally, cytokines (IL-10, IL-35, TGF-β) related to the immunosuppression process and co-inhibitory checkpoints (CTLA-4, PD-1, and LAG-3) were all upregulated in the high-LUGs score group, which validated that the immunosuppression induced by Tregs exists in high-LUGs score tumors.

Immune checkpoint inhibitors can block immune checkpoints on the cell membrane, which become a promising strategy in the treatment of cancer. Although a variety of immune checkpoint inhibitors has been widely applied in the front-line treatment of HCC, many advanced LIHC patients are resistant to immune checkpoint therapy (Donisi et al., 2020). Our study reveals multiple immune checkpoints (like PD-1, PD-L1, and CTLA4) expression upregulated in high-risk groups. Low TIDE score and high TME score mean a high probability of response to immune checkpoint blockade therapy. We observed that TME scores were significantly higher in high-LFG score groups than those with low-LFG score groups and TME score is completely opposite. Meanwhile, patients with low LFG scores had high expression of multiple immune checkpoints (CTLA4, CD247, HAVCR2, LAG3, PDCD1, and TIGIT). Therefore, we estimate the LFG score possibly can predict the response of immune checkpoint therapy, and combined immunotherapy may be a better choice for the treatment of LIHC.

Nonetheless, several limitations were notable in our study. First, since all data were collected retrospectively, the potential

bias of clinicopathological features is inevitable. Second, the two gene sets may be too large to economize on the sequencing costs. Finally, large-scale prospective studies and functional and mechanistic experimental studies are needed to support our findings.

CONCLUSION

In summary, we discover two LIHC-progression characteristic gene sets and created two LIHC-progression GSVA scores with great diagnostic and prognostic values for hepatocellular carcinoma. Our findings are of great importance in developing new prognostic markers and molecular targets for LIHC.

DATA AVAILABILITY STATEMENT

The datasets presented in this study can be found in online repositories. The names of the repository/repositories and accession number(s) can be found in the article/ **Supplementary Material**.

AUTHOR CONTRIBUTIONS

QH designed the experiments and wrote the paper. BF was mainly responsible for data analysis, and PD was mainly responsible for data collection. YJ was responsible for manuscript review and providing constructive comments. All authors approved the final manuscript.

ACKNOWLEDGMENTS

We gratefully acknowledge The Cancer Genome Atlas, International Cancer Genome Consortium, Gene Expression Omnibus, cBioPortal for Cancer Genomics, GEPIA, and Gene Set Cancer Analysis databases.

SUPPLEMENTARY MATERIAL

The Supplementary Material for this article can be found online at: https://www.frontiersin.org/articles/10.3389/fcell.2022.806989/full#supplementary-material

REFERENCES

Ashida, R., Okamura, Y., Ohshima, K., Kakuda, Y., Uesaka, K., Sugiura, T., et al. (2017). CYP3A4 Gene Is a Novel Biomarker for Predicting a Poor Prognosis in Hepatocellular Carcinoma. *Cancer Genomics Proteomic* 14 (6), 445–453. doi:10.21873/cgp.20054

Barbie, D. A., Tamayo, P., Boehm, J. S., Kim, S. Y., Moody, S. E., Dunn, I. F., et al. (2009). Systematic RNA Interference Reveals that Oncogenic KRAS-Driven Cancers Require TBK1. *Nature* 462 (7269), 108–112. doi:10.1038/nature08460

Barrett, T., Wilhite, S. E., Ledoux, P., Evangelista, C., Kim, I. F., Tomashevsky, M., et al. (2013). NCBI GEO: Archive for Functional Genomics Data Sets-Update. *Nucleic Acids Res.* 41 (Database issue), D991–D995. doi:10.1093/nar/gks1193

Bindea, G., Mlecnik, B., Tosolini, M., Kirilovsky, A., Waldner, M., Obenauf, A. C., et al. (2013). Spatiotemporal Dynamics of Intratumoral Immune Cells Reveal the Immune Landscape in Human Cancer. *Immunity* 39 (4), 782–795. doi:10.1016/j.immuni.2013.10.003

Calderaro, J., Ziol, M., Paradis, V., and Zucman-Rossi, J. (2019). Molecular and Histological Correlations in Liver Cancer. *J. Hepatol.* 71 (3), 616–630. doi:10.1016/j.jhep.2019.06.001

Cao, H., Phan, H., and Yang, L. X. (2012). Improved Chemotherapy for Hepatocellular Carcinoma. *Anticancer Res.* 32 (4), 1379–1386.

Chen, T.-W., Yin, F.-F., Yuan, Y.-M., Guan, D.-X., Zhang, E., Zhang, F.-K., et al. (2019). CHML Promotes Liver Cancer Metastasis by Facilitating Rab14 Recycle. *Nat. Commun.* 10 (1), 2510. doi:10.1038/s41467-019-10364-0

Dhodapkar, M. V., Steinman, R. M., Krasovsky, J., Munz, C., and Bhardwaj, N. (2001). Antigen-specific Inhibition of Effector T Cell Function in Humans after Injection of Immature Dendritic Cells. *J. Exp. Med.* 193 (2), 233–238. doi:10.1084/jem.193.2.233

Donisi, C., Puzzoni, M., Ziranu, P., Lai, E., Mariani, S., Saba, G., et al. (2020). Immune Checkpoint Inhibitors in the Treatment of HCC. *Front. Oncol.* 10, 601240. doi:10.3389/fonc.2020.601240

Dustin, D., Gu, G., and Fuqua, S. A. W. (2019). ESR1 Mutations in Breast Cancer. *Cancer* 125 (21), 3714–3728. doi:10.1002/cncr.32345

Foerster, F., Hess, M., Gerhold-Ay, A., Marquardt, J. U., Becker, D., Galle, P. R., et al. (2018). The Immune Contexture of Hepatocellular Carcinoma Predicts Clinical Outcome. *Sci. Rep.* 8 (1), 5351. doi:10.1038/s41598-018-21937-2

Geeleher, P., Cox, N., and Huang, R. S. (2014). pRRophetic: an R Package for Prediction of Clinical Chemotherapeutic Response from Tumor Gene Expression Levels. *PLoS One* 9 (9), e107468. doi:10.1371/journal.pone.0107468

Hänzelmann, S., Castelo, R., and Guinney, J. (2013). GSVA: Gene Set Variation Analysis for Microarray and RNA-Seq Data. *Bmc Bioinformatics* 14, 7. doi:10.1186/1471-2105-14-7

Hinshaw, D. C., and Shevde, L. A. (2019). The Tumor Microenvironment Innately Modulates Cancer Progression. *Cancer Res.* 79 (18), 4557–4566. doi:10.1158/0008-5472.CAN-18-3962

Huo, J., Wu, L., and Zang, Y. (2020). A Prognostic Model of 15 Immune-Related Gene Pairs Associated with Tumor Mutation Burden for Hepatocellular Carcinoma. *Front. Mol. Biosci.* 7, 581354. doi:10.3389/fmolb.2020.581354

Jiang, H., Cao, H.-J., Ma, N., Bao, W.-D., Wang, J.-J., Chen, T.-W., et al. (2020). Chromatin Remodeling Factor ARID2 Suppresses Hepatocellular Carcinoma Metastasis via DNMT1-Snail axis. *Proc. Natl. Acad. Sci. USA* 117 (9), 4770–4780. doi:10.1073/pnas.1914937117

Jiang, P., Gu, S., Pan, D., Fu, J., Sahu, A., Hu, X., et al. (2018). Signatures of T Cell Dysfunction and Exclusion Predict Cancer Immunotherapy Response. *Nat. Med.* 24 (10), 1550–1558. doi:10.1038/s41591-018-0136-1

Jiang, Y., Chen, S., Li, Q., Liang, J., Lin, W., Li, J., et al. (2021). TANK-binding Kinase 1 (TBK1) Serves as a Potential Target for Hepatocellular Carcinoma by Enhancing Tumor Immune Infiltration. *Front. Immunol.* 12, 612139. doi:10.3389/fimmu.2021.612139

Josefowicz, S. Z., Lu, L.-F., and Rudensky, A. Y. (2012). Regulatory T Cells: Mechanisms of Differentiation and Function. *Annu. Rev. Immunol.* 30, 531–564. doi:10.1146/annurev.immunol.25.022106.141623

Kumar, P., Bhattacharya, P., and Prabhakar, B. S. (2018). A Comprehensive Review on the Role of Co-signaling Receptors and Treg Homeostasis in Autoimmunity and Tumor Immunity. *J. Autoimmun.* 95, 77–99. doi:10.1016/j.jaut.2018.08.007

Lian, Q., Wang, S., Zhang, G., Wang, D., Luo, G., Tang, J., et al. (2018). HCCDB: A Database of Hepatocellular Carcinoma Expression Atlas. *Genomics, Proteomics & Bioinformatics* 16 (4), 269–275. doi:10.1016/j.gpb.2018.07.003

Liu, C.-J., Hu, F.-F., Xia, M.-X., Han, L., Zhang, Q., and Guo, A.-Y. (2018). GSCALite: a Web Server for Gene Set Cancer Analysis. *Bioinformatics* 34 (21), 3771–3772. doi:10.1093/bioinformatics/bty411

Liu, Z., Liu, L., Jiao, D., Guo, C., Wang, L., Li, Z., et al. (2021a). Association of RYR2 Mutation with Tumor Mutation Burden, Prognosis, and Antitumor Immunity in Patients with Esophageal Adenocarcinoma. *Front. Genet.* 12, 669694. doi:10.3389/fgene.2021.669694

Liu, Z., Lu, T., Li, J., Wang, L., Xu, K., Dang, Q., et al. (2021b). Clinical Significance and Inflammatory Landscape of aNovel Recurrence-Associated Immune Signature in Stage II/III Colorectal Cancer. *Front. Immunol.* 12, 702594. doi:10.3389/fimmu.2021.702594

Liu, Z., Lu, T., Wang, L., Liu, L., Li, L., and Han, X. (2021c). Comprehensive Molecular Analyses of a Novel Mutational Signature Classification System with Regard to Prognosis, Genomic Alterations, and Immune Landscape in Glioma. *Front. Mol. Biosci.* 8, 682084. doi:10.3389/fmolb.2021.682084

Llovet, J. M., Villanueva, A., Lachenmayer, A., and Finn, R. S. (2015). Advances in Targeted Therapies for Hepatocellular Carcinoma in the Genomic Era. *Nat. Rev. Clin. Oncol.* 12 (7), 408–424. doi:10.1038/nrclinonc.2015.103

Marengo, A., Rosso, C., and Bugianesi, E. (2016). Liver Cancer: Connections with Obesity, Fatty Liver, and Cirrhosis. *Annu. Rev. Med.* 67, 103–117. doi:10.1146/annurev-med-090514-013832

Mayakonda, A., Lin, D.-C., Assenov, Y., Plass, C., and Koeffler, H. P. (2018). Maftools: Efficient and Comprehensive Analysis of Somatic Variants in Cancer. *Genome Res.* 28 (11), 1747–1756. doi:10.1101/gr.239244.118

Novikova, M. V., Khromova, N. V., and Kopnin, P. B. (2017). Components of the Hepatocellular Carcinoma Microenvironment and Their Role in Tumor Progression. *Biochem. Mosc.* 82 (8), 861–873. doi:10.1134/S0006297917080016

Piñero, F., Dirchwolf, M., and Pessôa, M. G. (2020). Biomarkers in Hepatocellular Carcinoma: Diagnosis, Prognosis and Treatment Response Assessment. *Cells* 9 (6), 1370. doi:10.3390/cells9061370

Ringelhan, M., Pfister, D., O'Connor, T., Pikarsky, E., and Heikenwalder, M. (2018). The Immunology of Hepatocellular Carcinoma. *Nat. Immunol.* 19 (3), 222–232. doi:10.1038/s41590-018-0044-z

Ritchie, M. E., Phipson, B., Wu, D., Hu, Y., Law, C. W., Shi, W., et al. (2015). Limma powers Differential Expression Analyses for RNA-Sequencing and Microarray Studies. *Nucleic Acids Res.* 43 (7), e47. doi:10.1093/nar/gkv007

Sebestyén, E., Singh, B., Miñana, B., Pagès, A., Mateo, F., Pujana, M. A., et al. (2016). Large-scale Analysis of Genome and Transcriptome Alterations in Multiple Tumors Unveils Novel Cancer-Relevant Splicing Networks. *Genome Res.* 26 (6), 732–744. doi:10.1101/gr.199935.115

Shen, Q., Fan, J., Yang, X.-R., Tan, Y., Zhao, W., Xu, Y., et al. (2012). Serum DKK1 as a Protein Biomarker for the Diagnosis of Hepatocellular Carcinoma: a Large-Scale, Multicentre Study. *Lancet Oncol.* 13 (8), 817–826. doi:10.1016/S1470-2045(12)70233-4

Subramanian, A., Tamayo, P., Mootha, V. K., Mukherjee, S., Ebert, B. L., Gillette, M. A., et al. (2005). Gene Set Enrichment Analysis: a Knowledge-Based Approach for Interpreting Genome-wide Expression Profiles. *Proc. Natl. Acad. Sci.* 102 (43), 15545–15550. doi:10.1073/pnas.0506580102

Szklarczyk, D., Gable, A. L., Nastou, K. C., Lyon, D., Kirsch, R., Pyysalo, S., et al. (2021). The STRING Database in 2021: Customizable Protein-Protein Networks, and Functional Characterization of User-Uploaded Gene/measurement Sets. *Nucleic Acids Res.* 49 (D1), D605–D612. doi:10.1093/nar/gkaa1074

Tang, Z., Li, C., Kang, B., Gao, G., Li, C., and Zhang, Z. (2017). GEPIA: a Web Server for Cancer and normal Gene Expression Profiling and Interactive Analyses. *Nucleic Acids Res.* 45 (W1), W98–W102. doi:10.1093/nar/gkx247

Tian, G., Yang, S., Yuan, J., Threapleton, D., Zhao, Q., Chen, F., et al. (2018). Comparative Efficacy of Treatment Strategies for Hepatocellular Carcinoma: Systematic Review and Network Meta-Analysis. *Bmj Open* 8 (10), e021269. doi:10.1136/bmjopen-2017-021269

Tomczak, K., Czerwińska, P., and Wiznerowicz, M. (2015). Review the Cancer Genome Atlas (TCGA): an Immeasurable Source of Knowledge. *Contemp Oncol (Pozn)* 1A (1A), 68–77. doi:10.5114/wo.2014.47136

Topalian, S. L., Drake, C. G., and Pardoll, D. M. (2015). Immune Checkpoint Blockade: A Common Denominator Approach to Cancer Therapy. *Cancer Cell* 27 (4), 450–461. doi:10.1016/j.ccell.2015.03.001

Uhlen, M., Oksvold, P., Fagerberg, L., Lundberg, E., Jonasson, K., Forsberg, M., et al. (2010). Towards a Knowledge-Based Human Protein Atlas. *Nat. Biotechnol.* 28 (12), 1248–1250. doi:10.1038/nbt1210-1248

Villanueva, A. (2019). Hepatocellular Carcinoma. *N. Engl. J. Med.* 380 (15), 1450–1462. doi:10.1056/NEJMra1713263

Wei, L., Chiu, D. K.-C., Tsang, F. H.-C., Law, C.-T., Cheng, C. L.-H., Au, S. L.-K., et al. (2017). Histone Methyltransferase G9a Promotes Liver Cancer Development by Epigenetic Silencing of Tumor Suppressor Gene RARRES3. *J. Hepatol.* 67 (4), 758–769. doi:10.1016/j.jhep.2017.05.015

Xiao, W.-K., Qi, C.-Y., Chen, D., Li, S.-Q., Fu, S.-J., Peng, B.-G., et al. (2014). Prognostic Significance of Glypican-3 in Hepatocellular Carcinoma: a Meta-Analysis. *Bmc Cancer* 14, 104. doi:10.1186/1471-2407-14-104

Yang, C., Huang, X., Liu, Z., Qin, W., and Wang, C. (2020). Metabolism-associated Molecular Classification of Hepatocellular Carcinoma. *Mol. Oncol.* 14 (4), 896–913. doi:10.1002/1878-0261.12639

Yoshihara, K., Shahmoradgoli, M., Martínez, E., Vegesna, R., Kim, H., Torres-Garcia, W., et al. (2013). Inferring Tumour Purity and Stromal and Immune Cell Admixture from Expression Data. *Nat. Commun.* 4, 2612. doi:10.1038/ncomms3612

Yu, G., Wang, L.-G., Han, Y., and He, Q.-Y. (2012). clusterProfiler: an R Package for Comparing Biological Themes Among Gene Clusters. *OMICS: A J. Integr. Biol.* 16 (5), 284–287. doi:10.1089/omi.2011.0118

Zeng, D., Wu, J., Luo, H., Li, Y., Xiao, J., Peng, J., et al. (2021). Tumor Microenvironment Evaluation Promotes Precise Checkpoint Immunotherapy of Advanced Gastric Cancer. *J. Immunother. Cancer* 9 (8), e002467. doi:10.1136/jitc-2021-002467

Zhang, C., Peng, L., Zhang, Y., Liu, Z., Li, W., Chen, S., et al. (2017). The Identification of Key Genes and Pathways in Hepatocellular Carcinoma by Bioinformatics Analysis of High-Throughput Data. *Med. Oncol.* 34 (6), 101. doi:10.1007/s12032-017-0963-9

Zhang, C., Wang, X., Fang, D., Xu, P., Mo, X., Hu, C., et al. (2021). STK39 Is a Novel Kinase Contributing to the Progression of Hepatocellular Carcinoma by the PLK1/ERK Signaling Pathway. *Theranostics* 11 (5), 2108–2122. doi:10.7150/thno.48112

Zhang, J., Bajari, R., Andric, D., Gerthoffert, F., Lepsa, A., Nahal-Bose, H., et al. (2019). The International Cancer Genome Consortium Data Portal. *Nat. Biotechnol.* 37 (4), 367–369. doi:10.1038/s41587-019-0055-9

Zhao, X., Qin, W., Jiang, Y., Yang, Z., Yuan, B., Dai, R., et al. (2020). ACADL Plays a Tumor-Suppressor Role by Targeting Hippo/YAP Signaling in Hepatocellular Carcinoma. *Npj Precis. Onc.* 4, 7. doi:10.1038/s41698-020-0111-4

Zhou, T., Cai, Z., Ma, N., Xie, W., Gao, C., Huang, M., et al. (2020). A Novel Ten-Gene Signature Predicting Prognosis in Hepatocellular Carcinoma. *Front. Cel Dev. Biol.* 8, 629. doi:10.3389/fcell.2020.00629

Zhou, Y., Zhou, B., Pache, L., Chang, M., Khodabakhshi, A. H., Tanaseichuk, O., et al. (2019). Metascape Provides a Biologist-Oriented Resource for the Analysis of Systems-Level Datasets. *Nat. Commun.* 10 (1), 1523. doi:10.1038/s41467-019-09234-6

Conflict of Interest: The authors declare that the research was conducted in the absence of any commercial or financial relationships that could be construed as a potential conflict of interest.

Publisher's Note: All claims expressed in this article are solely those of the authors and do not necessarily represent those of their affiliated organizations, or those of the publisher, the editors, and the reviewers. Any product that may be evaluated in this article, or claim that may be made by its manufacturer, is not guaranteed or endorsed by the publisher.

Advantages of publishing in Frontiers

OPEN ACCESS
Articles are free to read for greatest visibility and readership

FAST PUBLICATION
Around 90 days from submission to decision

HIGH QUALITY PEER-REVIEW
Rigorous, collaborative, and constructive peer-review

TRANSPARENT PEER-REVIEW
Editors and reviewers acknowledged by name on published articles

Frontiers
Avenue du Tribunal-Fédéral 34
1005 Lausanne | Switzerland

Visit us: www.frontiersin.org
Contact us: frontiersin.org/about/contact

REPRODUCIBILITY OF RESEARCH
Support open data and methods to enhance research reproducibility

DIGITAL PUBLISHING
Articles designed for optimal readership across devices

FOLLOW US
@frontiersin

IMPACT METRICS
Advanced article metrics track visibility across digital media

EXTENSIVE PROMOTION
Marketing and promotion of impactful research

LOOP RESEARCH NETWORK
Our network increases your article's readership